Protection of major transmission lines using travelling-waves.

David William Phillip Thomas B.Sc., M.Phil.

Thesis submitted to the University of Nottingham
for the degree of Doctor of Philosophy, May, 1990

Acknowledgements

I would like to acknowledge the invaluable assistance of many individuals during my work on this project.

Firstly I would like to express my thanks to my supervisor Dr. C. Christopoulos of Nottingham University. Thanks are also due to Prof. A Wright of Nottingham University for some useful discussions on distance protection and Dr. P.A. Crossley for insight into travelling-wave problems.

I am indebted to GEC Measurements for supplying equipment and an industrial philosophy to distance protection, the staff of Cripps Computing Centre for sorting out many problems and my colleagues in the Electrical and Electronic Engineering Department for their assistance.

I greatfully acknowledge the financial support of the Science and Engineering Research Council of Great Britain and GEC Measurements, Stafford, U.K.

Contents

Abstract.

An ultra high speed relay for the protection of long EHV transmission lines is described in this thesis.

The need for ultra high speed relays is first discussed. From a brief review of protection based on "impedance" distance algorithms or methods using post fault transients, it is shown that at present, there is no truly ultra high speed relay available for the protection of long EHV transmission lines.

The proposed relay operates on the incident fault transient travelling-waves received at the relaying point only. After the arrival of the first incident transient at the relaying point all subsequent incident travelling-waves are detected using the cross-correlation of the first reflected wave with the incident transient waves. From the amplitudes of the subsequent incident transients, two fault resistance estimates are obtained. These two fault resistance estimates are in agreement only for the subsequent incident wave which is caused by direct reflection from the fault. The fault location can then be determined from the time of arrival of this wave. Additional checks based on the ground mode delay or the line round trip wave amplitude, are incorporated to enhance further the security of the scheme.

Good fault discrimination is shown to be possible over a large range of fault resistances for symmetric three phase faults to ground, phase to ground faults and phase to phase faults. Double circuit transmission lines and compensated transmission lines can also be protected.

The relay has good noise tolerance and a reasonable bandwidth requirement. A real time implementation of the basic algorithm for an internal phase-a to ground fault shows that an ultra high speed relay response with good accuracy can be achieved using currently available digital hardware.

Symbols

$\mathbf{v}$	=	Voltage phasor .
$\mathbf{i}$	=	Current phasor .
v	=	Relaying voltage (= $Re(\mathbf{v})$).
i	=	Relaying current (= $Re(\mathbf{i})$).
Δv	=	Incremental voltage (i.e. system frequency removed from the relaying signal).
Δi	=	Incremental current (i.e. system frequency removed from the relaying signal).
$\mathbf{V}$	=	Root mean square voltage magnitude.
$\mathbf{I}$	=	Root mean square current magnitude.
V	=	Travelling wave voltage amplitude.
I	=	Travelling wave current amplitude.
V_1	=	The initial incident voltage amplitude at the protection point.
V_{r1}	=	The initial reflected voltage amplitude at the protection point.
V_{i2}	=	The voltage amplitude of the second incident transient travelling wave at the protection point.
R	=	The line resistance.
L	=	The line inductance.
C	=	The line capacitance.
χ	=	The line reactance.
Z_l	=	The line impedance.
Y_l	=	The line shunt conductance.
Z_s	=	The line surge impedance.
z^s_{12}	=	Elements of the surge impedance matrix.
z^s_{dd}	=	Diagonal elements of the surge impedance matrix of a fully transposed line.
z^s_{ce}	=	Off diagonal elements of the surge impedance matrix of a fully transposed line.
γ	=	The line propagation constant .
α	=	The travelling wave attenuation along a transmission line.
β	=	The propagation phase coefficient.

τ	=	The transient travelling-wave travel time along the protected line length.
t_1	=	The transient travelling-wave travel time from the protection point to the internal fault location.
$[S]$	=	The modal voltage transform matrix.
$[Q]$	=	The modal current transform matrix.
$[Z_m]$	=	The modal surge impedance matrix.
$[Z_s]$	=	The phase surge impedance matrix.
$[Y_f]$	=	The fault conductance matrix.
R_f	=	The fault resistance.
k_{vf}	=	The fault travelling-wave reflection coefficient.
k_{v1}	=	The protection point travelling-wave reflection coefficient.
k_{v2}	=	The far busbar travelling-wave reflection coefficient.
x	=	Distance along the transmission line.
$\phi(\nu)$	=	The cross-correlation function.
ν	=	The delay time of the cross-correlation function.
A	=	The auto-correlation function.
f_0	=	The power frequency.
ω_0	=	The power angular frequency ($2\pi f_0$).
c	=	The speed of light.
u	=	The velocity of the transient-travelling waves.
>1A	=	Hexadecimal notation (i.e. >1A = 26 decimal).

Subscripts

m	=	modes.
i	=	incident.
r	=	reflected.
l	=	per unit length.
12	=	elements of matricies.
1	=	The first relaying transient.
0	=	Power frequency parameters

Superscripts

a	=	aerial mode.
g	=	ground mode.
p	=	positive sequence.

Introduction.

This thesis describes an ultra high speed relay for the protection of long extra high voltage transmission lines.

The need for ultra high speed relays is first explained in chapter 1. The principle of the proposed travelling-wave algorithm is then outlined in chapter 2. In chapter 3 is shown how the first and subsequent incident waves at the relaying point are detected and processed.

In Chapter 4 the implementation of the algorithm to three common fault types is discussed. The fault types investigated are; symmetric three phase faults to ground, phase to ground faults and phase to phase faults. The application of the relay to double circuit lines and compensated transmission lines and its noise immunity and bandwidth requirements are outlined in chapter 5.

In chapter 6 the implementation in real time of the basic relay algorithm for the protection against phase-a to ground faults is demonstrated. It is shown that good accuracy and fast response times are achievable with currently available signal processing technology.

The conclusions are given in chapter 7 where it is shown that the travelling-wave relay algorithm offers a highly secure ultra high speed trip for internal faults over a wide range of system conditions and fault types without over reach. The proposed relaying scheme should then be a useful addition to current distance protection schemes.

The use of jargon is unavoidable in this thesis and certain constantly recurring terms are listed below.

bit A digit in the binary system.

busbar An electrical connection of zero impedance joining a transmission line to other lines or systems.

EHV transmission lines These are extra high voltage transmission lines typically between 200 to 800 kV.

fault In this thesis this is taken to be a short circuit between transmission line conductors and/or earth.

load This can mean either a collection of devices which consume electricity or the power or current being passed through a line or machine.

RAM Read/write memory.

relay A device which indicates abnormal conditions such as faults and activates circuit breakers.

ROM Read only memory in which information is stored during or immediately after fabrication and not changed later.

source A machine which exchanges net power to the system.

systems This is used to describe the complete network, generators, loads and prime movers.

wait state An extra cycle added to the instruction cycle in order to allow for slower devices on the bus to respond.

CHAPTER 1

The Benefits and Designs of Fast Fault Clearing Relays on Long Extra High Voltage Transmission Lines

1.1 Introduction

Extra high voltage or EHV transmission lines transmit electrical power at typically 275 kV and 400 kV in Britain or 345 kV, 765 kV and 500 kV in North America. The term "long transmission lines" is usually applied to lines that are longer than about 100 km and are best represented by distributed rather than lumped parameters, as travelling waves become significant. "Ultra high speed relays" are usually those which can respond within a few milliseconds from fault inception ($< 5\,ms.$). This chapter presents the main features of EHV transmission line relaying and the motives behind the development of ultra high speed relays for long EHV transmission lines.

The first section outlines the advantages that are gained from faster relay response times on power systems with long EHV transmission lines. The evolution of faster relays is then described in the following sections. It is shown that the limited response time of impedance type relays (greater than half a system cycle) has led to the development of travelling wave relays.

The conclusions are that, despite recent progress in the development of travelling wave relays, there is still a need for further improvements. Rapid fault clearance may be best achieved by a travelling wave relay which can operate within a few milliseconds using transient information available at just one end of a transmission line.

1.2 Benefits of fast relay speeds

The main reason for reducing the relay fault clearing time is to increase the secure loading of long EHV transmission lines [1]. Reduced fault clearing times also give rise to other important benefits which include; reduced damage to insulators and conductors from flashovers, a decrease in safety hazards to substation personnel and linesmen, also the mechanical stresses in major substation equipment are significantly reduced as the increase in rotational kinetic energy is proportional to the square of the fault time [2].

The main features and methods of improving power system stability were outlined by Kimbark [2]. For a first order approximation of an intertie network, given in figure 1.1. A finite machine with internal voltage **E** supplies power P_u at voltage **V** to an infinite bus over a circuit of total inductive reactance χ given by

$$P_u = \frac{\mathbf{EV}}{\chi} \sin \delta \tag{1.1}$$

where δ is the phase angle by which **E** leads **V**.

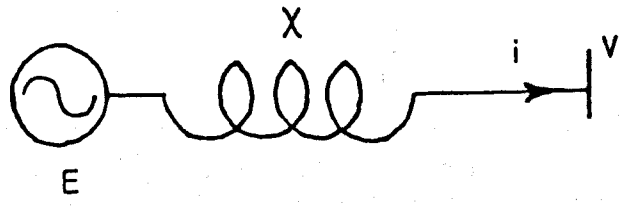

Figure 1.1 A first order intertie network between a source and load.

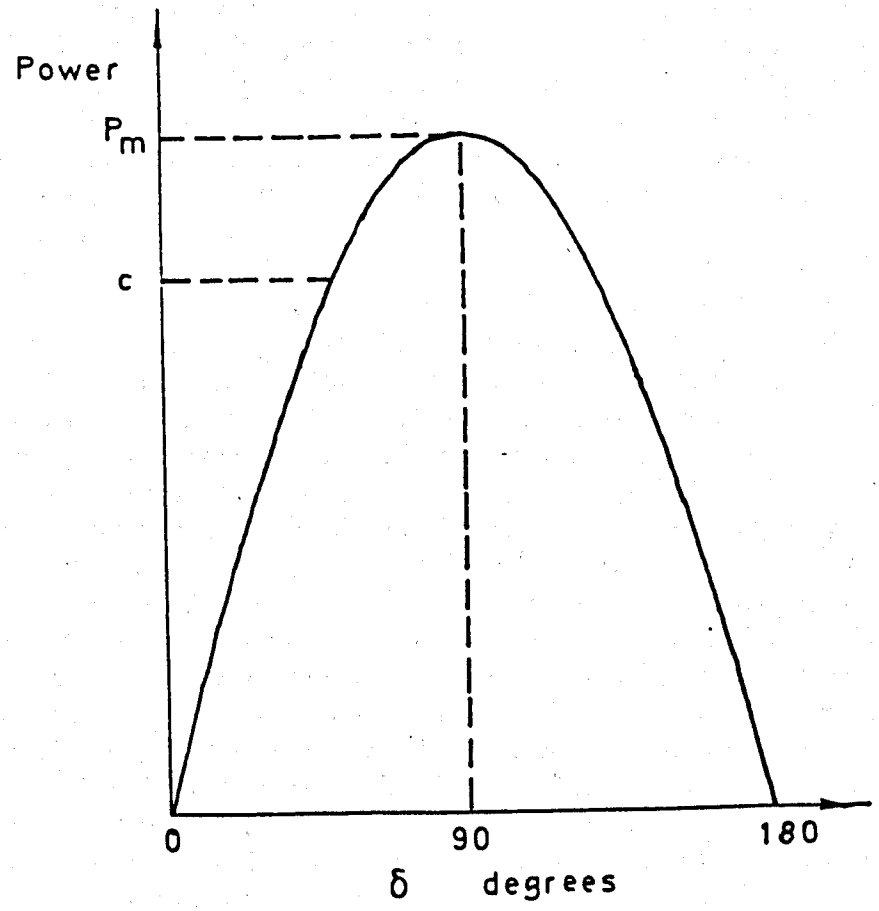

Figure 1.2 Power curve of supplied power against voltage phase angle difference δ between source and load for a first order intertie network as given in figure 1.1.

The mechanical power input P_i to the machine is independent of δ, therefore, the accelerating power P_a of the machine is given by

$$P_a = P_i - \frac{EV}{\chi} \sin \delta \tag{1.2}$$

The resulting power curve is given in figure 1.2. Point c represents the normal steady state operating position where P_a is zero. It can be shown [2] that equation 1.2 is still valid when more than one machine supplies an intertie. In the case of more than one machine, P_i represents the total input minus the local loads at the machine end.

It appears in figure 1.2 that stability, where zero acceleration is maintained, is not possible beyond the point of maximum power P_m. This is because, beyond the maximum P_m, the delivered power decreases as the phase difference δ increases. Slight perturbations will then cause the machine to move away from the operating point rather than back towards it. At operating positions approaching P_m stability will be greatly impaired.

Rapid fault clearing increases stability and, therefore, offers the opportunity of increasing power output by operating near the steady state stability limit. Figure 1.3 shows the improvement in power transmission capability as fault clearing times are reduced. The values were calculated by Bergland et al. [1], for the 500 kV power line between Pacific Northwest and California. Such increases in power transfer capability would also result in reduced transmission costs. Hicks and Butt [3] calculated that a reduction from 3 cycle to 1 cycle fault clearing times, for a 150 mile 500 kV transmission line, could yield savings of $29 million (Assuming transmission investment at $400,000 / mile *c.* 1979).

Fault clearing times, however, involve the combined action of relays and circuit breakers. Clearance times will be limited by breaker interruption occurring, at best, only at the first available current zero. The decrease in fault duration will not then be directly proportional to the reduction in relay operation time. Figure 1.4 shows the maximum total fault duration against relay operation times for various system reactance to resistance (χ/R) impedance ratios, deduced by Thorp et al., [4]. These times of fault duration will be reduced by the breaker arc impedance which temporarily reduces the reactance to resistance ratio (χ/R) of the fault current path [3]. Such analysis of the operation of high speed breakers has led Hicks and Butt [3] to suggest that a one cycle fault duration may be achievable if relay schemes, which can operate within a quarter of a cycle, are developed.

Reduction in relay timing is then particularly beneficial on long EHV intertie lines. It leads to substantial benefits in system performance allowing increased loading with corresponding increases in revenue. These advantages and the development of fast 1 cycle circuit breakers [1] have given a stimulus for the development of high speed relays that can respond within half a cycle and possibly within a quarter of a cycle.

1.3 Distance relays

At the present, distance protection involves the estimation of the line to fault impedance at the system power frequency (50 or 60 Hz). This is achieved by phase or amplitude comparisons of the voltage and current fundamental components. The time delays, introduced by mechanical time constants in

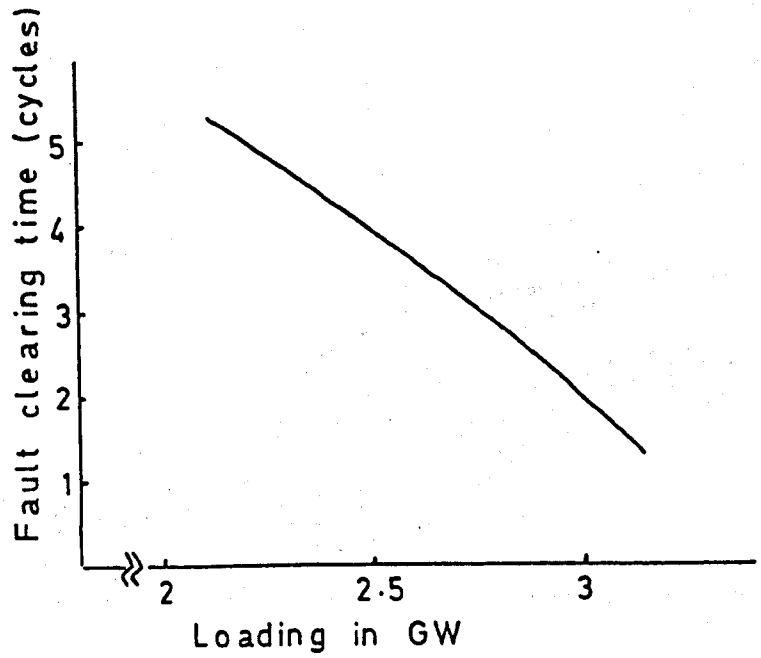

Figure 1.3 The effect of fault clearing time on power transmission with constant stability, after Berglund et al. [1].

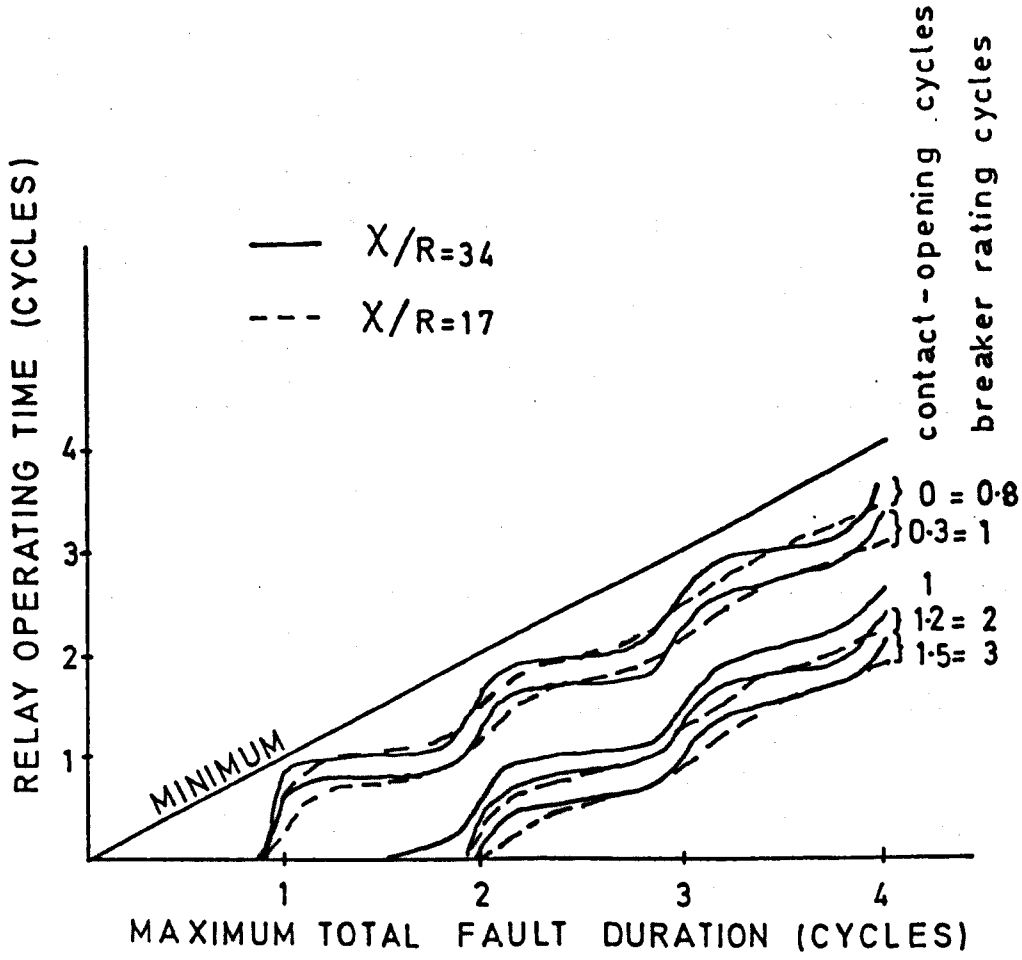

Figure 1.4 Maximum total fault duration vs. relay operating time for various breaker ratings and line inductance to reactance ratios χ/R, after Thorp et al. [4].

early electromagnetic moving armatures, offered adequate rejection of non-power frequency components in the relay input signals.

Higher frequency components, in relay signals, are mainly due to travelling waves. The characteristic frequency lies between $1/2\tau$ and $1/4\tau$ [5], where τ is the aerial mode travel time between the fault and the relaying point (Appendix A), depending on whether the source impedance at the relaying point is greater or less than the line impedance. Other transients consist primarily of exponentially decaying d.c. currents and voltages [6,7]. The amplitude of the d.c. components depends on the initial system voltage at the fault location. The current d.c. transient is usually the most significant. The decay time constant depends on the impedance ratio χ/R of the protection transformer primaries and the section of line between the fault and the protection point.

Successful designs of mechanical relays give good rejection of non-fundamental components combined with an operating time of the order of one cycle [8].

The advent of transistor comparators afford greater freedom of design for both static characteristics and dynamic performance. In particular the block average comparators [9] have a potential 10 milliseconds minimum operating time. The need to filter non-fundamental components, in order to limit relay over reach, reduces their operating times to the order of one cycle [9].

For long multiple phase EHV transmission lines several authors [10,11] have also suggested that high speed comparators can over reach during single phase to ground faults. This is mainly due to the variation in impedances presented by the different modes of propagation of the fault transients [12].

The introduction of digital techniques, not only creates greater freedom in relay design characteristics but also, allows completely new principles of operation to be incorporated.

Rockefeller [13] adapted, for a digital computer, the principles of analogue compensation for transmission lines and suggested a complete group of programmes for transformer and bus protection. Computer speed in initiating tripping was a maximum of 4 milliseconds for severe close faults or 10 milliseconds for moderate or distant faults.

Mann and Morrison [7] suggested that the line impedances can be calculated from estimated peak values of the voltage and current sinusoids which are given by their instantaneous amplitudes and derivatives in the form

$$a_{pk}^2 = a^2 + (a'/\omega_0)^2 \tag{1.3}$$

where;

$\omega = 2\pi f_0$

f_0 is the power frequency

a is the sampled amplitudes

a' is the sampled derivatives

This has the advantage that the peak values are independent of the phase angles at the time of fault inception. Non-system frequencies were removed by a digital filter. The exponential d.c. offset was reduced by impedances

on the transformer secondaries that mimic the χ/R impedance ratio of the primaries plus 90 % of the protected line.

With a sampling rate of about 0.5 milliseconds and the use of a suitable interpolation of the amplitudes and derivatives, they suggest a reasonable accuracy in impedance estimation could be achieved within 5 milliseconds. Though this timing is a reasonable estimate for the simulated high voltage 23 mile line, it is doubtful whether this can be achieved for long multiphase EHV transmission lines where travelling wave effects become significant.

Phadke et al. [14] showed that line impedance estimation can be reduced to one calculation that covers all expected line faults, when symmetrical components are used. Gilbert and Shovlin [15] developed an efficient algorithm to estimate the line impedance assuming the transient voltages and currents were purely sinusoidal. The need to remove non-system frequencies would, however, severely limit the response time of relays using these algorithms.

Application of digital techniques to comparator type relays is limited, therefore, by the need to remove non-system frequencies. The use of active analogue filters [16] or digital filters [17] can reduce the required waveforms to 10 milliseconds but the filtering process could add as much as 10 milliseconds to the minimum relay response time [17].

The presence of significant travelling waves, on long EHV transmission lines, can further reduce the performance of comparator type relays. Johns and Aggarwal [18] found that, for voltage maximum faults on long EHV transmission lines, mho and block average comparator relays would only give reasonable accuracy after more than one system cycle had elapsed,

An alternative method of rejecting non-system frequencies is to convolve a half cycle of the transient waveforms with two orthogonal functions [19]. The use of sine and cosine orthogonal functions is equivalent to the Fourier transform of the half cycle window at the system frequency. The transients would still have to be low pass filtered down to as little as 450 Hz to prevent aliasing. Hope et al. [20] found that a 200 km EHV transmission line could then be accurately protected within about 3/4 of a system power frequency cycle.

A Wiszniewski [21] suggested that Fourier analysis by means of correlating sine and cosine functions of periods equal to a reduced window length would be more efficient. Such a method would reduce the least square errors in estimating the system frequency and phase, however, harmonic noise gives rise to significant errors. The need to severely filter the transients will then more than compensate for the time gained in using a much reduced window length.

The use of Fourier transforms could, of course, be extended to finding the line impedance at any given frequency. Johns and Martin [22] found that such a method would give adequate protection of long EHV transmission lines with a response time within about 3/4 of a system cycle.

Another variation in impedance relaying is to approximate the fault transient circuit by the differential equation

$$v = Ri + L\frac{di}{dt} \tag{1.4}$$

where;-

L = the line inductance

R = the line resistance

v, i = The relaying voltage and current signals

This algorithm directly accounts for the transient d.c. offset and integrating produces a degree of harmonic rejection [23]. The line inductance is then found by integrating equation 1.4 over two data windows in the time domain.

The use of several windows gives improved low pass filtering [24] and the algorithm can be adapted for compensated transmission lines [23]. Such an algorithm is, unfortunately, limited to short lines where the line shunt capacitance and travelling waves are negligible.

Smolinski [25] developed this method further by approximating the line as a single π equivalent section. On long transmission lines where transient wave travel time is significant, the relay response time would, however, be degraded.

Jeyasurya and Smolinski [26] reviewed and appraised many of these digital protection algorithms. They evaluated the accuracy and computational requirements of the algorithms to a range of faults on a 100 mile transmission line. From their results they concluded that the best response could be achieved with a combination of a third order recursive low pass filter and a relay based on the solution of the differential equations in the time domain. Typical response times may then approach half a cycle.

Recently more advanced filtering techniques have been evaluated as a means of improving relay response times of distance schemes. If the transient frequency components are considered to be purely random, then, an optimum response recursive digital filter such as a Kalman filter [27] can be used to extract the system frequency components. Given a reasonable approximation of the expected variance or scatter of the transient signals [28], it is expected that the impedance calculations can be achieved at least 75% faster than a half cycle Fourier transform algorithm [28,29].

For faults on transmission lines the transients can be characterised as; a decaying d.c., fundamental frequencies and higher frequencies. Sachdev and Baribeau [30] then suggested that an efficient digital filter using the least squares approach could be formed which filtered a decaying d.c. component and some harmonics. The expected transient waveforms were represented by the first three terms of the expanded Taylors series. The filter parameters could then be found from the first three terms.

Dash and Panda [31] also proposed that an efficient recursive discrete time filter could be used that explicitly filters the decaying d.c. components and some harmonics. The filter they considered was an interpolating "spectral observer" constructed to give the required Fourier coefficients. Such a filter is highly efficient and gave a relay response time, for a 200 mile 230 kV transmission line, between 1/2 and 3/4 of a power frequency cycle.

In conclusion, it appears that the optimum response of an impedance type distance relay may only approach half a power frequency cycle for long transmission lines. The most sophisticated and efficient transient filters do not improve the relay timing beyond this limit. Faster relays will therefore have to use a completely different operating philosophy.

1.4 Travelling wave relays

It was shown in section 1.2 that the time of response of impedance type distance relays, on long EHV transmission lines, is limited to about half a system cycle. A completely different criteria will then have to be utilised for ultra high speed relaying.

The first few milliseconds of fault transients on long EHV transmission lines are dominated by the travelling wave effects outlined in appendix A. Relays which can accurately fault locate using measurements on travelling-wave, therefore, offer the possibility of fast response within a few milliseconds.

The travelling waves, instigated by an internal fault on a long EHV transmission line, have the form given by the Bewley lattice diagram in figure 1.5. These travelling waves are superimposed on the steady state voltage and current signals. The transient travelling waves can then be found from the incremental signals, where the steady state signals are removed.

For a multi-phase transmission line of " n " phases, it is shown in appendix A that, the travelling wave transients can be considered to propagate as " n " independent modes [32] . The modal waves can be extracted from the relay incremental signals using

$$[\Delta v_m] = [S][\Delta v] \quad (1.5)$$

$$[\Delta i_m] = [Q][\Delta i] \quad (1.6)$$

where;

$\Delta v_m, \Delta i_m$ = the incremental modal voltages and currents respectively.

$\Delta v, \Delta i$ = the incremental phase voltages and currents respectively.

$[S], [Q]$ = the modal transformation matrices.

A multi-phase transmission line usually has asymmetric impedance and conductance matrices due to the asymetry of the line geometry. To compensate for this, discrete transformations of the phases are some times placed at points along the line. This can be too expensive to be used extensively on long EHV transmission lines. Therefore, though many transmission lines can be assumed to be fully transposed with symmetric impedance and conductance matrices this may not be the case for long EHV transmission lines.

Studies have found that, on untransposed EHV transmission lines, the modal transformation matrices can be approximated by constant real values over the frequency range 50–5000 Hz [33, 34, 35]. It is also shown in appendix A that, the incident and reflected transient travelling waves can be found at the relaying location from

$$[V_{im}] = \frac{[\Delta v_m] - [Z_m][\Delta i_m]}{2.0} \quad (1.7)$$

$$[V_{rm}] = \frac{[\Delta v_m] + [Z_m][\Delta i_m]}{2.0} \quad (1.8)$$

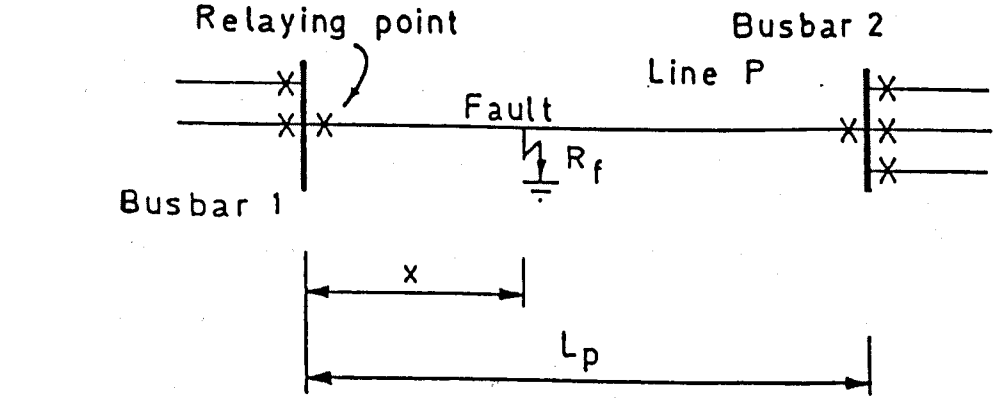

(a)

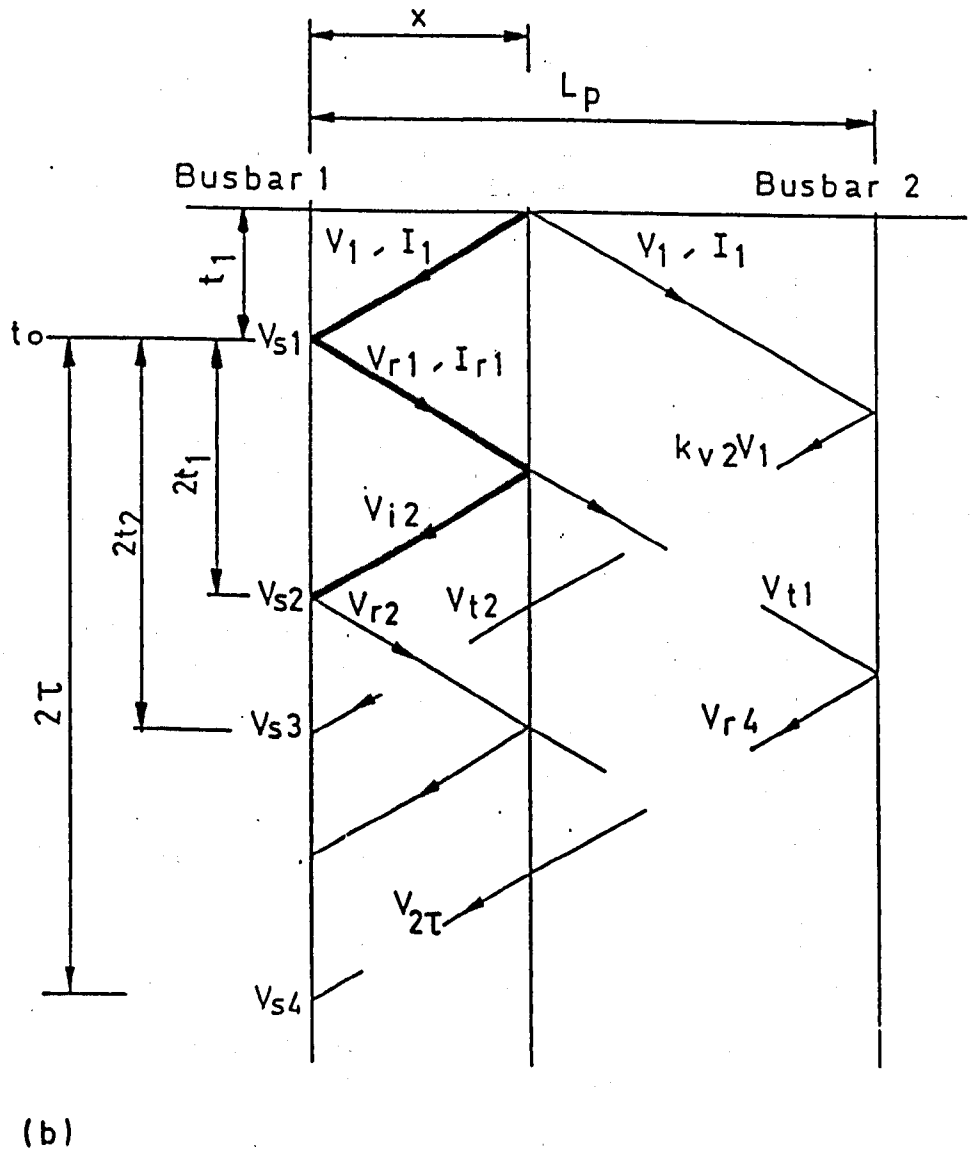

(b)

Figure 1.5 An internal fault on a general line configuration (a.) The subsequent travelling-wave Bewley lattice diagram of the fault transients is given in (b.)

where $[Z_m]$ is the diagonal modal surge impedance matrix.

Travelling wave relays were first designed as directional discriminating relays. Such relays determine from which side of the relay the fault is located using the initial travelling wave amplitudes. Two directional relays, at each end of the protected line and connected by a communication channel, can then decide whether the fault is an internal fault located within the protection region or an external fault located outside the protection region.

Dommel and Michels [36] showed that the incident aerial modes at the relay can be given as travelling waves at the power frequency, the amplitude of which can be found from

$$|V_{im}|^2 = [\Delta v_m - Z_m \Delta i_m]^2 + \left[\frac{1}{2\pi f_0}[\frac{d\Delta v_m}{dt} - Z_m \frac{d\Delta i_m}{dt}]\right]^2 \qquad (1.9)$$

where;

f_0 = the power system frequency

Δv_m = the modal incremental voltage

Δi_m = the modal incremental current

The modal quantities they used, which assumed that the line was fully transposed line, were obtained by the Clark transformation matrices [37]

$$[S]^{-1} = [Q]^{-1} = \frac{1}{3}\begin{bmatrix} 1 & 1 & 1 \\ 2 & -1 & -1 \\ 0 & \sqrt{3} & -\sqrt{3} \end{bmatrix} \qquad (1.10)$$

The quantity $|V_{im}|$ is related to the magnitude of the voltage phasor at the fault location and is, therefore, independent of the voltage phase angle at the fault location at the time of fault instigation. This can be compared with equation [1.3] which also led to an amplitude independent of the voltage phase angle. A significant value of $|V_{im}|$, deduced from the fault transients, will then indicate a fault forward of the relay location at any initial fault voltage phase angle.

An evaluation of this and other ultra high speed travelling wave algorithms by E.P.R.I. [35] found that the derivative terms gave unacceptably large errors. Better results were achieved when $|V_{im}|$ is compared with the reflected transient wave magnitude at the protection point given by

$$|V_{rm}|^2 = [\Delta v_m + Z_m \Delta i_m]^2 + \left[\frac{1}{2\pi f_0}[\frac{d\Delta v_m}{dt} + Z_m \frac{d\Delta i_m}{dt}]\right]^2 \qquad (1.11)$$

It is then assumed that the incident amplitude $|V_{im}|$ will only be larger than $|V_{rm}|$ for forward faults.

Maisour and Swift [38] further developed the Dommel and Michels [36] algorithm to include fault classification. The line types they considered were only fully transposed. It is doubtful, therefore, whether complete classification can also be achieved for untransposed lines.

Vitins [39] presented a geometrical approach to the detection of fault direction, for directional comparison schemes. The principle of this scheme can be understood by considering the initial incremental signals instigated

by the travelling wave transients. From equation A.7 of appendix A, for a forward fault we can put

$$Z_s \Delta i = \pm A - \Delta v \tag{1.12}$$

where A is an arbitrary constant.
For a reverse fault, from equation A.8

$$Z_s \Delta i = \pm A + \Delta v \tag{1.13}$$

The subsequent voltage amplitude will also be related to the initial fault voltage amplitude, which can be expressed by

$$\Delta v \propto -|v_f| \cos(2\pi f_0 t + \delta_0) \tag{1.14}$$

where

$|v_f|$ = The fault voltage magnitude

f_0 = The system frequency

δ_0 = Voltage phase angle at fault inception

t = The time since fault inception

A plot of Δi against Δv will then lead to a clockwise trajectory for a forward fault and an anticlockwise trajectory for a reverse fault. This trajectory and the quadrant where the trajectory crosses a boundary in the plane of incremental voltage versus incremental current can be used for directional discrimination. Studies [35] have shown that such relay tripping was not possible within 4 milliseconds but this algorithm had the advantage that directional information was available several cycles after fault initiation.

The analysis of the incremental signals can be further simplified, for directional comparison schemes, to the comparison of the incremental voltage and current amplitudes. From equations A.7 and A.8 of appendix A it appears that, for forward faults Δv and Δi will be of opposite sign and for reverse faults Δv and Δi will have the same sign. This forms the basis of the RALDA type directional comparison ultra high speed relays first proposed by Chamia and Leberman [40]. The RALDA scheme has been successfully applied, in an analogue form, to 500 kV power systems by B.P.A. [41] and offers fault clearing times within 8 milliseconds. For close up faults where travelling wave effects are short lived, however, the relay may malfunction [35].

A directional scheme based on comparing the incident wave voltage amplitude given in equation A.7 to a threshold level has been developed by Johns et al., [42, 43, 44, 45]. The signal processing and relay logic have been carefully designed to allow for; good system noise rejection, coverage of all fault inception angles, and difficult configurations like double circuit feeders. Extensive testing of a similar algorithm [46] has shown that rapid response within a few milliseconds is possible. The relay has been tested on 400 kV CEGB systems [46] and offers tripping within 8 milliseconds.

Bollen [46] developed a rapid phase selection procedure for directional comparison schemes which could also be incorporated in most travelling relay algorithms. Such a routine could further reduce travelling-wave relay response times.

Tagaki et al., [47, 48] proposed a travelling wave relay algorithm, known as a travelling wave current differential relay, which requires numerical information from both ends of the protected line. The relays, at each end of the protected line, analyse the signals $\epsilon(t)$ given by

$$\epsilon(t) = \frac{1}{Z_s}[v_s(t) - v_r(t-\tau)] - [i_s(t) - i_r(t-\tau)] \tag{1.15}$$

where τ is the travelling wave propagation time on the line, subscript s refers to the locally measured values and subscript r is the communicated values from the remote end.

For an external fault $\epsilon(t)$ is zero and for an internal fault it can be shown that $\epsilon(t)$ is related to the delayed current at the fault location.

$$\epsilon(t) = i_f(t-\tau_1) \tag{1.16}$$

where τ_1 is the travelling wave propagation time from the fault location to the relay.

The operating speed of this algorithm is, unfortunately, limited by the need to transmit such a large amount of data between the two line ends. It has been found that detection times for internal faults can be in excess of 20 milliseconds [35].

Directional comparison schemes can, therefore, lead to rapid fault clearing within a quarter of a cycle. Their dependence on a communications channel between the relays, however, limits such high speed relay responses to transmission lines that are shorter than about 290 miles [35] and also reduces the relay security. When the relay is positioned near a strong source, the initial small transient current may also make directional information difficult to obtain. There is a need, then, for an Ultra High Speed relay which can operate from the transients observed at only one end of a protected transmission line and give a response time within 4 milliseconds on long transmission lines.

Several methods of Ultra High Speed non-unit relays, which operate from just one end of a EHV transmission line, have been proposed. The initial travelling waves set up by an internal fault can be represented by the Bewley lattice diagram [49] given in figure 1.5 . Non-unit travelling wave relays will have to make use of as much information in these initial travelling waves as possible.

Non-unit travelling wave schemes have their origin in Type-A travelling wave fault locators [50, 51]. In the Type-A travelling wave fault locator the initial wave $[V_1, I_1]$ travels to a station at one end of the line, where it starts a timing device. It is reflected at the station bus, back down the line to the fault, where it is reflected back to the station again $[V_{i2}, I_{i2}]$. The time interval $2t_1$ between the arrival of the first wave $[V_1, I_1]$ and the second wave $[V_{i2}, I_{i2}]$ at the station is measured by the timing device and is proportional to the distance to the fault.

Vitins [52] outlined an algorithm where the phase of the first reflected travelling wave $[V_{r1}, I_{r1}]$, at the protection point, is compared with the phase of the second incident wave $[V_{i2}, I_{i2}]$. The vector representation of the two waves is found by correlating with two orthogonal functions. The phase angle at which the vector of V_{i2} becomes parallel with the vector of V_{r1}

was shown to indicate the distance of the fault from the protection point. Reasonable accuracy was only achieved, however, for correlation window lengths of the order of half a cycle. This, plus the possible need for low pass filters, in certain hostile conditions, would increase the relay response beyond half a cycle.

Another approach, first suggested by Crossley and McLaren [53, 54], is to correlate the first reflected wave V_{r1} , at the protection point, with all subsequent incoming transients. It is then suggested that the maximum peak, in the cross correlation function, occurs at the time of arrival of the second incident travelling wave V_{i2}. From the time of arrival of the second transient wave V_{i2} the fault location can be calculated and appropriate relay action taken. The cross-correlation function with mean removal (the covariance function) was found to be ideal for this and is given as [53, 54]

$$\phi(\nu) = \frac{1}{T}\int_0^T [V_{im}(t+\nu) - \overline{V_{im}}][V_{r1m}(t) - \overline{V_{r1m}}]dt \qquad (1.17)$$

where the mean values are given by

$$\overline{V_{im}} = \frac{1}{T}\int_0^T V_{im}(t+\nu)dt \qquad (1.18)$$

$$\overline{V_{r1m}} = \frac{1}{T}\int_0^T V_{r1m}(t)dt \qquad (1.19)$$

The incident and reflected modal waves V_{im} and V_{r1m} are found from equation A.30 and A.31 of appendix A. The modes can either correspond to that of a fully transposed line or the transformation matrices for a untransposed line can be incorporated into the algorithm.

Field tests [35] indicated, unfortunately, that the Crossley and McLaren algorithm [53, 54] has poor fault discrimination. The main criticisms were that; fault distance estimates were different for aerial modes and ground modes, the magnitude of the covariance function decreased dramatically as the fault initiation angle approached voltage zero, other covariance peaks are produced by wave reflections from different parts of the system, asymmetrical faults cause errors due to modal mixing at the fault location.

Several authors have carried out further work, however, and suggested enhancements to the Crossley and McLaren routine [53, 54]. Rajendra and McLaren [55, 56], from the consideration of travelling waves generated by faults on teed networks, suggest a method of auto-correlating the covariance function will give reliable fault discrimination on teed networks. The period between successive peaks in the auto-correlation were very similar for internal faults whereas significant differences occurred for external faults. It is unfortunately difficult to rigorously prove whether this result is true for all type of faults and locations. The problems of modal mixing at the fault location was also left unresolved.

Shehab-Eldin et al., [57] discussed further modifications of the Crossley and McLaren routine [53, 54] to cover all fault locations along the protection zone and faults occurring near zero voltage. They suggest that when close up faults occur the root mean square of the cross-correlation function, over a period equal to twice the line transient wave travel time, will exceed a given threshold level. Tripping will then be initiated if this level is exceeded

regardless of whether the second incident transient wave is detected. For good fault location along the whole transmission line it was also necessary to incorporate two cross-correlation window lengths. The long correlation window was of the order of the transmission line transient wave travel time τ and the short window length was of the order of 0.25 ms.

Though a correction factor was applied to the relaying signals for improved response near voltage zero, Shehab-Eldin et al., [57] concede that a conventional zone 2 type distance relay would also have to be incorporated for protection when faults occur near voltage zero.

For the Crossley and McLaren routine [53, 54] good coverage of all initial voltage phase angles may be achieved if the incident and reflected modal waves are calculated by equations 1.9 and 1.11 as suggested by Koglin and Zhang [58]. The errors generated in the derivative term of equations 1.9 and 1.11 reported by EPRI [35], may, however, lead to unacceptable errors in the convolution function.

A non-unit travelling wave scheme which does not need to resolve individual wave fronts has been proposed by Nimmersjö and Saha [59]. This scheme is based on comparisons between the fault transient voltage levels measured at the protection point and the estimated voltage level for a location near the far end of the protection zone. The voltage level at a point near the far end V_b is given by

$$V_b(t) = \frac{D}{2}[\Delta v(t-\tau) + Z_s \Delta i(t-\tau)] + \frac{1}{2D}[\Delta v(t+\tau) + Z_s \Delta i(t+\tau)] \quad (1.20)$$

where D is the travelling wave attenuation factor and the other terms are as defined in section 1.4.

The main assumptions used in the Nimmersjö and Saha algorithm [59] are that; the steady state line voltage does not vary along the line length and the fault resistances are negligible. High fault resistances towards the far line end may cause the routine to incorrectly locate an internal fault as an external fault. Long transmission lines with long propagation times and significant voltage variation along the lines will also present problems. The algorithm does, however, offer the opportunity of extremely high speed relay response times and accurate fault location for close faults where individual wave fronts will not be detectable.

In conclusion, it appears that ultra-high speed relaying may be possible using travelling wave relays. Non-unit travelling wave relays operating from just the information at one line termination might provide ultra-high speed relaying within 4 milliseconds for all transmission line lengths. Unfortunately, at present none of the non-unit travelling wave relays described above can offer complete fault discrimination for all fault types and transmission line configurations. Studies [35] have also shown that some of the non-unit travelling wave algorithms described above are not precise enough for EHV transmission line protection.

In this thesis the development of a novel ultra high speed non-unit relay that should provide good fault discrimination for all fault types and transmission line configurations will be described. The work has been carried out

at Nottingham in colaboration with GEC measurements of Stafford and the general theory has been developed in several papers [60, 61, 62].

CHAPTER 2

The Principle of the Proposed Protective Scheme

2.1 Introduction

This chapter outlines the fundamental principles of the proposed protective scheme for long three phase EHV transmission lines.

The first section outlines the basic scheme as applied to a single phase line. The fault location is given by the separation of the first and second primary incident travelling-wave transients. The incident waves are identified by comparing two estimates of the fault resistance which are evaluated from the travelling-wave amplitudes and their time of arrival.

The performance of the relay scheme, in discriminating between an internal and an external fault, is examined in section 2.3. It is found that additional checks have to be incorporated into the basic algorithm to ensure consistent fault discrimination.

The adaptation of the relaying scheme to three phase transmission lines is then described in section 2.4. The fault resistance estimates are evaluated in terms of the fault conductance matrix. The different modal velocities of the transient travelling-waves are also included as an additional fault discriminating feature.

2.2 Relay fundamentals on a single phase line

The principle of the proposed protective scheme was first outlined by Christopoulos and Wright [60] and further elaborated by Christopoulos,Thomas and Wright [61],[62]. This relaying scheme can be described by considering, for simplicity, a protected single phase loss free transmission line P connected between busbars 1 and 2 as shown in figure 1.5a

If a fault of resistance R_f occurs at a distance x from the relaying point at Busbar 1, when the instantaneous voltage at the fault location is v_f, it will instigate travelling-wave fault transients which are superimposed on the steady state voltage and currents. The form of the fault transients is given by the Bewley lattice diagram [49] in figure 1.5b. The first voltage wave amplitude V_1 incident at the relaying point will have an initial value given by

$$V_1 = -\frac{Z_s}{Z_s + 2R_f} v_f \tag{2.1}$$

The accompanying current wave I_1 will have an initial value given by

$$I_1 = -\frac{V_1}{Z_s} = \frac{1}{Z_s + 2R_f} v_f \tag{2.2}$$

Positive current flow is taken to be from Busbar 1 to Busbar 2.

The superimposed waves can be extracted from transducer output quantities with the use of the filter arrangement, given in figure 2.1, developed

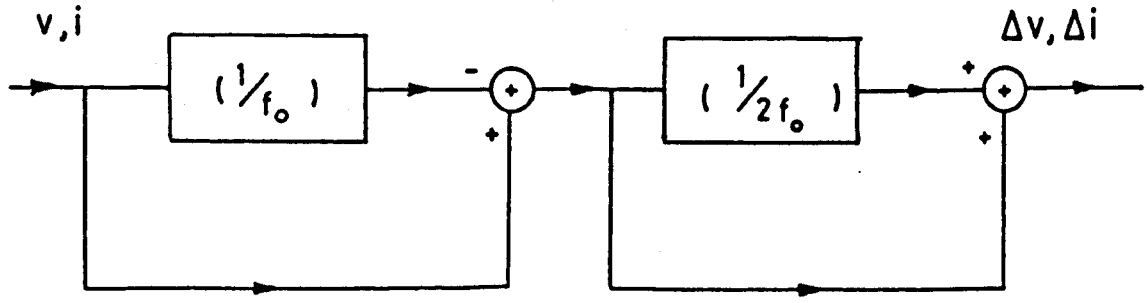

Figure 2.1 Digital superimposed filtering arrangement for the removal of the system steady state voltages and currents, after Johns and Walker [45].

by Johns et al., [45]. This filter consists of a two stage process. In the first stage, sampled values of a full cycle of data are stored and then subtracted from the next cycle of data. In the second stage sampled values of a half cycle of data are added to the next cycle of data. It is claimed that [45] this arrangement almost totally rejects any frequency components within ±3 Hz of the nominal power frequency, thus eliminating any need for adjusting filter delays for power frequency variations. This filter will, of course, only give a half cycle of incremental data but this should be adequate for ultra high speed relaying.

The incident and reflected voltage waves, at the relaying point, can then be resolved using equations A.7 and A.8 given in appendix A. A comparison between the amplitudes of the incident and reflected voltage waves is used as an initial directional check, as with the directional relay developed by Johns et al., [45].

Further information is available when the transient wave, reflected at the protection point [V_{r1}, I_{r1}],is again reflected at the fault location and returns to the relaying point [V_{i2}, I_{i2}]. The travelling-wave reflection coefficient at the fault location is given by

$$k_{vf} = -\frac{Z_s}{Z_s + 2R_f} \tag{2.3}$$

The time of arrival of the second incident wave [V_{i2}, I_{i2}] at the protection point can be used for fault locating. This type of fault location is the basis of a type "A" fault locator [50, 51] and has been developed for ultra high speed relaying [52] — [58]. The problem, as discussed in section 1.4, is to distinguish confidently the second incident wave [V_{i2}, I_{i2}] from all the other incident waves which have been reflected from other parts of the network.

The proposed method of confidently locating the second incident wave $[V_{i2}, I_{i2}]$, is to deduce two estimates of the fault resistance from the first two primary waves $[V_1, I_1]$, $[V_{i2}, I_{i2}]$, and the steady state waveform. The identification of the second incident wave $[V_{i2}, I_{i2}]$ is then confirmed when the two fault resistance estimates agree. The fault location x is then given by the time separation $2t_1$ of the first two primary waves $[V_1, I_1]$ and $[V_{i2}, I_{i2}]$, since, from the Bewley lattice diagram of an internal fault (figure 1.5b)

$$x = ut_1 \tag{2.4}$$

where u is the wave propagation velocity.

The fault will be recognised as being internal provided that its location x is less than the protected line length L_p.

The first estimate of the fault resistance R_{f1} is found from equation 2.1 using the amplitude of the initial incident voltage wave V_1 and the steady state voltage at the fault location v_f at the time of the fault instigation. The initial fault voltage v_f is found from the steady state voltage and current at the protection point and the time separation of the two primary waves incident at the relaying point $2t_1$.

For a transmission line, of series impedance Z_l and shunt admittance Y_l per unit length as shown in figure 2.2, the propagation constant γ and the line surge impedance Zs are given by [63]

$$\gamma = \sqrt{Z_l Y_l} = \alpha + j\beta \tag{2.5}$$

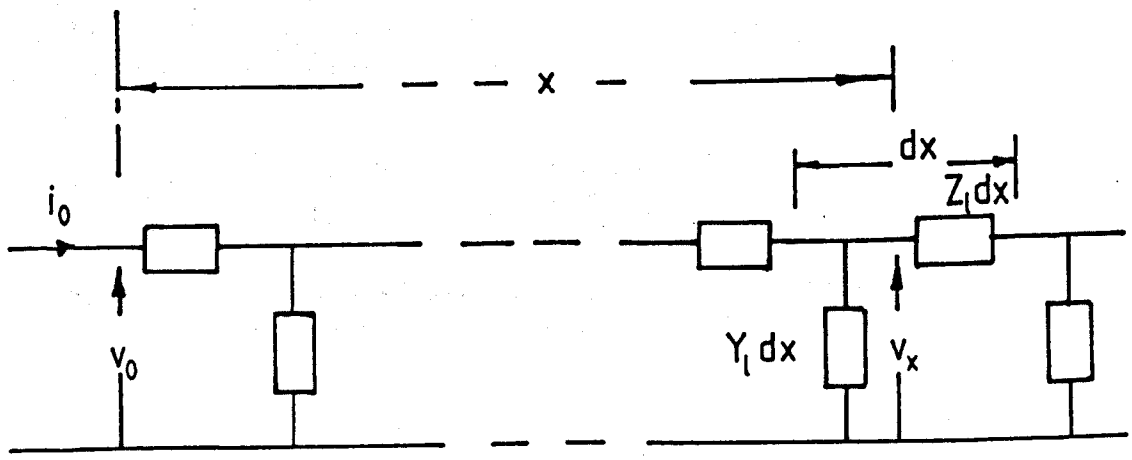

Figure 2.2 Distributed transmission line showing line elements.

$$Z_s = \sqrt{\frac{Z_l}{Y_l}} \tag{2.6}$$

In general α, β, γ are frequency dependent though Z_s is, to a good approximation [36], constant for EHV transmission lines.

The steady state voltage and current solutions for a.c. power transmission are then given by [63]

$$\mathbf{v_x} = \mathbf{v_0} cosh(\gamma_0 x) - \mathbf{i_0} Z_s sinh(\gamma_0 x) \tag{2.7}$$

$$\mathbf{i_x} = \mathbf{i_0} cosh(\gamma_0 x) - \frac{\mathbf{v_0}}{Z_s} sinh(\gamma_0 x) \tag{2.8}$$

where the subscript o refers to parameters at the power frequency f_0, $\mathbf{v_0}$ and $\mathbf{i_0}$ are the voltage and current phasors at the relaying point.

For a single phase loss less transmission line (i.e. $\alpha = 0$) we can then write

$$\mathbf{v_x} = \mathbf{v_0} \cos\beta_0 x - jZ_s \mathbf{i_0} \sin\beta_0 x \tag{2.9}$$

$$\mathbf{i_x} = \mathbf{i_0} \cos\beta_0 x - j\frac{\mathbf{v_0}}{Z_s} \sin\beta_0 x \tag{2.10}$$

At the time of arrival of the initial transient wave [V_1, I_1] at the protection point the steady state voltage and current at the relaying point can be given by

$$\mathbf{v_0}(t_0) = |\mathbf{v_0}| e^{j\theta_1} \tag{2.11}$$

$$\mathbf{i_0}(t_0) = |\mathbf{i_0}| e^{j\theta_2} \tag{2.12}$$

where $|\mathbf{v_0}|$ and $|\mathbf{i_0}|$ are the steady state voltage and current magnitudes. θ_1 and θ_2 are the steady state voltage and current phase angles at the relaying point ($x = 0$).

The time of propagation t_f of the initial wave $[V_1, I_1]$ will be

$$t_f = x/u = \frac{\beta_0 x}{2\pi f_0} \tag{2.13}$$

where; f_0 is the power frequency and u is the velocity of the fault transients.

The steady state voltage and current at the relaying point at the time of fault instigation can then be expressed as

$$\mathbf{v_0}(t_0 - t_1) = |\mathbf{v_0}| e^{j[\theta_1 - \beta_0 x]} \tag{2.14}$$

$$\mathbf{i_0}(t_0 - t_1) = |\mathbf{i_0}| e^{j[\theta_2 - \beta_0 x]} \tag{2.15}$$

From equations 2.9 , 2.14 and 2.15 the initial fault voltage v_f at the time of fault instigation is then given by

$$\mathbf{v_f} = |\mathbf{v_0}| e^{j[\theta_1 - \beta_0 x]} \cos\beta_0 x - jZ_s |\mathbf{i_0}| e^{j[\theta_2 - \beta_0 x]} sin\beta_0 x \tag{2.16}$$

and

$$v_f = Re(\mathbf{v_f}) \tag{2.17}$$

The phase angle delay $\beta_0 x$ can be found from the time separation $2t_1$ of the first and second incident waves $[V_1, I_1]$ and $[V_{i2}, I_{i2}]$, since from figure 1.5 it appears that

$$2\pi f_0 t_1 = 2\pi f_0 t_f = \beta_0 x \tag{2.18}$$

The initial fault voltage at the fault location can be estimated, therefore, from the steady state voltage and current phasors at the time of arrival of the initial fault transient and the time separation $2t_1$ of the first two incident waves [V_1, I_1] and [V_{i2}, I_{i2}].

The first estimate of the fault resistance can then be found by rearranging equation 2.1 to give

$$R_{f1} = -\frac{Z_s}{2}\left[1 + \frac{v_f}{V_1}\right] \tag{2.19}$$

The second estimate of the fault resistance is found by comparing the amplitude of the first reflected wave at the relaying point [V_{r1}] with amplitude of the second incident wave [V_{i2}]. The incident and reflected wave voltage amplitudes at the relaying point being given by equations A.7 and A.8 . It is assumed that there is negligible attenuation and dispersion of the travelling-waves propagating from the relaying point to the fault and back. The second estimate of the fault resistance is then be found from the reflection coefficient given by equation 2.3 which is rearranged into the form

$$R_{f2} = -\frac{Z_s}{2}\left[1 + \frac{V_{r1}}{V_{i2}}\right] \tag{2.20}$$

If the two estimates of the fault resistance agree then it is assumed that the second incident wave [V_{i2}, I_{i2}] has been correctly identified. If the location of the fault given by equation 2.4 indicates an internal fault then tripping of the circuit breakers can be initiated.

In the following section the situations which can prevent correct fault discrimination are described, necessitating the inclusion of extra checks. A suitable extra discriminating check is then also described.

2.3 Relay response to an external fault

In the preceding section consideration was only given to internal faults at a distance x from the protection point. The behaviour of the proposed protective scheme during external faults is considered below to indicate how the necessary discrimination between internal and external faults could be achieved.

In section 2.2 it was stated that directional fault discrimination is implemented on the initial fault transients. Forward external faults beyond the far busbar should then only create problems.

A typical external fault, at a distance x from the far busbar (busbar 2), is shown in figure 2.3a. The resulting travelling wave transients can be represented by the Bewley lattice diagram given in figure 2.3 b. It appears that after the initial incident transient wave V_{pt1} , there are many incident travelling waves at the relaying point which can be confused with the second incident travelling wave V_{i2} of an internal fault (figure 1.5).

For example the second incident wave at the protection point V_{pt2}, of the external fault transients, can be confused with the second incident wave V_{i2} of an internal fault. From the time separation alone, between the transient waves V_{pt1} and V_{pt2}, the external fault transients will indicate an internal fault at a distance x from the relaying point.

If the travelling-wave reflection coefficient of the busbar at the protection point (busbar 1) is k_{v1} and the reflection coefficient of the far busbar (busbar

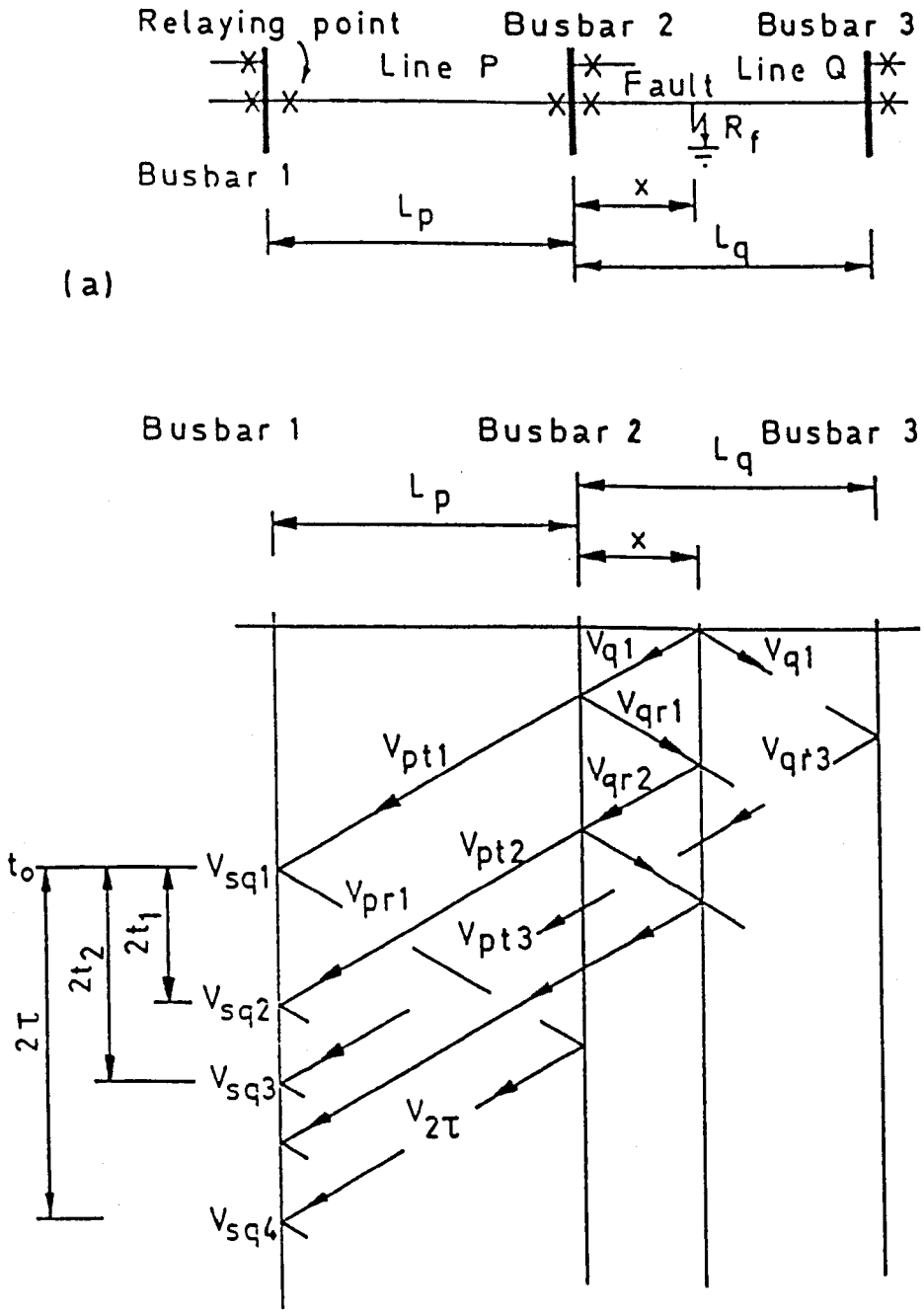

Figure 2.3 The line configuration and Bewley lattice diagram of an external fault.

2) is k_{v2}, then, from equation 2.20 the second estimate of the fault resistance R_{f2} for an external fault will be

$$\begin{aligned} R_{f2} &= -\frac{Z_s}{2}\left[1+\frac{V_{pt1}}{V_{pt2}}\right] \\ &= -\frac{Z_s}{2}\left[1+\frac{(1+k_{v2})k_{ve}k_{v2}v_e}{k_{v1}(1+k_{v2})v_e}\right] \\ &= -\frac{Z_s}{2}\left[1+\frac{k_{v2}k_{ve}}{k_{v1}}\right] \end{aligned} \tag{2.21}$$

where k_{ve} is the travelling-wave reflection coefficient at the external fault and v_e is the initial external fault voltage level.

Note that if $k_{v1} = k_{v2}$ then the second estimate of the fault resistance given by equation 2.21 will yield the true fault resistance.

The estimated fault resistance from equation 2.21 will be less than zero if the fault resistance is

$$R_f < \frac{Z_s}{2}[1 - k_{v1}/k_{v2}] \tag{2.22}$$

The transients would then be ignored without any further computation as negative resistances are physically unacceptable.

The first estimate of the fault resistance is found from equation 2.19 which, for an external fault, gives

$$R_{f1} = -\frac{Z_s}{2}\left[1+\frac{v_f}{V_{pt1}}\right] \tag{2.23}$$

The initial fault voltage v_f will be estimated from equation 2.16 as before with $\beta_0 x$ given by equation 2.18. using the time separation of waves V_{pt1} and V_{pt2}.

The steady state voltage phase angle at the fault location can be related to the voltage and current phase angle at the protection point by

$$\theta_f = \delta_1 + \theta_1 \tag{2.24}$$

$$= \delta_2 + \theta_2 \tag{2.25}$$

where θ_1 and θ_2 are the steady state voltage and current phase angles at the protection point and δ_1 and δ_2 are constants.

If the true fault voltage phasor $\mathbf{v_e}$ is given by

$$\mathbf{v_e} = |\mathbf{v_e}|e^{j\theta_f} \tag{2.26}$$

It follows that; from combining equations 2.16, 2.18, 2.21, 2.23, 2.24 and 2.25, there are two positions in the system cycle where the two fault resistance estimates agree which are given by

$$\tan\theta_f = \frac{(k_{v2}+1)k_{v1}|\mathbf{v_e}|}{k_{v2}[Z_s i_s \sin\beta_0 x \sin\psi_2 - v_s \cos\beta_0 x \sin\psi_1]} - \frac{v_s \cos\beta_0 x \cos\psi_1 + Z_s i_s \sin\beta_0 x \sin\psi_2}{Z_s i_s \sin\beta_0 x \sin\psi_2 - v_s \cos\beta_0 x \sin\psi_1} \tag{2.27}$$

where

$$\psi_1 = \delta_1 + \omega_0 t_e - \beta_0 x$$
$$\psi_2 = \delta_2 + \omega_0 t_e - \beta_0 x$$

and t_e = the propogation time of the fault transient-wave from the fault to the protection point.

There will always be two solutions over one system cycle for the fault voltage phase angle θ_f from equation 2.27. Thus for all fault locations and line geometries there will be two phase angles, within a system cycle, where the fault resistance estimates will be in agreement for an external fault.

For example, consider the single phase line geometry given in figure 2.3a. Typical parameters for an external fault 40 km from the protected line of length 200 km are:-

δ_1	=	20.31^o	k_{v2}	=	$-1/3$
δ_2	=	1.607^o	k_{v1}	=	$-1/2$
$\omega_0 t_e$	=	14.4^o	v_s	=	$357.6\ kV$
$\beta_0 x$	=	2.461^o	i_s	=	$1.7362\ kA$
Z_s	=	$262\ \Omega$	v_e	=	$315.36\ kV$

The loci of the fault resistance estimates for different initial voltage phase angles at the fault location are given in figure 2.4. The two fault resistance estimates agree when

$$\theta_f = 3.09\ radians\ or\ 6.23\ radians \tag{2.28}$$

It is concluded that the condition that the two fault resistance estimates must agree is not, on its own, a sufficient discriminant between an internal and an external fault. Extra checks will then have to be incorporated into the algorithm to ensure complete fault discrimination between internal and external faults.

One discriminant between an internal and external fault is to verify that the fault resistance estimates are positive. Only in a few special special cases, however, will an external fault lead to a negative fault resistance estimate.

A check that is applicable to a single phase line, is to examine the amplitude of the incident wave which arrives at twice the protected line wave transit travel time 2τ after the initial incident transient wave V_1. From figure 1.5 it appears that this wave at 2τ has to propagate through the fault location twice for an internal fault to give the wave amplitude $V_{2\tau}$. For an external fault, shown in figure 2.3 , the travelling-wave amplitude $V_{2\tau}$ results from a wave which travels along the healthy lines of the protected region and will not then be significantly attenuated. It should then be possible to discriminate between an internal and external fault by examining the amplitude of the incident travelling wave which arrives at a time 2τ after the initial incident wave V_1.

The transmission coefficient at the fault location T_{vf} is given by

$$T_{vf} = 1 + k_{vf} \tag{2.29}$$

Let the travelling-wave reflection coefficient of the far busbar (busbar 2) be k_{v2}. For an internal fault the incident wave amplitude at time 2τ will then

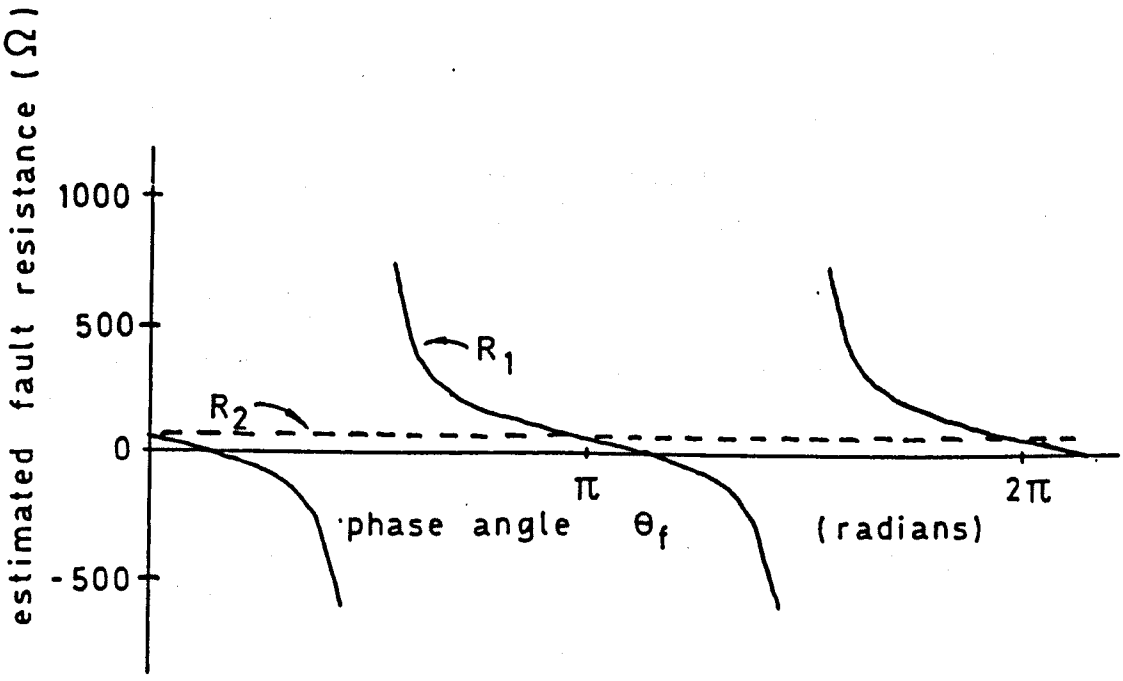

Figure 2.4 Loci of the theoretical fault resistance estimates for external faults on a single phase line with the configuration given in figure 2.3a.

be

$$V_{2\tau} = (1 + k_{vf})V_{r4} + k_{vf}V_{r5}$$
$$= k_{v1}(1 + k_{vf})^2 k_{v2}V_1 + k_{v1}k_{v2}(1 + k_{vf})k_{vf}V_1$$
$$= k_{v1}k_{v2}(1 + 2k_{vf})(1 + k_{vf})V_1 \qquad (2.30)$$

This can be compared with the first reflected travelling-wave amplitude V_{r1} given that

$$V_{r1} = k_{v1}V_1 \qquad (2.31)$$

then

$$\frac{V_{2\tau}}{V_{r1}} = k_{v2}(1 + 2k_{vf})(1 + k_{vf}) \qquad (2.32)$$

Substituting equation 2.3 gives

$$\frac{V_{2\tau}}{V_{r1}} = k_{v2}\left[\frac{2R_f}{Z_s + 2R_f}\right]\left[\frac{2R_f - Z_s}{Z_s + 2R_f}\right] \qquad (2.33)$$

For an external fault to be possible there must be at least one other line connected to the far busbar. It is, therefore, reasonable to assume that far busbar reflection coefficient will be negative, thus $V_{2\tau}/V_{i2}$ will be positive provided that

$$R_f < \frac{Z_s}{2} \qquad (2.34)$$

For an external fault the amplitude of the incident travelling-wave $V_{2\tau}$ which arrives at a time 2τ after the arrival of the first transient wave V_1 at the protection point is given by

$$V_{2\tau} = k_{v2}V_{pr1} \qquad (2.35)$$

thus

$$\frac{V_{2\tau}}{V_{pr1}} = k_{v2} \qquad (2.36)$$

This ratio ($V_{2\tau}/V_{pr1}$) should then always be negative. this is in contrast with that of an internal fault given by equation 2.33 which is positive provided that the condition 2.34 is met. Faults of higher resistance will have to be protected against using another approach, although, their low fault current will not necessitate rapid fault clearing.

It should then be possible to achieve complete fault discrimination of low impedance faults between an internal fault, in the protection region, and an external fault, outside the protection region, using the procedure given by the flow diagram of figure 2.5.

2.4 Application of the algorithm to three phase transmission lines

This section describes how the relay procedure, outlined in sections 2.2 and 2.3, can be applied to three phase lines. Allowance is made for the different modes of propagation of the transient waves on a multiphase line (Appendix A) and for different fault types.

The transmission line configuration given in figure 1.5 is now considered to be a three phase transmission line. When a fault occurs at a distance

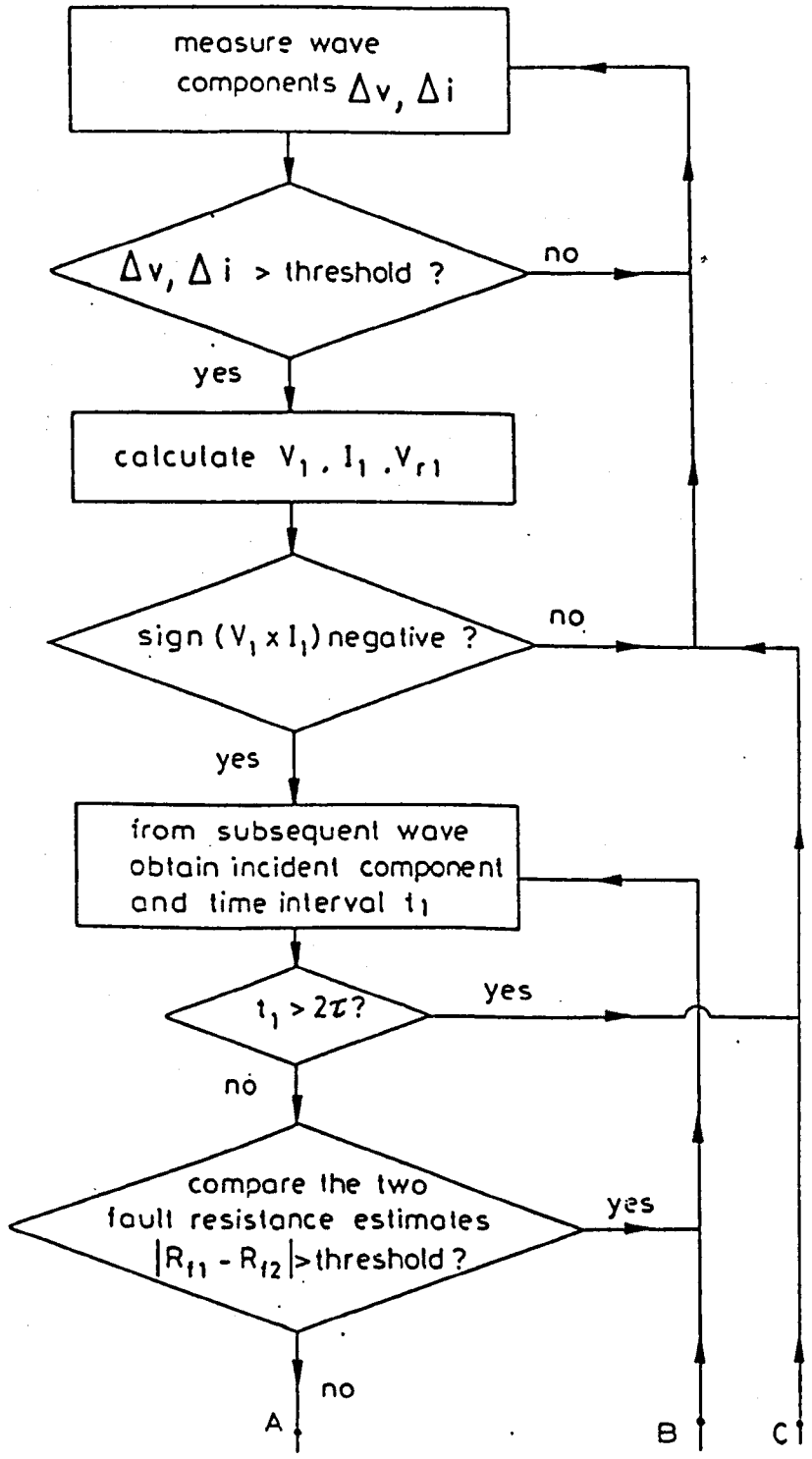

Flow chart of the decision procedure

Figure 2.5 Flow chart of the basic decision procedure. Points A, B and C refer to the extra necessary checks which will be described in more depth later.

x from the relaying point at busbar 1, the fault transients will take the form of three modal travelling waves of different velocities and amplitudes which will be superimposed on the original conditions. These modal waves are independent when propagating along the transmission lines but modal mixing may occur at points of discontinuity such as busbars or faults. The simple Bewley lattice [49] diagram given in figure 1.5 will only be correct if no modal mixing takes place in the system. In general the degree of modal mixing may have to be estimated or allowed for.

The incremental voltage and current values can still be extracted from the relaying voltages and currents by filtering out the system frequency on each phase, in the manner outlined in section 2.2. This will give three phase incremental voltages and currents.

For a three phase transmission line a general three phase fault shown in figure 2.6 can be represented by a conductance matrix given as [64]

$$[Y_f] = \begin{bmatrix} \frac{1}{R_{aa}} + \frac{1}{R_{ab}} + \frac{1}{R_{ac}} & -\frac{1}{R_{ab}} & -\frac{1}{R_{ac}} \\ -\frac{1}{R_{ab}} & \frac{1}{R_{bb}} + \frac{1}{R_{ab}} + \frac{1}{R_{bc}} & -\frac{1}{R_{cb}} \\ -\frac{1}{R_{ac}} & -\frac{1}{R_{cb}} & \frac{1}{R_{cc}} + \frac{1}{R_{ac}} + \frac{1}{R_{bc}} \end{bmatrix} \tag{2.37}$$

It is then shown in appendix B that the first transient wave, which travels along the transmission line from the fault to the relaying point, will then have a voltage amplitude $[V_1]$ given by the matrix equation

$$[V_1] = -[2[U] + [Z_s][Y_f]]^{-1}[Z_s][Y_f][v_f] \tag{2.38}$$

where;

$[U]$	=	The unit matrix.
$[Z_s]$	=	The line surge impedance matrix.
$[v_f]$	=	The initial amplitude of the phase voltages at the fault location.

This will initiate three independent transient modes which will propagate towards the relaying point with amplitude

$$[V_1^m] = [S]^{-1}[V_1] \tag{2.39}$$

where $[S]$ is the modal transform matrix defined in appendix A.

At the relaying point the incident and reflected modal voltages can be resolved using equations A.30 and A.31 of appendix A or the phase voltages can be found from

$$[V_i] = [[\Delta V] - [Z_s][\Delta I]]/2 \tag{2.40}$$

$$[V_r] = [[\Delta V] + [Z_s][\Delta I]]/2 \tag{2.41}$$

These initial incremental values can be used for directional discrimination as described in section 1.4.

The line parameters of EHV transmission lines are frequency dependent, however, studies have found that the modal transform matrices $[S]$ and $[Q]$ can be approximated by constant real values over the 50—5000 Hz [32, 33, 34]. It has then been found that reasonable accuracy can be achieved if the line parameters are given by constant values deduced at about one kHz.

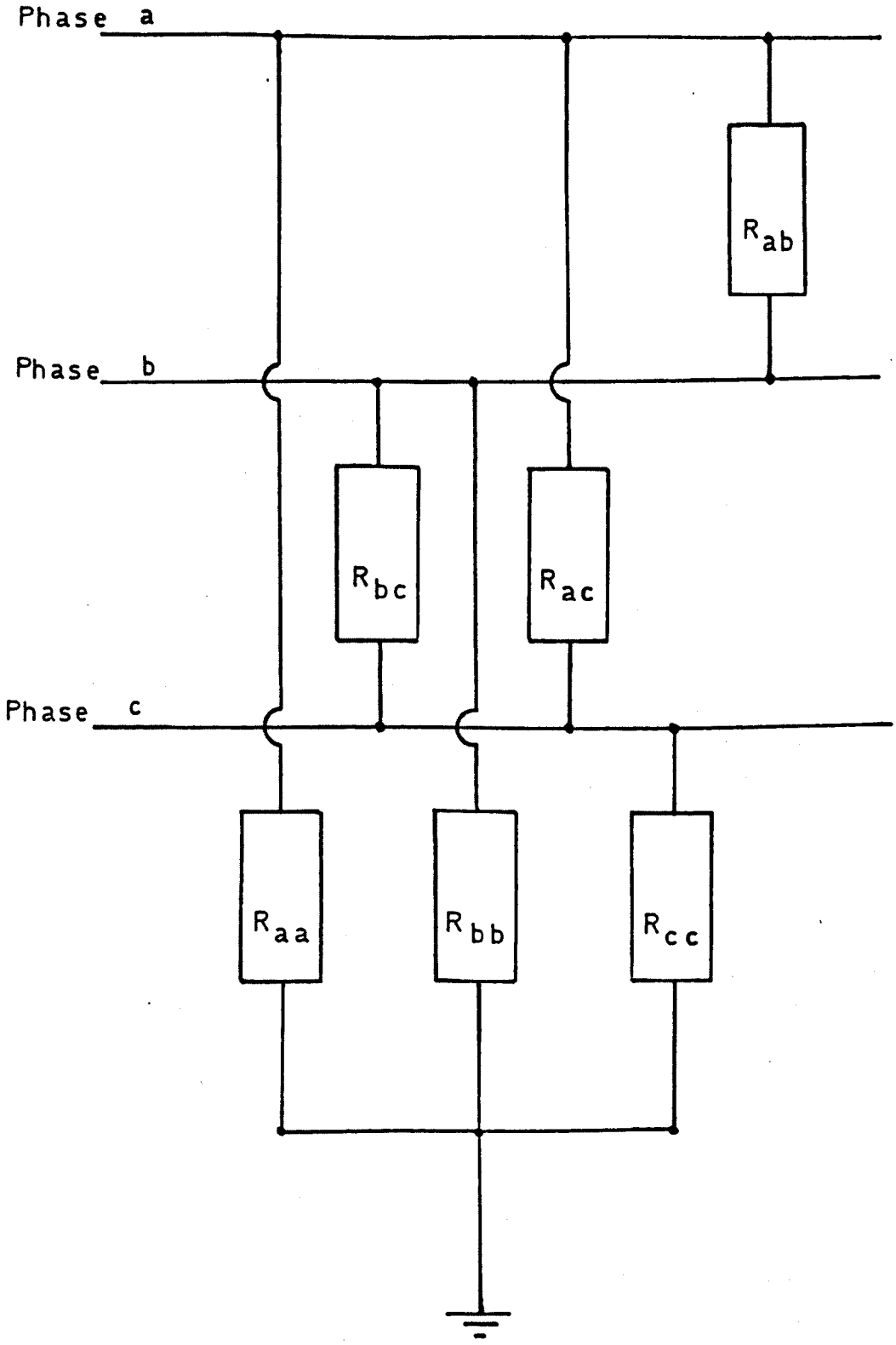

Figure 2.6 General three phase fault configuration.

Further information will be available when the modal transients reflected at the relaying point $[V_r^m]$ are further reflected at the fault location and then return to the relaying point $[V_{i2}^m]$. Given the fault conductance matrix $[Y_f]$ it is shown in appendix B that the phase voltage reflection matrix at the fault location can be given by

$$[k_{vf}] = -[2[U] + [Z_s][Y_f]]^{-1}[Z_s][Y_f] \tag{2.42}$$

From equation 2.39 it follows that the modal reflection matrix at the fault is then

$$[k_{vf}^m] = [S][k_{vf}][S]^{-1} \tag{2.43}$$

Note that in general the fault modal reflection coefficient $[k_{vf}^m]$ will not be diagonal, therefore, mixing of the modes of propagation will occur at the fault location. For some fault types this modal mixing will have to be allowed for.

It follows that, provided the attenuation and dispersion of modal propagation is negligible, the second incident transient travelling-waves will have amplitudes

$$[V_{i2}^m] = [k_{vf}^m][k_{v1}^m][V_1^m] \tag{2.44}$$

The time of arrival of each of the modes of the second incident modal wave $[V_{i2}^m]$ will be different due to the different propagation velocities. In principle this could then give three independent estimates of the fault location. In practice, the two aerial modes both propagate at close to the speed of light and the ground mode or mode 1 travels at a much reduced velocity which depends on the ground conductivity. There will then only be two possible independent fault location estimates. The ground mode or mode 1 will only give a crude estimate of the fault location as the ground conductivity is very variable [62,63].

As with the single phase line example, the fault location can only be found provided the second incident wave $[V_{i2}^m]$ is correctly identified. This will now be achieved by comparing two estimates of the fault conductance matrix $[Y_f]$ which are formed from the amplitudes of the first two incident transient modal waves $[V_1^m]$, $[V_{i2}^m]$ and the estimate of the initial fault voltages $[v_f]$.

In a similar manner to the single phase case (section 2.2), the first estimate of the fault conductance matrix is obtained from equation 2.38 using the initial transient modal wave amplitude $[V_1^m]$ and the estimate of the initial steady state voltage amplitude at the fault location $[v_f]$.

The steady state voltage at the fault location is given by the steady state voltages and currents at the relaying point and the time separation of the incident transient modes $[V_1^m]$ and $[V_{i2}^m]$. If the steady state transmitted power is balanced positive sequence only, as is the usual practice [64], then, from equation 2.7 the steady state voltage can be given by

$$\mathbf{v}^{\mathbf{p}}(x) = \mathbf{v}_0^{\mathbf{p}} \cosh \gamma_0^p x - Z_s^p \, \mathbf{i}_0^{\mathbf{p}} \sinh \gamma_0^p x \tag{2.45}$$

where the superscript p refers to positive sequence values.

For fully transposed three phase transmission lines the positive sequence surge impedance is given by [65]

$$Z_s^p = z_{dd}^s - z_{ee}^s \tag{2.46}$$

where z^s_{dd} and z^s_{ee} are the elements of the surge impedance matrix given as

$$[Z_s] = \begin{bmatrix} z^s_{dd} & z^s_{ee} & z^s_{ee} \\ z^s_{ee} & z^s_{dd} & z^s_{ee} \\ z^s_{ee} & z^s_{ee} & z^s_{dd} \end{bmatrix} \tag{2.47}$$

For an untransposed three phase transmission line it has been found that reasonable accuracy in estimating the fault voltage can be obtained with the following approximation

$$Z^p_s = \frac{z^s_{11} + z^s_{22} + z^s_{33}}{3} - \frac{z^s_{12} + z^s_{13} + z^s_{23}}{3} \tag{2.48}$$

where the surge impedance is given by

$$[Z_s] = \begin{bmatrix} z^s_{11} & z^s_{12} & z^s_{13} \\ z^s_{12} & z^s_{22} & z^s_{23} \\ z^s_{13} & z^s_{23} & z^s_{33} \end{bmatrix} \tag{2.49}$$

The positive sequence is an aerial mode and therefore, assuming that the attenuation is negligible over the line span, the propagation constant γ^p_0 can be approximated by

$$\gamma^p_0 \approx \beta^p_0 \approx \frac{\omega_0}{c} \tag{2.50}$$

In the same manner as for the single phase line (section 2.2), the initial fault voltage at the fault location can then be found from

$$\mathrm{v}^{\mathrm{p}}_{\mathrm{f}} = |\mathrm{v}^{\mathrm{p}}_0| e^{j[\theta_1 - \beta^p_0 x]} \cos(\beta^p_0 x) - j Z^p_s |\mathrm{i}^{\mathrm{p}}_0| e^{j[\theta_2 - \beta^p_0 x]} \sin(\beta^p_0 x) \tag{2.51}$$

where $|\mathrm{v}^{\mathrm{p}}_0|$ and $|\mathrm{i}^{\mathrm{p}}_0|$ are the steady state positive sequence voltage and current magnitudes with θ_1 and θ_2 being the initial voltage and current phase angles at the time of reception of the first transient wave $[V^m_1]$.

The phase angle delay $\beta^p_0 x$ is found from equation 2.19 using the time separation of the aerial modes V^{am}_1 and V^{am}_{i2} which have a propagation velocity at close to the speed of light.

The initial phase voltage at the fault location at the time of the fault inception is then found from the transform [65].

$$[\mathrm{v_f}] = \begin{bmatrix} 1 & 1 & 1 \\ 1 & h^2 & h \\ 1 & h & h^2 \end{bmatrix} \begin{bmatrix} 0 \\ \mathrm{v}^{\mathrm{p}}_{\mathrm{f}} \\ 0 \end{bmatrix} \tag{2.52}$$

where $h = e^{j2\pi/3}$ and

$$[v_f] = Re([\mathrm{v_f}]) \tag{2.53}$$

The first estimate of the fault conductance matrix can then be found from equation 2.38 where the initial wave amplitude has been given by equation 2.40 and the initial fault voltage has been found from equations 2.51 and 2.19. Note that from equation 2.37 there are six unknown resistances $[R_{aa}, R_{ab}, R_{ac}, R_{bb}, R_{cc}, R_{ac}]$ but only three possible independent equations. It is necessary, therefore, to reduce the fault geometry to a maximum of three unknown resistances for unique solutions to be found. It is shown

in this thesis that, for the three fault types studied, the fault conductance matrix can be reduced to three unknown fault types.

The second estimate of the fault resistance can be derived from a comparison of the amplitude of the first reflected wave $[V_{1\tau}^m]$ and the amplitude of the second incident wave $[V_{i2}^m]$ given by equation 2.44 assuming negligible attenuation and dispersion as

$$[V_{i2}^m] = [k_{vf}^m][V_{1\tau}^m] \tag{2.54}$$

If the two estimates of the fault conductance matrix coincide then it is assumed that the second incident transient wave $[V_{i2}^m]$ has been correctly identified and the relay action proceeds. As with the single phase line example, however, there are still points in the system cycle where external faults may be confused with internal faults. Extra discrimination features will also have to incorporated for multiphase lines.

The amplitude of the incident wave $[V_{2\tau}]$ which arrives at a time 2τ after the first incident transient $[V_1]$, as described in section 2.1, can also be used on multiphase lines. This is provided that the modal mixing is negligible at the fault location. It has been found that the line to line voltage between the two faulted phases of a phase to phase fault can be monitored as an independent mode of propagation and transmission through the fault location. When a phase to phase fault occurs, the amplitude of the $V_{2\tau}$ line to line voltage wave can then be used for fault discrimination between an internal and an external phase to phase faults as described in section 2.1.

If sufficient ground mode or mode 1 transients are produced by a fault, the time delay of the incident ground or mode 1 can also be used as a fault discriminant. The ground mode propagates at a much slower velocity than the aerial modes, also, the ground mode velocity depends on the ground conductivity which is very variable. Phase to phase faults and symmetric faults do not produce ground modes of sufficient amplitude for realistic measurements. The ground mode is then only used for phase to ground faults, as a crude fault location discriminant.

For symmetric three phase to ground faults each phase can be processed independently to give estimates of the fault conductance matrix. Only one of the phases can be at the problem phase angle where internal and external faults can be confused. Fault discrimination between internal and external symmetric faults can then be achieved by insisting that at least two phases must indicate an internal fault before relay action is taken.

2.5 Conclusion

In conclusion the principle of an ultra high speed relay algorithm for EHV three phase transmission lines has been described. The location of the fault is given by the time separation of the first and second incident transient modal waves at the relaying point. The second incident transient travelling-wave is identified by a comparison between two estimates of the fault resistance. These estimates of the fault resistance are found from the time of arrival and amplitudes of the incident transients and the steady state voltages and currents measured at the relaying point.

Extra checks have also been incorporated to ensure complete fault discrimination between internal and external faults. The checks include the

ground mode or mode 1 propagation delay and the measurement of the incident transient travelling wave amplitude at a time 2τ.

The measurement of the incident transient wave amplitudes and the application of the algorithm to specific fault types are discussed in the following chapters. It will be shown that the implicit assumption that the line parameters are frequency independent do not lead to unrealistic errors.

CHAPTER 3

Detection of incident waves using the cross-correlation function.

3.1 Introduction

The cross-correlation function gives the degree of similarity and their relative displacement for a common variable, when two functions are linearly dependent. It is a powerful method of extracting signals from noisy data [66].

The relay routine, outlined in this chapter, involves the detection of incident waves at the protection point. After the arrival of the first incident travelling wave V_1, the subsequent incident travelling waves of interest V_{i2} and $V_{2\tau}$ can be considered to be linearly dependent on the first reflected wave at the protection point V_{r1}. It is therefore proposed to extract the amplitude and arrival times of the incident waves V_{i2} and $V_{2\tau}$, by cross-correlating the first reflected wave at the protection point V_{r1} with all subsequent incident waves. This procedure, for locating the second incident wave V_{i2}, was first proposed for protective relaying by Crossley and McLaren [53]. In this study not only is the second incident wave V_{i2} detected but also its amplitude is measured using the cross-correlation routine.

This section then describes the use of the cross-correlation function for the detection and measurement of the incident waveforms V_{i2} and $V_{2\tau}$. In this description it is assumed that the transmission line is a single phase line. The application of the cross-correlation technique to multiphase transmission lines is discussed in subsequent chapters.

3.2 The cross-correlation theory

The degree of similarity between two time dependent functions x and y can be expressed by the covariance function [66]

$$\phi(\nu) = \lim_{T\to\infty} \frac{1}{T} \int_0^T [x(t) - \bar{x}][y(t+\nu) - \bar{y}]dt \tag{3.1}$$

where the mean values $\bar{x}$ and $\bar{y}$ are given by

$$\bar{x} = \lim_{T\to\infty} \frac{1}{T} \int_0^T x(t)dt \tag{3.2}$$

$$\bar{y} = \lim_{T\to\infty} \frac{1}{T} \int_0^T y(t+\nu)dt \tag{3.3}$$

This is often loosely referred to as the cross-correlation function by engineers [66]. To be pedantic, the cross-correlation function is the normalised form of the covariance function.

The time delay ν and the amplitude of a peak in the covariance function gives the relative time displacement of the functions x and y and characteristics of the linear relationship.

In this analysis it is assumed that the fault reflection coefficient, of the transient waves, is time independent and can be given by equation 2.3. In particular V_{i2} is given by

$$V_{i2} = k_{vf} V_{r1} \tag{3.4}$$

If the reflected wave V_{r1} is cross-correlated with the incident waves V_i, then, a peak in the cross-correlation function should indicate the time of arrival of the second incident wave V_{i2}. The amplitude of the cross-correlation peak should also be related to the fault reflection coefficient k_{vf}. In other words the time dependent equations y and x of equation 3.1 are replaced by

$$x = V_{r1}(t) \tag{3.5}$$

$$y = V_i(t) \tag{3.6}$$

which gives

$$\phi(\nu) = \lim_{T\to\infty} \frac{1}{T} \int_0^T [V_i(t+\nu) - \bar{V}_i(\nu)][V_{r1}(t) - \bar{V}_{r1}]dt \tag{3.7}$$

From the Bewley lattice diagram given in figure 1.5 it follows that at time $\nu = 2t_1$ we can put

$$V_i(t+2t_1) = V_1(t+2t_1) + V_{i2}(t) \tag{3.8}$$

thus from equation 3.7

$$\begin{aligned}
\phi(2t_1) &= \lim_{T\to\infty} \frac{1}{T} \int_0^T [V_1(t+2t_1) - \bar{V}_1(2t_1)][V_{r1}(t) - \bar{V}_{r1}]dt \\
&+ \lim_{T\to\infty} \frac{1}{T} \int_0^T [V_{i2}(t) - \bar{V}_{i2}][V_{r1}(t) - \bar{V}_{r1}]dt \\
&= \lim_{T\to\infty} \frac{1}{T} \int_0^T [V_1(t+2t_1) - \bar{V}_1(2t_1)][V_{r1}(t) - \bar{V}_{r1}]dt \\
&+ k_{vf} \lim_{T\to\infty} \frac{1}{T} \int_0^T [V_{r1}(t) - \bar{V}_{r1}]^2 dt
\end{aligned} \tag{3.9}$$

The first term of equation 3.9 varies slowly over the time of interest and can be approximated by a constant given at an earlier reference time t_r. The second term is the auto-correlation of the reference wave form multiplied by the fault travelling wave reflection coefficient. The fault reflection coefficient can then be found from

$$k_{vf} = \frac{\phi(2t_1) - \phi(t_r)}{A} \tag{3.10}$$

where A is the auto-correlation of the reference wave form given by

$$A = \lim_{T\to\infty} \frac{1}{T} \int_0^T [V_{r1}(t) - \bar{V}_{r1}]^2 dt \tag{3.11}$$

and it is assumed that

$$\begin{aligned}
\phi(t_r) &= \lim_{T\to\infty} \frac{1}{T} \int_0^T [V_1(t+t_r) - \bar{V}_1(t_r)][V_{r1}(t) - \bar{V}_{r1}]dt \\
&\approx \lim_{T\to\infty} \frac{1}{T} \int_0^T [V_1(t+2t_1) - \bar{V}_1(2t_1)][V_{r1}(t) - \bar{V}_{r1}]dt
\end{aligned} \tag{3.12}$$

where $2t_1$ is time of the peak in the cross-correlation function and t_r is a reference time after the arrival of the initial transients.

In the ideal case T approaches infinity, however, in order to limit the calculation time, the correlation window is kept as small as possible. The wave forms will also be sampled waveforms, so that the cross-correlation is given in the discrete form as [66]

$$\phi(\nu) = \frac{\frac{1}{N}\sum_{h=1}^{N}[V_i(h\Delta t+\nu) - \bar{V}_i(\nu)][V_{r1}(h\Delta t) - \bar{V}_{r1}]}{A} \tag{3.13}$$

where

Δt = The wave form sample time

$N\Delta t$ = T

$$\bar{V}_i(\nu) = \frac{1}{N}\sum_{h=1}^{N} V_i(h\Delta t+\nu)$$

$$\bar{V}_{r1} = \frac{1}{N}\sum_{h=1}^{N} V_{r1}(h\Delta t)$$

$$A = \frac{1}{N}\sum_{h=1}^{N}[V_{r1}(h\Delta t) - \bar{V}_{r1}]^2$$

This is the discrete cross-correlation function as applied by the relay algorithm to locate and measure the second incident transient travelling-wave V_{i2} and the line round trip wave V_{2r}. From a detailed consideration of the cross-correlation function response to the transient travelling-waves, the choice of sample window lengths will be derived in the following section.

The sampled reflected wave will include a section of zero samples before the reflected transient wave occurs. For a reference length of N samples there will be n_b initial zero samples. If the incident and reflected wave forms are step functions, as given in figure 3.1, then the auto-correlation function A will have a maximum when $n_b/N = 0.5$. A large auto-correlation function A implies an increase the signal to noise ratio of the cross-correlation function given in equation 3.13. In practice the incremental transients will have a finite rise time and the auto-correlation A will have a maximum for n_b/N less than 0.5. A value of $n_b/N = 1/3$ was found to give good results for a range of fault types, line configurations and correlation window lengths.

The cross-correlation of sampled reflected waves V_{r1} with the sampled incident waves V_i for the rectangular wave forms of figure 3.1a and figure 3.1b are shown in figure 3.1c. Initially the cross-correlation function will have a value at zero delay time ($\nu = 0$) of

$$\phi(0) = \frac{n_b}{N}(1 - \frac{n_b}{N})k_{v1}V_1^2 \tag{3.14}$$

In figure 3.1 $n_b = 4$ and $N = 8$. The cross-correlation function then decreases until delay time $n_b\Delta t$ when

$$\phi(n_b\Delta t) = 0 \tag{3.15}$$

The reference time t_r of equation 3.10 will then be taken to be

$$t_r = n_b\Delta t \tag{3.16}$$

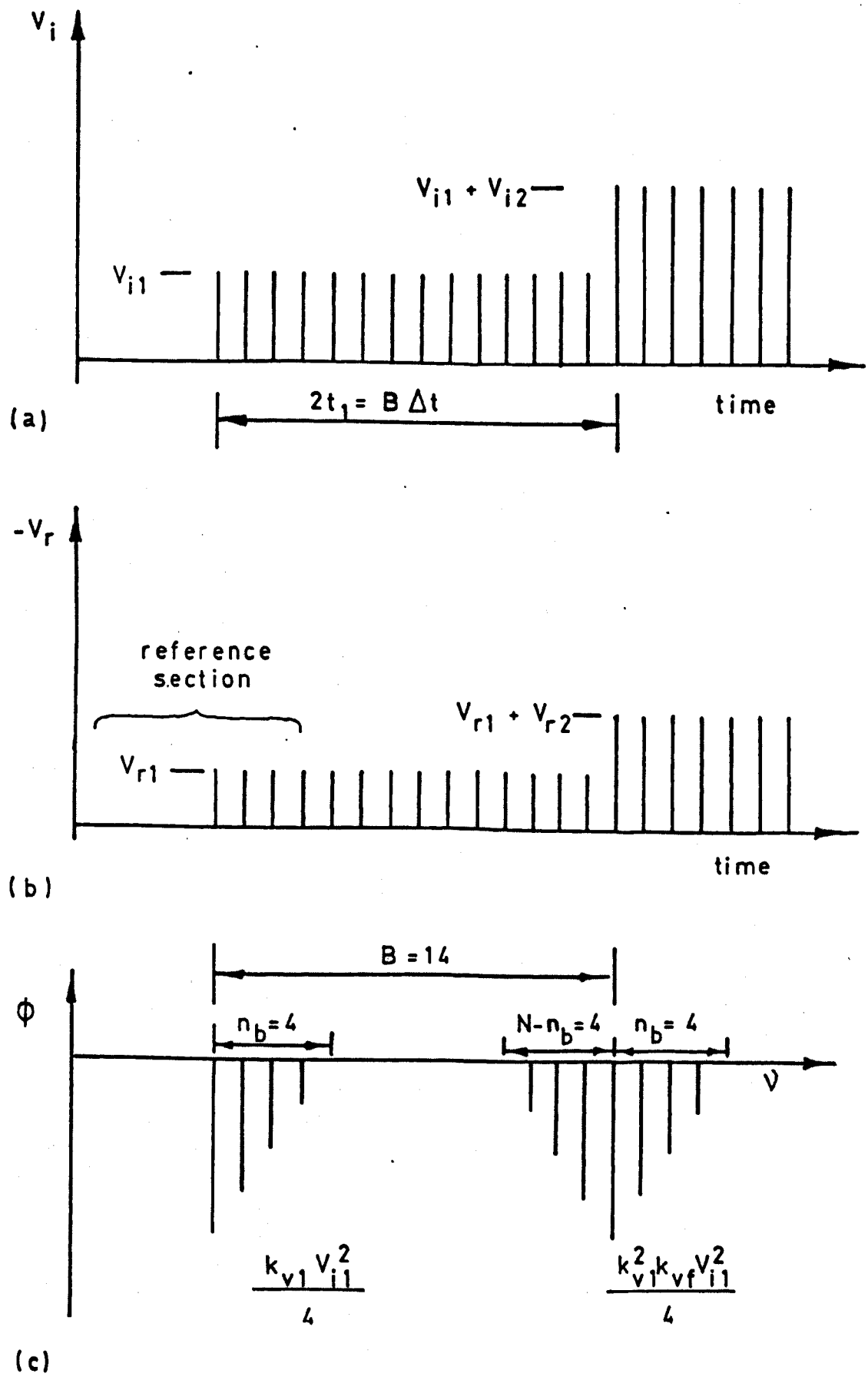

Figure 3.1 Ideal rectangular incident and reflected voltages at the relaying point (a) and (b). The resulting cross-correlation function with mean removal (c).

The cross-correlation function then remains at zero until the arrival of the second incident wave V_{i2} at the protection point at time $2t_1$. The incident voltage amplitude then becomes

$$V_i = V_1 + V_{i2} \tag{3.17}$$

As the delay time ν is incremented from $\nu = B-(N-n_b)$ to $\nu = B$, where B is the arrival time of the second incident wave in sample steps ($B = 2t_1/\Delta t$), the cross-correlation function increases linearly until at $\nu = B$ it reaches a maximum amplitude of

$$\phi(B) = \frac{n_b(N-n_b)}{N^2} k_{v1}^2 k_{vf} V_1^2 \tag{3.18}$$

Examination of the equation 3.18 with equation 3.15 indicates that equation 3.10 is correct provided that the condition 3.16 is used. Thereafter the cross-correlation function decreases linearly to zero at $\nu = B + n_b$.

Since the reflection coefficient of a fault k_{vf} will always be negative the peak in the cross-correlation function, as given by equation 3.9, will always be negative. The incident waves V_{i2} and $V_{2\tau}$ will then be indicated by troughs in the actual cross-correlation functions.

The actual travelling waves will also not be rectangular functions as depicted in figure 3.1. For a loss free transmission line, the transient wave amplitudes will vary sinusoidally due to the sinusoidal variation of the steady state fault voltage. For a fault on a single phase line the transients are then expected to be of the form given in figure 3.2 where

$$V_i(t) = |V_{pk}| sin(\alpha + \omega_0(t - t_0)) \tag{3.19}$$

$$V_{r1}(t) = k_{v1} V_i(t) \tag{3.20}$$

$$V_{i2}(t) = k_{vf} k_{v1} V_i(t - 2t_1) \tag{3.21}$$

The resulting cross-correlation functions using these incident and reflected wave forms can then be calculated.The normalised cross-correlation functions ϕ/A for various initial fault voltage phase angles α are given in figure 3.3. The initial level is unity as $k_{v1} = 1$, but the function does not then reduce linearly to zero. Over the range $n_b\Delta t < \nu < (B - (N - n_b))\Delta t$ the cross-correlation function varies sinusoidally. For reasonable line lengths (i.e. less than 400 km), however, this variation as depicted in figure 3.3 is small. The estimate of the fault reflection coefficient given by equation 3.10 was then found to give results of acceptable accuracy.

In conclusion it should be possible to identify the incident waves using the cross-correlation function and find the incident wave amplitudes with respect to the initial reflected wave amplitude V_{r1}. From the amplitude of the second incident wave V_{i2} the fault resistance can be estimated and from the time of arrival of the second incident wave the fault location can be found.

3.3 Cross-correlation window length and errors

It has already been stated that, in order to reduce the errors in the cross-correlation routine, the cross-correlation window length has to be as large as possible. The actual usable window length is, however, limited to the period

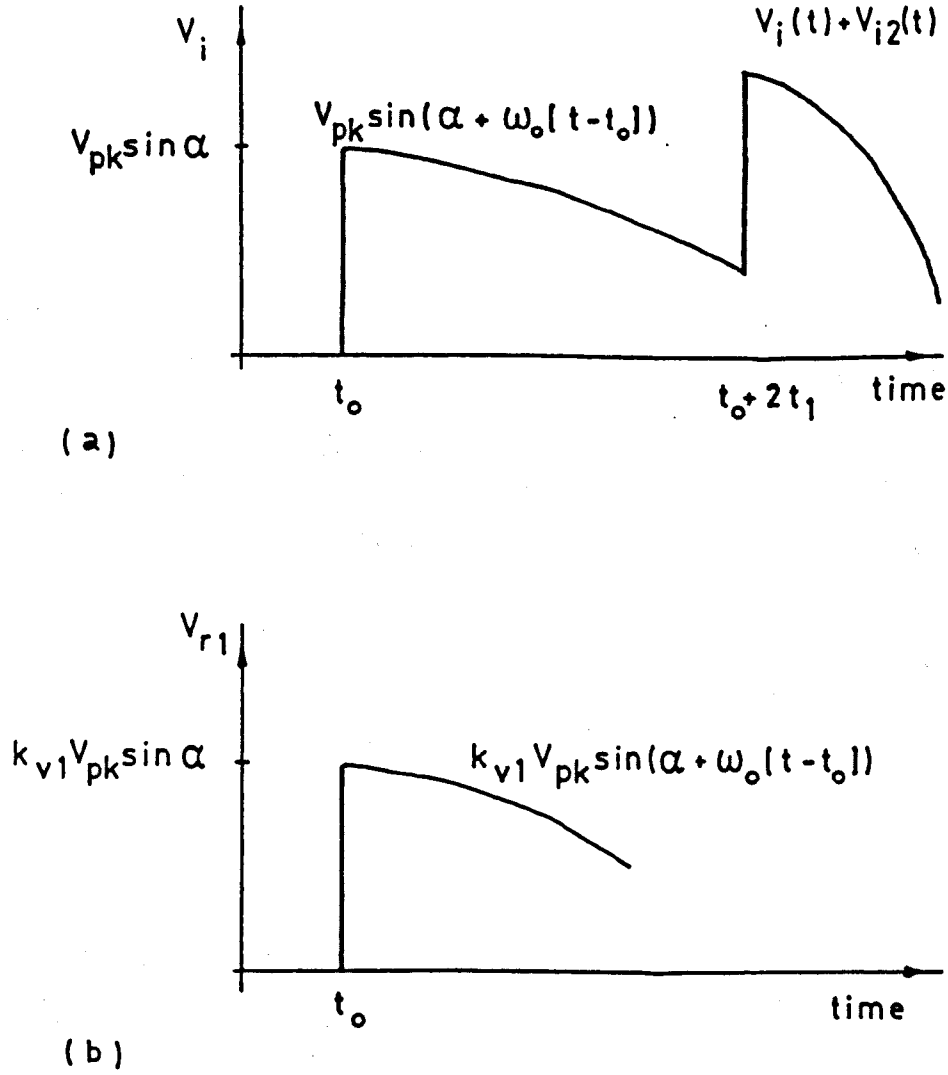

Figure 3.2 Sinusoidal incident voltage (a) and reflected voltage (b) at the relaying point.

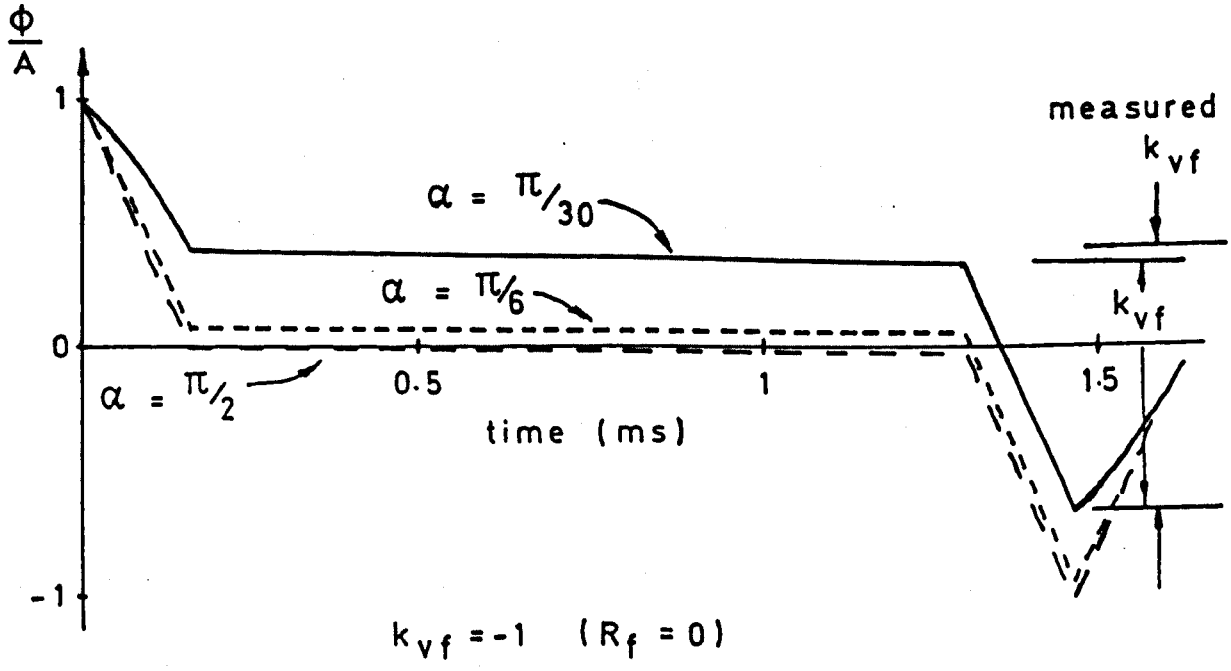

Figure 3.3 The normalised cross-correlation function with mean removal for different values of initial voltage phase angle (α) of the sinusoidal transients given in figure 3.2.

when only one reflected wave form is present (V_{r1}). From figure 1.5 it appears that the incident wavefronts generated by an internal fault are separated by a period $2t_1$. The cross-correlation window length is then limited to

$$(N - n_b)\Delta t < 2t_1 \tag{3.22}$$

A realistic limit of 40 km was set, for the resolution of close up faults by the travelling-wave routine. Closer faults will be resolved by a routine that does not require the identification of individual wave fronts. This then limits the cross-correlation window length to

$$(N - n_b)\Delta t < 2.7ms. \tag{3.23}$$

In general the transducer signals will be noisy. A noise level of as much as 5 % of the per unit levels is expected [45]. This will then give about a 5 % per unit noise level in the deduced travelling wave amplitudes. For good fault discrimination, the cross-correlation function should at least approach the accuracy of the first fault resistance estimate where $\frac{v_f}{V_1}$ can be found to about a 20% accuracy up to within $\pi/12$ of voltage zero. It follows then that, the signal to noise ratio of the cross-correlation trough amplitude should be about 5. If sinusoidal transducer signals have broad band random noise with a signal to noise ratio of ρ_s, it can be shown that [66, 67], the cross-correlation function will have a signal to noise ratio given by

$$\rho_\phi = \sqrt{\frac{N}{1 + 2\rho_s^{-2}}} \tag{3.24}$$

Over the small window length used by this algorithm, the sampled waveforms will resemble the rectangular functions discussed in section 3.1. The signal to noise ratio of the cross-correlation trough for the rectangular functions given in figure 3.1 can be expressed as

$$\rho_\phi = \sqrt{\frac{n_b[N - n_b]N}{[N - 2n_b]^2 + N^2\rho_s^{-2}}} \tag{3.25}$$

This signal to noise ratio will have a maximum at $n_b = N/2$ of

$$\rho_\phi = \sqrt{\frac{N\rho_s^2}{4}} \tag{3.26}$$

This implies that four samples are sufficient for reasonable correlation accuracy to within fifteen degrees of voltage zero. The incident waves, however, may have a finite rise time and a significant sinusoidal variation. Good cross-correlation signal to noise ratios, greater than four, were only achieved using a cross-correlation window with a minimum of 8 samples and $n_b = 3$. For such a cross-correlation window it follows that, equation 3.23 can be rearranged to give

$$\Delta t \leq \frac{0.27}{5}\, ms./sample \tag{3.27}$$

This indicates that a sampling rate of at least 19 kHz with a cross-correlation window length of 8 samples is required for the resolution of faults

within 40 km of the relaying point. In practice it is found that, some of the calculations can be simplified if a sampling rate of 25.6 kHz is used.

The sampling rate of 25.6 kHz is rapid and is a lot greater than that used in currently installed travelling-wave relays [45] ($\approx$ 4 kHz). Sampling rates greater than 25.6 kHz have been investigated [35, 46] and though this sampling rate is high the required transducer resolution will be shown to be only a few kHz. It was therefore felt that a sampling rate of about 25.6 kHz was realistic.

Along the whole length of the protection zone sufficient accuracy is not achieved, unfortunately, by the use of an eight sample cross-correlation window length. For faults located beyond the first half of the protection zone from protection point, other waves will be incident at the protection point before the arrival of the second incident wave V_{i2}. This is illustrated in figure 3.4. These other incident waves may reduce the signal to noise ratio of the second incident travelling-wave at the protection point V_{i2} down to as little as two. The signal to noise ratio of the cross-correlation function will then be at best $\sqrt{N}$. The cross-correlation window length must therefore be at least sixteen samples, for a signal to noise ratio of four. In practice a long cross-correlation length defined as; $N = 21$ and $n_b = 7$, has been found to consistently give good signal to noise ratios. For faults of near zero resistance the signal to noise ratio of the troughs using, this long window, was of the order of 5 and as the fault resistances approached the line surge impedance (approximately 240 ohms) the trough signal to noise ratio dropped to about 4.

A sampling rate of 25.6 kHz and a cross-correlation window of at least 16 samples implies that faults within 70 km of the protection point will not be resolved. Full fault resolution along the whole length of the protection zone, to within 40 km of the protection point, will only be possible if a combination of short and long cross-correlation window lengths are incorporated into the relay algorithm. The protected line must also be at least 140 km long so that faults beyond half the line length can be resolved with the longer cross-correlation window length.

It has been found that good results were obtained on multiphase transmission lines when a combination of; a short window length defined by; $N = 8$, $n_b = 3$ and a long window length defined by $N = 21$, $n_b = 7$ were used in the cross-correlation routine.

The introduction of two cross-correlation window lengths resulted in the following steps in the processing being incorporated into the relay algorithm.

1. Initially, after the arrival of a significant incident transient travelling-wave, the cross-correlation process will commence using the shorter window length ($N = 8$, $n_b = 3$).

2. If a cross-correlation peak is detected in a time less than that needed for travelling-waves to traverse at least 170 km, an internal fault will be indicated. The algorithm will then complete the necessary checks before tripping

3. If an internal fault has not been identified within 85 km of the protection point, the longer cross-correlation window will be used ($N =$

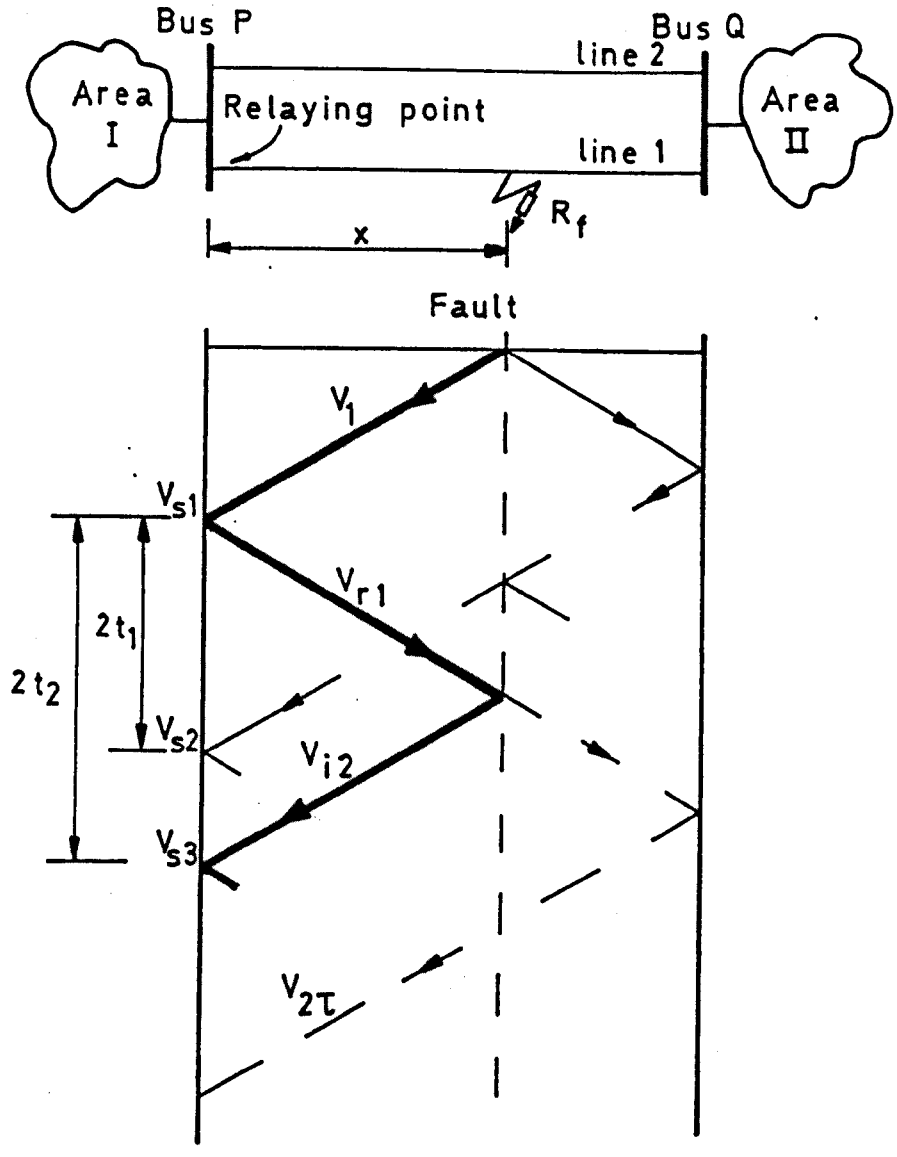

Figure 3.4 A general line configuration and Bewley lattice diagram of an internal fault beyond half the protected line length from the relaying point.

21, $n_b = 7$). Fault locations, between 85 km from the protection point to the far end of the protection zone, will then be investigated.

3.4 Conclusion

It is proposed to locate and measure the second incident transient travelling-wave V_{i2} using the cross-correlation routine. The use of two cross-correlation windows ($N = 8$ *and* $N = 21$) and a sampling rate of 25.6 kHz should be sufficient to resolve the second incident wave for any fault location along the defined protection zone with sufficient accuracy for fault discrimination.

The amplitude of the cross-correlation trough can be used to measure the fault reflection coefficient. The timing of the cross-correlation function trough will give the location of the fault.

CHAPTER 4

Application of the protection algorithm to a range of simulated faults.

4.1 Introduction

Using the principles outlined in chapters 2 and 3, the relay algorithm is now applied to three major fault types. The fault types considered are; symmetric three phase to ground faults, single phase to ground faults and phase to phase faults. In this analysis, it is assumed that the faults are non-arcing and that they do not develop into different fault types.

Ideally the faults would be generated in the field on a test network monitored with wide band transducers connected to recording equipment. These transients would then be used to evaluate the relay algorithm. Such an approach, however, would be impracticable due to the low fault rate on EHV transmission lines [68] and the lack of suitable test lines on which to induce faults. It was therefore necessary to simulate the fault transients off line, in non-real time, using a programmable power system implemented on a computer. The relay algorithm is then applied in non-real time to the fault transients generated by the simulation programme.

The results show how the relay will provide good fault discrimination for a range of faults on long multiphase transmission lines. The relay response time will then be discussed in a later chapter.

4.2 Fault transient simulation

Two main fault transient simulation programmes were available for non-real time relay analysis. One model is the well known electromagnetic transients program (EMTP) [69] which is the most widely used transients programme in the world. The other simulation programme was the GEC MCZ1022A power simulation programme developed by GEC Measurements [70].

The EMTP simulation is based on the time domain approach to transient analysis [71] which inherently has difficulty in resolving frequency dependent properties such as; propagation constants, characteristic impedances and modal matrices. These frequency dependent wave propagation effects can be resolved in the time domain, to a certain extent, by incorporating time dependent convolutions [71, 74, 75] and convolutions within the modal framework [77]. Frequency dependent parameters, however, are modelled far more accurately in the frequency domain using Fourier or Laplace transforms where they are automatically included [78].

The GEC MCZ1022A power simulation programme developed by GEC Measurements, is a frequency domain programme based on the modified Fourier transform [80] and the modal analysis methods [54, 70, 81]. This simulation has the advantage that frequency dependent parameters will be

precisely modeled, but, time dependent features such as arcing or developing faults are not fully simulated.

In this initial analysis, time dependent features will not be considered. As it is important to simulate the transients as precisely as possible, the GEC MCZ1022A frequency domain programme will be used for generating the transients analysed in this chapter.

In the MCZ1022A frequency domain programme; the transmission lines are represented by uniformly distributed parameters calculated from the given line geometries, and each simulated source represents a system connected to the line terminals with an equivalent impedance derived from its short circuit capacity.

The line geometries considered were the single circuit CEGB type 01L vertical tower, shown in figure 4.1. This vertical line geometry were thought to be the most difficult, as it yields a large degree of asymmetry in the modal transients. Double circuit lines will be discussed in a later chapter.

In the UK, systems connected to the EHV grid (400 kV) have short circuit capacities typically between 1–35 GVA [45]. The short circuit capacities chosen for the sources then reflect these typical values.

The voltage and current transients generated by the fault transient programme were sampled at 25.6 kHz to give the optimum relay performance (Section 3.4). The programmed relay algorithm is then applied to the simulated transients, off line in non-real time, so that the relay performance can be observed. This type of analysis will be ideal, of course, as no transient distortion or transducer noise will be present on the transient signals. The effects of signal noise and limited bandwidth will be discussed in a later chapter.

4.3 Symmetric three phase to ground faults.

A symmetric three phase to ground fault is the least common of the faults presented [68]. A fault involving all three phases would, however, produce the biggest problems for power system stability [68]. It is important, therefore, to include three phase faults in any high speed relaying scheme.

4.3.1 Symmetric fault conductance estimation.

A symmetric three phase fault, as depicted in figure 4.2, will have a fault conductance matrix that can be given as

$$[Y_f] = \begin{bmatrix} \frac{1}{R_f} & 0 & 0 \\ 0 & \frac{1}{R_f} & 0 \\ 0 & 0 & \frac{1}{R_f} \end{bmatrix} \tag{4.1}$$

Substituting equation 4.1 into equation 2.42 gives the travelling wave reflection coefficient for a symmetric fault. Given that ground mode transients are not produced at the fault location, the fault travelling wave reflection coefficient on a fully transposed line is

$$[k_{vf}] = -\begin{bmatrix} \frac{Z_s}{Z_s+2R_f} & 0 & 0 \\ 0 & \frac{Z_s}{Z_s+2R_f} & 0 \\ 0 & 0 & \frac{Z_s}{Z_s+2R_f} \end{bmatrix} \tag{4.2}$$

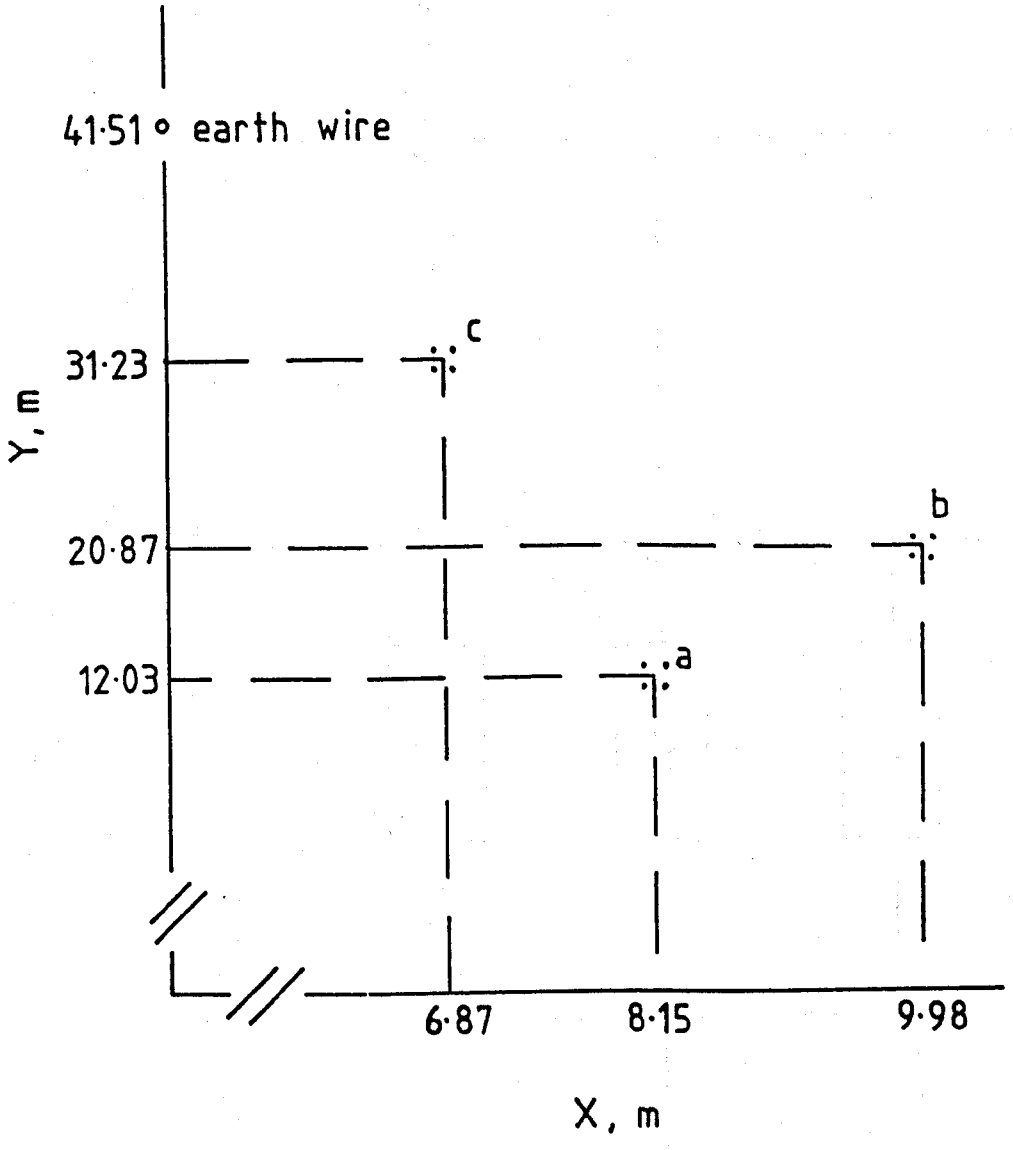

Figure 4.1 Configuration of overhead single circuit line with quad conductors usually used by CEGB on 400 kV systems.

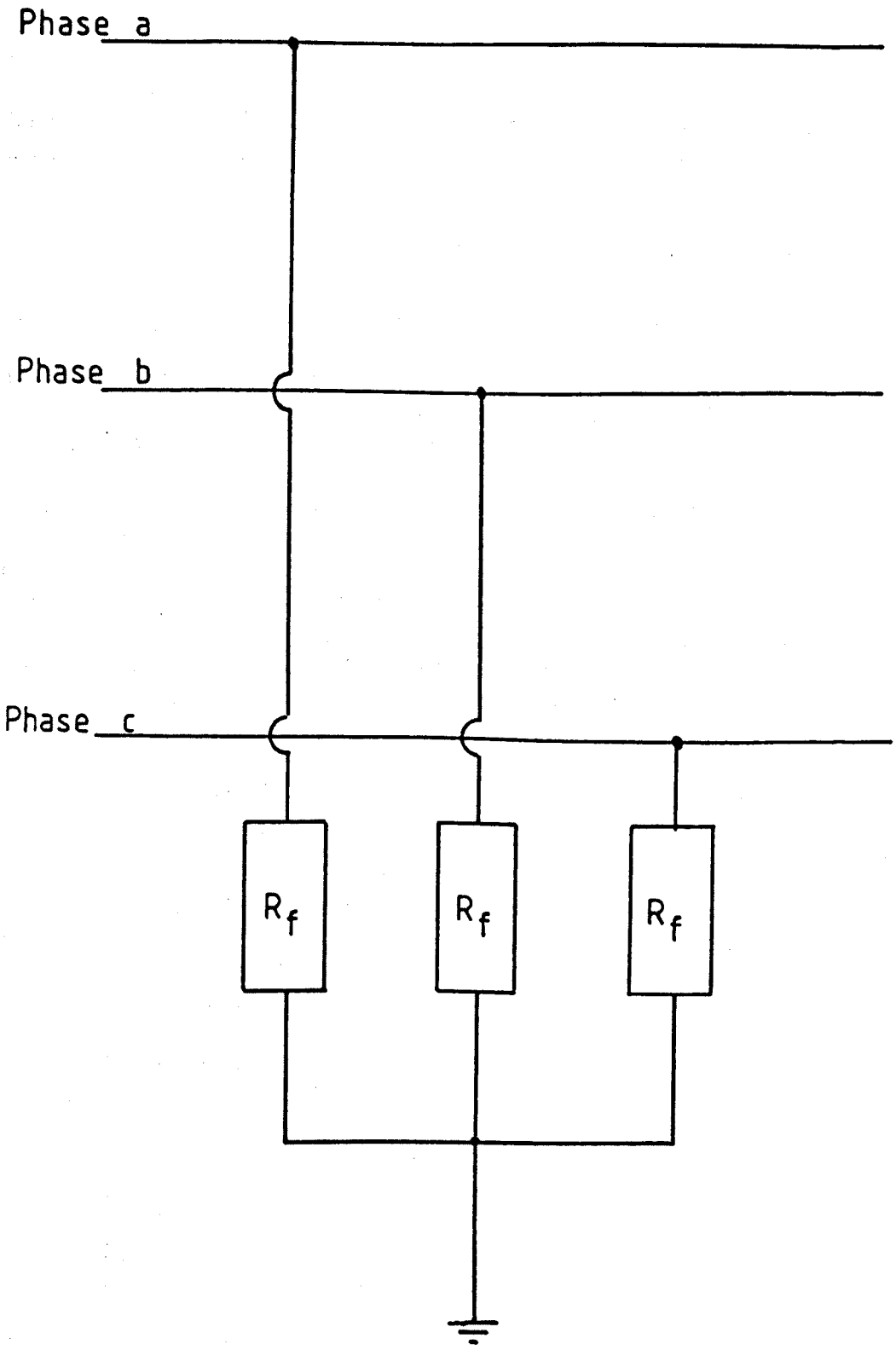

Figure 4.2 Three phase symmetric fault to ground representation.

where $Z_a = z^s_{dd} - z^s_{ee}$ which is the surge impedance for the aerial transient travelling-waves.

The initial fault conductance matrix estimate, from equation 2.38, can then be rearranged to give three independent estimates of the fault resistances

$$R_{f1}(n) = -\frac{Z_a}{2} - \frac{Z_a v_f(n)}{2V_1(n)} \tag{4.3}$$

where n = the phases a, b or c. The initial fault voltage $v_f(n)$ is found from equations 2.51 and 2.52.

On a general three phase line with a symmetric three phase to ground fault, it can be shown that modal mixing is negligible at the fault location and the fault transients are all aerial mode travelling-waves. The aerial transient travelling-waves propagate at approximately the same velocity. It follows, therefore, that all the transient waves can be assumed to propagate, without distortion, at the aerial mode velocity. The calculations are then all carried out with the phase values, which, behave as independent modes propagating at the aerial mode velocity.

The initial amplitude $[V_1]$ is measured two sample steps (0.08 ms.) after the instigation of fault transients. This is because the modal unit impulse of travelling-wave step functions can be represented, to a good approximation, by the sum of two exponentials [49, 71, 74] giving

$$V_{im} = a(1 - e^{-\alpha(t-t_0)}) + (1-a)(1 - e^{-\beta(t-t_0)}) \tag{4.4}$$

For a three phase single circuit CEGB type 01L transmission line of length 250 km, the parameters t_0, a, α and β calculated using the EMTP "SEMLYEN SETUP" [69] are given in table 4.1. From the parameters for the aerial modes (modes 2 and 3) it follows that, at a time 0.08 milliseconds after the arrival of the aerial transients t_0 the aerial transient amplitudes should be within 97% of their initial amplitude.

Table 4.1 Modal parameters L=250 km

Mode 1	a	0.91412
	α	7741.0
	β	755.3
	t_0	0.93274 ms.
Mode 2	a	0.91658
	α	339440.0
	β	17165.0
	t_0	0.83489 ms.
Mode 3	a	0.89147
	α	800340.0
	β	55541.0
	t_0	0.8333 ms.

Given that the relaying sample rate will be 25.6 kHz (0.04 ms.), it is therefore proposed to measure the amplitude of the first incident transient $[V_1]$ two sample steps after its arrival. The measured voltage amplitude should then be a good approximation of its initial value at the fault location,

before it propagates to the relaying point, for transmission lines up to 300 km in length. These measured amplitudes are used for the first estimate of the fault resistances given by equation 4.3.

The fault travelling-wave modal reflection matrix, given by equation 2.44, can also be reduced to phase values in the form

$$[V_{i2}] = [k_{vf}][k_{v1}][V_1] = [k_{vf}][V_{r1}] \tag{4.5}$$

The second estimate of the fault conductance matrix, given by equations 2.42, 2.54 and 4.5, is then rearranged into three independent estimates of the fault resistances in the form

$$R_{f2}(n) = -\frac{Z_a}{2} - \frac{Z_a V_{r1}(n)}{2V_{i2}(n)} \tag{4.6}$$

where n = the phases a, b or c.

The ratio $V_{r1}(n)/V_{i2}(n)$ is found from the cross-correlation function, described in chapter 3, applied independently to each phase.

These two sets of three independent equations means that each phase can be processed independently, thus giving a high degree of security. The problem of external faults occurring at the special angle, as discussed in section 2.3, will be overcome as only one phase can be at the special angle at any one time on a balanced three phase system.

For a untransposed transmission line the ground mode transients generated by a symmetric three phase fault to ground are also negligible. The aerial transient travelling-wave reflection coefficient can also be approximated by equation 4.2 where Z_a is given by

$$Z_a = \frac{z^s_{11} + z^s_{22} + z^s_{33} - z^s_{12} - z^s_{13} - z^s_{23}}{3} \tag{4.7}$$

The two fault resistance estimates are then be given by

$$R_{f1} = -\frac{Z_a}{2}[1 + \frac{v_f(n)}{V^a_1(n)}] \tag{4.8}$$

$$R_{f2} = -\frac{Z_a}{2}[1 + \frac{V^a_{r1}(n)}{V^a_{i2}(n)}] \tag{4.9}$$

where the superscript a refers to the phase transients with the ground mode removed, which are approximated by

$$V^a(n) = V(n) - V_g = V(n) - \frac{1}{3}(V(a) + V(b) + V(c)) \tag{4.10}$$

These transient values consist mostly of the aerial modes (modes 2 and 3) which propagate at approximately the same velocity. The aerial phase transients then approximate to independent modes of propagation. It follows therefore that the calculations can be applied independently to each aerial phase waveform, as with the phase values of a fully transposed transmission line.

4.3.2 Simulation results

Symmetric faults have been studied using the simulated data from a range of network configurations. The configuration shown in figure 4.3 is a particularly difficult configuration, as strong sources near the line terminations create complex reflected travelling waves during fault conditions. This configuration is then used to provide example results from fault transients simulated with the GEC MCZ1022A frequency domain programme.

Figure 4.4 shows the simulated incremental voltage and current transients, at the relaying point, from an internal symmetric three phase to ground fault on the configuration given in figure 4.3. The fault occurred at phase-a voltage maximum 140 km from the relaying point with phase resistances R_f of 10 ohms. The deduced incident and reflected transient waves, using equations 2.40 and 2.41, are given in figures 4.5a and 4.5b.

The three normalised cross-correlation functions are given by equations 3.13 with the substitutions;

$$V_i = V_i^a(n) \tag{4.11}$$

$$V_{r1} = V_{r1}^a(n) \tag{4.12}$$

where $n = a, b$ or c.

The cross-correlation functions, for the long and short window lengths, are given in figures 4.5c and 4.5d.

The sampling rate of 25.6 kHz, at best, gives a 6 km resolution of the fault location. This also implies that the initial estimate of the fault voltage amplitude v_f will have about a 5 % error. It is also expected that the transducer noise levels may be as high as 5 % of the per unit levels. The error in the first estimate of the fault resistance ΔR_{f1}, to within $\pi/12$ of phase voltage zero, should then be within

$$\Delta R_{f1} = \pm 30\Omega \quad \text{for } R_f \to 0 \tag{4.13}$$

$$\frac{\Delta R_{f1}}{R_{f1}} = \pm 30\% \quad \text{for } R_f \to \infty \tag{4.14}$$

The error in the cross-correlation amplitudes were limited to 25 % by the use of the two correlation windows discussed in chapter 3. The error in the second estimate of the fault resistance ΔR_{f2} should be within

$$\Delta R_{f2} = \pm 30\Omega \quad \text{for } R_f \to 0 \tag{4.15}$$

$$\frac{\Delta R_{f2}}{R_{f2}} = \pm 30\% \quad \text{for } R_f \to \infty \tag{4.16}$$

Agreement between the two fault resistances is then defined as

$$|R_{f1} - R_{f2}| < 60\Omega \quad \text{for} \quad R_{f1} \to 0 \tag{4.17}$$

$$\frac{|R_{f1} - R_{f2}|}{R_{f1}} < 60\% \quad \text{for} \quad R_{f1} \to \infty \tag{4.18}$$

The fault resistance estimates from the transients given in figures 4.4 and 4.5 are given in table 4.2 are only in agreement for the trough V_{i2} of

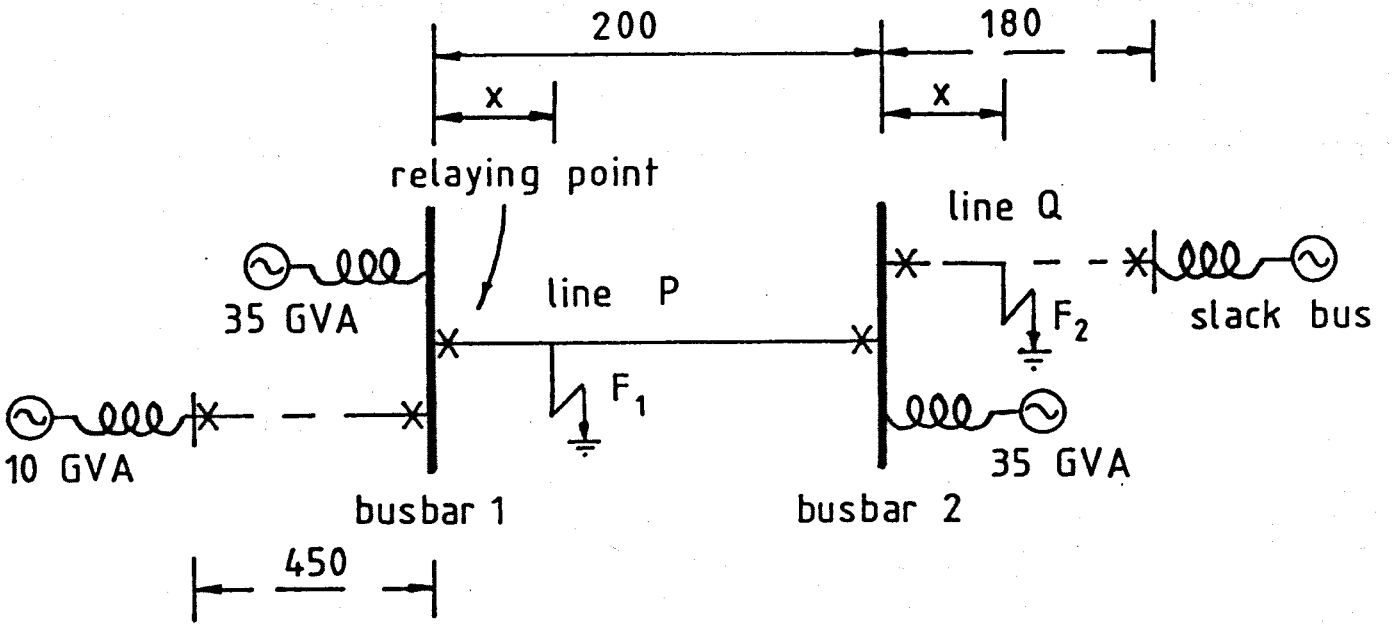

Figure 4.3 System network configuration used for the simulations of the faults studied in this chapter (distances in km).

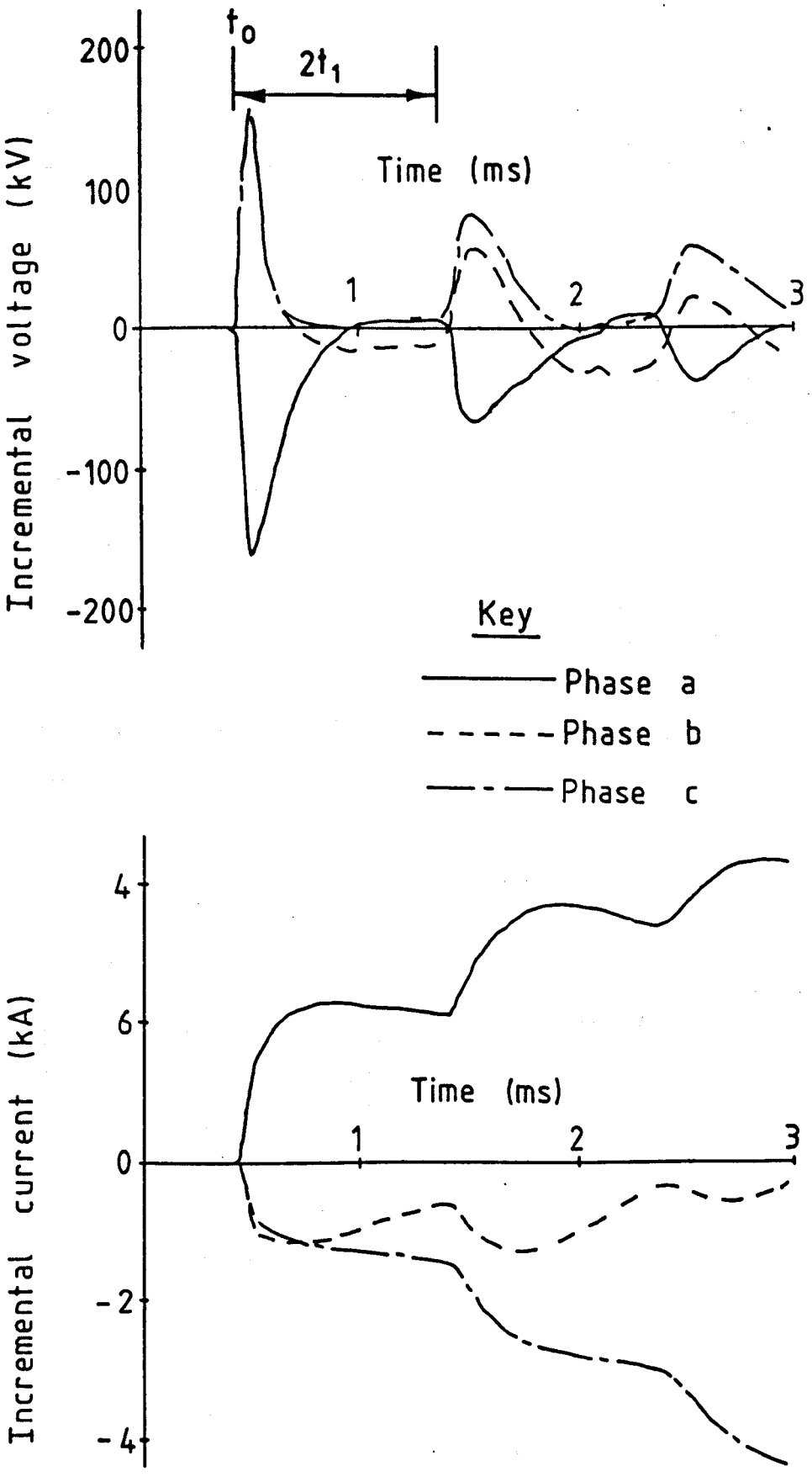

Figure 4.4 Incremental voltage and current transients produced during an internal symmetrical fault 140 km from the relaying point. The fault resistance on each phase was 10 ohms to ground and the fault occurred at phase-a voltage maximum.

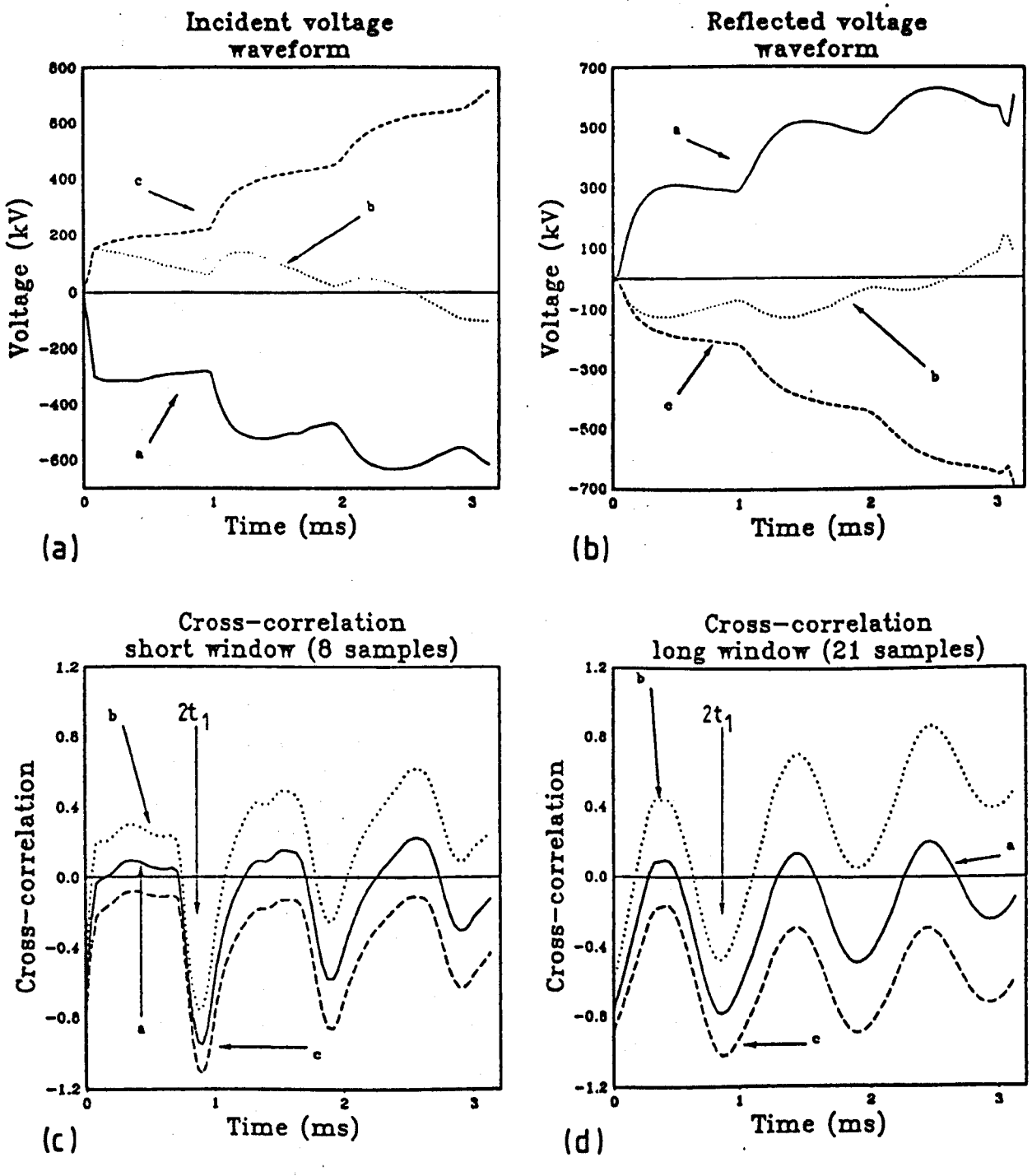

Figure 4.5 The relay outputs produced from the internal symmetric fault transients given in figure 4.4.
(a) The incident aerial voltage at the relaying point. (b) The reflected aerial voltage at the relaying point. (c) The cross-correlation function using the short window length of 8 samples (0.32 ms). (d) The cross-correlation function using the long window length of 21 samples (0.84 ms).

the long cross-correlation window ($N = 21$). This trough time is at 0.94 milliseconds which indicates a fault location at

$$x_a = 141 \pm 6\ km. \tag{4.19}$$

Table 4.2 Internal fault x=140 km

Phase	R_{f1} (Ω)	R_{f2} (Ω)	Trough time (ms.)	$x_a(km)$
a	18.0	16.0	0.94	141
b	26.0	12.0	0.94	141
c	10.0	21.0	0.94	141

The internal symmetric three phase fault has therefore been correctly identified.

The corresponding results for an external fault occurring 140 km from the far busbar (busbar 2), are given in figures 4.6, 4.7 and table 4.3. From these results it appears that the fault resistance estimates are never consistent for all three phases. The external fault should then be correctly identified as being beyond busbar 2.

Table 4.3 External fault x=340 km

Phase	R_{f1} (Ω)	R_{f2} (Ω)	Trough time (ms.)	$x_a(km)$
a	128.0	247.0	0.51	76
b	-171.0	228.0	0.55	82
c	452.0	267.0	0.51	76
a	143.0	-32.0	0.94	141
b	-105.0	-38.0	0.94	141
c	403.0	-24.0	0.94	141

The fault resistance estimates, for internal symmetric faults 140 km from the relaying point with of different initial fault voltage phase angles, are shown in figures 4.8. Near voltage zero there is a large error in the fault resistance estimates. This algorithm is then limited to within $\pi/12$ of voltage zero. Good agreement between the fault resistance estimates is then only required on two of the three phases. Since only one phase can be within $\pi/12$ of voltage zero at any one time, all the faults are correctly identified as being internal.

The fault resistance estimates, for the external symmetric fault at different initial voltage phase angles are shown in figures 4.9. The results for the cross-correlation trough indicating a location at 141 km are only shown as the other trough is not significant and gives similar results. The relay algorithm is intended to protect the line against faults of resistance up to the aerial mode surge impedance of the line (240 ohms). The confidence limits in figure 4.9 are then shown at the maximum acceptable value of 150 ohms (60 % of 240 ohms). There is only agreement between the fault resistance estimates at the special angle, which is discused in chapter 2. Since only one phase is at the special angle at any time, all the faults are correctly identified as being external.

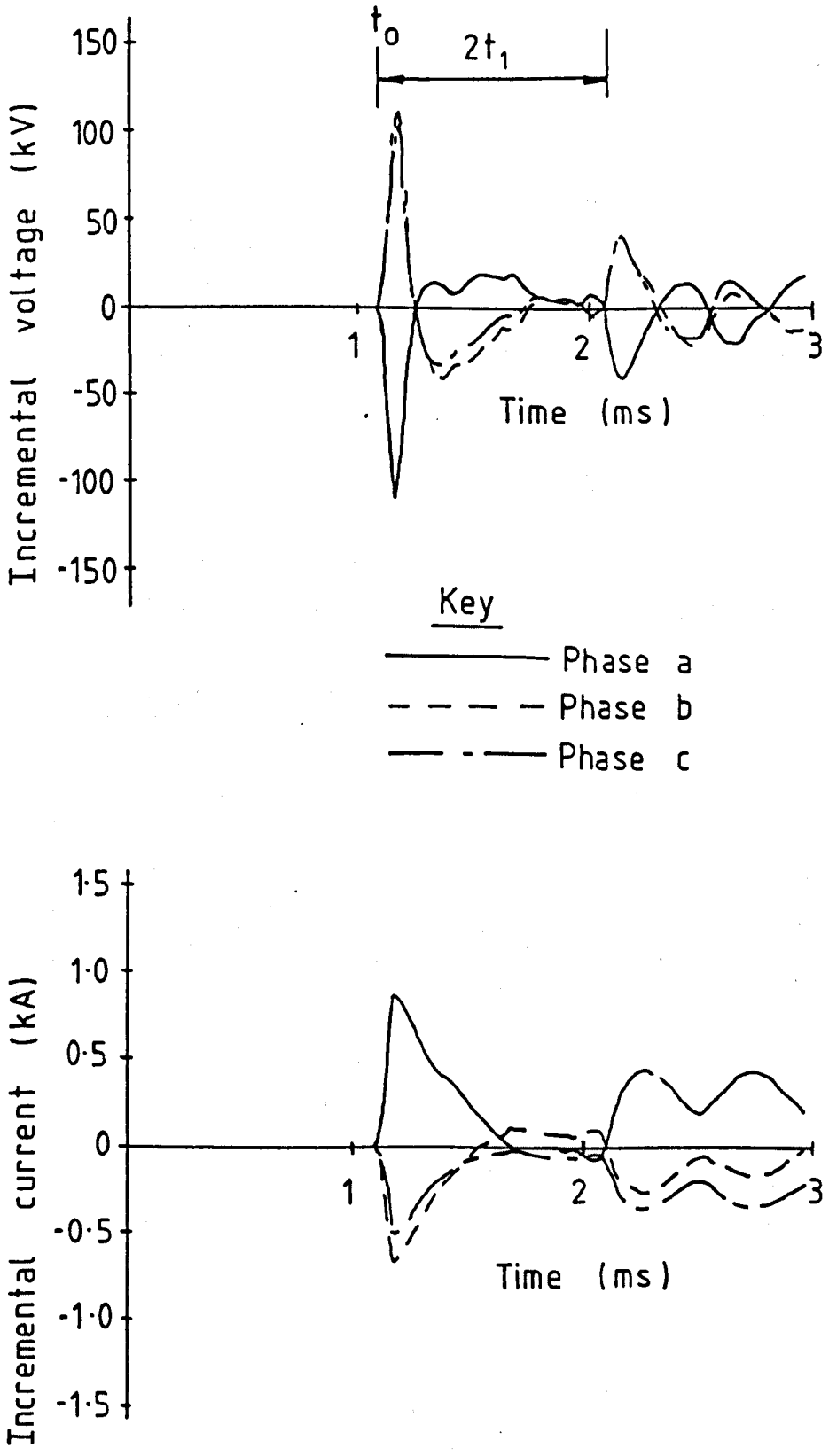

Figure 4.6 Incremental voltage and current transients produced during an external symmetrical fault 340 km from the relaying point (140 km from the far busbar). The fault resistance on each phase was 10 ohms to ground and the fault occurred at phase-a voltage maximum.

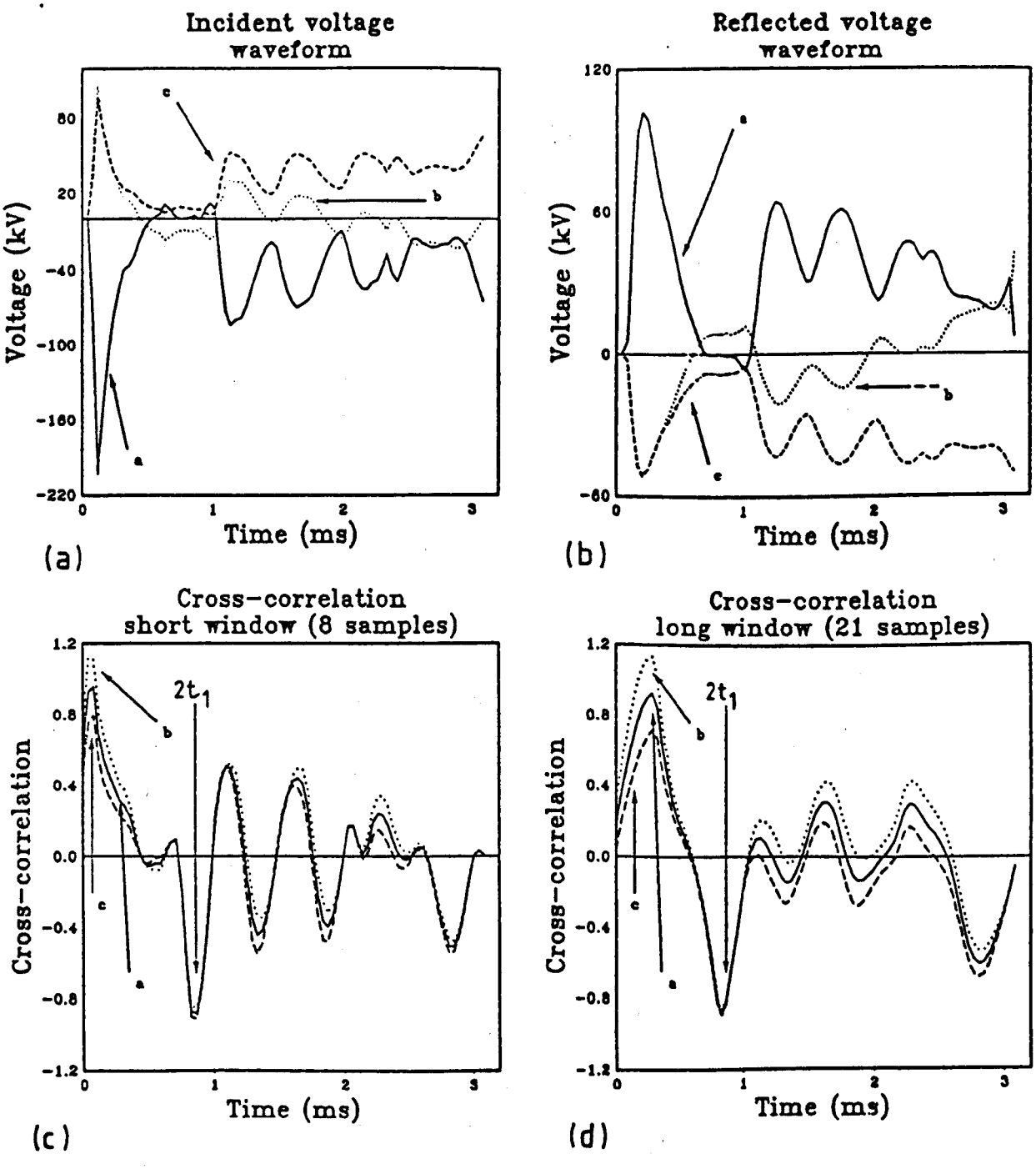

Figure 4.7 The relay outputs produced from the external symmetric fault transients given in figure 4.6.
(a) The incident aerial voltage at the relaying point. (b) The reflected aerial voltage at the relaying point. (c) The cross-correlation function using the short window length of 8 samples (0.32 ms). (d) The cross-correlation function using the long window length of 21 samples (0.84 ms).

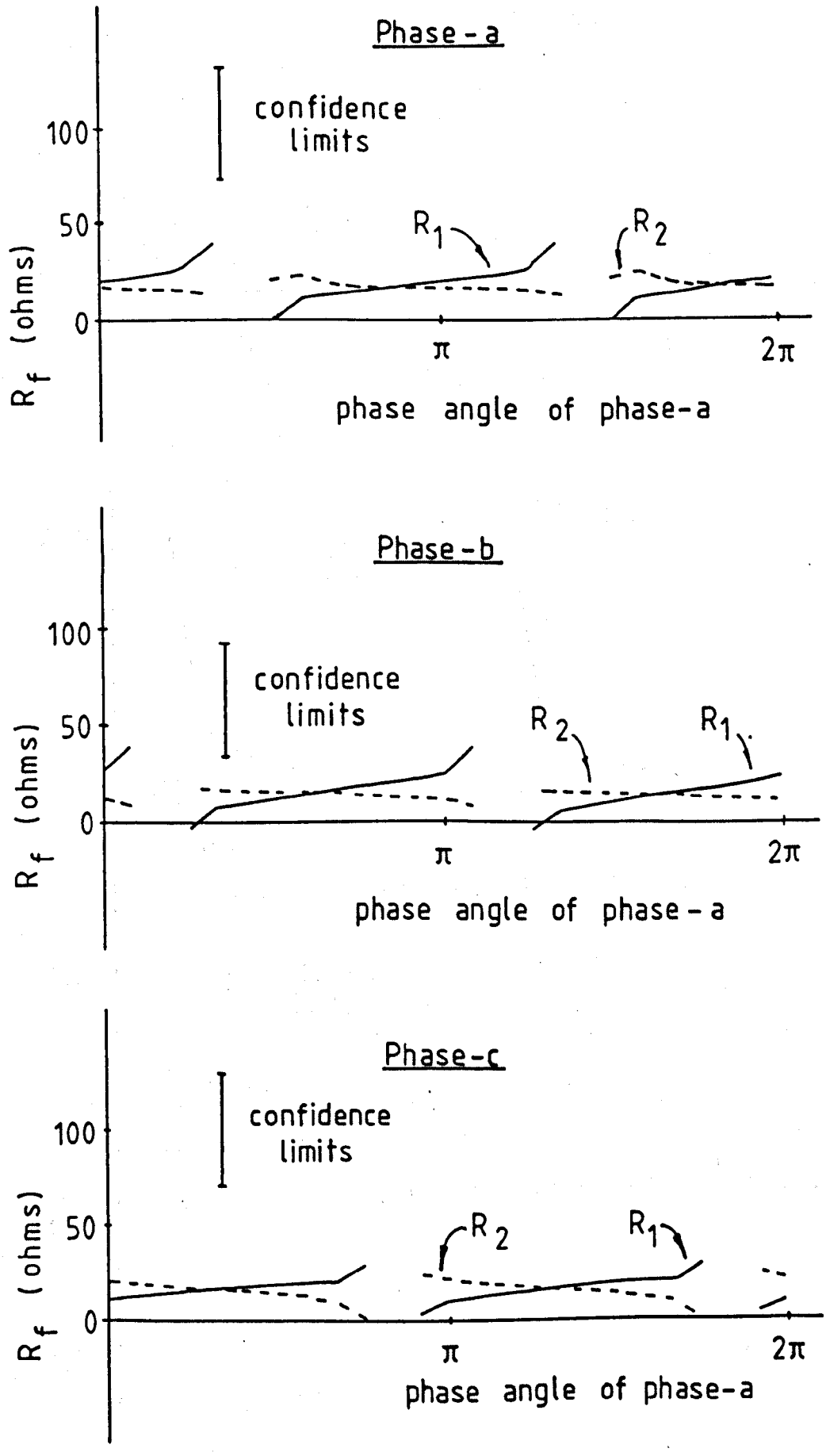

Figure 4.8 Fault resistance estimates for internal symmetric faults 140 km from the relaying point for various initial voltage phase angles. Good agreement for at least two phases indicates an internal fault.

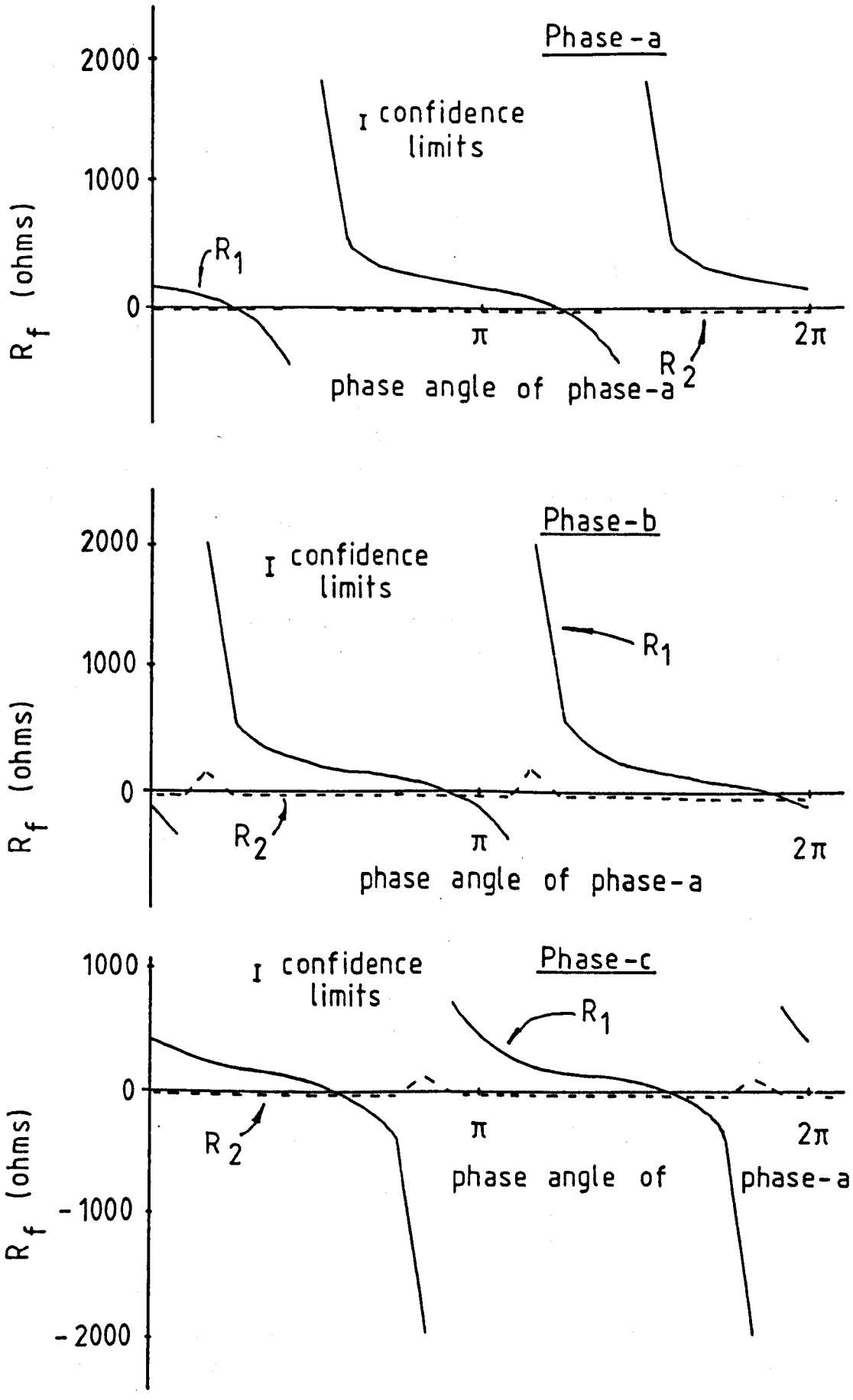

Figure 4.9 Fault resistance estimates for external symmetric faults 140 km from the relaying point for various initial voltage phase angles. Poor agreement for at least two phases indicates an external fault.

4.3.3 Conclusion for symmetric faults.

From these results it appears that good fault discrimination between internal and external symmetric faults is possible with this high speed travelling wave relay. Processing three independent phase waveforms ensures that complete protection over the whole system cycle is achieved. The confidence limits have been set so that all internal faults can be identified and all external faults are ignored.

As a result of using a high sampling rate, the algorithm can protect against symmetric faults occurring to within 40 km of the relaying point and faults can be located to within 6 km.

4.4 Single phase to ground faults.

In this section the application of the algorithm to single phase to ground faults will be described. For brevity only the application to a phase-a to ground fault will be discussed, as the other phase to ground faults will be processed in an identical manner. It is found that the ground mode delay has to be monitored, to ensure good fault discrimination for all fault conditions. The results then show that the internal and external faults will be correctly identified and the correct relay action taken.

4.4.1 Single phase fault conductance estimation

Figure 4.10 shows a schematic of a phase-a to ground fault. This will have a fault conductance matrix of the form

$$[Y_f] = \begin{bmatrix} \frac{1}{R_f} & 0 & 0 \\ 0 & 0 & 0 \\ 0 & 0 & 0 \end{bmatrix} \tag{4.20}$$

where R_f is the fault resistance

The fault reflection coefficient is then found by substituting equation 4.20 into equation 2.42 which gives for a fully transposed line

$$[k_{vf}] = -\begin{bmatrix} \frac{z^s_{dd}}{z^s_{dd}+2R_f} & 0 & 0 \\ \frac{z^s_{ce}}{z^s_{dd}+2R_f} & 0 & 0 \\ \frac{z^s_{ce}}{z^s_{dd}+2R_f} & 0 & 0 \end{bmatrix} \tag{4.21}$$

where z^s_{dd} are the diagonal elements of the surge impedance matrix and z^s_{ce} are the off diagonal elements of the surge impedance matrix.

It follows that the reflection coefficient for the aerial mode phase voltages found using equation 4.10 is then

$$[k^a_{vf}] = -\begin{bmatrix} \frac{2[z^s_{dd}-z^s_{ce}]}{3[z^s_{dd}+2R_f]} & 0 & 0 \\ \frac{[z^s_{ce}-z^s_{dd}]}{3[z^s_{dd}+2R_f]} & 0 & 0 \\ \frac{[z^s_{ce}-z^s_{dd}]}{3[z^s_{dd}+2R_f]} & 0 & 0 \end{bmatrix} \tag{4.22}$$

The initial fault conductance matrix estimate using equation 2.38 can therefore be rearranged into the form of a fault resistance estimate given by

$$R_{f1} = -\frac{1}{2}\left[z^s_{dd} + \frac{2}{3}[z^s_{dd} - z^s_{ce}]\frac{v_f(a)}{V^a_1(a)}\right] \tag{4.23}$$

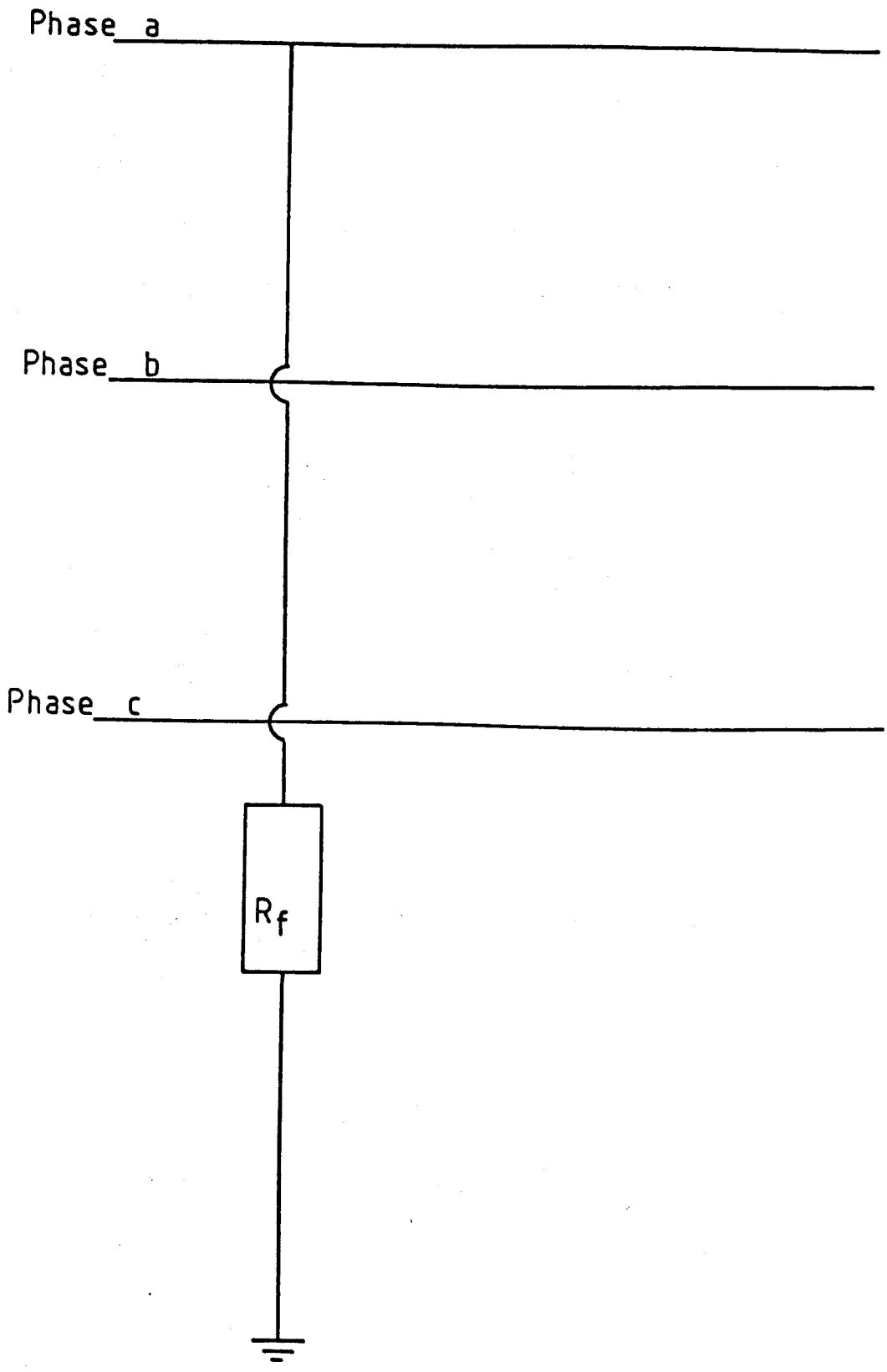

Figure 4.10 Phase-a to ground fault representation.

where $v_f(a)$ is the estimate of the initial fault voltage of the faulted phase (phase a) found from equations 2.51 and 2.52. $V_1^a(a)$ is the first incident aerial wave amplitude on the faulted phase. Due to the similarity in the aerial mode velocities, the aerial phase voltages propagate like independent modes. The aerial phase voltages can then be used without decomposing the transients into modes. It is also assumed that the aerial transients reach full amplitude within 0.08 milliseconds, as with the symmetric faults. Note that the other two phases also provide a fault resistance estimate but they are not independent equations as they are all only dependent on the initial faulted phase voltage (phase-a).

The second estimate of the fault conductance matrix given by equations 2.42, 2.54 and 4.22 can also be rearranged into the form

$$R_{f2} = -\frac{1}{2}\left[z^s_{dd} + \frac{2}{3}[z^s_{dd} - z^s_{ee}]\frac{V_{r1}(a)}{V^a_{i2}(a)}\right] \tag{4.24}$$

where V_{r1} is the first reflected phase voltage amplitude at the protection point and V^a_{i2} is the amplitude of the second incident aerial phase transient travelling wave.

The ratio $V_{r1}(a)/V^a_{i2}(a)$ is found from the cross-correlation function described in chapter 3, using equations 3.13 with the substitutions

$$V^i_1 = V^a_i(a) \tag{4.25}$$
$$V^i_r = V_{r1}(a) \tag{4.26}$$

The fault resistance estimates have been defined in terms of the phase values to simplify the calculations. The fault resistance estimates can also be defined in terms of the incident propagating modal waves but the gain in accuracy has been found to be minimal.

On untransposed transmission lines the fault conductance estimates can also be written in the form of fault resistance estimates given by

$$R_{f1} = -\frac{1}{2}\left[z^s_{11} + \frac{1}{3}[2z^s_{11} - z^s_{12} - z^s_{13}]\frac{v_f(a)}{V^a_1(a)}\right] \tag{4.27}$$

$$R_{f2} = -\frac{1}{2}\left[z^s_{11} + \frac{1}{3}[2z^s_{11} - z^s_{12} - z^s_{13}]\frac{V_{r1}(a)}{V^a_{i2}(a)}\right] \tag{4.28}$$

where z^s_{11}, z^s_{12} and z^s_{13} are the elements of the line surge impedance matrix.

4.4.2 Modal mixing at the fault location

From equation 4.22 it appears that the reflected aerial transient waves depend on the total incident voltage on the faulted phase (phase-a). In other words a degree of modal mixing occurs at a single phase to ground fault.

For a single phase to ground fault on a fully transposed transmission line model transient wave reflection is given by

$$[V_{rm}] = -[S]^{-1}[k_{vf}][S][V_{im}] \tag{4.29}$$

where $[V_{rm}]$ are the reflected modal transients at the fault, $[V_{im}]$ are the incident modal transients at the fault and $[S]$ is the transformation matrix of the modal voltages.

The general form of the transformation matrix of the modal voltages for a fully transposed line can be given by [82]

$$[S] = \begin{bmatrix} 1 & X_1 & Y_1 \\ 1 & X_2 & Y_2 \\ 1 & -[X_1+X_2] & -[Y_1+Y_2] \end{bmatrix} \tag{4.30}$$

thus the modal reflection matrix for the fault is

$$[k_{vf}^m] = \frac{-1}{3[Y_2X_1 - Y_1X_2]} \begin{bmatrix} ad & X_1ad & Y_1ad \\ b[Y_1+2Y_2] & X_1b[Y_1+2Y_2] & Y_1b[Y_1+2Y_2] \\ b[X_1+2X_2] & X_1b[X_1+2X_2] & Y_1b[X_1+2X_2] \end{bmatrix} \tag{4.31}$$

where

$$\begin{aligned} a &= \frac{z_{dd}^s + 2z_{ee}^s}{z_{dd}^s + 2R_f} \\ b &= \frac{z_{dd}^s - z_{ee}^s}{z_{dd}^s + 2R_f} \\ d &= [Y_2X_1 - Y_1X_2] \end{aligned}$$

Thus for a reflected mode to be independent of the ground mode $V_{im}(0)$ either one of the following conditions must be true.

$$a[Y_2X_1 - Y_1X_2] = 0 \text{ or} \tag{4.32}$$

$$b[Y_1 + 2Y_2] = 0 \text{ or} \tag{4.33}$$

$$b[X_1 + 2X_2] = 0 \tag{4.34}$$

These conditions, however, lead to the trivial solution of a reflected mode of zero amplitude. All reflected transients are therefore dependent on the amplitude of the incident ground mode travelling wave.

It follows that, the reflection coefficient at the fault location cannot be derived from the cross-correlation of only the initial reflected aerial transient V_{r1}^a with the incident aerial transient waves. An estimate of the ground mode delay, with respect to the aerial modes, has to be found so that the total initial incident wave at the fault location V_{r1f} can be given. This total initial incident wave at the fault location can then be cross-correlated with the incident aerial transient travelling waves at the relaying point to find the fault reflection coefficient.

The ground mode transients are very dispersed compared with the aerial mode transients. Over the reference window length (about 1 ms.) the ground modes or transients given by equation 4.4 can be approximated by

$$V_i^g \approx a\alpha V_1^g(t-t_0) + (1-a)\beta V_1^g(t-t_0) \tag{4.35}$$

$$V_{r1}^g \approx a\alpha V_{r1}^g(t-t_0) + (1-a)\beta V_{r1}^g(t-t_0) \tag{4.36}$$

The dispersion of the ground mode of the first reflected wave at the fault location should be approximately twice that at the relaying point as the wave will have propagated twice the distance. The expected wave amplitude incident at the fault is then

$$V_{r1f}^{g} \approx a\frac{\alpha}{2}V_{r1}^{g}(t-t_0)+(1-a)\frac{\beta}{2}V_{r1}^{g}(t-t_0) \tag{4.37}$$

$$\approx \frac{V_{r1}^{g}}{2} \tag{4.38}$$

For near faults, within half the protected line length of the relaying point, an adequate estimate of the amplitude of the first incident transient travelling wave at the fault location can then be given by

$$V_{r1f} = V_{r1}^{a} + \frac{1}{2}V_{r1}^{g} \tag{4.39}$$

where

V_{r1}^{a} is the initial reflected aerial transient at the relaying point and V_{r1}^{g} is the initial reflected ground mode transient at the relaying point.

For more distant faults the ground mode has to be more precisely defined. Adequate results can be provided by the approximation

$$V_{r1f}(t) = V_{r1}^{a}(t) + DV_{r1}^{g}(t-\tau) \tag{4.40}$$

where τ is the ground mode propagation delay measured from the first incident wave V_1 and D is approximated as the ground mode attenuation for a wave propagating along three quarters of the line length.

These estimates of the incident voltage wave amplitude at the fault location are then used in the cross-correlation routine (equation 4.26) to deduce the fault refection coefficient and hence the fault resistance to ground. They have been found to provide reasonable accuracy even on untransposed transmission lines.

4.4.3 Ground mode delay

At the fault location of a single phase to ground fault, the nature of the modal mixing, is difficult to predict. The amplitude of the line round trip wave $V_{2\tau}$ is therefore too unreliable to be used for discrimination against external phase to ground faults occurring at the special angle. Fortunately, a single phase to ground fault creates significant ground mode transients on a fully transposed transmission line or significant mode 1 transients on a untransposed transmission line. The time delay between the propagation of ground mode or mode 1 transients, with respect to the aerial transients, can then be used as a crude fault locator during single phase faults.

The crude fault location given by the ground mode delay when used in combination with the precise fault location given by the cross-correlation function trough then acts as a good fault discriminating feature between internal and external faults.

For the initial transient modal waves which, are incident at the relaying point V_{1m}, the time of propagation from the fault to the relaying point is

$$t_{1m} = x/u_m \tag{4.41}$$

where x is the distance between the fault and the relaying point and u_m is the modal propagation velocity.

The time difference Δt_{1m}, between the arrival of the modes of propagation at the relaying point is then

$$\Delta t_{1m} \approx \left| \frac{x \Delta u_m}{u_m^2} \right| \tag{4.42}$$

where Δu_m is the velocity difference between the independent modes of propagation

Thus the fault location can be estimated from

$$x \approx \left| \frac{\Delta t_{1m} u_m^2}{\Delta u_m} \right| \tag{4.43}$$

For a three phase transmission line the aerial modes propagate at close to the speed of light "c" and the ground mode or mode 1 propagate at a much reduced velocity which can be given as

$$u_g = c(1 + \xi) \tag{4.44}$$

where ξ is less than zero

The ground mode or mode 1 velocity is strongly dependent on the ground conductivity which is very variable. For a reasonable range of ground conductivities (20-500 ohm meters) ξ may vary by as much as 25% . ξ is then given as

$$\xi = 0.2 \pm 0.05 \tag{4.45}$$

Given a sampling rate of 25.6 kHz, the ground mode or mode 1 delay will then be known to a precision of 0.039 milliseconds (one sample). The fault location given by the ground mode delay (equation 4.43) can then be found to a precision of

$$x_g = \frac{-c \Delta t_m}{\xi} \pm (60 + 0.25x) \text{ km.} \tag{4.46}$$

The fault location given by the cross-correlation function is known to an accuracy of 6 km (see section on symmetric faults). For the location given by the ground mode delay to agree with the incorrect fault location given by the P_{t2} incident wave of an external fault x_a (see figure 2.) then

$$x_a(maximum) > x_g(minimum) \tag{4.47}$$

thus

$$6 > L - 60 - 0.25(L + x) \text{ km.} \tag{4.48}$$

where L is the length of the protected line and x is the distance of the external fault from the far busbar which has a minimum value of zero. The minimum length of the protected line, which ensures that condition 4.47 is never satisfied, is then

$$L < 88 \text{ km} \tag{4.49}$$

Thus if the protected line was less than 88 km in length, then the ground mode delay could not be used as a fault discriminant.

It has been shown that, despite the variability of the ground mode or mode 1 delay time with respect to the aerial modes, this delay time can be used as an extra discriminant between internal and external faults. This is provided that the protected line length is greater than 88 km. Note that, for instance, if the sampling rate was halved then the minimum protectable line length would be double (i.e. 176 km.).

4.4.4 Simulation results

The algorithm outlined is then applied when single phase to ground faults occur. Simulated transients of phase-a to ground faults, generated by the GEC MCZ1022A frequency domain programme, were then processed to demonstrate that good fault discrimination is possible. A typical set of results are now given.

As stated in section 4.2, the errors in the fault voltage estimate v_f and initial travelling wave voltage amplitude V_1 are expected to be about 5 %. For a single phase to ground fault, for protection to within $\pi/12$ of phase voltage zero, the error in the first fault resistance estimate should then be within

$$\Delta R_{f1} = \pm 30\Omega \quad \text{for} \quad R_f \rightarrow 0 \tag{4.50}$$

$$\frac{\Delta R_{f1}}{R_{f1}} = \pm 30\% \quad \text{for} \quad R_f \rightarrow \infty \tag{4.51}$$

The error in the cross-correlation function trough amplitude was limited to 25 % by the use of the window lengths discussed in chapter 3. The error in the second estimate of the fault resistance should then be within

$$\Delta R_{f2} = \pm 30\Omega \quad \text{for} \quad R_f \rightarrow 0 \tag{4.52}$$

$$\frac{\Delta R_{f2}}{R_{f2}} = \pm 30\% \quad \text{for} \quad R_f \rightarrow \infty \tag{4.53}$$

Agreement between the two fault resistance estimates is then given as

$$|R_{f1} - R_{f2}| < 60\Omega \quad \text{for} \quad R_{f1} \rightarrow 0 \tag{4.54}$$

$$\frac{|R_{f1} - R_{f2}|}{R_{f1}} < 60\% \quad \text{for} \quad R_{f1} \rightarrow \infty \tag{4.55}$$

Figure 4.11 shows the simulated incremental voltage and current transients at the relaying point, from an internal phase-a to ground fault on the configuration given in figure 4.3. The fault occurred at phase-a voltage maximum 140 km from the relaying point with phase resistance R_f of 10 ohms. The deduced incident and reflected transient waves, using equations 2.40 and 2.41, are given in figures 4.12a and 4.12b.

The resulting normalised cross-correlation functions for the two window lengths are shown in figures 4.12c and 4.12d. The incident modal voltage wave form is shown in figure 4.13.

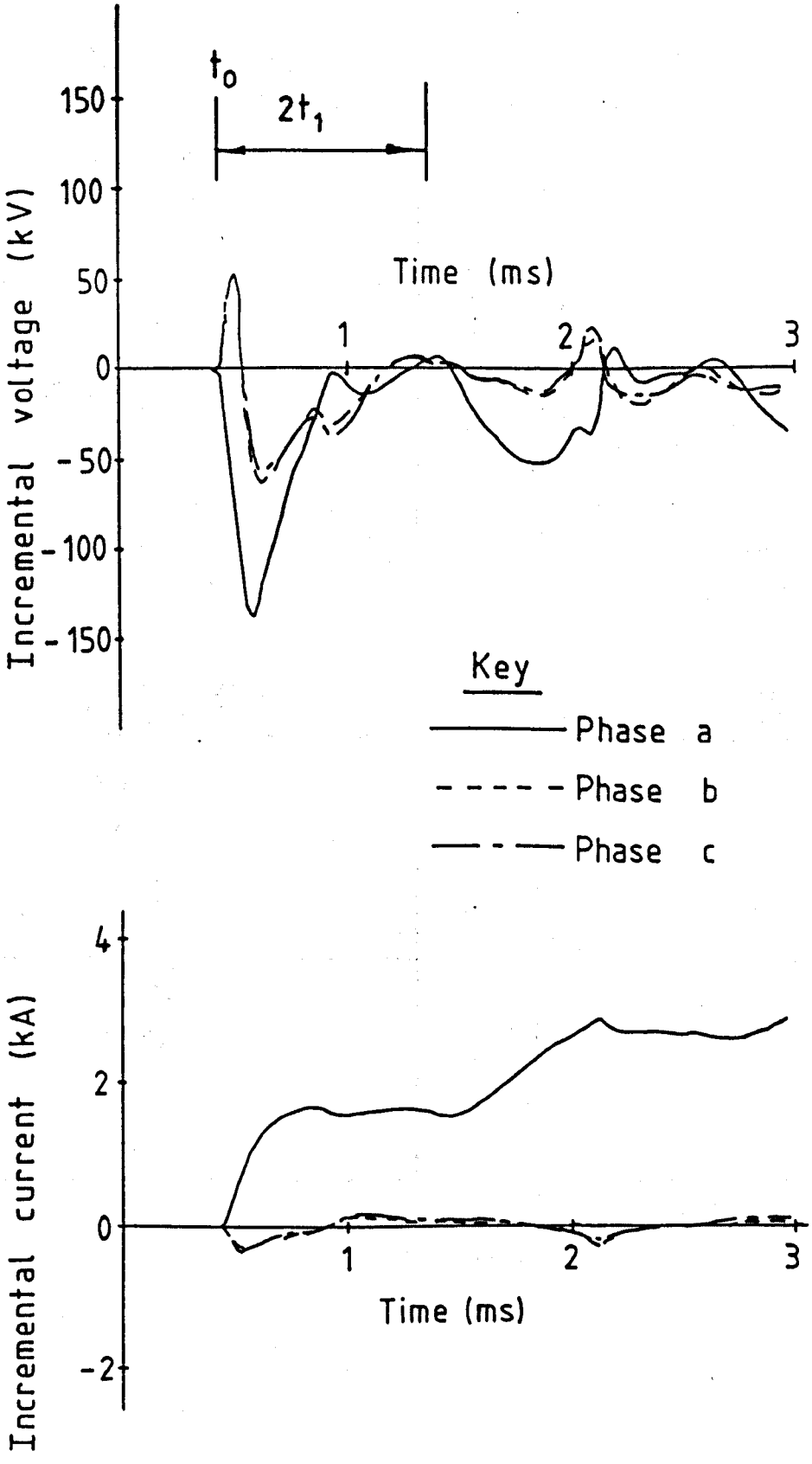

Figure 4.11 Incremental voltage and current transients produced during an internal phase-a to ground fault 140 km from the relaying point. The fault resistance on phase-a was 10 ohms to ground and the fault occurred at phase-a voltage maximum.

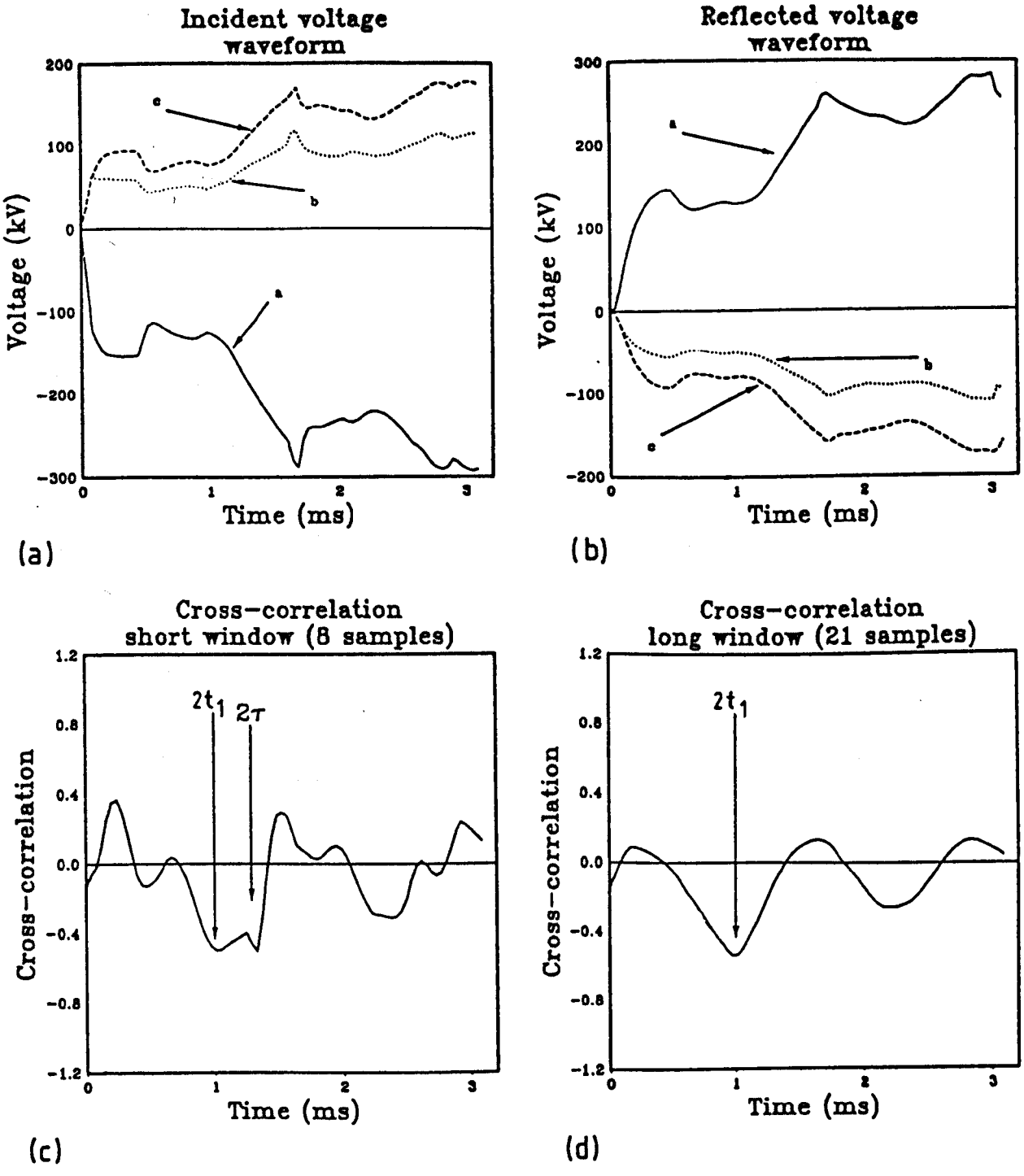

Figure 4.12 The relay outputs produced from the internal phase-a to ground fault transients given in figure 4.11.
(a) The incident aerial voltage at the relaying point. (b) The reflected aerial voltage at the relaying point. (c) The cross-correlation function using the short window length of 8 samples (0.32 ms). (d) The cross-correlation function using the long window length of 21 samples (0.84 ms).

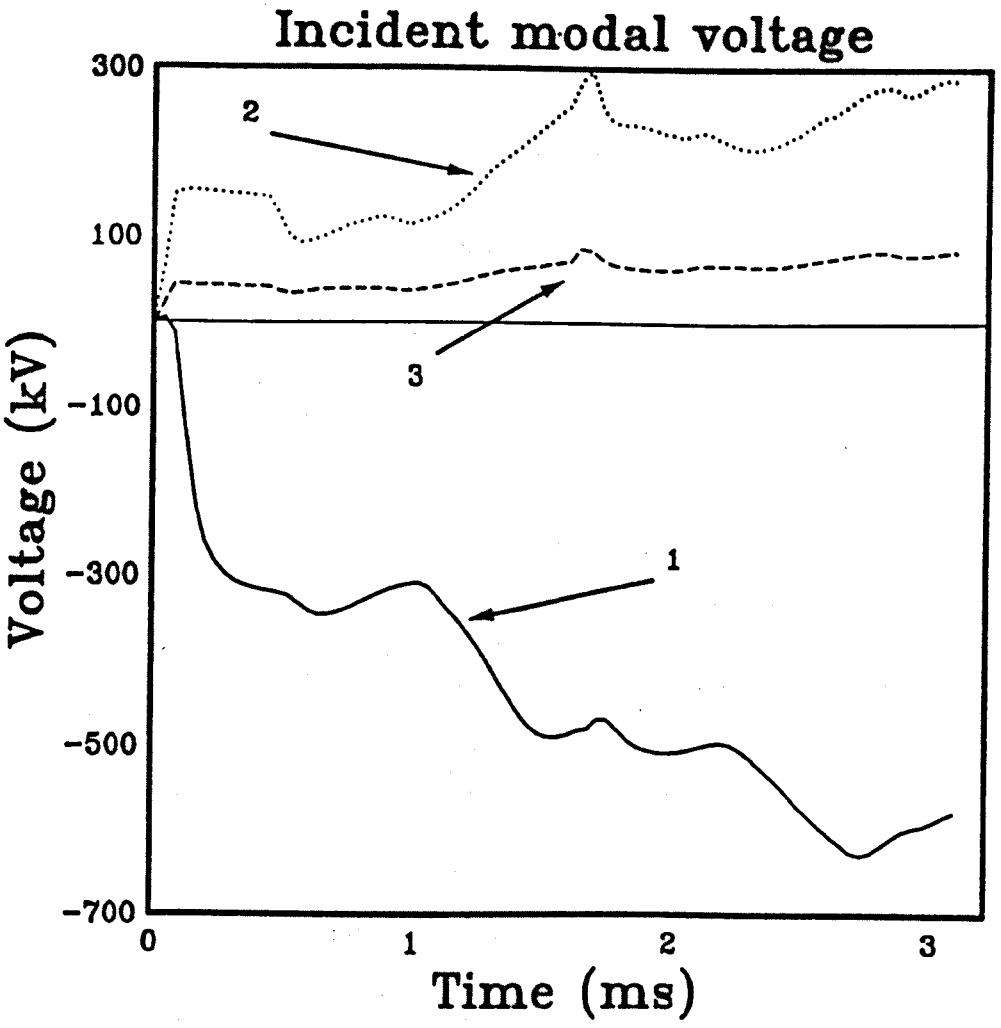

Figure 4.13 The incident model transients deduced from the internal phase-a to ground fault transients given in figure 4.11.

The fault resistance estimates given in table 4.4 are only in agreement for the trough V_{i2} of the long cross-correlation window ($N = 21$). This indicates a fault location at

$$x_a = 141 \pm 6 \; km. \tag{4.56}$$

Table 4.4 Internal fault x=140 km

$R_{f1}(\Omega)$	$R_{f2}(\Omega)$	Trough time (ms.)	x_a (km)
31.0	596.0	0.51	76.0
30.0	-18.0	0.94	141.0

The ground mode delay indicates a fault location at

$$x_g = 117 \pm 98 \; km. \tag{4.57}$$

The internal phase-a to ground fault is therefore correctly identified.

The corresponding results for an external fault occurring 140 km from the far busbar (busbar 2), are given in figures 4.14 to 4.16 and table 4.5. From these results it can be seen that the fault resistance estimates do not agree so the fault is correctly identified as being beyond the far busbar.

The mode 1 delay indicated a fault location at

$$x_g = 293 \pm 133 \; km \tag{4.58}$$

This also confirms the fault is external.

Table 4.5 External fault x=340 km

$R_{f1}(\Omega)$	$R_{f2}(\Omega)$	Trough time (ms.)	x_a (km)
421.0	-117.0	0.54	82.0
465.0	-117.0	0.94	141.0

The fault resistance estimates, for the internal phase-a to ground fault at different initial voltage phase angles, are given in figure 4.17a. The algorithm is limited to within $\pi/12$ of voltage zero as there is a low signal to noise ratio at the lower voltage amplitudes. From these results it appears that the internal fault can be correctly identified for most phase angles except near voltage zero.

The fault resistance estimates, for an external phase-a to ground fault at different initial voltage phase angles, are given in figure 4.17b. The fault resistance estimates given by the wave amplitude V_{pt2} are only given as these indicate a fault location closer to that given by the mode 1 delay. The fault resistance estimates presented show agreement at the special phase angle discussed in chapter 2. External single phase to ground faults occurring at these special phase angles could therefore be confused with an internal fault. The extra discriminating feature of the ground mode delay will have to be incorporated so that external single phase to ground faults are always correctly identified.

From the cross-correlation trough timing, the fault location is given as

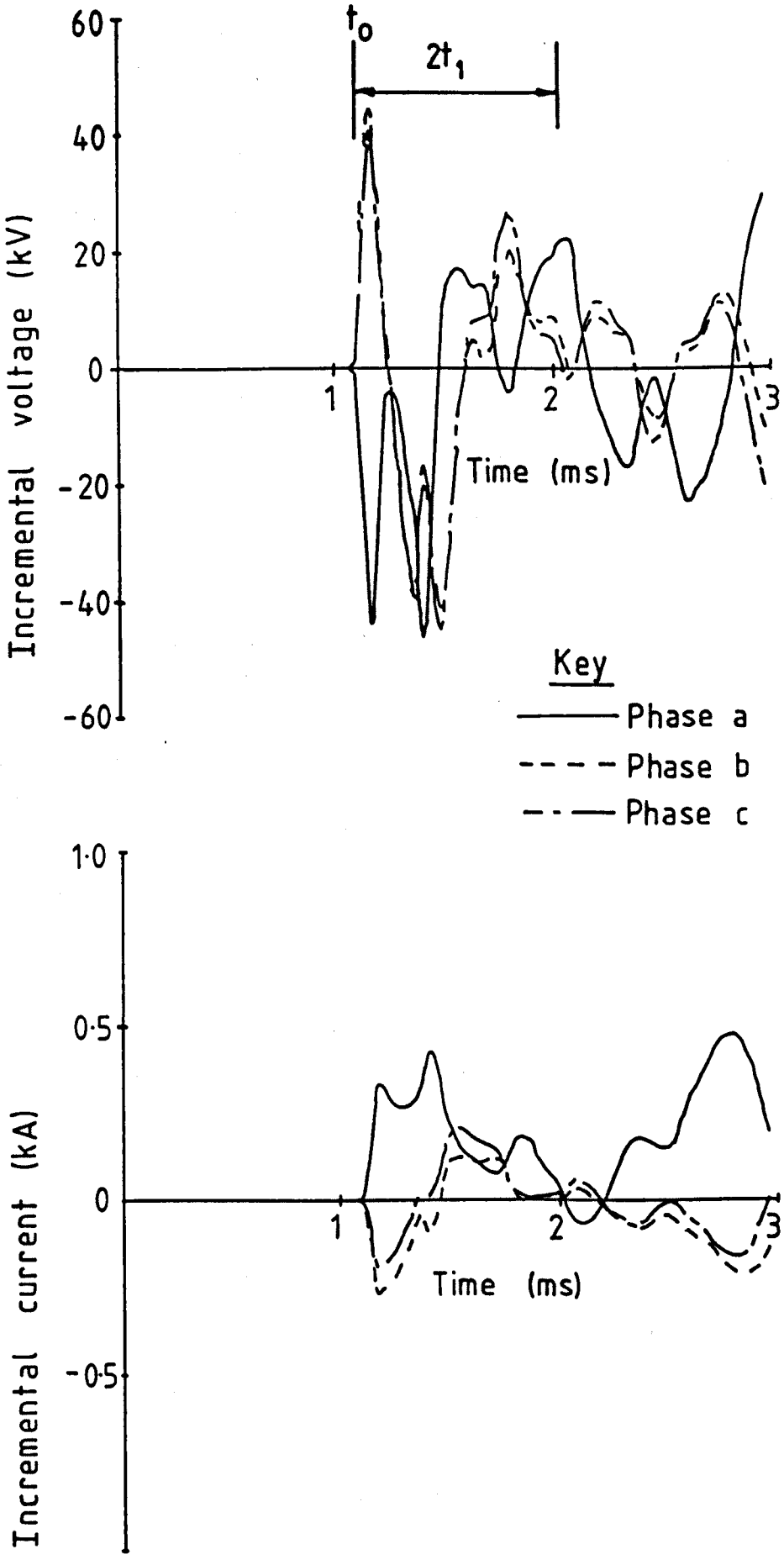

Figure 4.14 Incremental voltage and current transients produced during an external phase-a to ground fault 340 km from the relaying point (140 km from the far busbar). The fault resistance on phase-a was 10 ohms to ground and the fault occurred at phase-a voltage maximum.

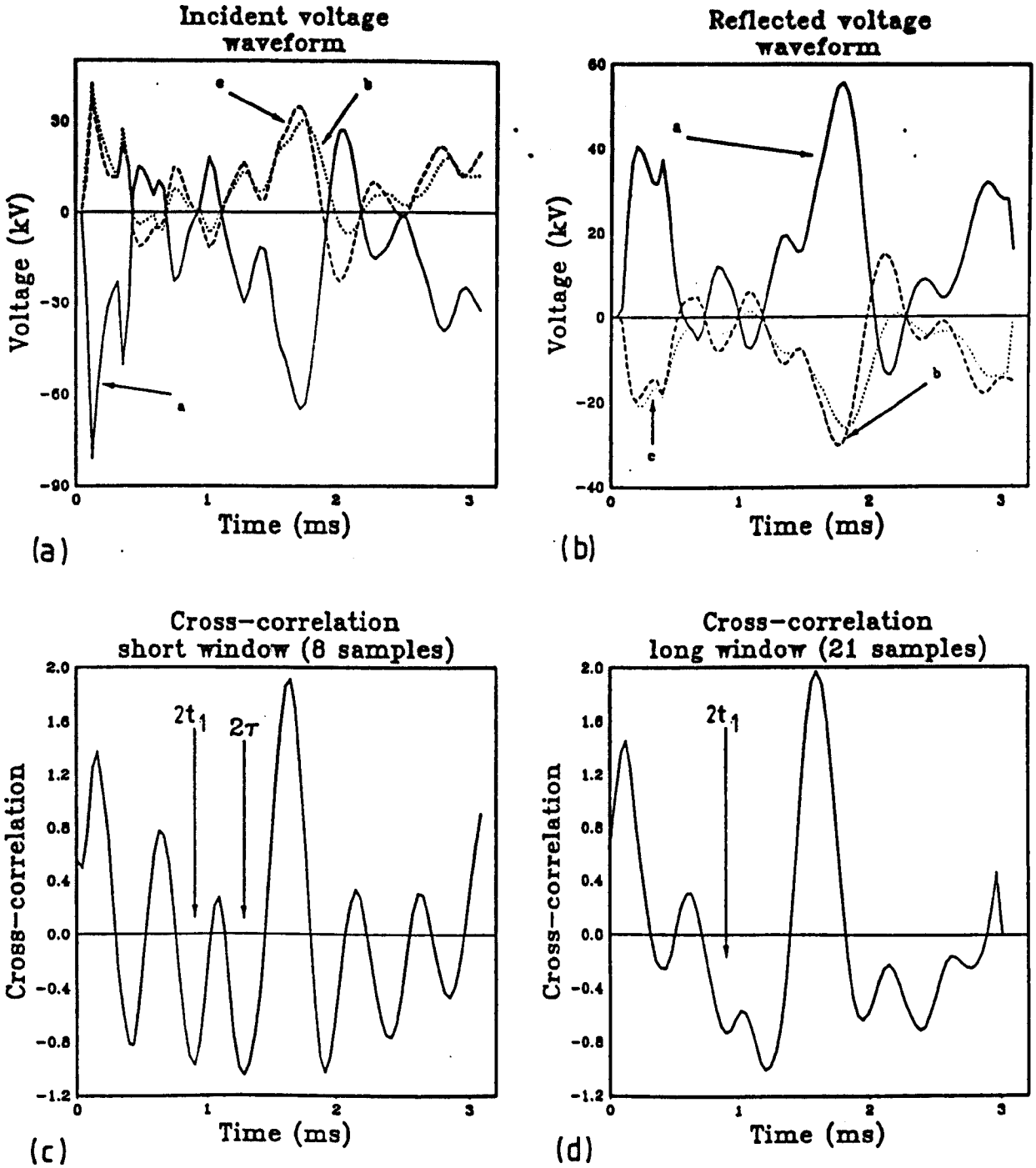

Figure 4.15 The relay outputs produced from the external phase-a to ground fault transients given in figure 4.14.
(a) The incident aerial voltage at the relaying point. (b) The reflected aerial voltage at the relaying point. (c) The cross-correlation function using the short window length of 8 samples (0.32 ms). (d) The cross-correlation function using the long window length of 21 samples (0.84 ms).

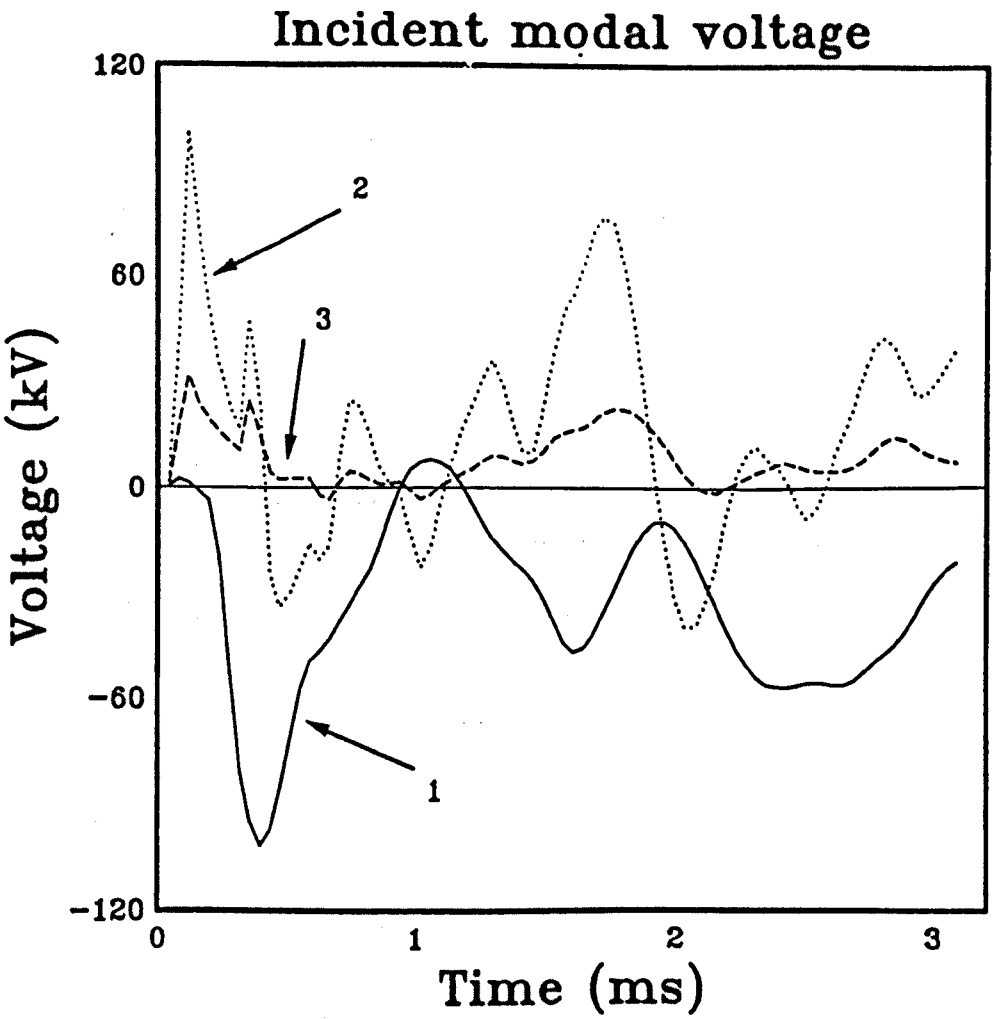

Figure 4.16 The incident model transients deduced from the external phase-a to ground fault transients given in figure 4.14.

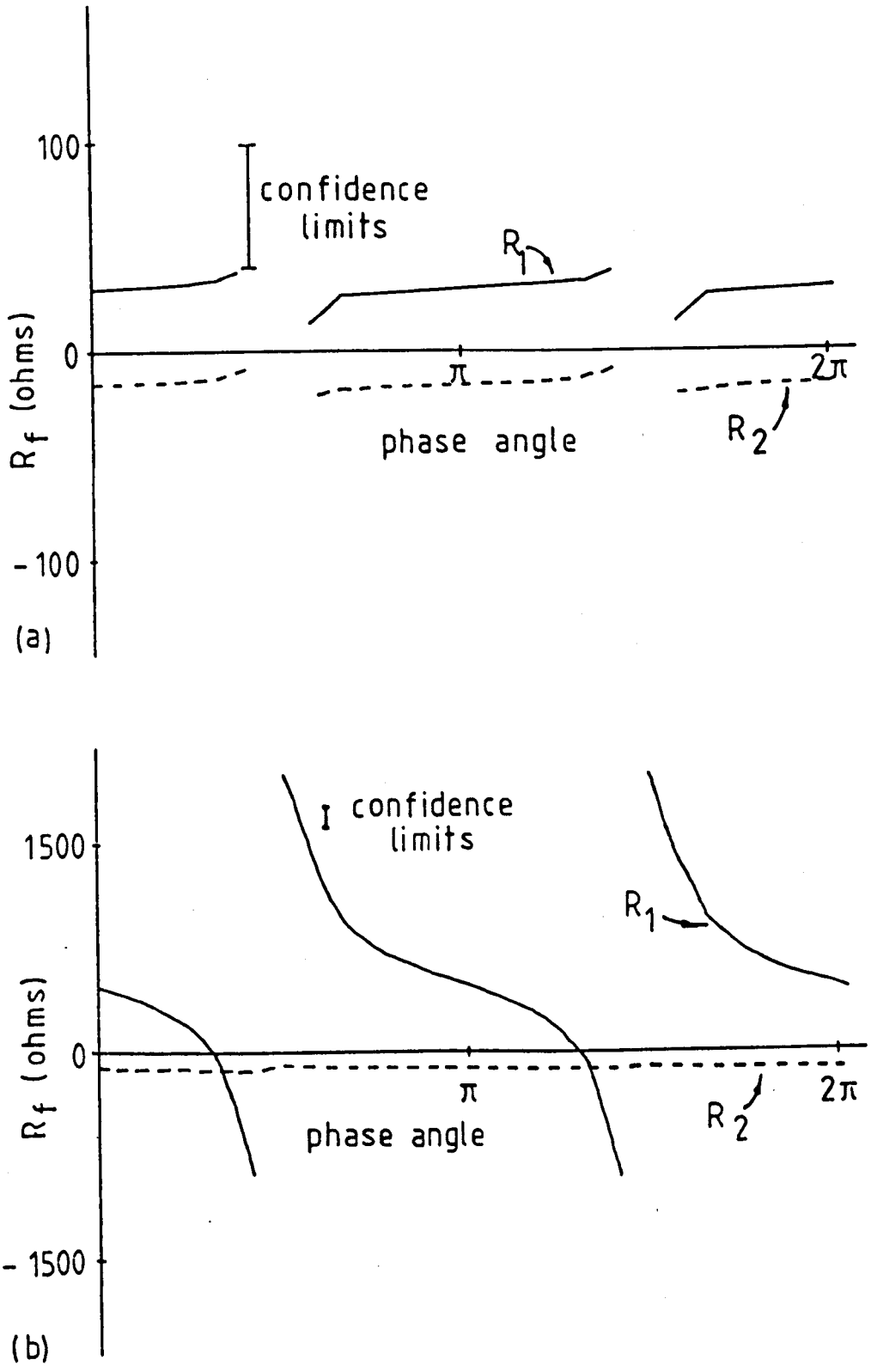

Figure 4.17 Fault resistance estimates for phase-a to ground faults against initial fault voltage phase angles. (a) Internal faults 140 km from the relaying point. The actual fault resistances to ground were 10 ohms. Good agreement is achieved for all phase angles not within $\pi/12$ of phase-a voltage zero ($\pi/2$ and $3\pi/2$).

(b) External faults 340 km from the relaying point (140 km from busbar 2). The actual fault resistances to ground were 10 ohms. Good agreement between the fault resistance estimates is only observed at two narrow regions in the cycle (special angles).

$$x_a = 140 \pm 6\ km \tag{4.59}$$

From the mode 1 delay, the fault location is

$$x_g = 293 \pm 133\ km \tag{4.60}$$

All the external faults are then correctly identified.

Identification of internal faults is possible over a large range of fault resistances up to about the aerial mode surge impedance of the line (260 ohms). Figure 4.18 shows the agreement between the two fault resistance estimates over a large range of fault resistances. The faults were located 40 km from the relaying point and the cross-correlation trough indicated a location at

$$x_a = 41 \pm 6\ km \tag{4.61}$$

The mode 1 delay indicates a fault location at

$$x_g = 59 \pm 75\ km \tag{4.62}$$

The fault resistance estimates over a range of initial phase angles, for internal and external phase-a to ground faults of resistance 150 ohms, are shown in figure 4.19. The internal fault locations were 40 km from the relaying point. The faults were measured to be at

$$x_a = 41 \pm 6\ km \tag{4.63}$$

$$x_g = 59 \pm 75\ km \tag{4.64}$$

The external faults were 240 km from the relaying point and there locations were measured to be at

$$x_a = 41 \pm 6\ km \tag{4.65}$$

$$x_g = 175 \pm 104\ km \tag{4.66}$$

This demonstrates that good fault discrimination is also possible for high fault resistances.

4.4.5 Conclusion for single phase to ground faults

It has been shown that this relay algorithm can protect transmission lines against severe single phase to ground faults. Internal faults of resistances up to 260 ohms can be identified for fault instigation times to within $\pi/12$ of phase voltage zero. All external faults are identified throughout the system cycle.

In order to ensure correct fault discrimination for external faults at all times, the ground mode or mode 1 delay has to be measured. Despite the variability of the ground mode or mode 1 velocities, it has been found their delay provides a reliable confirmation of the fault location for transmission lines longer than 88 km.

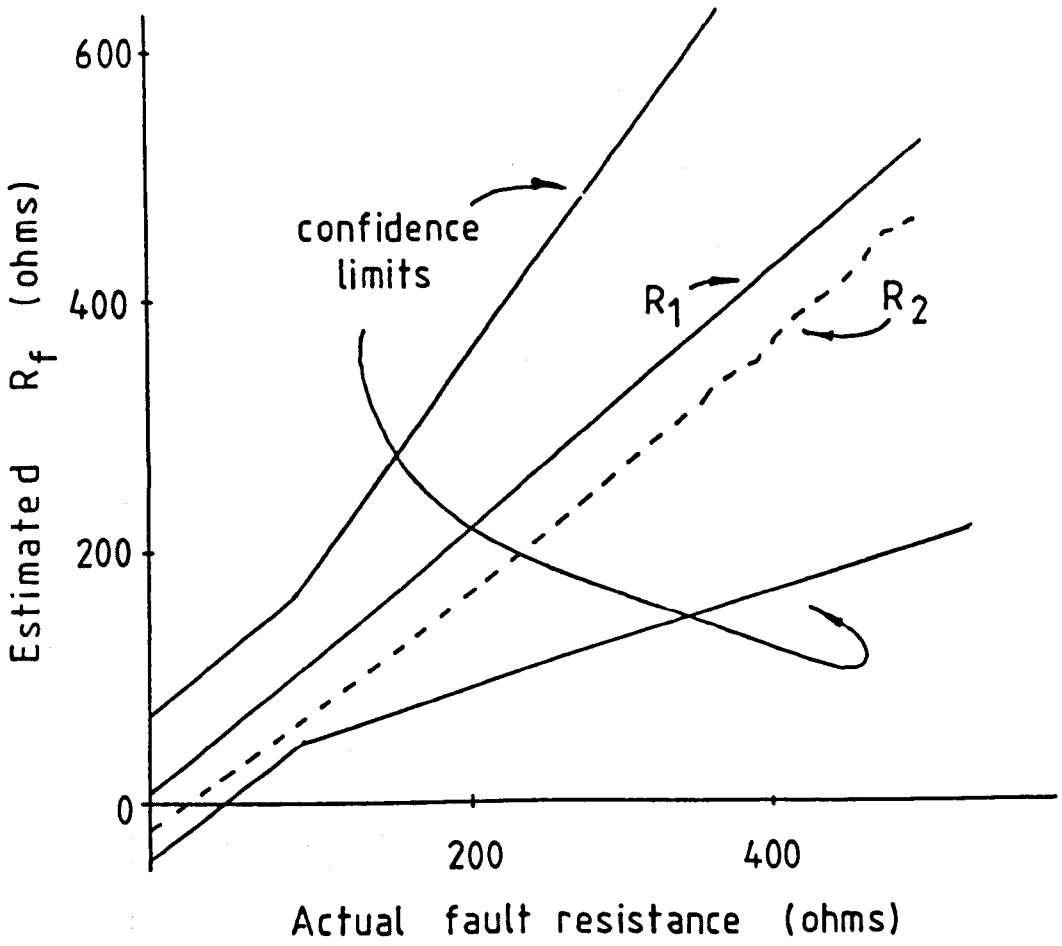

Figure 4.18 Fault resistance estimates for internal phase-a to ground faults 40 km from the relaying point against the actual fault resistance. The faults occurred at phase-a voltage maximum. Good agreement between the fault resistance estimates is possible for fault resistances up to at least the line aerial mode surge impedance ($Z_a \approx 240\Omega$).

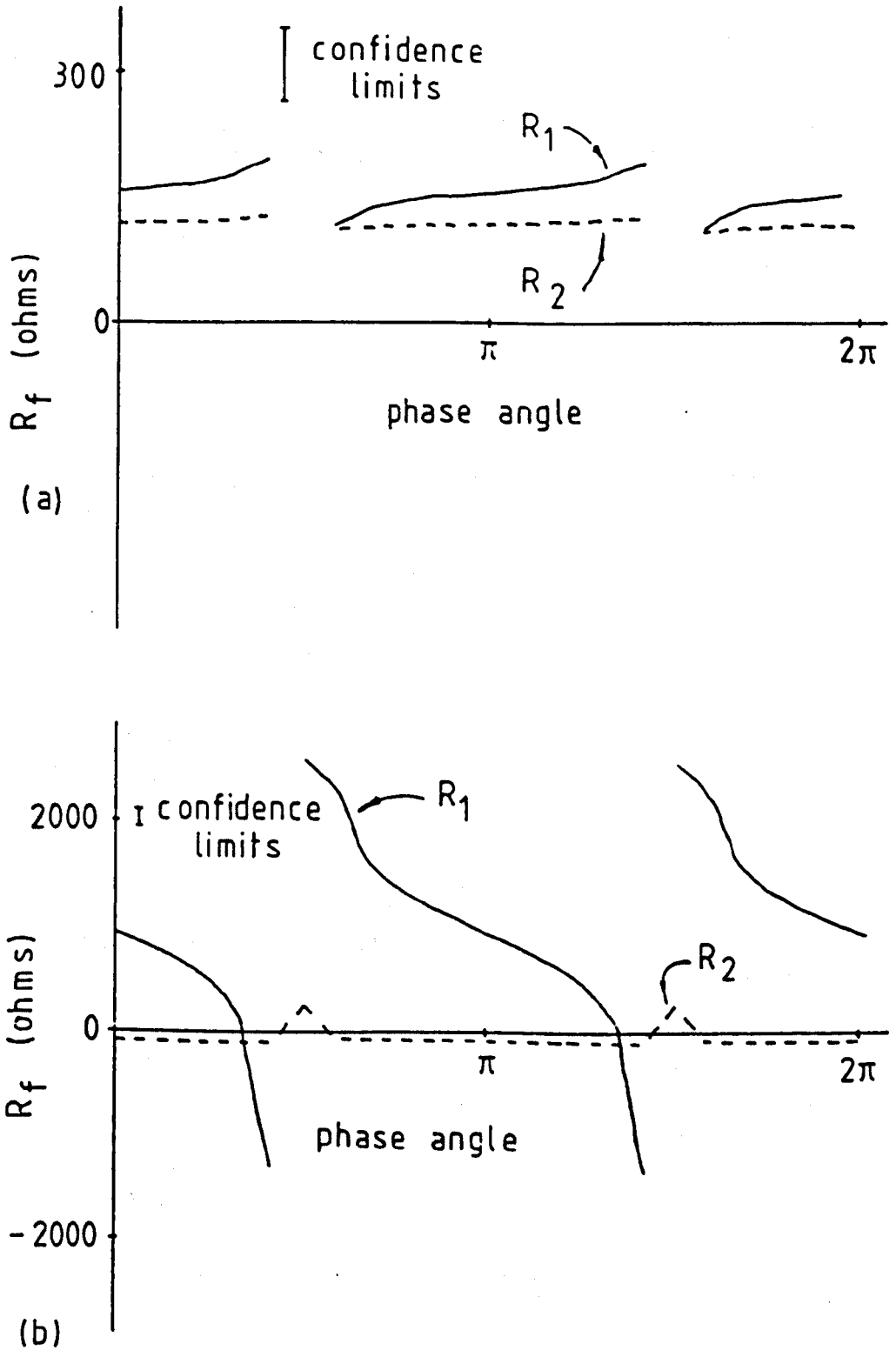

Figure 4.19 Fault resistance estimates for phase-a to ground faults against initial fault voltage phase angles. (a) Internal faults 40 km from the relaying point. The actual fault resistances to ground were 150 ohms. Good agreement is achieved for all phase angles not within $\pi/12$ of phase-a voltage zero ($\pi/2$ and $3\pi/2$).
(b) External faults 240 km from the relaying point (40 km from busbar 2). The actual fault resistances to ground were 150 ohms. Good agreement between the fault resistance estimates is only observed at two narrow regions in the cycle (special angles).

4.5 Phase to phase faults

In this section the application of the algorithm to phase to phase faults will be described. For brevity only the phase-a to phase-b fault type will be considered as the other fault types will be processed in an identical manner.

It is found that, in order for good fault discrimination to be achieved, the line round trip wave amplitude $V_{2\tau}$ has to be monitored. It is then shown, from the simulated results, that the internal and external faults can be correctly identified.

4.5.1 Fault conductance estimation

A phase-a to phase-b fault as shown in figure 4.20 has a fault conductance matrix which can be given as

$$[Y_f] = \begin{bmatrix} \frac{1}{R_f} & -\frac{1}{R_f} & 0 \\ -\frac{1}{R_f} & \frac{1}{R_f} & 0 \\ 0 & 0 & 0 \end{bmatrix} \tag{4.67}$$

The fault reflection coefficient given by equation 2.42 for a fully transposed transmission line is then

$$[k_{vf}] = -\frac{1}{2R_f + 2z^s_{dd} - 2z^s_{ee}} \begin{bmatrix} z^s_{dd} - z^s_{ee} & z^s_{ee} - z^s_{dd} & 0 \\ z^s_{ee} - z^s_{dd} & z^s_{dd} - z^s_{ee} & 0 \\ 0 & 0 & 0 \end{bmatrix} \tag{4.68}$$

where z^s_{dd} are the diagonal elements of the surge impedance of a fully transposed line and z^s_{ee} are the off diagonal elements of the surge impedance.

Since no ground mode transients are produced by a phase to phase fault on a fully transposed transmission line we can put that the aerial phase reflection coefficient is given by the phase reflection coefficient, that is

$$[k^a_{vf}] = [k_{vf}] \tag{4.69}$$

The initial fault conductance matrix estimate using equations 2.38 and 4.68 is then rearranged into the form of a fault resistance estimate given as

$$R_{f1} = -(z^s_{dd} - z^s_{ee}) - (z^s_{dd} - z^s_{ee}) \left[\frac{v_f(a) - v_f(b)}{V^a_1(a) - V^a_1(b)} \right] \tag{4.70}$$

where $v_f(a)$ and $v_f(b)$ are given by equations 2.51 and 2.52, $V^a_1(a)$ and $V^a_1(b)$ are the initial aerial voltage transients found from equations 4.10 and 2.40

The second estimate of the fault conductance matrix using equations 2.42, 2.54 and 4.68 can also be rearranged into the form

$$R_{f2} = -(z^s_{dd} - z^s_{ee}) - (z^s_{dd} - z^s_{ee}) \left[\frac{V^a_{r1}(a) - V^a_{r1}(b)}{V^a_{i2}(a) - V^a_{i2}(b)} \right] \tag{4.71}$$

The ratio $\frac{V_{r1}(a) - V_{r1}(b)}{V^a_{i2}(a) - V^a_{i2}(b)}$ is found from the cross-correlation function given by equation 3.13 with the substitution

$$V_i = V^a_i(a) - V^a_i(b) \tag{4.72}$$

$$V_{r1} = V^a_{r1}(a) - V^a_{r1}(b) \tag{4.73}$$

$$\tag{4.74}$$

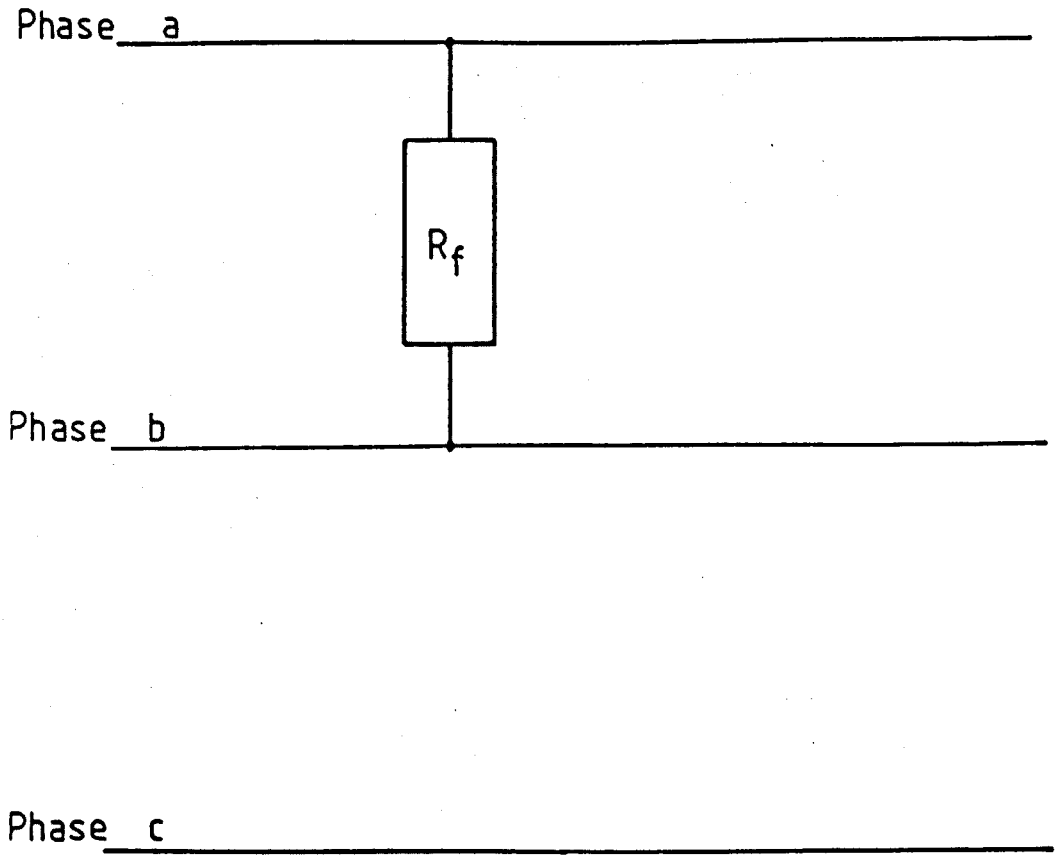

Figure 4.20 Phase-a to phase-b fault representation.

Note that the values $V(a) - V(b)$ are the line voltages between the two faulted phases. On a fully transposed transmission line the line voltage can be considered to be an independent mode of propagation, which propagates at the aerial mode velocity. Fault discrimination for a phase to phase fault can then be reduced to a single phase problem using the line voltages between the faulted phases. Even on untransposed transmission lines the line voltage is, to a good approximation, an independent aerial mode and modal mixing at a phase to phase fault is found to be minimal.

For an untransposed transmission line the fault conductance estimates can also be put in a form of two resistance estimates given by

$$R_{f1} = -\frac{z^s_{11} + z^s_{22} - 2z^s_{12}}{2} - \frac{z^s_{11} + z^s_{22} - 2z^s_{12}}{2}\left[\frac{v_f(a) - v_f(b)}{V^a_1(a) - V^a_1(b)}\right] \quad (4.75)$$

$$R_{f2} = -\frac{z^s_{11} + z^s_{22} - 2z^s_{12}}{2} - \frac{z^s_{11} + z^s_{22} - 2z^s_{12}}{2}\left[\frac{V^a_{r1}(a) - V^a_{r1}(b)}{V^a_{i2}(a) - V^a_{i2}(b)}\right] \quad (4.76)$$

where z^s_{11}, z^s_{22} and z^s_{12} are the elements of the surge impedance matrix.

The fault conductance matrix estimates can then be reduced to fault resistance estimates using the line voltage between the faulted phase. Since only one line voltage can be used another discriminating feature has to be incorporated to ensure correct identification of external faults occurring at the special angle. For phase to phase faults the line voltage transients are treated as an independent mode and the protected line round trip wave, as described in chapter 2, can be successfully used for discrimination. External faults are therefore confirmed by a trough in the cross-correlation functions at a time 2τ.

4.5.2 Simulation results

Phase-a to phase-b faults have been studied using simulated data from a range of network configurations. Example results for the configuration 4.3 are given here.

Figure 4.21 shows the incremental voltage and current transients for an internal phase-a to phase-b fault 140 km from the relaying point. The fault resistance R_f was 10 ohms and the fault occurred at phase-a voltage maximum. The deduced incident and reflected voltage transients using equations 2.40 and 2.41 are given in figures 4.22a and 4.22b.

The normalised cross-correlation functions for the two window lengths, using equation 3.13, are given in figures 4.22c and 4.22d.

For a sampling rate of 25.6 kHz, noise level of 5 % of the per unit levels and protection within $\pi/12$ of line to line voltage zero, the error in the first estimate of the fault resistance ΔR_{f1} should be within

$$\Delta R_{f1} = \pm 30\Omega \quad \text{for } R_f \to 0 \quad (4.77)$$

$$\frac{\Delta R_{f1}}{R_{f1}} = \pm 30\% \quad \text{for } R_f \to \infty \quad (4.78)$$

The errors in the cross-correlation trough amplitudes should also be within 25% for phase to phase faults. The errors in the second estimate of the fault resistance ΔR_{f2} should then be within

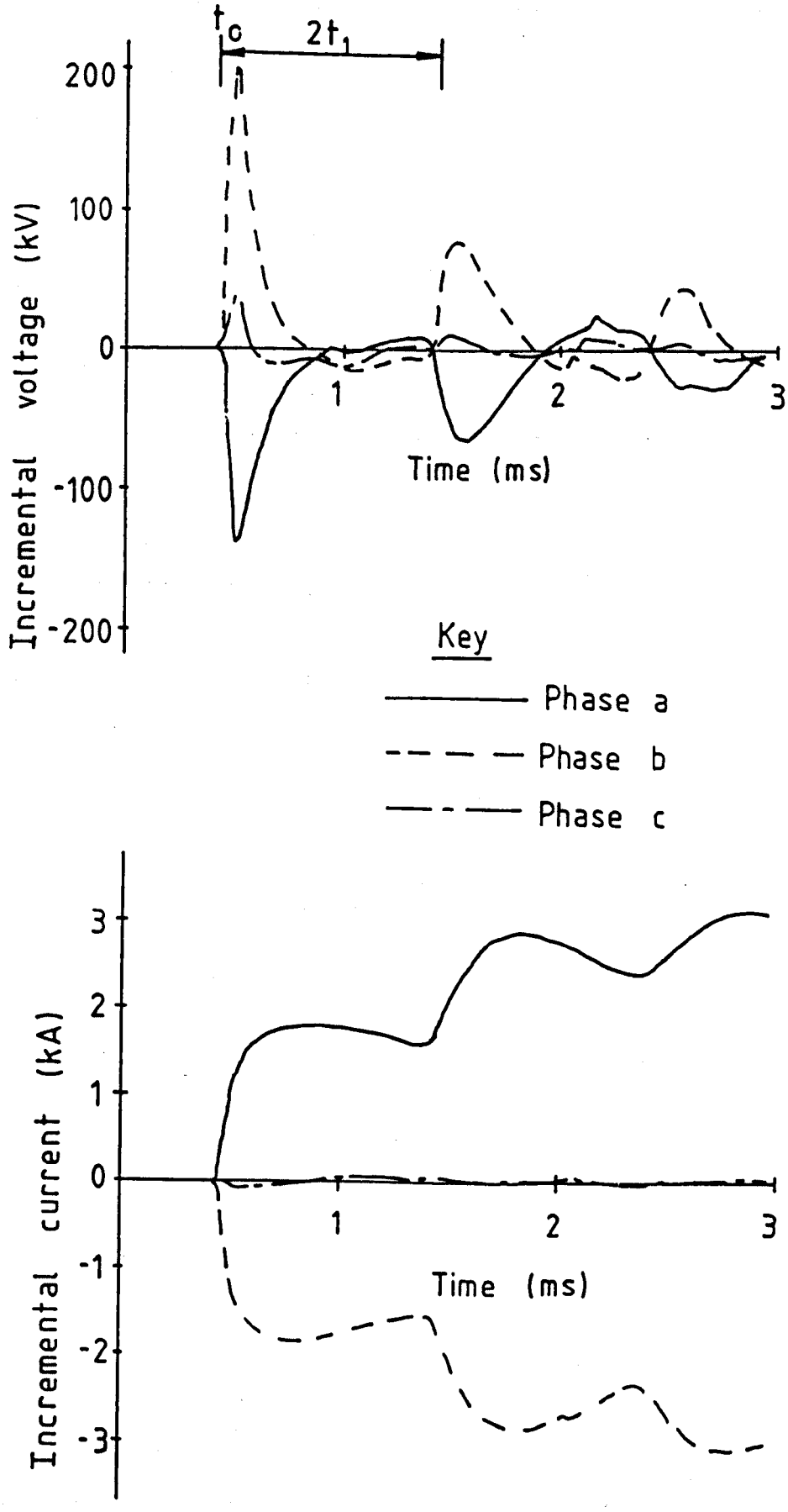

Figure 4.21 Incremental voltage and current transients produced during an internal phase-a to phase-b fault 140 km from the relaying point. The fault resistance on was 10 ohms phase to phase and the fault occurred at phase-a voltage maximum.

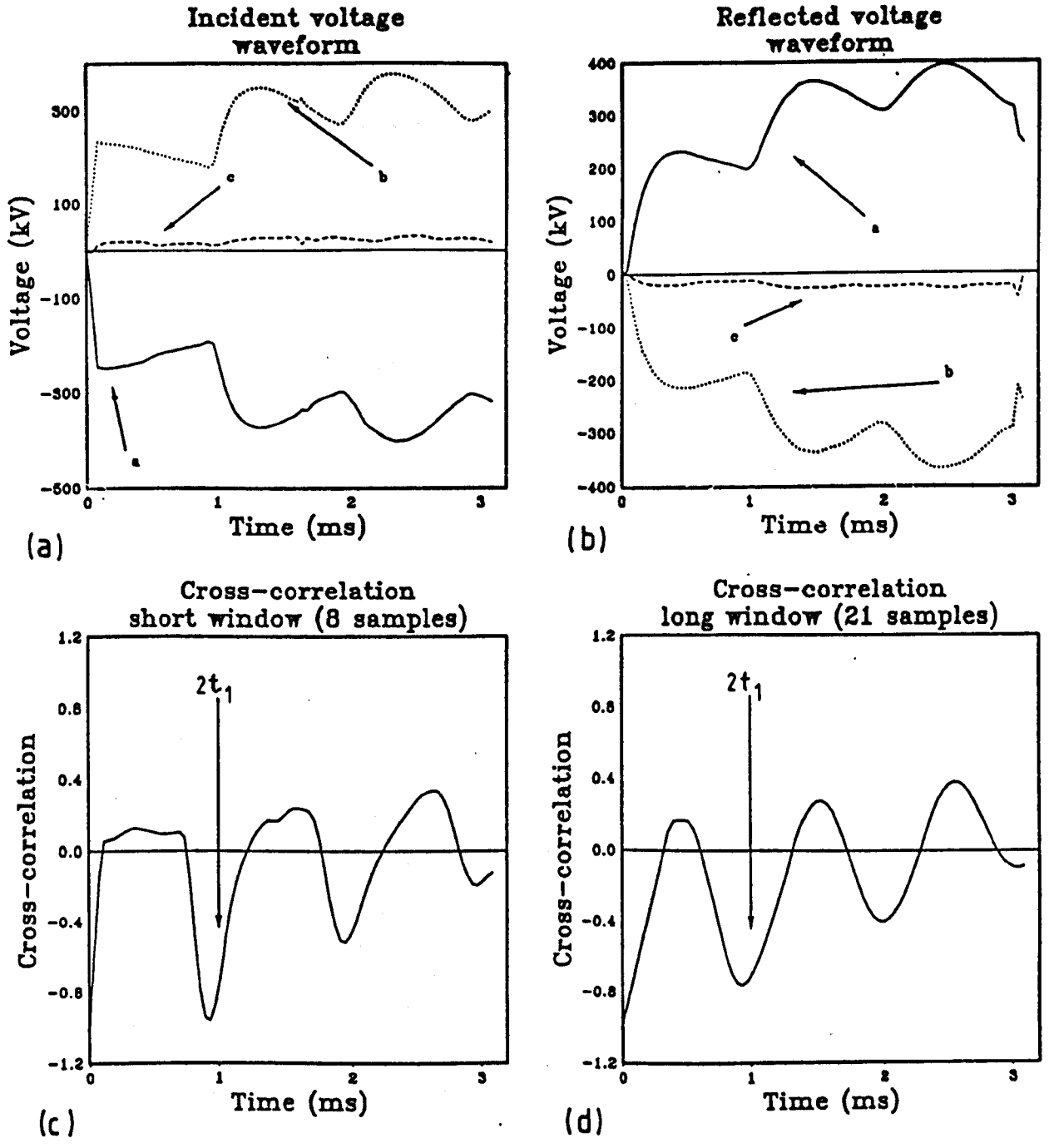

Figure 4.22 The relay outputs produced from the internal phase-a to phase-b fault transients given in figure 4.21.
(a) The incident aerial voltage at the relaying point. (b) The reflected aerial voltage at the relaying point. (c) The cross-correlation function using the short window length of 8 samples (0.32 ms). (d) The cross-correlation function using the long window length of 21 samples (0.84 ms).

$$\Delta R_{f2} = \pm 30\Omega \quad \text{for } R_f \to 0 \tag{4.79}$$

$$\frac{\Delta R_{f2}}{R_{f2}} = \pm 30\% \quad \text{for } R_f \to \infty \tag{4.80}$$

As with the other fault types, agreement between the two fault resistance estimates is then defined as

$$|R_{f1} - R_{f2}| < 60\Omega \quad \text{for} \quad R_{f1} \to 0 \tag{4.81}$$

$$\frac{|R_{f1} - R_{f2}|}{R_{f1}} < 60\% \quad \text{for} \quad R_{f1} \to \infty \tag{4.82}$$

The fault resistance estimates for the transients given in figures 4.21 and 4.22 are given in table 4.6. There is agreement between the fault resistance estimates for the trough at time$2t_1$for the long window (21 samples) of the cross-correlation function. The trough time is at 0.94 milliseconds which indicates a fault location at

$$x_a = 141 \pm 6 \qquad km \tag{4.83}$$

Table 4.6 Internal fault x=140 km

$R_{f1}(\Omega)$	$R_{f2}(\Omega)$	Trough time (ms.)	x_a (km)
18.0	5.0	0.94	141.0

The line round trip amplitude at time 1.33 milliseconds was positive (0.3) which then confirms the fault is internal.

The corresponding results for an external fault occurring 140 km from the far busbar (busbar 2), are given in figures 4.23 and 4.24 and table 4.7. These results show no agreement between the fault resistance estimates and the trough amplitude at time 2τ (1.33 ms) is negative (-1.4). The fault is then identified and confirmed as being an external fault beyond the far busbar.

Table 4.7 External fault x=340 km

$R_{f1}(\Omega)$	$R_{f2}(\Omega)$	Trough time (ms.)	x_a (km)
-44.0	296.0	0.16	47.0
63.3	-110.0	0.94	141.0

The fault resistance estimates, for phase-a to phase-b faults 140 km from the relaying point, as the fault resistance varies are given in figure 4.25a. There is good agreement between the fault resistance estimates up to about the aerial mode surge impedance (260 ohms). Larger fault resistance have a high wave transmission coefficient so other incident waves, from the far busbar, distort the second incident wave V_{2i}. The second estimate of the fault resistance then becomes unreliable.

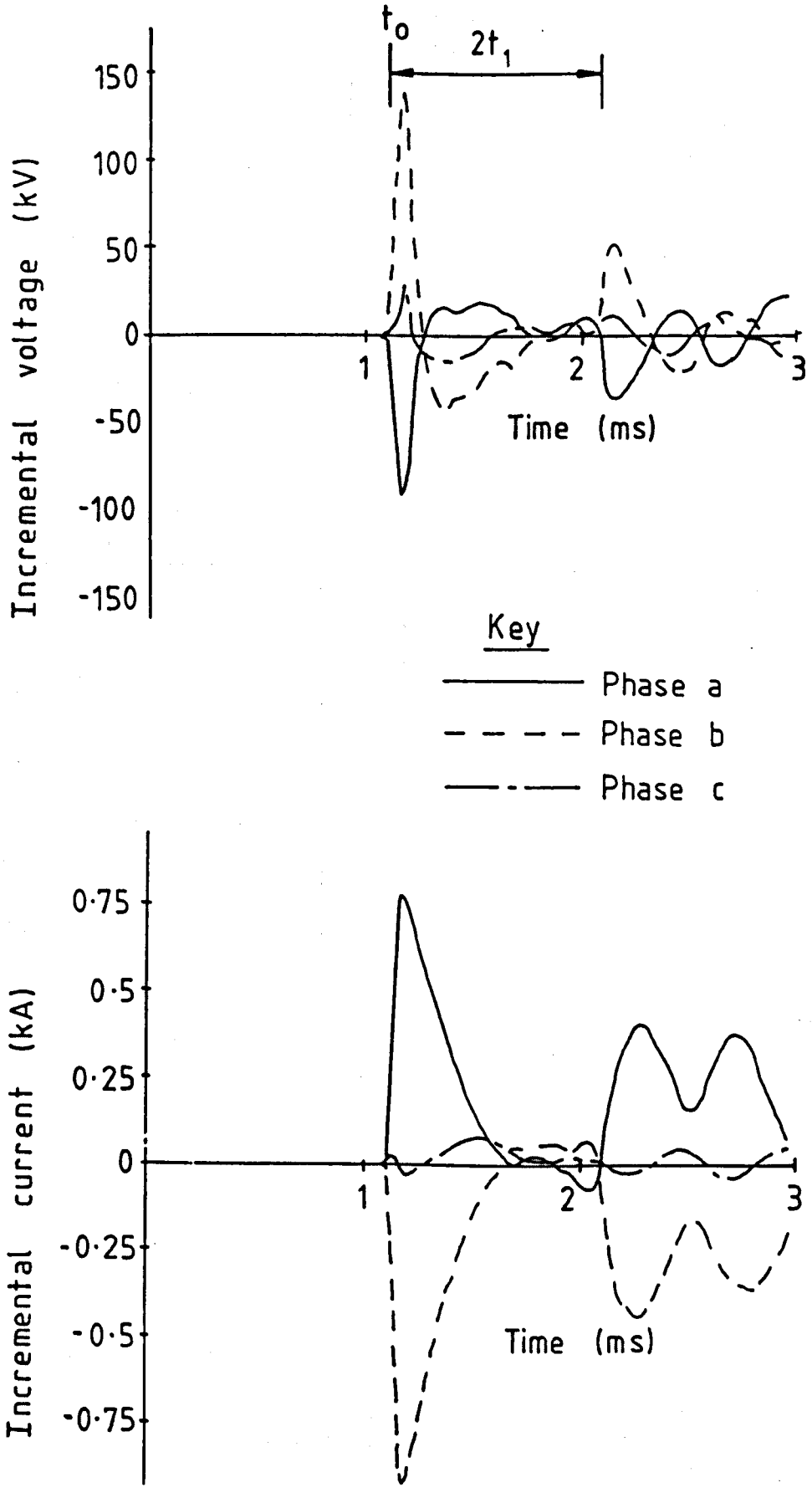

Figure 4.23 Incremental voltage and current transients produced during an external phase-a to phase-b fault 340 km from the relaying point (140 km from the far busbar). The fault resistance on was 10 ohms phase to phase and the fault occurred at phase-a voltage maximum.

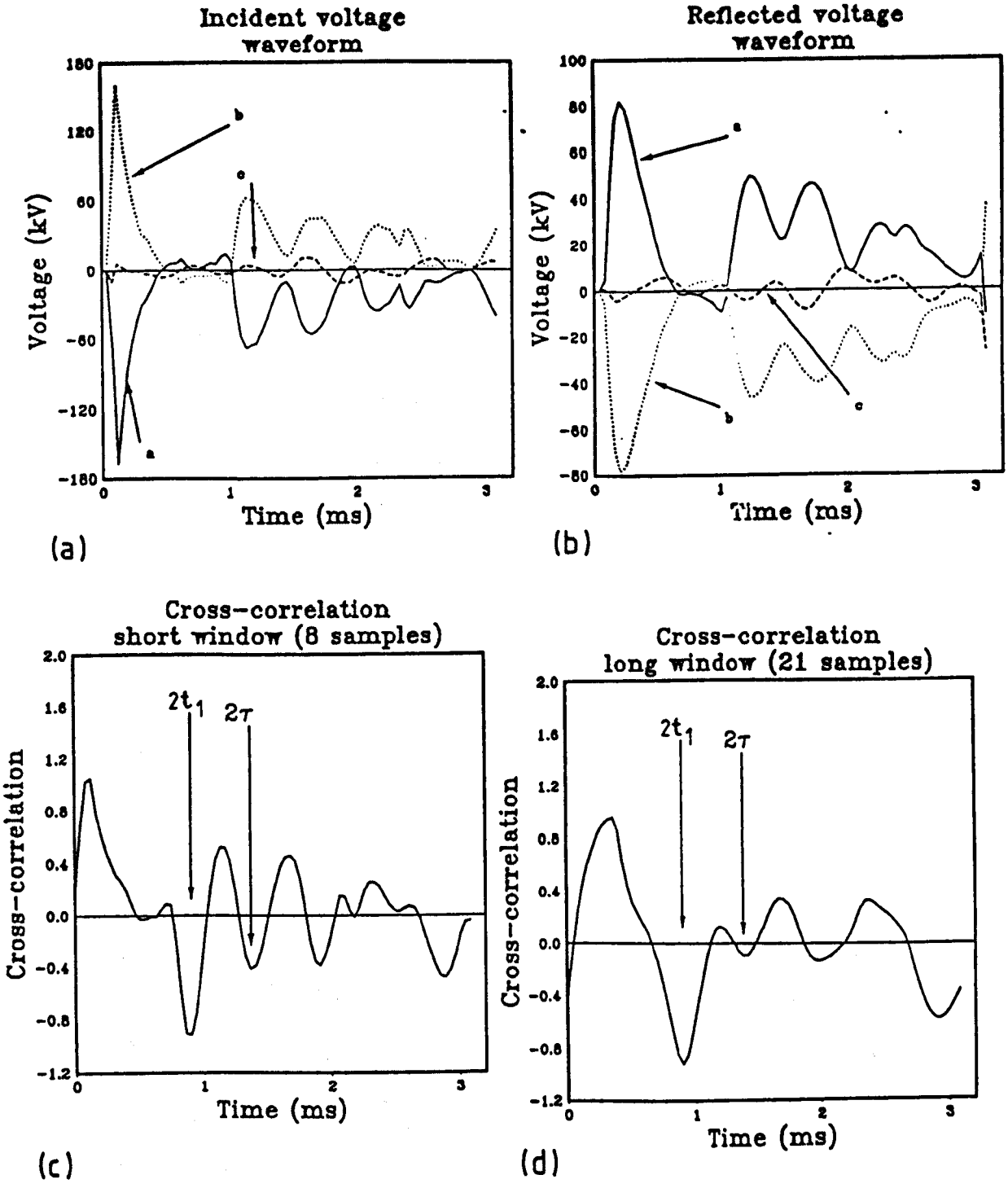

Figure 4.24 The relay outputs produced from the external phase-a to phase-b fault transients given in figure 4.23.
(a) The incident aerial voltage at the relaying point. (b) The reflected aerial voltage at the relaying point. (c) The cross-correlation function using the short window length of 8 samples (0.32 ms). (d) The cross-correlation function using the long window length of 21 samples (0.84 ms).

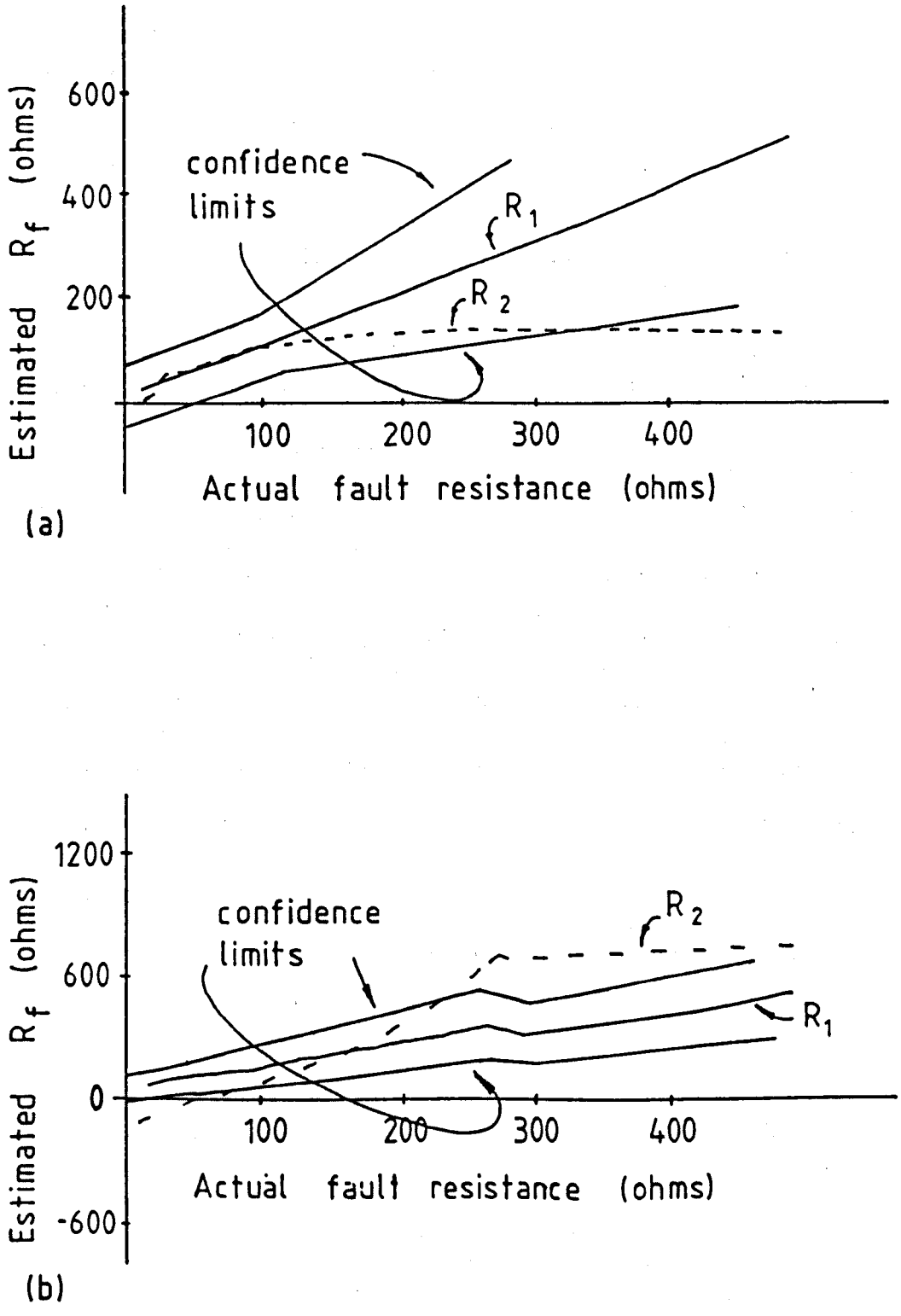

Figure 4.25 Fault resistance estimates for phase-a to phase-b faults against the actual fault resistance. (a) Faults 140 km from the relaying point occurring at phase-a voltage maximum. Good agreement between the fault resistance estimates is possible for fault resistances up to at least the line aerial mode surge impedance ($Z_a \approx 240\Omega$). (b) External faults 340 km from the relaying point (140 km from busbar 2) occurring at phase-a voltage maximum.

Figure 4.26 shows the amplitude of the line round trip wave given by the cross-correlation trough at time 1.33 milliseconds for the internal fault. From this it can be seen that the line round trip wave amplitude $V_{2\tau}$ is only positive with respect to the first reflected wave amplitude $V_{\tau 1}$ for resistances less than about $Z_a/2$ (130 ohms). This is in agreement with the theory given in chapter 2.

Internal phase to phase faults can therefore only be identified for fault resistances up to about 130 ohms ($Z_a/2$). This should not be a severe restriction as phase to phase faults usually have low fault resistances.

The fault resistance estimates against the actual fault resistance, for external faults 140 km from the far busbar (busbar 2), are shown in figure 4.25b. The faults occurred at phase-a voltage maximum which is close to the special phase angle of resistance estimate agreement. As the fault resistance increases the fault resistance estimates move into agreement, however, the line round trip wave is always negative with respect to the first reflected wave $V_{\tau 1}$ as shown in figure 4.26. All the external faults are therefore identified as being outside the protected line.

The variation of the estimated fault resistances as the initial voltage phase angle changes are shown in figure 4.27. The results for an internal fault 40 km from the relaying point of resistance 10 ohms are given in figure 4.27a. As with the single phase to ground fault, the resistance estimates are only reliable for initial fault voltage levels outside $\pi/12$ of voltage zero. In this case line voltage zero between phase-a and phase-b(phase-a phase angles 120^o and 300^o). All the line round trip waves were positive with respect to the first reflected wave (typically $V_{2\tau}/V_{\tau 1} \approx 0.3$).

Figure 4.27b shows the fault resistance estimates for an external fault 40 km from the far busbar with fault resistance 10 ohms. The estimates agree at only the special phase angles, however, the line round trip wave is always negative with respect to the first reflected wave (≈ -1.4). All the external faults will therefore be correctly identified as being beyond the far busbar.

4.5.3 Conclusions for phase to phase faults

Phase to phase fault resolution can be reduced to a single phase line fault solution. In doing so, however, it leads to the problem of using the line round trip wave $V_{2\tau}$ for complete fault discrimination. This then limits the identifiable internal faults to those of fault resistance below half the aerial mode surge impedance (120 ohms). Internal faults occurring within $\pi/12$ of line voltage zero may also not be identified.

This is not thought to be a severe limitation as phase to phase faults will have a low impedance as they do not involve the ground.

All external faults, however, are correctly identified so relay over reach should not occur.

4.6 Phase selection

Since there are three very different routines for the different fault types, there will have to be an initial phase selection procedure to select the correct routine.

A suitable phase selection procedure is that proposed by Bollen [46] which can successfully distinguish between symmetric faults, phase to ground faults and phase to phase faults. Unfortunately, at some phase angles, the

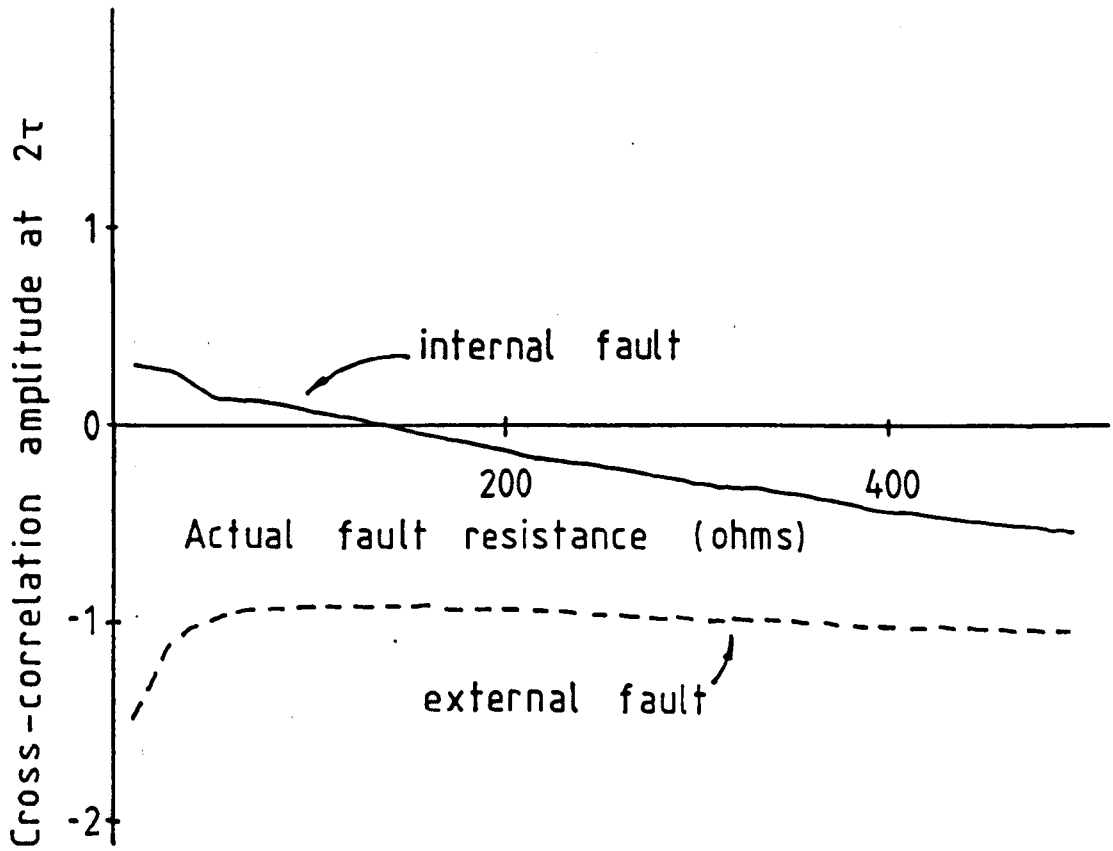

Figure 4.26 The amplitude of the line round trip wave compared with the first reflected wave $V_{2\tau}/V_{\tau 1}$ against the actual fault resistance. The ratio is found from the amplitude of the cross-correlation function with the long window (21 samples) at time 2τ.

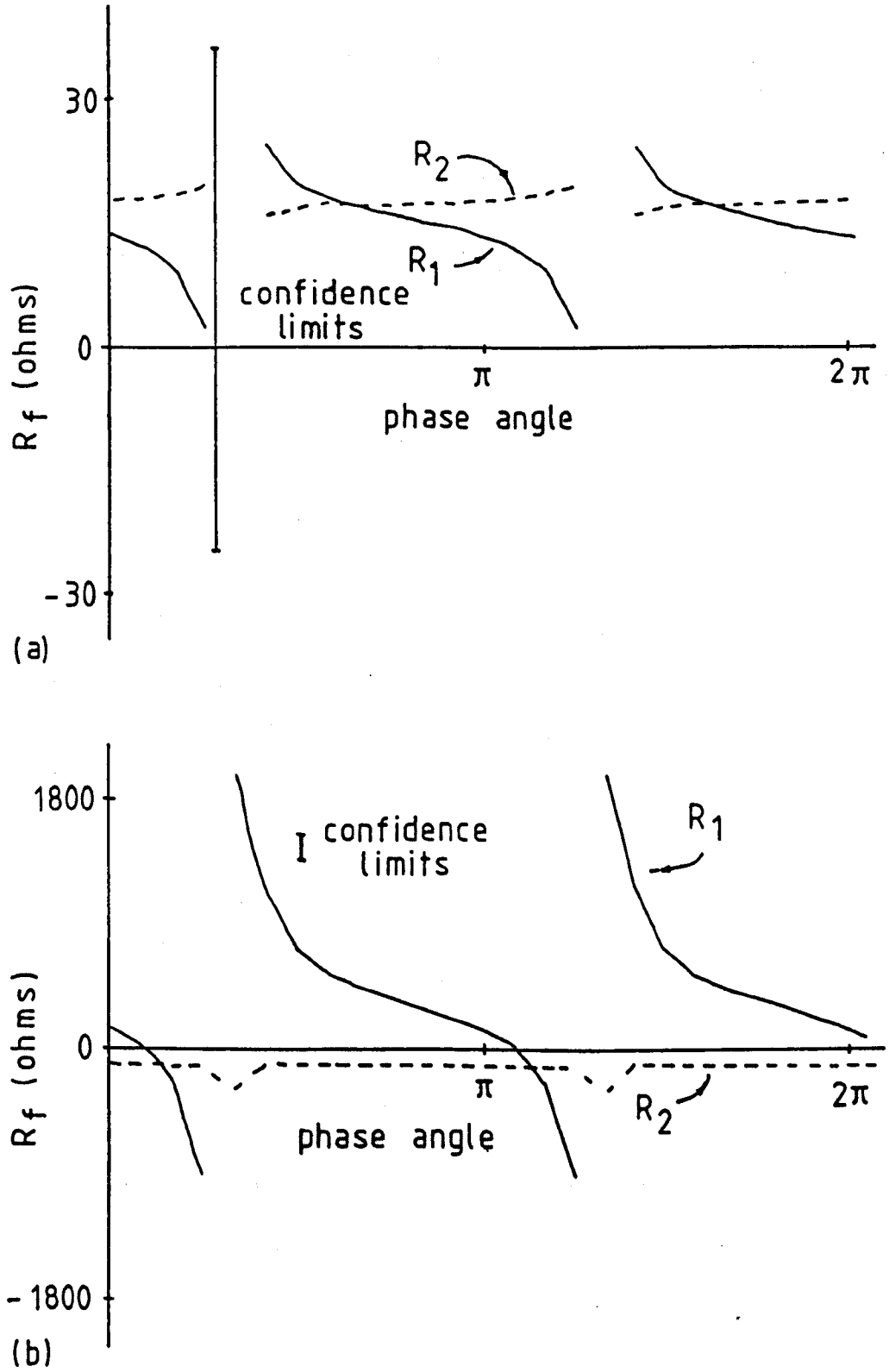

Figure 4.27 Fault resistance estimates for phase-a to phase-b faults against initial phase-a fault voltage phase angles. (a) Internal faults 40 km from the relaying point. The actual fault resistances were 10 ohms phase to phase. Good agreement is achieved for all phase angles not within $\pi/12$ of line voltage zero (phase-a $\pi/3$ and $5\pi/6$). (b) External faults 240 km from the relaying point (40 km from busbar 2). The actual fault resistances were 10 ohms phase to phase. Good agreement between the fault resistance estimates is only observed at two narrow regions in the cycle (special angles).

routine takes an excessive time to distinguish between symmetric faults and single phase to ground faults. It is therefore necessary to include in the procedure an assessment of the ground mode or mode 1 amplitude, so that symmetric and single phase to ground faults can be distinguished rapidly. The other features of the phase selection procedure described here are then comparable to that proposed by Bollen [46].

At a suitable point after fault transients have been received at the protection point, the incident aerial voltage wave amplitudes $[V_i^a]$ are sampled and used for phase selection. Six parameters are set from the aerial voltage amplitudes and one is given by the incident ground mode. The seven parameters are defined as

$$\begin{aligned} S_1 &= b_1 V_1^a(b) - b_2 V_1^a(a) \\ S_2 &= b_3 V_1^a(c) - b_4 V_1^a(a) \\ S_3 &= b_5 V_1^a(b) - b_6 V_1^a(c) \\ S_4 &= V_1^a(c) \\ S_5 &= V_1^a(b) \\ S_6 &= V_1^a(a) \\ S_7 &= V_1^g \end{aligned} \tag{4.84}$$

where V_1^a is the incident aerial voltages , V_1^g is the incident ground mode voltage and the parameters b are given by

$$\begin{aligned} b_1 &= \frac{3(2z_{13}^s - z_{23}^s - z_{33}^s)}{z_{11}^s + z_{22}^s + z_{33}^s - z_{12}^s - z_{13}^s - z_{23}^s} \\ b_2 &= \frac{3(2z_{23}^s - z_{13}^s - z_{33}^s)}{z_{11}^s + z_{22}^s + z_{33}^s - z_{12}^s - z_{13}^s - z_{23}^s} \\ b_3 &= \frac{3(2z_{12}^s - z_{23}^s - z_{22}^s)}{z_{11}^s + z_{22}^s + z_{33}^s - z_{12}^s - z_{13}^s - z_{23}^s} \\ b_4 &= \frac{3(2z_{23}^s - z_{12}^s - z_{22}^s)}{z_{11}^s + z_{22}^s + z_{33}^s - z_{12}^s - z_{13}^s - z_{23}^s} \\ b_5 &= \frac{3(2z_{13}^s - z_{12}^s - z_{11}^s)}{z_{11}^s + z_{22}^s + z_{33}^s - z_{12}^s - z_{13}^s - z_{23}^s} \\ b_6 &= \frac{3(2z_{12}^s - z_{13}^s - z_{11}^s)}{z_{11}^s + z_{22}^s + z_{33}^s - z_{12}^s - z_{13}^s - z_{23}^s} \end{aligned}$$

where z_{jk}^s are elements of the line surge impedance matrix

The parameters b ensure that correct tripping occurs on untransposed transmission lines. From examination of the equations giving the amplitude of the first incident aerial voltage transient given in the previous sections (equations 2.38, 4.2, 4.22 and 4.68), it can be shown that the following phase selection criterion is valid.

$\|S_1\| < \delta$, all others $> \delta$	c-ground fault
$\|S_2\| < \delta$, all others $> \delta$	b-ground fault
$\|S_3\| < \delta$, all others $> \delta$	a-ground fault
$\|S_4\| < \delta$, all others $> \delta$	a-b fault
$\|S_5\| < \delta$, all others $> \delta$	a-c fault
$\|S_6\| < \delta$, all others $> \delta$	b-c fault
$\|S_7\| < \delta_g$, at least $5 > \delta$	symmetric fault

$\delta = 0.1$ p.u.

Note that,when a symmetric fault occurs; $|S_7|$ is less than δ_g and one other parameter can also be less than δ. However, for single phase faults, the ground mode is much greater than any of the other parameters. Therefore δ_g is set to the largest of the first six parameters so that correct phase selection between single phase to ground faults and symmetric faults occurs.

It should also be noted that, the sample point must be at a point when the initial ground mode transients have been received. This is typically at least 0.25 milliseconds after the arrival of the initial aerial transient, for lines up to 300 km in length. The data is therefore sampled at this point and averaged over three samples to reduce the effect of noise.

Faults within 40 km may cause incorrect phase selection due to the multiple travelling wave reflections that may occur within 0.25 milliseconds. Such faults would however be processed by another protection scheme.

Results indicate that correct phase selection is then possible with this routine for most faults at a distance of 40 to 300 km from the relaying point. Only symmetric faults occurring when one phase is at voltage zero causes incorrect phase selection to occur. In these cases the symmetric fault transients are identical to a phase to phase fault. In fact it has been found that, symmetric faults occurring when one phase is at voltage zero can be processed using the phase to phase routine for fault discrimination. The use of the line round trip wave $V_{2\tau}$ is also valid in these cases. Fault discrimination should not then be compromised.

Correct phase selection is shown in figure 4.28 which shows the S parameters for the three fault types presented in figures 4.4, 4.11, and 4.21

In conclusion, a rapid phase selection routine similar to that suggested by Bollen, but supplemented by an additional test to increase the speed of phase selection and additional coefficients to give correct phase selection on untransposed lines, is incorporated into the initial stages of the relay algorithm. Only symmetric faults occurring when one phase is at voltage zero and faults within 40 km of the relaying routine causes incorrect phase selection. Despite this fault discrimination is not compromised as such symmetric faults can be processed by the selected phase to phase fault routine and close up faults within 40 km of the relay will be left for another algorithm.

4.7 Conclusions from initial simulations

From the simulations of the three typical fault types, it appears that good fault discrimination is possible. The fault type can be rapidly identified and the correct procedure successfully implemented.

For symmetrical faults all internal and external faults can be correctly identified over a wide range of fault resistances and over the complete system cycle. This is important as, although symmetric faults are not common, they present the biggest problems to power system stability [82]. All external faults are rejected.

Internal phase to ground faults can only be identified for fault resistances up to about the aerial mode surge impedance ($Z_a \approx 240\Omega$). Internal faults occurring within $\pi/12$ of voltage zero can also not be identified. This should be adequate as rapid tripping is not important on less severe faults which can be protected with normal distance schemes.

External phase to ground faults are rejected provided that their location is confirmed by the ground mode delay. Despite the variability of the ground

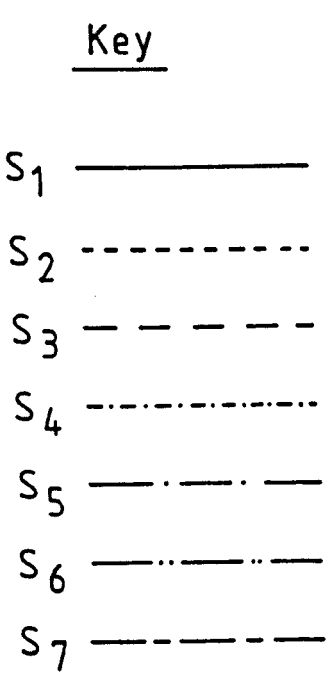
Key
S_1
S_2
S_3
S_4
S_5
S_6
S_7

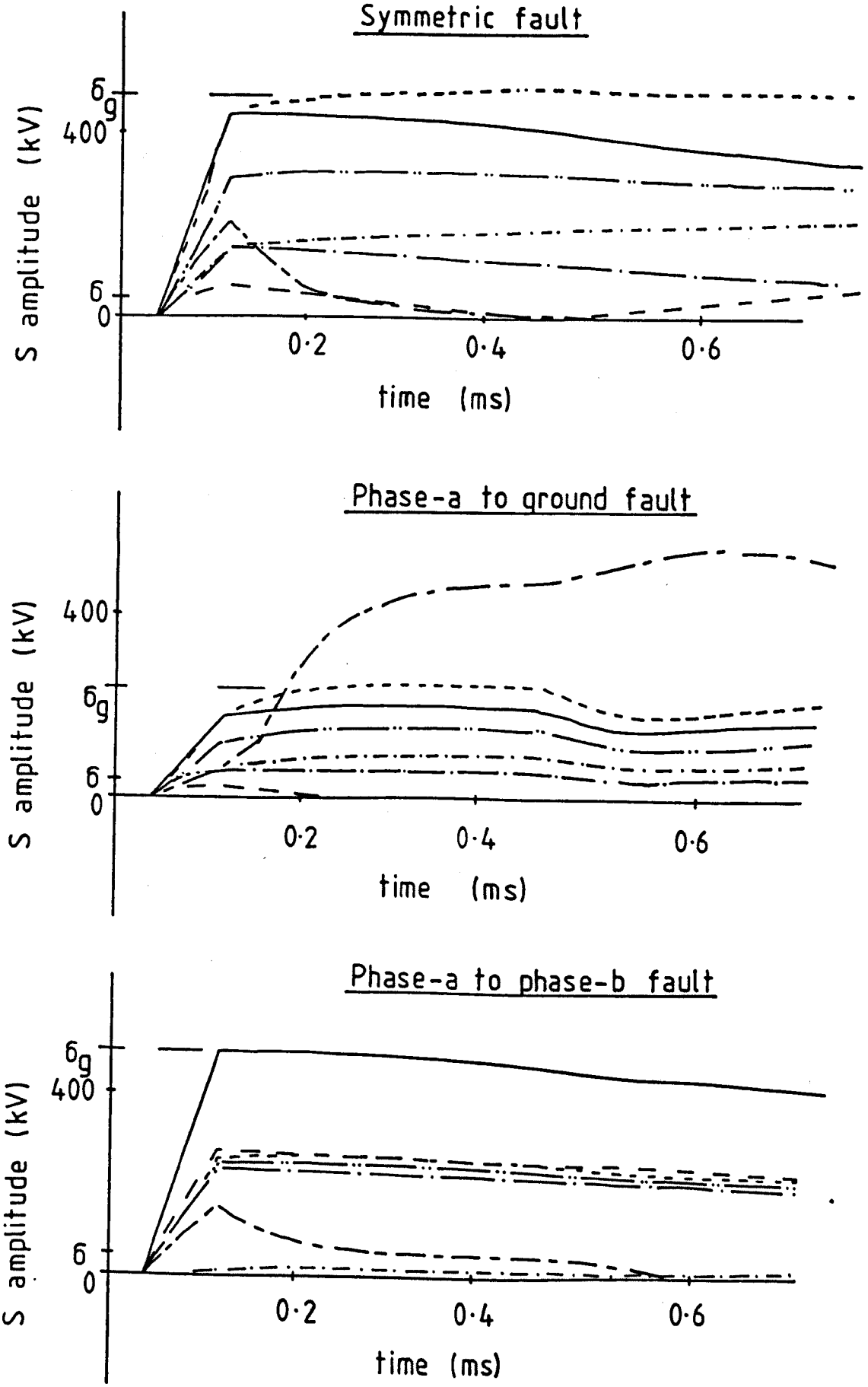

Figure 4.28 The phase selection S parameters for the three fault types given in figures 4.4, 4.11 and 4.21.

mode propagation velocity, good fault discrimination is possible for lines longer than about 90 km. All external phase to ground faults will then be rejected and relay over reach should not occur.

Internal phase to phase faults can only be detected for low fault resistances below half the aerial mode surge impedance ($Z_a/2 \approx 120\Omega$). The faults must also occur $\pi/12$ outside the line voltage zero. This is thought to be adequate as rapid fault clearing will only be important on severe faults and phase to phase fault resistances should be low as they do not involve the ground.

External phase to phase faults can be discriminated provided that they are confirmed by the presence of a large line round trip wave $V_{2\tau}$. The line round trip wave being signaled by a significant trough in the cross-correlation function at time 2τ. All external faults are then excluded and relay over reach does not occur.

From these results it can be seen that care has been taken to ensure that relay over reach does not occur. Excellent discrimination is achieved up to very substantial fault resistances.

CHAPTER 5

Compensated lines, Double circuit lines, bandwidth and noise.

5.1 Introduction

In the previous chapter the action of the algorithm was described, during three common line fault types. The line conditions considered were single circuit fully transposed or untransposed transmission lines. In this chapter the application of the algorithm to more complicated, but never the less quite common, system conditions will be examined. The effects of transducer bandwidth and noisy signals will also be investigated.

The first section will describe the application of the algorithm to compensated transmission lines and the next section will discuss the approach necessary for the protection of double circuit lines. Both compensated lines and double circuit lines are very common features of long transmission lines, so it is important to ensure that this algorithm will provide good fault discrimination for these cases. In the last section the required transducer bandwidth and signal to noise ratio, necessary for the resolution of the fault transient travelling-waves, will be specified.

The results shown in this chapter indicate that this relay algorithm is applicable to real EHV transmission line environments.

5.2 Protection of series compensated lines

The load capability and performance of many existing and future high voltage transmission lines can be improved by the installation of series capacitors [83]. Consequently, series capacitors are finding increased use in EHV systems. The main advantages are [83]; improved stability, an increase in transmissible power, improved voltage control, and proper power division among circuits operated in parallel and having different transmission capacities.

There appears to be some disagreement on the optimal series capacitor locations. Locations along the line are preferred in Scandinavia as shown in figure 5.1 [84], while locations at the line terminations are used by the majority of U.S. utilities [85], as shown in figure 5.2. The mid-point gives optimal compensation [83] but locating the series capacitors at the line terminations reduces the installation and maintenance costs [85].

Typical configurations are therefore either; 50 % compensation at the line centre or up to 70 % compensation split between the two line terminations. Note that for 400 kV or 500 kV transmission lines the line resistance to reactance ratio is about 1/10 therefore compensation greater than about 70 % leads to prohibitive line loss for the increased power transmission levels [83].

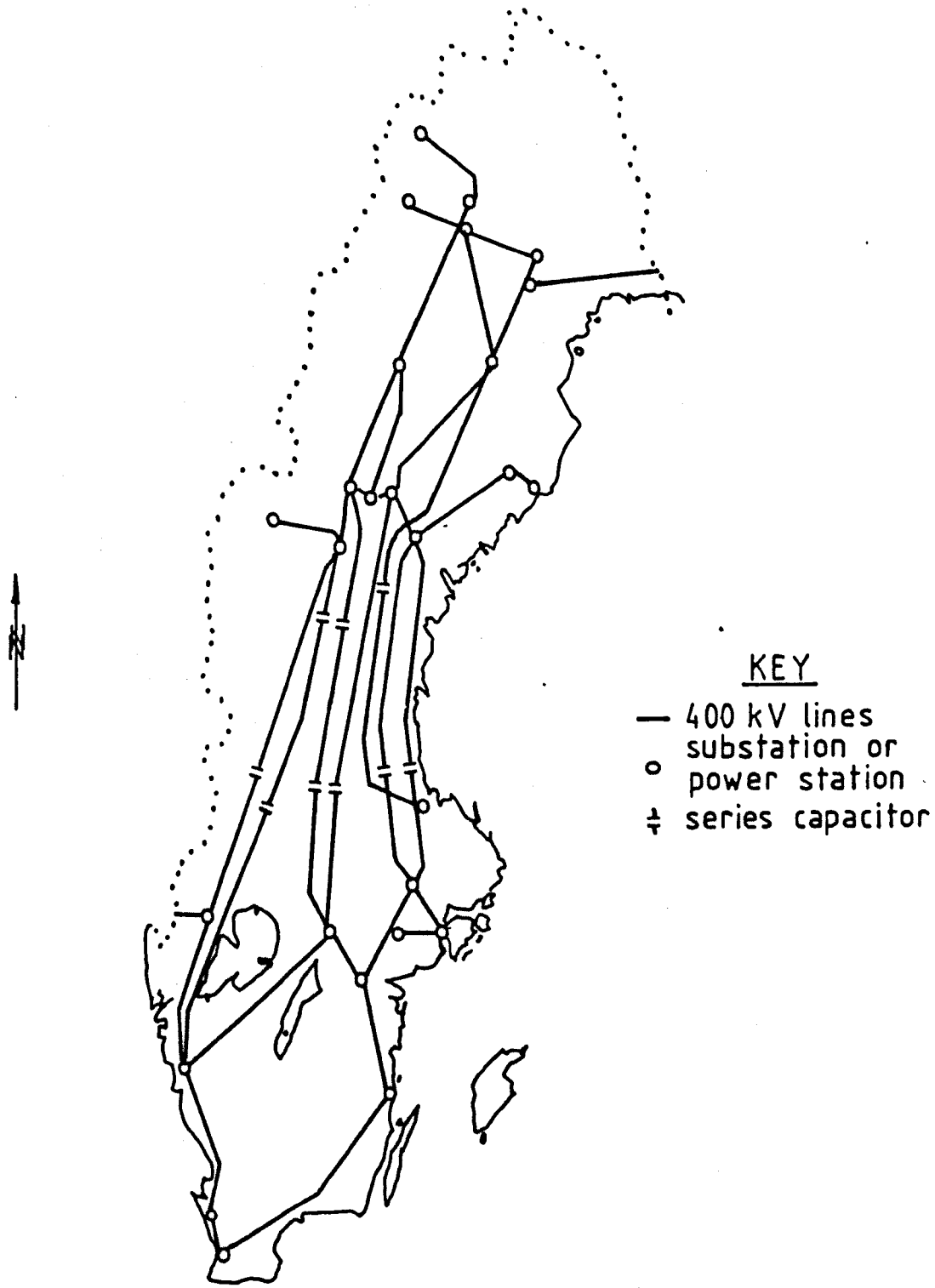

Figure 5.1 The Swedish 400 kV transmission line system in 1973. After Jancke et al., 1975 [84].

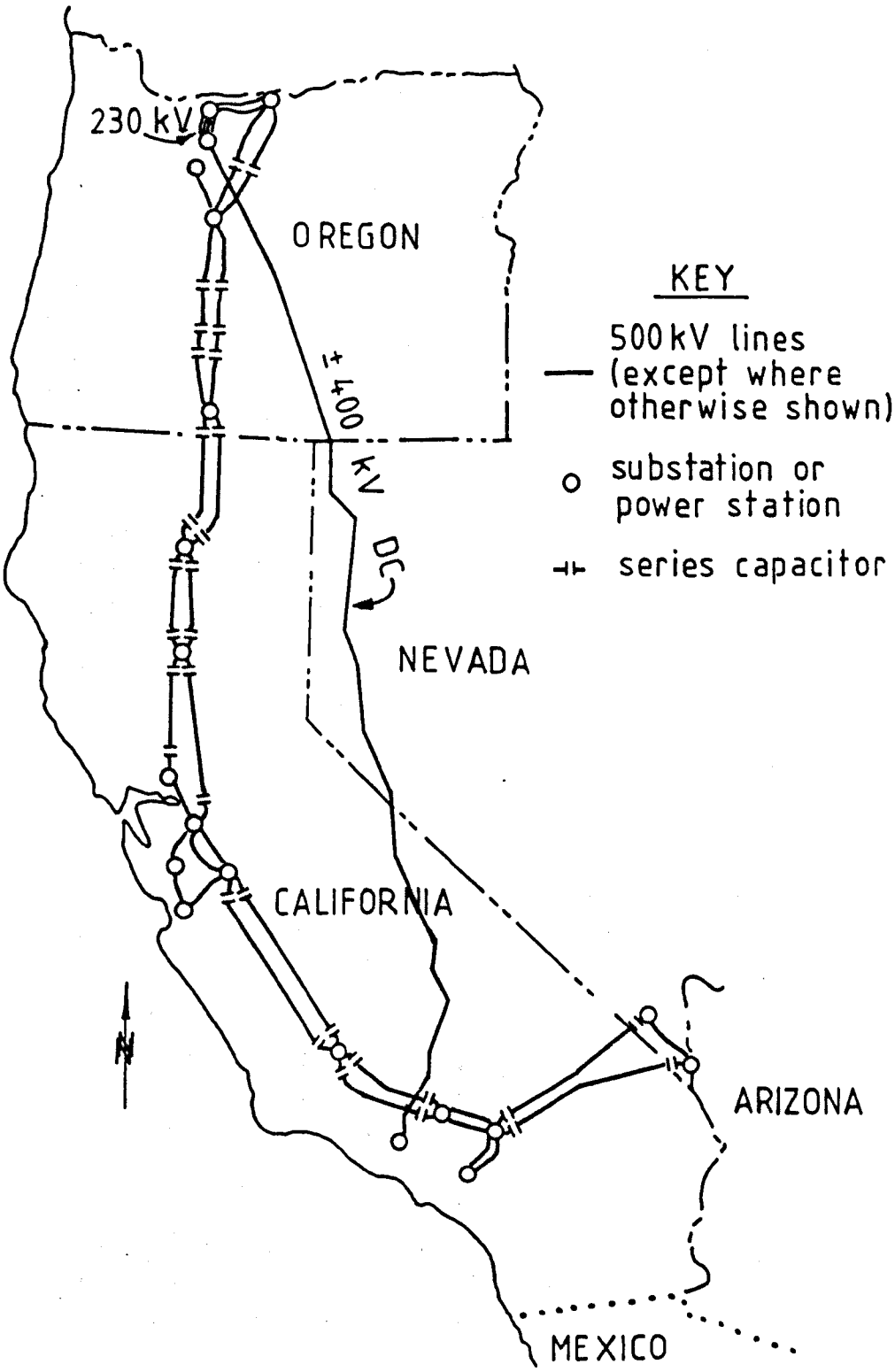

Figure 5.2 The United States Pacific EHV transmission line system and adjacent systems in 1970. After Maneatis et al., 1971 [85].

It is, therefore, a reasonable assumption that all future long EHV transmission lines will be compensated by one of the above mentioned schemes and any EHV protective equipment must be adaptable for such compensated lines. This section then outlines the adaptation of this high speed relay algorithm to these compensated lines. The results presented then show that correct fault discrimination between internal and external faults is possible.

The compensated line configurations studied are given in figure 5.3. It is expected that the series capacitors will be virtually "transparent" to the fault travelling-waves as they consist of high frequency transients ($> 500Hz$). The fault transients are then only distorted by the capacitor spark gap flashover.

The main features of the application of the relay algorithm to compensated lines are then; an adjustment of the initial steady state fault voltage estimation to include the series capacitor reactance, followed by, an assessment of the likelihood and effect of rapid series capacitor spark gap flashover within the relay operating times.

It is then shown that this travelling-wave relay can protect compensated lines satisfactorily, unlike conventional distance schemes which have severe problems due to possible voltage and/or current inversion [86] and [87].

5.2.1 Compensated Steady State Voltage Profile

With a series capacitor in the centre of a lossless single phase transmission line of length l, the line voltage v_x at a distance x from the relaying point shown in figure 5.4 is given by three two port networks in cascade. The first section is a line section of length $x - l/2$. The voltage and current at position x can then be found in terms of the voltages and current at the far side of the series compensation v_3, i_3 using equations 2.9 and 2.10 which gives

$$\begin{bmatrix} \mathrm{v_x} \\ \mathrm{i_x} \end{bmatrix} = \begin{bmatrix} \cos\beta_0(x-l/2) & -jZ_s\sin\beta_0(x-l/2) \\ -\frac{j}{Z_s}\sin\beta_0(x-l/2) & +\cos\beta_0(x-l/2) \end{bmatrix} \begin{bmatrix} \mathrm{v_3} \\ \mathrm{i_3} \end{bmatrix} \tag{5.1}$$

The next section is a series capacitance that has a reactance of χ_c, at the system frequency, thus

$$\begin{bmatrix} \mathrm{v_3} \\ \mathrm{i_3} \end{bmatrix} = \begin{bmatrix} 1 & j\chi_c \\ 0 & 1 \end{bmatrix} \begin{bmatrix} \mathrm{v_2} \\ \mathrm{i_2} \end{bmatrix} \tag{5.2}$$

The last section is a line section of length $l/2$ from the series compensation to the relaying point, so we can put

$$\begin{bmatrix} \mathrm{v_2} \\ \mathrm{i_2} \end{bmatrix} = \begin{bmatrix} \cos\beta_0 l/2 & -jZ_s\sin\beta_0 l/2 \\ -\frac{j}{Z_s}\sin\beta_0 l/2 & +\cos\beta_0 l/2 \end{bmatrix} \begin{bmatrix} \mathrm{v_0} \\ \mathrm{i_0} \end{bmatrix} \tag{5.3}$$

The equations 5.1, 5.2 and 5.3 can then be combined to give

$$\begin{aligned} \mathrm{v_x} = & \\ & \mathrm{v_0}(\cos\beta_0 x + \chi_c/Z_s\cos\beta_0(x-l/2)\sin\beta_0 l/2) \\ & +\mathrm{i_0}(-jZ_s sin\beta_0 x + j\chi_c\cos\beta_0 l/2\cos\beta(x-l/2)) \end{aligned} \tag{5.4}$$

Let the voltage and current phasors, at the protection point at the time of arrival of the initial fault transients, be given as

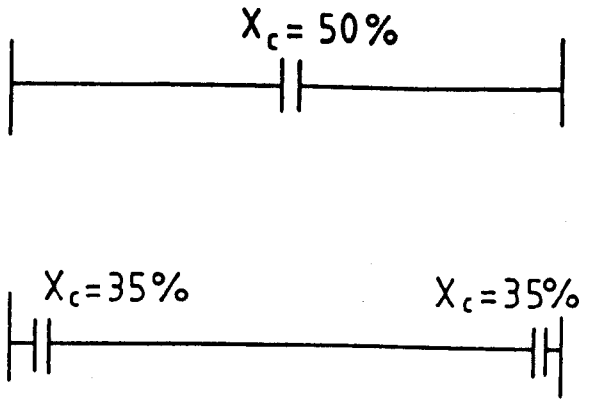

Figure 5.3 The two compensated line configurations considered in this study.

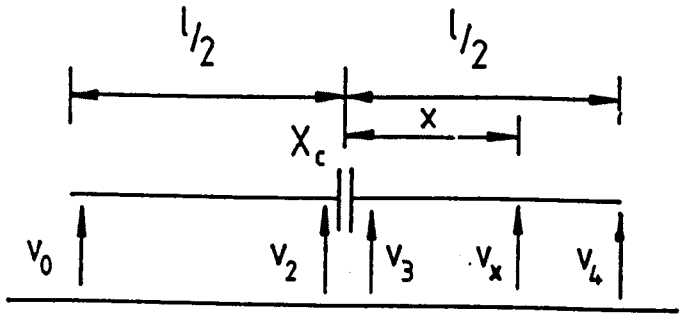

Figure 5.4 The phase voltages at points along a compensated transmission line.

$$v_0(t_0) = |v_0|e^{j\theta_1} \quad (5.5)$$

$$i_0(t_0) = |i_0|e^{j\theta_2} \quad (5.6)$$

From the timing of the cross-correlation trough and equation 2.18 the steady state voltage at the relaying point at the time of fault instigation can then be traced back using equations 2.14 and 2.16. The initial fault voltage can then be expressed in terms of the fault voltage at the relaying point at the onset of the fault transients. The initial fault voltage level is then given as

$$\begin{aligned} &v_f(t_0 - t_1) = \\ &\quad |v_0|e^{\theta_1 - \beta_0 x}(\cos\beta_0 x + \chi_c/Z_s cos\beta_0(x - l/2)\sin\beta_0 l/2) \\ &\quad +|i_0|e^{\theta_2 - \beta_0 x}(-jZ_s\sin\beta_0 x + j\chi_c\cos\beta_0 l/2\cos\beta_0(x - l/2)) \end{aligned} \quad (5.7)$$

For a three phase transmission line with balanced voltage and current levels, the initial fault voltage can be given in terms of the positive sequence values as given in section 2.4 which in this case gives

$$\begin{aligned} &v_f^p(t_0 - t_1) = \\ &\quad |v_0^p|e^{\theta_1 - \beta_0^p x}(\cos\beta_0^p x + \chi_c^p/Z_s^p cos\beta_0^p(x - l/2)\sin\beta_0^p l/2) \\ &\quad +|i_0^p|e^{\theta_2 - \beta_0^p x}(-jZ_s^p\sin\beta_0^p x + j\chi_c^p\cos\beta_0^p l/2\cos\beta_0^p(x - l/2)) \end{aligned} \quad (5.8)$$

where

$$\beta_0^p \approx \omega_0/c \quad (5.9)$$

$$Z_s^p \approx \frac{z_{11}^s + z_{22}^s + z_{33}^s - z_{12}^s - z_{23}^s - z_{13}^s}{3} \quad (5.10)$$

(5.11)

χ_0^p is the shunt capacitive reactance on each phase and θ_1, θ_2 are the initial voltage and current phase angles at the relaying point

The phase voltages can then be found from the transform given in equation 2.54.

When a fault occurs within the first half of the protected line, equation 2.51 will still be valid. The relay will then have to first check for faults on the relay side of the series compensation making use of equation 2.51 and then, if necessary, check for a possible fault location beyond the series compensation using equation 5.8. This can be synchronised with the switching between the cross-correlation window lengths, outlined in chapter 3, provided that the series compensation is at the line centre.

For series compensation located at the line terminations equation 5.8 can be used with the substitution; $l/2$ equals the distance from the relaying point to the series compensation. Equation 5.8 will then be valid for the region between the two series capacitor banks.

Thus it should be possible to estimate the initial fault voltage levels from; the steady state voltages and currents at the relaying point, the time

separation of the fault transient waves V_1 and V_{i2}, and a knowledge of the amount and type of series compensation on the transmission line. The relay algorithm will then proceed to calculate the first fault resistance estimate as described in the earlier chapters.

5.2.2 Flashover of the series capacitor spark gap.

In order to protect the series capacitors during fault conditions, spark gaps are fitted to limit the capacitor voltage. It will be shown that rapid capacitor protective spark gap flashover, within the time of arrival of the second incident wave V_{i2} to the relaying point, is very unlikely. The travelling wave routine should then operate correctly for all resolvable internal faults (faults at a distance greater than 40 km). Closer internal faults will have to be resolved with another routine and an initial current maximum check should ensure that this travelling wave routine does not operate for close internal faults (less than 40 km) which generate extremely rapid spark gap flashovers (within 0.3 milliseconds). External faults, which cause rapid spark gap flashover on external compensation, can not be distinguished by the initial fault current level. This travelling wave routine will therefore have to be shown to operate correctly during such external faults.

Typical over voltage limits are 2-3 p.u. [88], that is, the voltage limit for spark gap flashover is given by

$$v_{limit} = \frac{1}{\omega_0 C}[2p.u.]i_{rating}\sqrt{2} \tag{5.12}$$

where i_{rating} is typically 1140-1600 Amps [88] , $\omega_0 = 2\pi/f_0$ and C is the series capacitance

If we put $i_{rating} = 1$ kAmp and since $\omega_0 = 314$ rads/sec. for a system frequency of 50 Hz then

$$v_{limit} \approx \frac{9}{C} \text{ Volts.} \tag{5.13}$$

For a 400 kV transmission line, the maximum initial travelling wave phase voltage due to a solid fault is 327 kV. The surge impedance Z_s is typically 290 ohms on EHV transmission lines. It therefore follows that, the maximum initial phase current due to the first incident travelling wave V_1 is

$$\Delta i_{pmax} = \pm\Delta v_{pmax} Z_s = \pm 1.126 \; kAmps \tag{5.14}$$

If at the line termination there is a very strong source, the initial reflected wave amplitude V_r will be

$$V_r = -V_i \tag{5.15}$$

The initial incremental current at the line termination will then be

$$\begin{aligned} \Delta i &= -\frac{\Delta v_1}{Z_s} + \frac{\Delta v_r}{Z_s} \\ &= -\frac{2v_i}{Z_s} \end{aligned} \tag{5.16}$$

Thus, the maximum possible incremental current at the line termination can be quantified as

$$\Delta i_{pmax} = \pm 2.25 \; kAmps \tag{5.17}$$

A series capacitance between the fault and this line termination could therefore receive a maximum fault current causing its protective spark gaps to be the first to flashover.

For protection using the proposed travelling wave routine, it will be an advantage if the capacitor gaps do not flashover before the time of arrival of the second incident wave at $2t_1$. This will ensure that the second incident wave V_{i2} of an internal fault will be reasonably undistorted on reception at the relaying point, allowing it to be readily identified.

The voltage across the series capacitors during fault conditions can be given by

$$V_c = \frac{1}{C}\int_0^t \Delta i dt + v_{cs} \tag{5.18}$$

where v_{cs} is the steady state voltage across the series compensation which can be given in terms of the series current i_{cs} as

$$v_{cs} = -\frac{j i_{cs}}{\omega_0 C} \tag{5.19}$$

For reasonable stability and power factors it is extremely unlikely that the steady state current will lag the steady state voltage by more than $\pi/4$ radians [89]. Thus the maximum voltage across the series compensation should be about

$$v_{cs}^{max} = \frac{i_{rating}}{\omega_0 C} \approx 3.2C \; Volts \tag{5.20}$$

From equations 5.13 and 5.18 it follows that, the series capacitor spark gaps will flashover when

$$\frac{9}{C} = \frac{1}{C}\int_0^t \Delta i dt + v_{cs} \tag{5.21}$$

Thus, for precise measurement of the second incident wave V_{2i}, the following condition must apply

$$\frac{9}{C} - \frac{3.2}{C} > \frac{1}{C}\int_0^{2t_1} \Delta i_{pmax} dt \tag{5.22}$$

therefore

$$t_1 < 1.3ms. \tag{5.23}$$

Given that the aerial transients propagate at close to the speed of light (300 km/ms.), this relay algorithm should then easily protect lines up to 400 km in length. The travelling wave distortion, caused by the capacitor spark gap flashover, need only be considered for; exceptionally long lines, periods of large load current, or for external faults close to strong sources.

Extremely rapid spark gap flashover is likely to occur for faults extremely close to series compensation which is in turn close to a strong source. For

internal faults such faults would be too close for this travelling wave relay to apply and is rejected by their extremely high fault current. For external faults, however, such an event must not cause the relay to trip.

Figure 5.5 shows the transient travelling-wave Bewley lattice diagram for an external fault where the transient wave "FLASH," is caused by a rapid capacitor spark gap flashover of the adjacent series capacitor to the fault. In this example, the timing of the spark gap flashover is sufficient to give a transient wave "FLASH" which can be confused with the arrival of the second incident wave of an internal fault V_{i2}.

A simulated example of an early capacitor spark gap flashover was produced using the line configuration given in figure 5.6. For this configuration the compensation of the faulted external line is connected to a strong source (35 GVA) which gives rise to high fault currents. The simulated fault was a phase-a to ground fault occurring at phase-a voltage maximum with a low fault resistance of 0.1 ohms. The transients were simulated using the EMTP "SEMLYEN SETUP" to give an accurate time response of the series capacitor spark gap flashover.

The protective spark gap circuits of the series compensation usually have a natural frequency of about 800 Hz and a quality factor of about 2 [88]. The simulated spark gap circuits were then formed to give approximately this response and were as shown in figure 5.7. Note that studies have found that the exact form of the spark gap circuits does not have a major effect on the fault transients [90].

The simulated transients at the relaying point are for a phase-a to ground fault, occurring at phase-a voltage maximum located as shown in figure 5.6 . Figure 5.8a shows the deduced incident transient waves forms at the relaying point. The transient voltage waveform produced by the spark gap flashover is indicated by the label "FLASH" in figure 5.8a. This transient voltage waveform appears to have a 0.2 millisecond duration.

This extremely rapid spark gap flashover does not occur fast enough to produce a transient wave which could be confused with the second incident wave V_{i2} of an internal fault within the first half of the protected line(i.e. less than 0.7 ms.). There is therefore no relevant cross-correlation trough apparent in the cross-correlation function of the short window length (8 samples), as shown in figure 5.8b.

The long cross-correlation window (21 samples) does not produce a cross-correlation trough at the time of arrival of the incident wave "FLASH",as shown in figure 5.8c, because the transients have too short a duration. The long cross-correlation window does however produce an earlier trough, indicated as "x" in figure 5.8c, but this is too early to be relevant.

The spark gap flashover transient travelling-wave, due to an external fault, will not then lead to a relevant trough in the cross-correlation function, due to its timing and short duration.

The spark gap flashover transient travelling-wave may combine, however, with the line round trip wave $V_{2\tau}$ and broaden it. This broadened line round trip wave may then create an earlier cross-correlation trough. This earlier $V_{2\tau}$ wave could be confused with that of an internal fault's second incident wave V_{i2} for a fault just within the protected line. Such an event occurs for an external phase-a to ground fault, at location F_3 in figure 5.6, which occurs at a phase-a voltage phase angle of $\frac{3\pi}{4}$ radians. Figure 5.9a shows

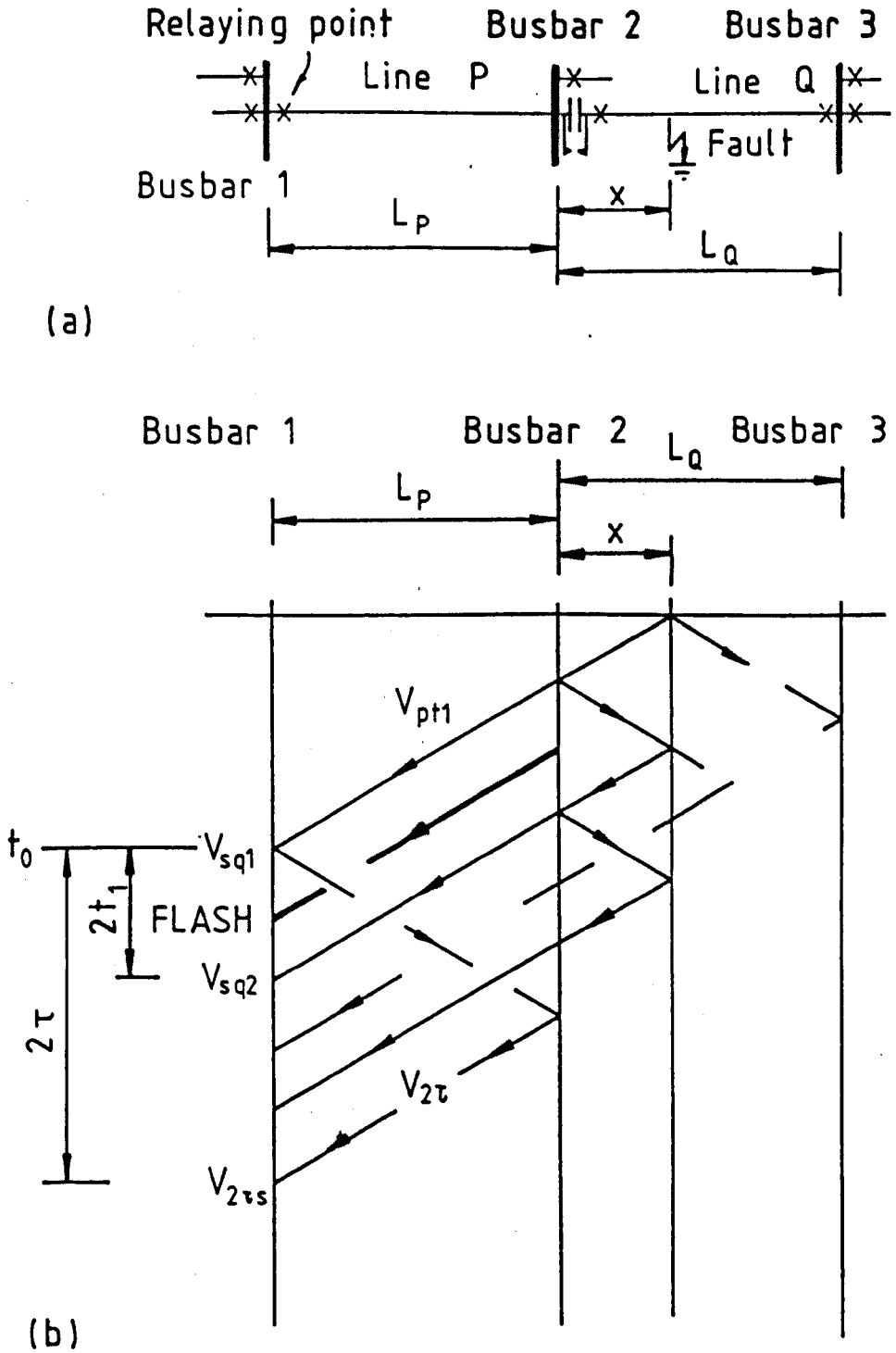

Figure 5.5 (a) A general line configuration with an external fault located near the series compensation. (b) The resulting fault transient Bewley lattice diagram, including the transient due to the capacitor spark gap flashover.

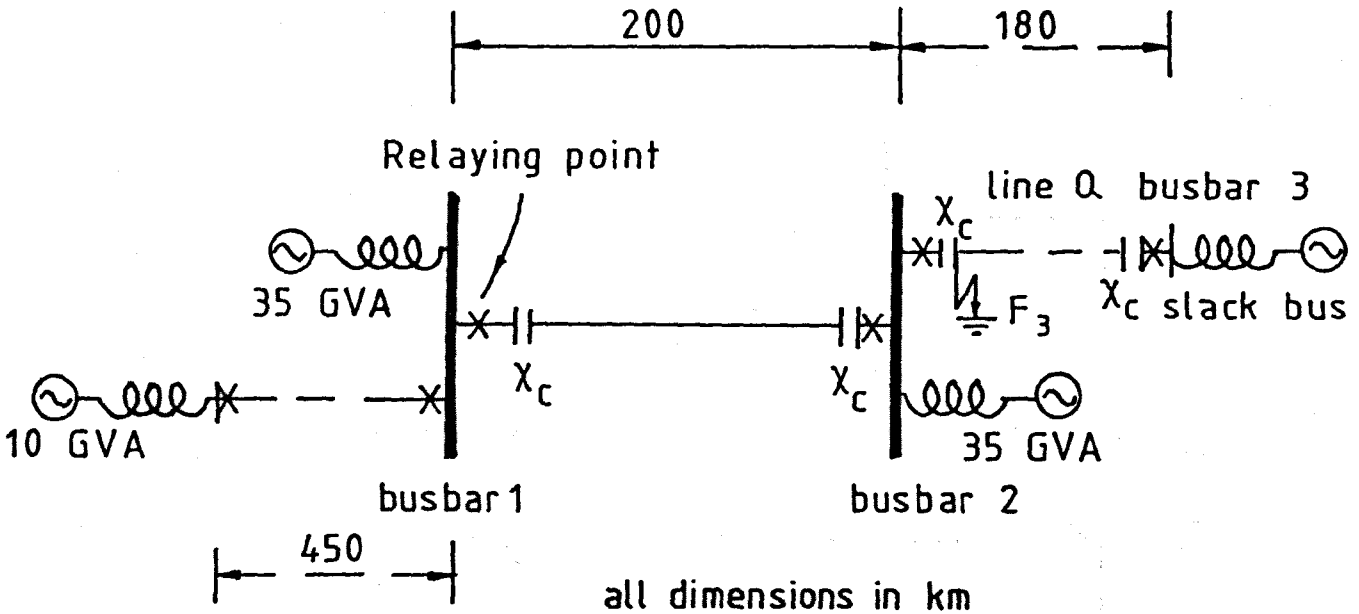

Figure 5.6 System configuration simulated to study the effects of capacitor spark gap flashover.

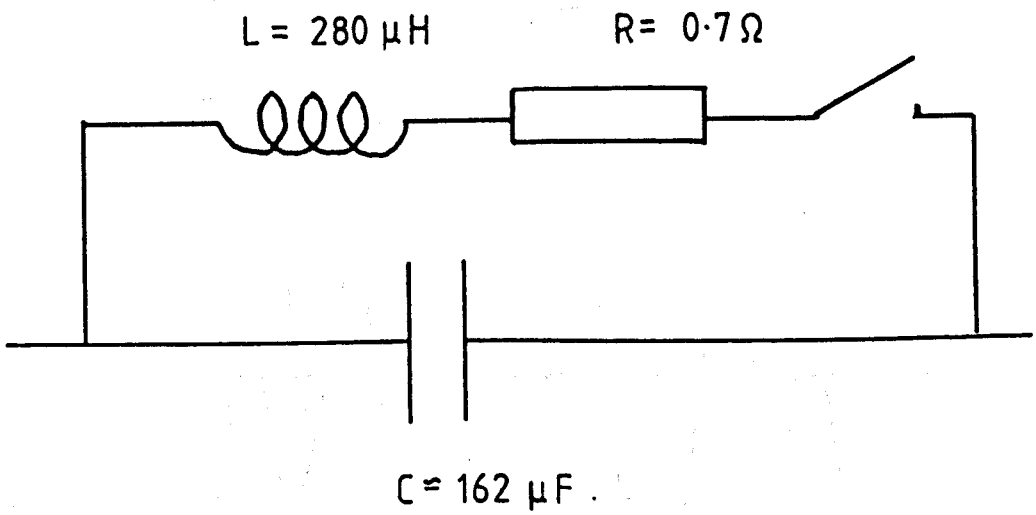

Figure 5.7 The modelled protective spark gap circuit.

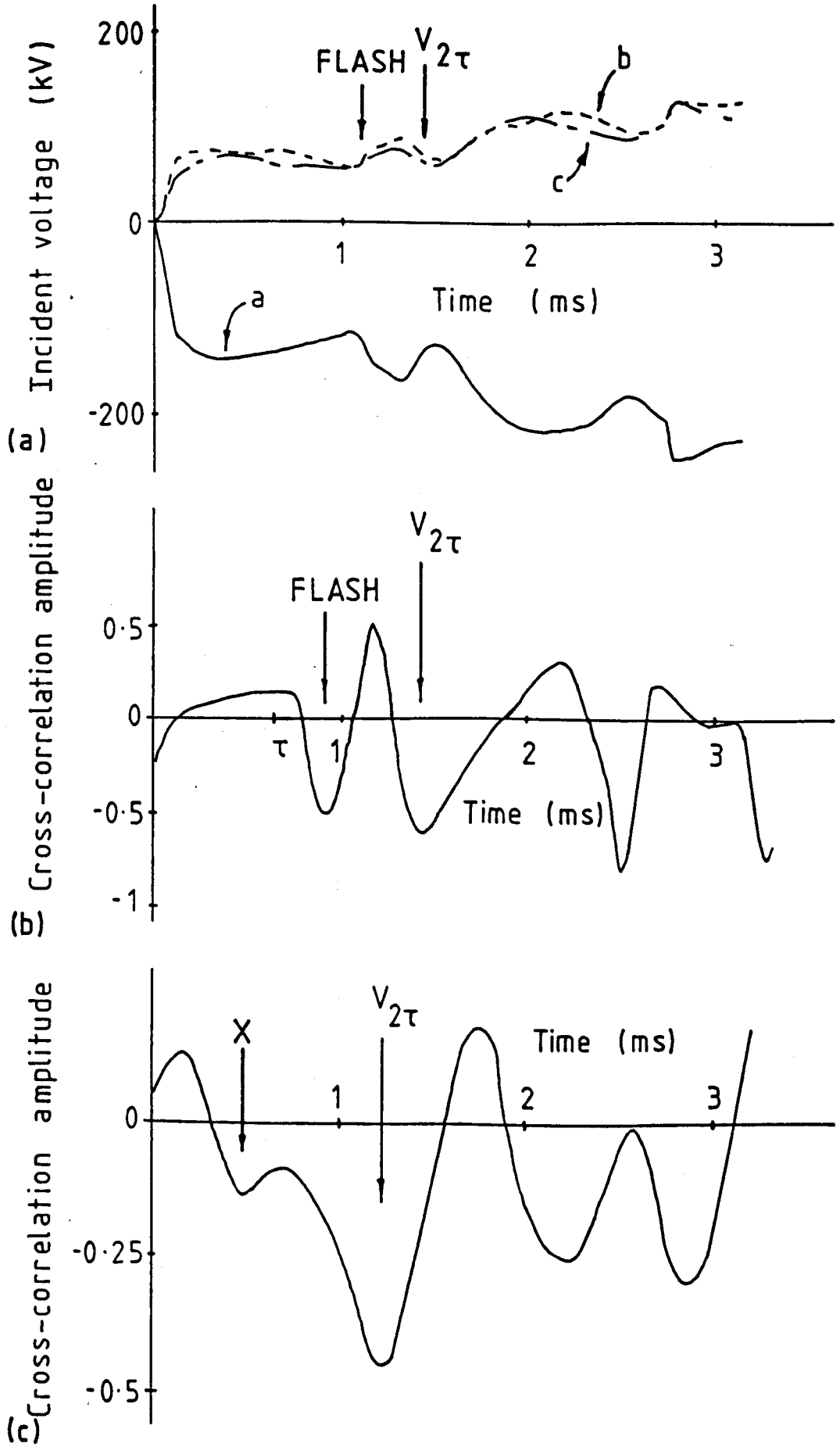

Figure 5.8 The relaying outputs for an external phase-a to ground fault occurring at phase-a voltage maximum and located at position F_3 on the configuration given in figure 5.6. (a) The deduced incident transient aerial waveforms with the transient due to the spark gap flashover indicated as "FLASH." (b) The cross-correlation using the short window (8 samples). (c) The cross-correlation using the long window (21 samples).

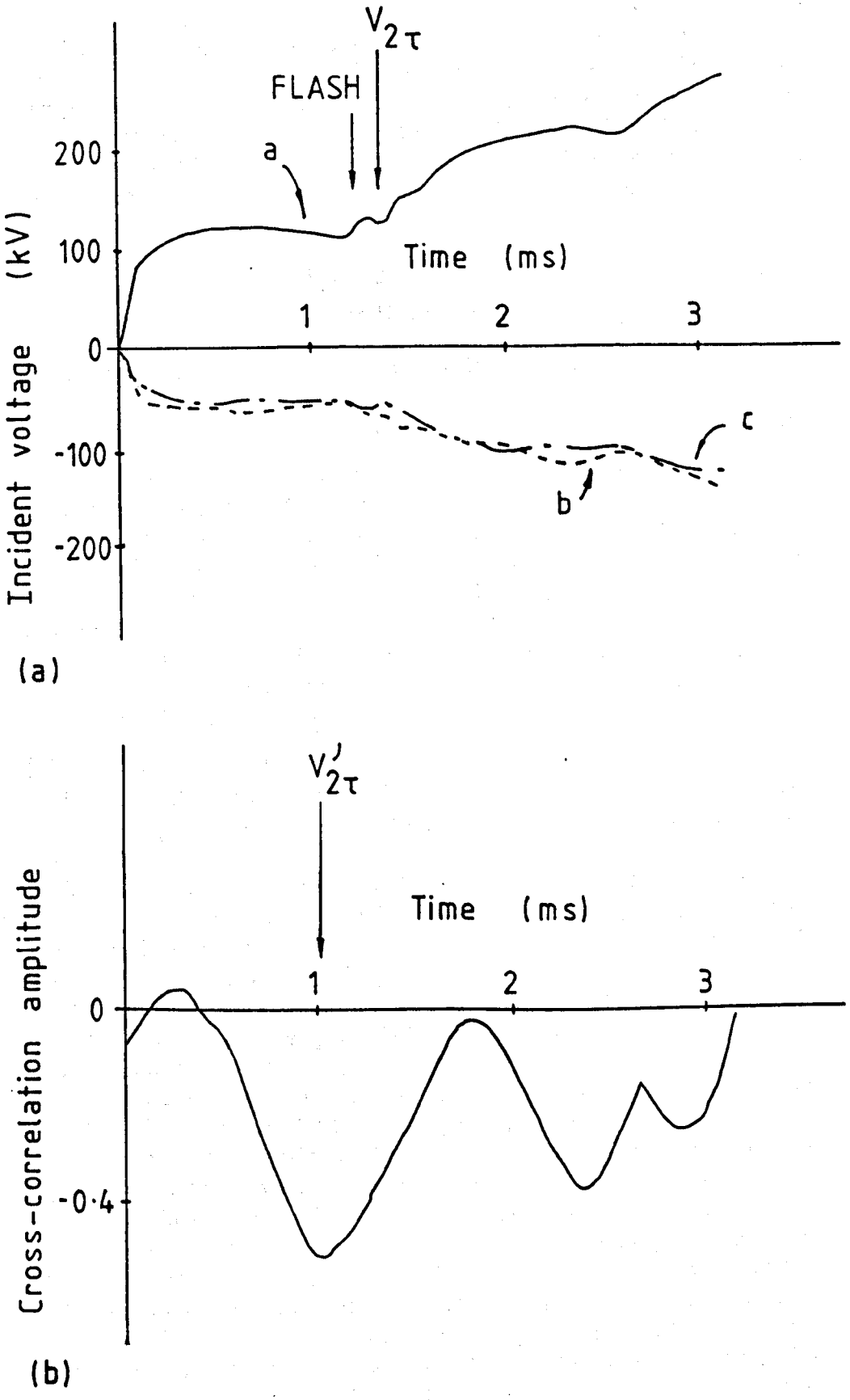

Figure 5.9 The relaying outputs for an external phas-a to ground fault occurring at phase-a voltage phase angle of $\frac{3\pi}{4}$ radians and located as for figure 5.8. (a) The deduced incident aerial waveform. (b) The cross-correlation using the long window (21 samples). The broadened line round trip wave is indicated as $V'_{2\tau}$.

the deduced incident aerial voltage transients for such a fault.

The merging of the spark gap flashover transient travelling-wave with the line round trip wave $V_{2\tau}$ gives an earlier cross-correlation trough $V'_{2\tau}$, for the long cross-correlation window, shown in figure 5.9b. This can be compared with the line round trip cross-correlation trough given in figure 5.8c. The timing of the cross-correlation trough given in figure 5.9b indicates an internal fault $176 \pm 6km$ from the relaying point. The two estimated fault resistance from the fault transients, using equations 4.27 and 4.28 were

$$R_{f1} = 29.3\ ohms \tag{5.24}$$

$$R_{f2} = 12.4\ ohms \tag{5.25}$$

The mode zero delay indicated a fault location at

$$x_g = 234 \pm 118\ km \tag{5.26}$$

From these results it appears that this external fault will be confused with an internal phase-a to ground fault.

As the transient travelling-waves due to the spark gap flashover have about a 0.2 millisecond duration, it is unlikely that the line round trip wave $V_{2\tau}$ will be broadened by more than 0.2 milliseconds. The distorted trough in the cross-correlation function $V'_{2\tau}$ will not then indicate a fault any closer than 25 km from the far line termination. If the protection zone is limited to 80% of the line length, over reach should not then occur for lines longer than about 150 km.

5.2.3 Results showing the relay response.

To illustrate the action of the relay algorithm on compensated lines, the results for a phase-a to ground fault on the two main line configurations are presented.

The first line configuration simulated, shown in figure 5.10, incorporates 70% compensation which is split between the two line terminations as 35% at each end. This configuration is typical of that adopted on the long EHV transmission lines in America [85].

The fault location simulated was 40 km from the relaying point. This is expected to be the severest possible fault location as close up faults give the earliest capacitor gap flashover.

Figure 5.11a shows the times of the capacitor gap flashover after fault inception, for various initial fault voltage phase angles. The capacitor gap setting, as given by equation 5.12, was 56 kV. From figure 5.11a it appears that the protective spark gaps will not flashover within 2.2 milliseconds for this fault. The second incident wave V_{i2} is then readily detected.

The two estimates of the fault resistance, at various inception fault voltage angles, are given in figure 5.12a. The initial voltage amplitude at the fault location was estimated using equations 5.8 and 2.54. The first estimate of the fault resistance was then given by equation 4.27. The second estimate of the fault resistance was found using the short correlation window (8 samples) and equation 4.28 as for the un-compensated case. The two estimates agree for all initial phase angles, except those near voltage zero

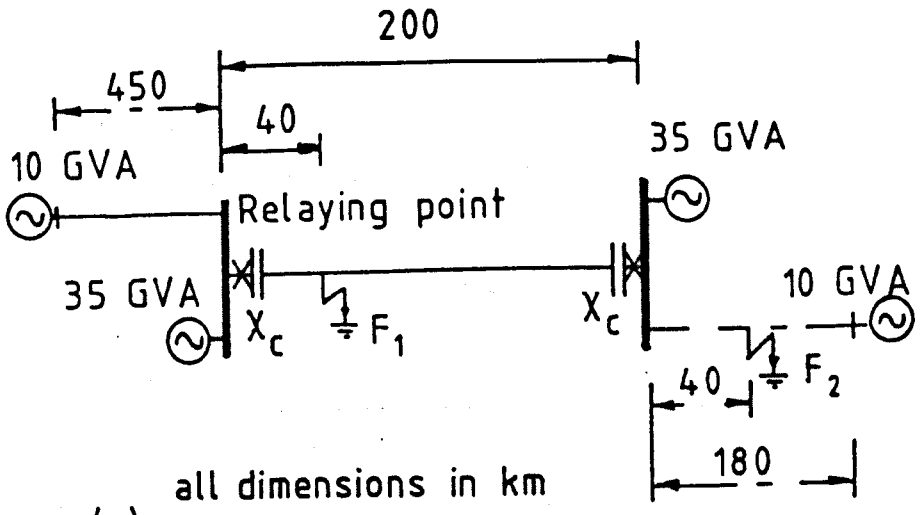

(a)

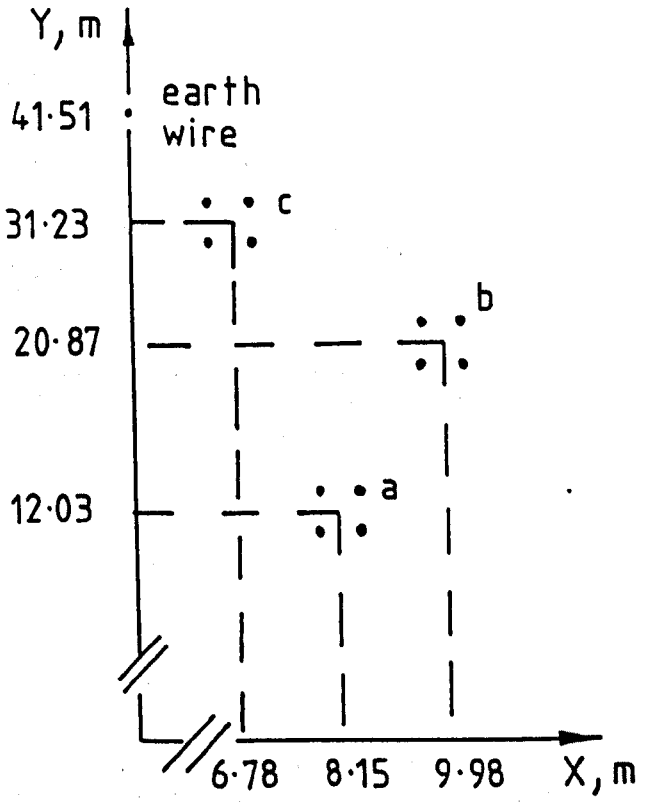

(b)

Figure 5.10 The simulated line configuration for the study of faults on lines with compensation at the line terminations.

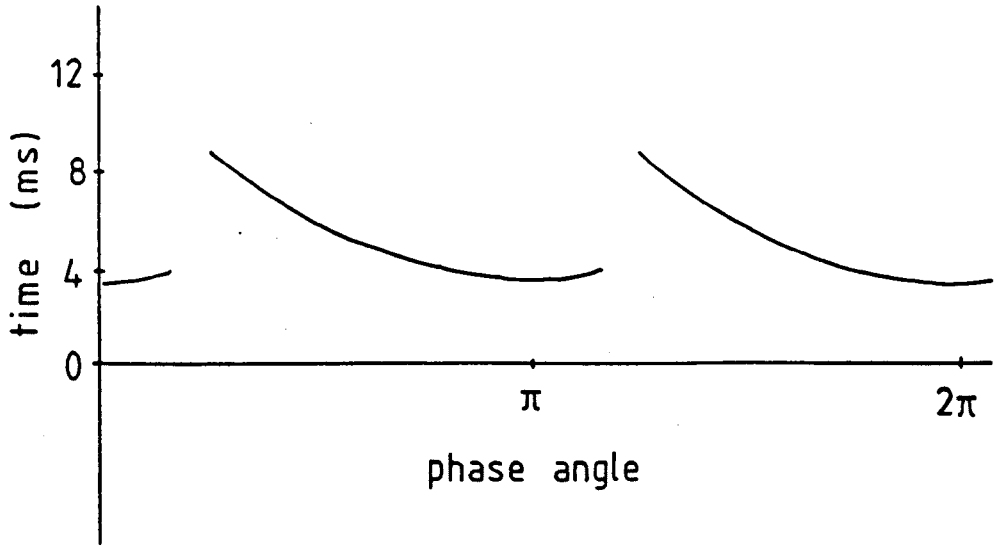

(a)

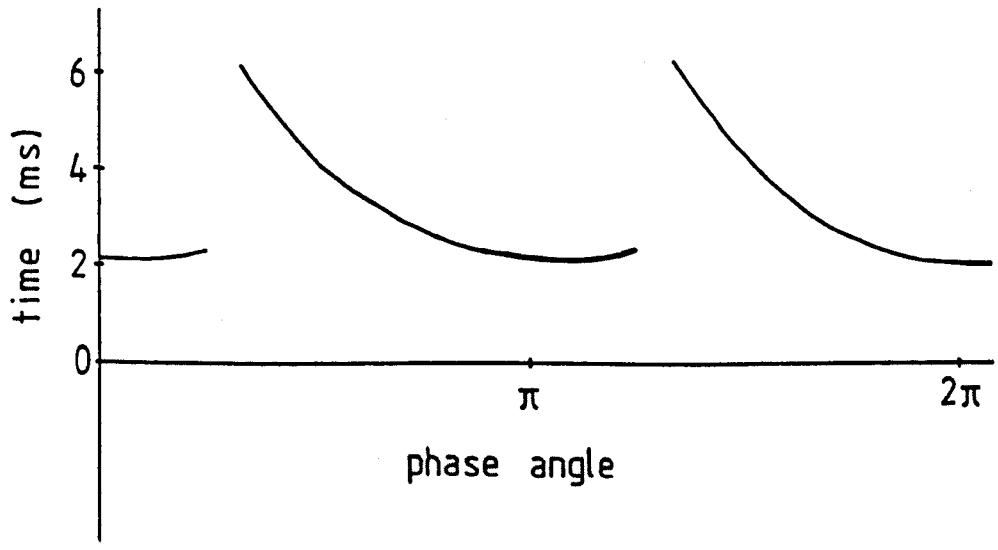

(b)

Figure 5.11 Minimum times for the capacitor spark gap flashover after the fault instigation against initial fault voltage phase angle.

(a) Results for the line configuration given in figure 5.10.

(b) Results for the line configuration given in figure 5.13.

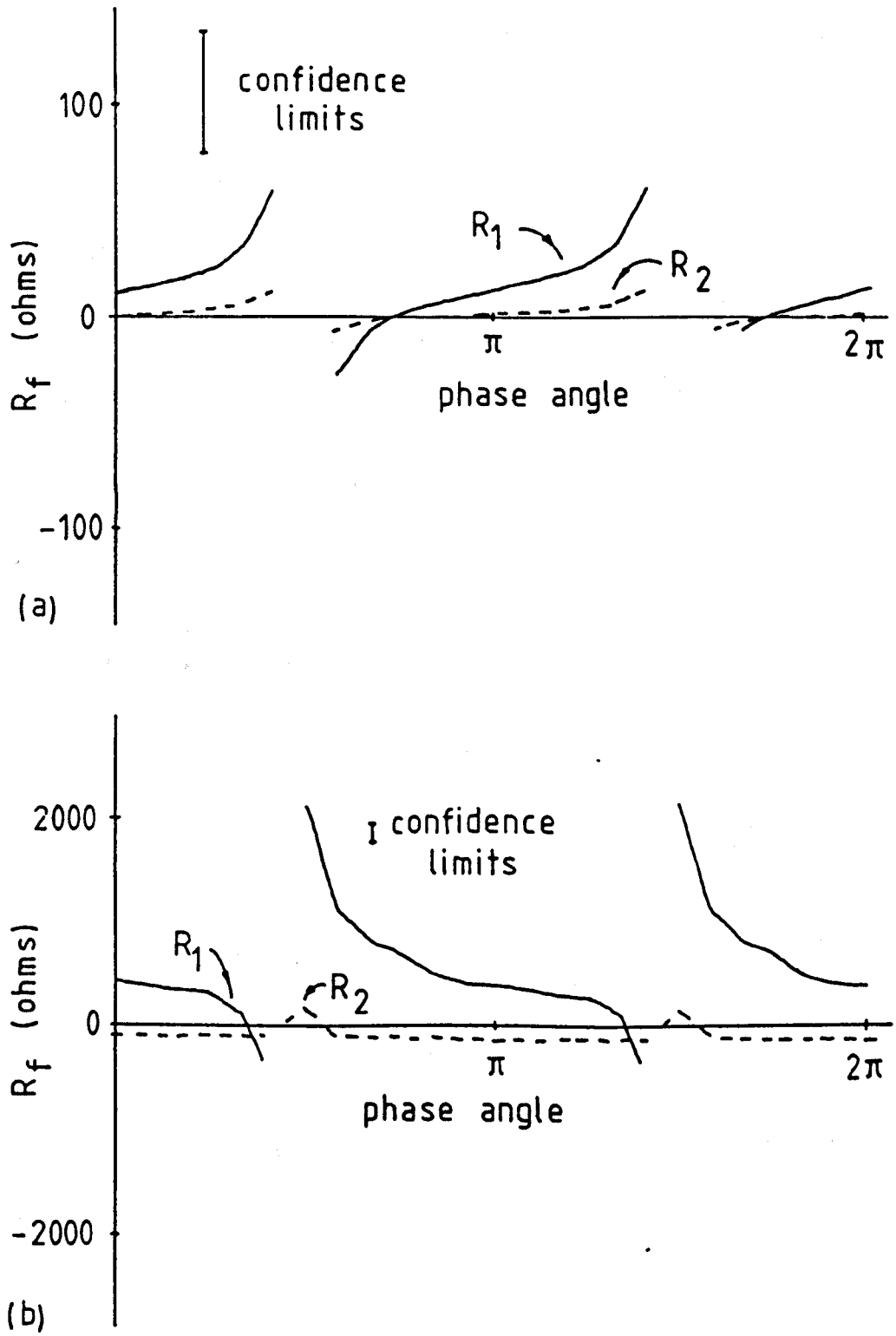

Figure 5.12 Fault resistance estimates against the initial phase-a voltage phase angle for phase-a to ground faults. The faults had a fault resistance of 10 Ω and were located on the line configuration given in figure 5.10. (a) Internal phase-a to ground faults 40 km from the relaying point. (b) External phase-a to ground faults 240 km from the relaying point (40 km from the far busbar).

(within $\pm\pi/12$ radians). The "mode 1" delay confirmed they were internal faults as it indicated a fault location of

$$x_g = 59 \pm 75 \; km \tag{5.27}$$

The results for an external fault 40 km from the far busbar are given in figure 5.12b. The capacitor spark gap flashover occurred at a time greater than 10 milliseconds after fault inception in all cases. The fault transients were then undistorted by the spark gap flashover within the time of interest (within 1.5 ms.). The two estimates of the fault resistance only agree at the special voltage phase angle, as discussed in chapter 2. The "mode 1" delay, however, indicates a fault location at

$$x_g = 234 \pm 119 \; km \tag{5.28}$$

This can be compared with that given by the timing of the cross-correlation trough, which gives

$$x_a = 40 \pm 6 \; km \tag{5.29}$$

The faults are then correctly identified as being external to the protected line.

These results indicate that the relay should be able to distinguish between internal and external faults for transmission lines with 35% compensation at each end. Travelling wave modal mixing is not significant at the compensation locations so that "mode 1" delay can be used as a fault discriminant.

The second line configuration studied, shown in figure 5.13, incorporates 50% compensation located at the line centre. This configuration is common in Scandinavia [84].

The internal fault location, simulated for this example, was located 140 km from the relaying point or 40 km from the series compensation.

Figure 5.11b. shows the times of the capacitor gap flashover after the fault inception. The capacitor gap setting given by equation 5.12 was 80 kV. It appears that such a fault will not produce a spark gap flashover within 4 milliseconds.

The two fault resistance estimates, at various fault voltage inception angles, are given in figure 5.14a. The initial voltage amplitude at the fault location was found using equation 5.8. The first estimate of the fault resistance was then given by equation 4.27. The second estimate of the fault resistance was found using the amplitude of the cross-correlation function, as for the un-compensated lines. The cross-correlation used the long window length of 21 samples as the faults were located beyond the first half of the protected line. The two estimates of the faults resistance agree for all initial fault voltage phase angles, except those within $\pi/12$ radians of voltage zero. The two fault location estimates were

$$x_a = 140 \pm 6 \; km \tag{5.30}$$

$$x_g = 117 \pm 90 \; km \tag{5.31}$$

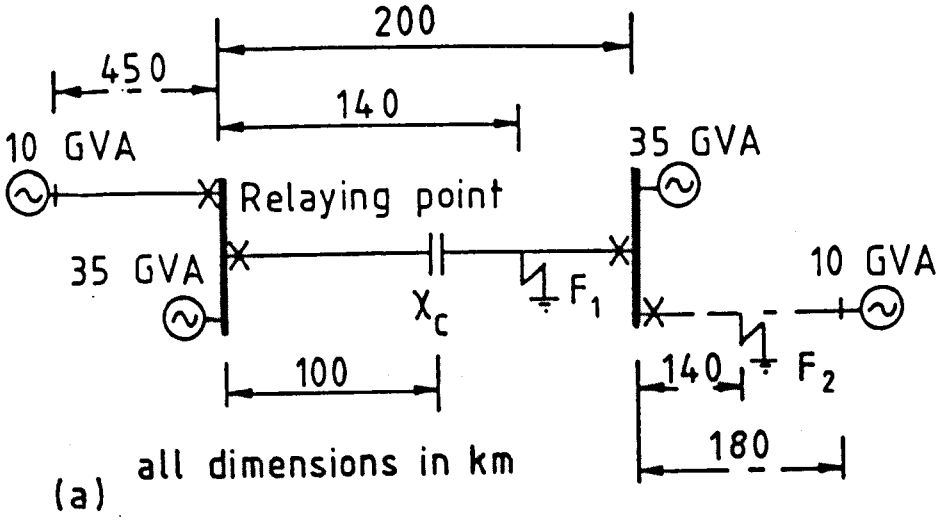

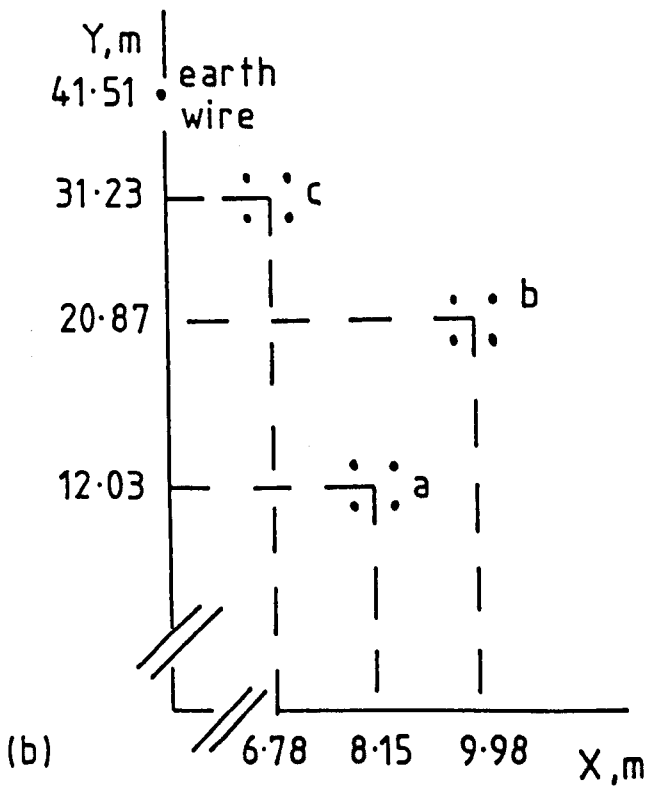

Figure 5.13 The simulated line configuration for the study of faults on lines with compensation at the line centre.

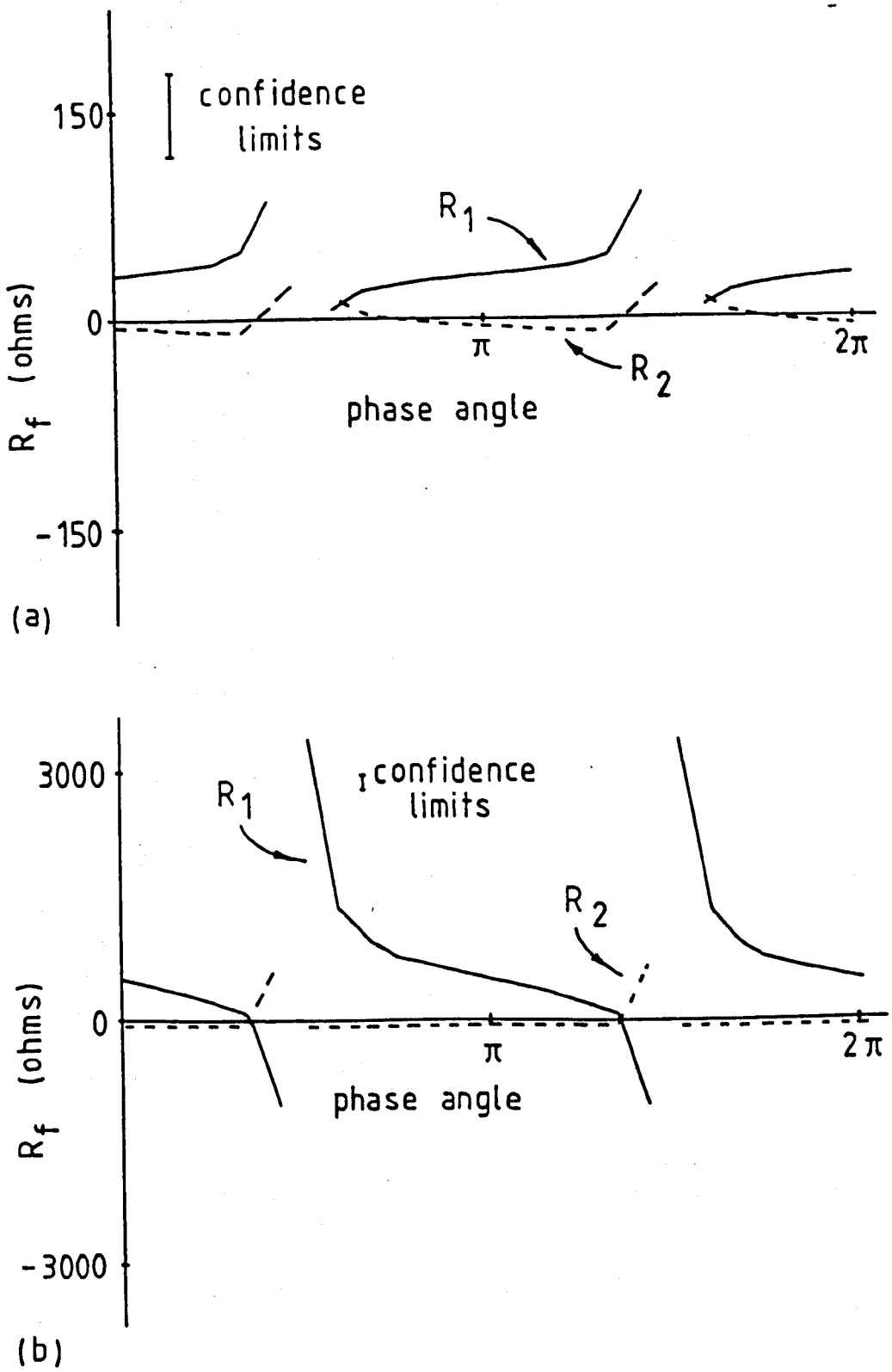

Figure 5.14 Fault resistance estimates against the initial phase-a voltage phase angle for phase-a to ground faults. The faults had a fault resistance of 10 Ω and were located on the line configuration given in figure 5.13. (a) Internal phase-a to ground faults 140 km from the relaying point (40 km from the compensation). (b) External phase-a to ground faults 340 km from the relaying point (140 km from the far busbar).

The results given in figure 5.14b are for an external fault 140 km from the far busbar. The capacitor spark gap flashover was greater than 10 milliseconds in all cases and the two fault resistance estimates only agreed at the "special angle". The two fault location estimates were

$$x_a = 140 \pm 6\ km \tag{5.32}$$

$$x_g = 293 \pm 133\ km \tag{5.33}$$

From these results it appears that the external faults should then be correctly identified.

The fault resistance estimates against actual fault resistance estimates are shown in figure 5.15, for internal phase-a to ground faults 140 km from the relaying point (40 km from the series compensation) occurring at phase-a voltage maximum. Figure 5.15 shows that, as with the un-compensated lines, internal faults up to about the line surge impedance (240 ohms) can be identified. The relay should then also be applicable to transmission lines compensated at the line centre.

5.2.4 Conclusions for compensated lines

The relay algorithm has been successfully applied to compensated transmission lines. The main features are; the adjustment of the estimate of the initial fault voltage to include the series compensation and allowance for the effect of the spark gap flashover waveform by limiting the protection to 80% of the line length.

The relay was shown to be able to protect lines compensated at either the line centre or at the the line ends. In fact any location for the series compensation should not produce any significant problems. Transmission lines of length greater than 400 km may cause problems as the spark gap flashover times will be less than the lines travelling wave transit time. Excessively loaded transmission lines, with close to twice the per unit current level, will also be difficult to protect due to the almost instantaneous capacitor protective spark gap flashover times.

In general, however, normally loaded compensated lines greater than 150 km and up to 400 km length can be protected by this algorithm against faults within 80% of the line length.

5.3 Double Circuit Lines

Most major EHV transmission lines are double circuit. It is important, therefore, to demonstrate that this relay algorithm can achieve good fault discrimination on double circuit lines.

On double circuit lines the relay could sample all six phases and the relay would then operate in much the same way as for the single circuit line. There would be twice as much data to cover twice as many faults plus intercircuit faults. It is then possible to show that the travelling-wave protection of double circuit lines is comparable to the travelling-wave protection of single circuit lines.

In general, however, information from only one circuit can be guaranteed, as one circuit may be disconnected for maintenance or because of a fault on that circuit. It is important, therefore, to show that the travelling-wave

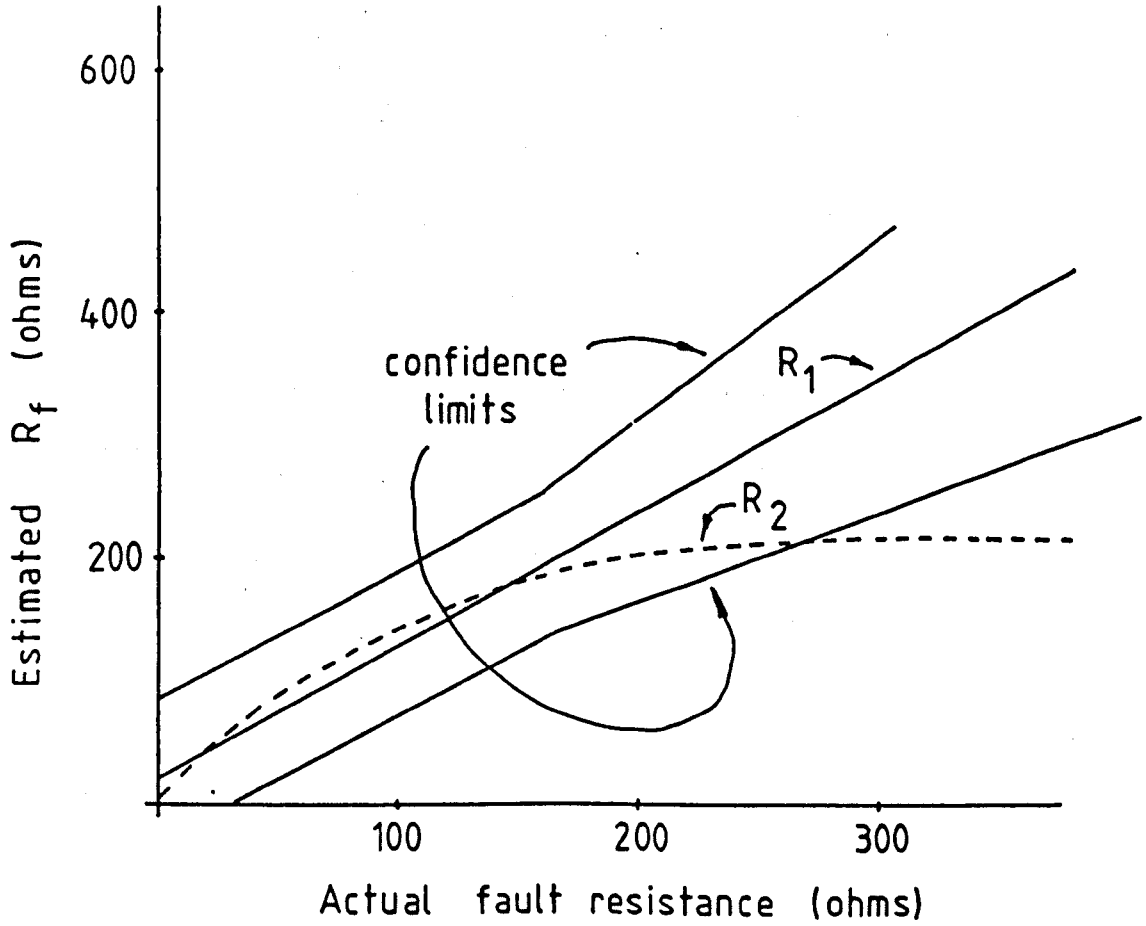

Figure 5.15 Fault resistance estimates against the actual fault resistance for internal phase-a to ground faults. The faults were located 140 km from the relaying point (40 km from the series compensation) on the line configuration given if figure 5.13.

relay can protect one circuit on a double circuit line with information from only that circuit which it is applied to. Intercircuit faults would have to be protected, in this case, by a separate scheme.

For the protection of one circuit on a double circuit line using this travelling-wave relay, the main issues are then: Can the incident and reflected fault travelling-waves be measured precisely when the line parameters have been altered by the presence of another circuit? Can the fault conductance matrices be found to a reasonable accuracy? Are the extra discriminating features of the ground mode delay and the line round trip wave amplitude still valid in a double circuit line?

In this section it will be shown that, when sampling only one circuit, not only can the fault transients be resolved accurately but that the extra discriminating features necessary for fault discrimination can also be used successfully on a double circuit line.

5.3.1 Fault conductance measurement on a double circuit line

The multiphase fault reflection coefficient and the amplitude of the initial transient travelling-wave $[V_1]$ can still be given by equations 2.42. The fault conductance matrix now being given by a six by six square matrix. For the general fault geometry given in figure 2.6 with the other circuit healthy, the fault conductance matrix on a double circuit line $[Y_{f6}]$ will have the form

$$[Y_{f6}] = \begin{bmatrix} [Y_f] & [0] \\ [0] & [0] \end{bmatrix} \tag{5.34}$$

where $[Y_f]$ is a 3 by 3 square matrix given by equation 2.37 and [0] is a 3 by 3 square matrix with all its elements being zero. Note that intercircuit faults are not considered in this study.

If each circuit is fully transposed on a double circuit transmission line then the line surge impedance matrix can be given by

$$[Z_s] = \begin{bmatrix} z^s_{dd} & z^s_{ee} & z^s_{ee} & z^s_{gg} & z^s_{gg} & z^s_{gg} \\ z^s_{ee} & z^s_{dd} & z^s_{ee} & z^s_{gg} & z^s_{gg} & z^s_{gg} \\ z^s_{ee} & z^s_{ee} & z^s_{dd} & z^s_{gg} & z^s_{gg} & z^s_{gg} \\ z^s_{gg} & z^s_{gg} & z^s_{gg} & z^s_{dd} & z^s_{ee} & z^s_{ee} \\ z^s_{gg} & z^s_{gg} & z^s_{gg} & z^s_{ee} & z^s_{dd} & z^s_{ee} \\ z^s_{gg} & z^s_{gg} & z^s_{gg} & z^s_{ee} & z^s_{ee} & z^s_{dd} \end{bmatrix} \tag{5.35}$$

where z^s_{dd} are the self impedance of the phases, z^s_{ee} are the mutual impedance between phases on the same circuit and z^s_{gg} are the mutual impedances between phases on different circuits.

For an untransposed transmission line the surge impedance matrix has the general form

$$[Z_s] = \begin{bmatrix} [A] & [B] \\ [B] & [A] \end{bmatrix} \tag{5.36}$$

where

$$[A] = \begin{bmatrix} z^s_{11} & z^s_{12} & z^s_{13} \\ z^s_{12} & z^s_{22} & z^s_{23} \\ z^s_{13} & z^s_{23} & z^s_{33} \end{bmatrix} \tag{5.37}$$

$$[B] = \begin{bmatrix} z^s_{14} & z^s_{15} & z^s_{16} \\ z^s_{15} & z^s_{25} & z^s_{26} \\ z^s_{16} & z^s_{26} & z^s_{36} \end{bmatrix} \tag{5.38}$$

The fault reflection matrices can then be found from equation 2.42 for the three fault types; symmetric, phase-a to phase-b and phase-a to ground. These are then

Symmetric faults

$$[k_{vf}] = -\frac{Z_a}{Z_a + 2R_f} \begin{bmatrix} 1 & 0 & 0 & 0 & 0 & 0 \\ 0 & 1 & 0 & 0 & 0 & 0 \\ 0 & 0 & 1 & 0 & 0 & 0 \\ 0 & 0 & 0 & 0 & 0 & 0 \\ 0 & 0 & 0 & 0 & 0 & 0 \\ 0 & 0 & 0 & 0 & 0 & 0 \end{bmatrix} \tag{5.39}$$

where

$$Z_a = \frac{1}{3}[z^s_{11} + z^s_{22} + z^s_{33} - z^s_{12} - z^s_{13} - z^s_{23}] \tag{5.40}$$

Phase-a to ground faults

$$[k_{vf}] = -\frac{1}{z^s_{11} + 2R_f} \begin{bmatrix} z^s_{11} & 0 & 0 & 0 & 0 & 0 \\ z^s_{12} & 0 & 0 & 0 & 0 & 0 \\ z^s_{13} & 0 & 0 & 0 & 0 & 0 \\ z^s_{14} & 0 & 0 & 0 & 0 & 0 \\ z^s_{15} & 0 & 0 & 0 & 0 & 0 \\ z^s_{16} & 0 & 0 & 0 & 0 & 0 \end{bmatrix} \tag{5.41}$$

or the aerial-phase reflection coefficient can be given as

$$[k^a_{vf}] = -\frac{1}{6[z^s_{11} + 2R_f]} \begin{bmatrix} Z_1 & 0 & 0 & 0 & 0 & 0 \\ Z_2 & 0 & 0 & 0 & 0 & 0 \\ Z_3 & 0 & 0 & 0 & 0 & 0 \\ Z_4 & 0 & 0 & 0 & 0 & 0 \\ Z_5 & 0 & 0 & 0 & 0 & 0 \\ Z_6 & 0 & 0 & 0 & 0 & 0 \end{bmatrix} \tag{5.42}$$

where

$$Z_p = 5z^s_{1p} - \sum_{r \neq p} z^s_{1r} \tag{5.43}$$

Phase-a to phase-b fault

$$[k_{vf}] = -\frac{Z_a}{2[Z_a + 2R_f]} \begin{bmatrix} 1 & -1 & 0 & 0 & 0 & 0 \\ -1 & 1 & 0 & 0 & 0 & 0 \\ 0 & 0 & 0 & 0 & 0 & 0 \\ 0 & 0 & 0 & 0 & 0 & 0 \\ 0 & 0 & 0 & 0 & 0 & 0 \\ 0 & 0 & 0 & 0 & 0 & 0 \end{bmatrix} \tag{5.44}$$

where

$$Z_a = \frac{1}{2}[z'_{11} + z'_{22} - 2z'_{12}] \tag{5.45}$$

For symmetric and phase to phase faults, from their reflection matrices, it appears that their transients are only dependent on the voltage levels on the faulted circuit and the transients are only induced on to the faulted circuit. The first estimate of the fault conductance matrix given by equation 2.38 can then be found from just the initial fault voltage levels $[v_f]$ and the initial travelling wave amplitude $[V_1]$ on the faulted circuit. The second estimate of the fault conductance matrix given by equation 2.42 can also be found from a comparison of the initial reflected waveform $[V_{r1}]$ and the second incident waveform $[V_{i2}]$ on just the faulted circuit.

The fault conductance estimates for symmetric and phase to phase faults on double circuit lines can be carried out, therefore, in an identical fashion to that outlined in chapter 4 for a single circuit. The line surge impedance matrix is now given by element $[A]$ of the full double circuit surge impedance matrix (equation 5.36). This then gives adequate precision in the fault conductance estimates for fault discrimination.

On single phase to ground faults, however, the transients generated at the fault are dependent only on the voltage levels on the faulted phase and they propagate on all six phases. Resolving the transients on just one circuit may not then give a complete picture of the fault transients.

As with the single circuit case, however, all the initial phase transients are linearly dependent as they are all fractions of the initial fault voltage on the faulted phase (in this case $v_f(a)$). The initial fault resistance estimates can then be found on the faulted phase from 4.27 where the line surge impedance is now given by matrix $[A]$ in equation 5.36.

On a fully transposed transmission line the modal transform matrices can be given by

$$[S]^{-1} = [Q]^{-1} = \frac{1}{6}\begin{bmatrix} 1 & 1 & 1 & 1 & 1 & 1 \\ 1 & 1 & 1 & -1 & -1 & -1 \\ -1 & 1/2 & 1/2 & -1 & 1/2 & 1/2 \\ 1 & -1/2 & -1/2 & -1 & 1/2 & 1/2 \\ 0 & 3/2 & -3/2 & 0 & -3/2 & 3/2 \\ 0 & 3/2 & -3/2 & 0 & 3/2 & -3/2 \end{bmatrix} \tag{5.46}$$

From the above given modal transformation matrices of a double circuit line with fully transposed circuits, it appears that, when sampling one circuit the ground mode transients will not be distinguishable from the mode 2 transients. The mode 2 transients circulate between the two circuits and propagate at close to the aerial mode velocities. The ground mode deduced from the transients of just one circuit will contain both mode 1 and mode 2 transients and will then appear to have little delay or dispersion. The estimate of the contribution of the ground mode to the first incident wave at the fault location V_{r1f}, given by equation 4.40, will then have a large error.

For the second estimate of the fault resistance, given by the cross-correlation function amplitude, the total contribution of all the modes to the faulted phase voltage level $V_{r1f}(a)$ is required. Resolution of the ground

mode or mode 1 transients from the mode 2 transients is therefore not necessary. The combined dispersion of modes 1 and 2 can be estimated and used for the estimate of the transient fault voltage level. The combined dispersion of modes 1 and 2 has then been found to be approximated adequately by 4.39 for the whole length of a double circuit transmission line.

The second estimate of the fault conductance matrix can be reduced, therefore, to the fault resistance given by equation 4.28. The two cross-correlation windows are used to estimate $V_{r1}(a)/V_{i2}^{a}(a)$ where $V_{r1}(a)$ is now given by equation 4.39 along the whole line length.

In conclusion, the fault conductance estimates for faulted circuits on double circuit lines can be found in much the same way as for the single circuit line. Only one circuit need be sampled and the confidence limits of the fault resistance estimates can be given by equations 4.17,4.18,4.54,4.55, 4.81 and 4.82, which is

$$|R_{f1} - R_{f2}| < 60\Omega \quad \text{for} \quad R_{f1} \rightarrow 0 \tag{5.47}$$

$$\frac{|R_{f1} - R_{f2}|}{R_{f1}} < 60\% \quad \text{for} \quad R_{f1} \rightarrow \infty \tag{5.48}$$

5.3.2 Ground mode delay on a double circuit line

On a double circuit line the fault resistance estimates for a phase to ground fault can only be carried out on one phase. There will therefore be a problem for external faults occurring at the special angle of fault resistance estimate agreement. An extra discriminating feature is required, therefore, to ensure relay over reach does not occur. It will be a distinct advantage if the ground mode delay can be utilised for fault discrimination.

It has already been shown, in the previous section, that the ground mode and mode 2 transients will be indistinguishable when sampling only one circuit on a double circuit line. The typical modal transformation matrices for an untransposed transmission line are given in appendix c which shows that the mode 1 and mode 2 transients will also be indistinguishable. Since the mode 2 transients propagate at close to the aerial mode velocities, it will not be possible to estimate the fault location from the ground mode delay.

Mode 2 on a double circuit line, however, is an asymmetrical mode. By asymmetric it is meant that the contribution to the mode from each circuit is of equal size but of opposite sign. Mode 1, on the other hand, is symmetric where the contributions from each circuit are of equal size and sign. If the corresponding phases of a double circuit line (e.g. a and a') are connected at the terminating busbars, as is the usual practice, then identical transients will be induced on each phase from an external fault. No asymmetrical modes should then exist on a double circuit line when an external fault occurs. In this case measurement of the ground mode or mode 1 delay should thus give a reasonable estimate of the fault location for external faults. Fault discrimination between internal and external faults should still be possible, therefore, on double circuit lines.

For double circuit lines, the mode 1 velocity has a far greater variation with ground conductivity. The mode 1 – aerial mode velocity difference ξ for a double circuit line is given by

$$\xi = -0.2 \pm 0.07 \tag{5.49}$$

This is still precise enough for the protection of lines longer than about 100 km.

The incident modal transients, for an internal phase-a to ground fault occurring 160 km from the relaying point at phase-a voltage maximum on a double circuit line, are given in figure 5.16a. The incident modes for an external fault, occurring 360 km from the relaying point (160 km from the far busbar) at phase-a voltage maximum, are given in figure 5.16b. From the modal transients given in figure 5.16 it can be seen that asymmetrical transients will not be present for an external fault.

The three modal values, deduced when sampling only the protected circuit, for the transients given in figure 5.16 are given in figure 5.17 In figure 5.17a no modal delay is detected which indicates an internal fault. In figure 5.17b there is clear mode 1 delay due to the absence of mode 2 transients, the fault location is indicated to be external at

$$x_g = 370 \pm 140\ km \tag{5.50}$$

It has been found therefore that the ground mode delay is enhanced on double circuit lines provided the two circuits are connected at the terminating busbar. Good fault discrimination between internal and external phase to ground faults should then be possible at all times and relay over reach should not occur.

5.3.3 Line round trip amplitude on a double circuit line.

The phase to phase fault resistance estimates on a double circuit line will be carried out using the line voltage in much the same way as for a fault on a single phase line. There will be problems, therefore, at the special angles where the fault resistance estimates are in agreement for an external fault. Good fault discrimination will only be possible if an extra discriminating feature, such as the line round trip wave, is included in the algorithm. It will be an advantage, therefore, if the line round trip amplitude can be utilized for phase to phase faults on double circuit lines.

On double circuit lines, however, there will be an extra healthy circuit for fault transients to propagate during internal faults. It has been found that internal phase to phase fault transients may still exhibit a significant line round trip travelling wave amplitude. Figure 5.18 shows the cross-correlation functions for an internal phase-a to phase-b fault 160 km from the relaying point and an external fault 360 km from the relaying point (160 km from the far busbar). From figure 5.18 it can be seen that the line round trip wave amplitude, given by the trough in the cross-correlation function, is significant for an internal fault but much smaller than that of an external fault. In fact it has been found that, if the criterion for the amplitude of the line round trip wave is now changed to insisting that it must give a cross-correlation trough greater than about -0.3, good fault discrimination is still possible between internal and external faults. In order to distinguish between internal and external faults the minimum line round trip amplitude when an external fault occurs must be greater than the maximum line round trip amplitude of an internal fault. This is only possible, however, provided

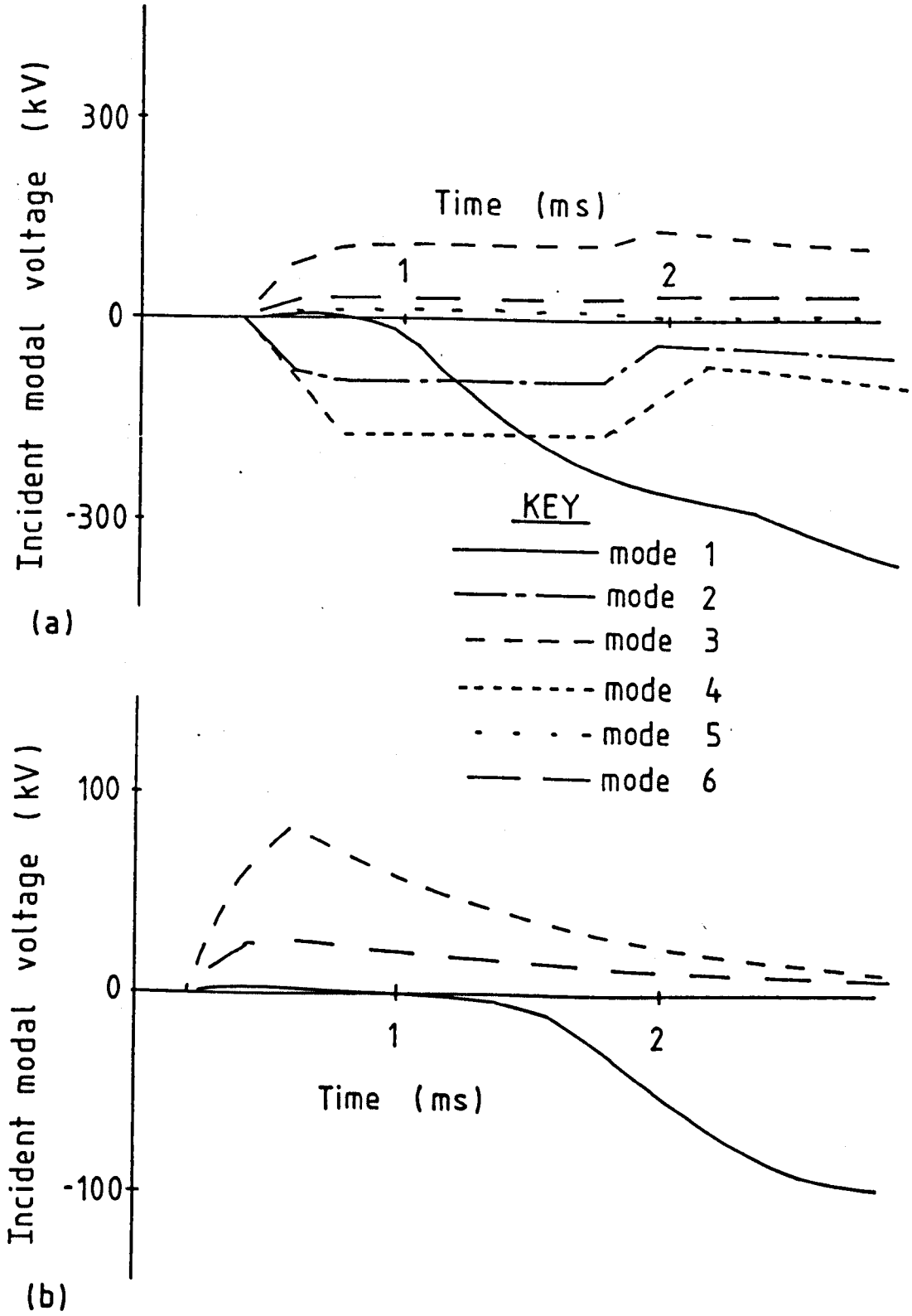

Figure 5.16 The incident modal transients for phase-a to ground faults on a double circuit line with each circuit connected in parallel.

(a) An internal fault located 160 km from the relaying point.

(b) An external fault located 360 km from the relaying point (160 km from the far busbar).

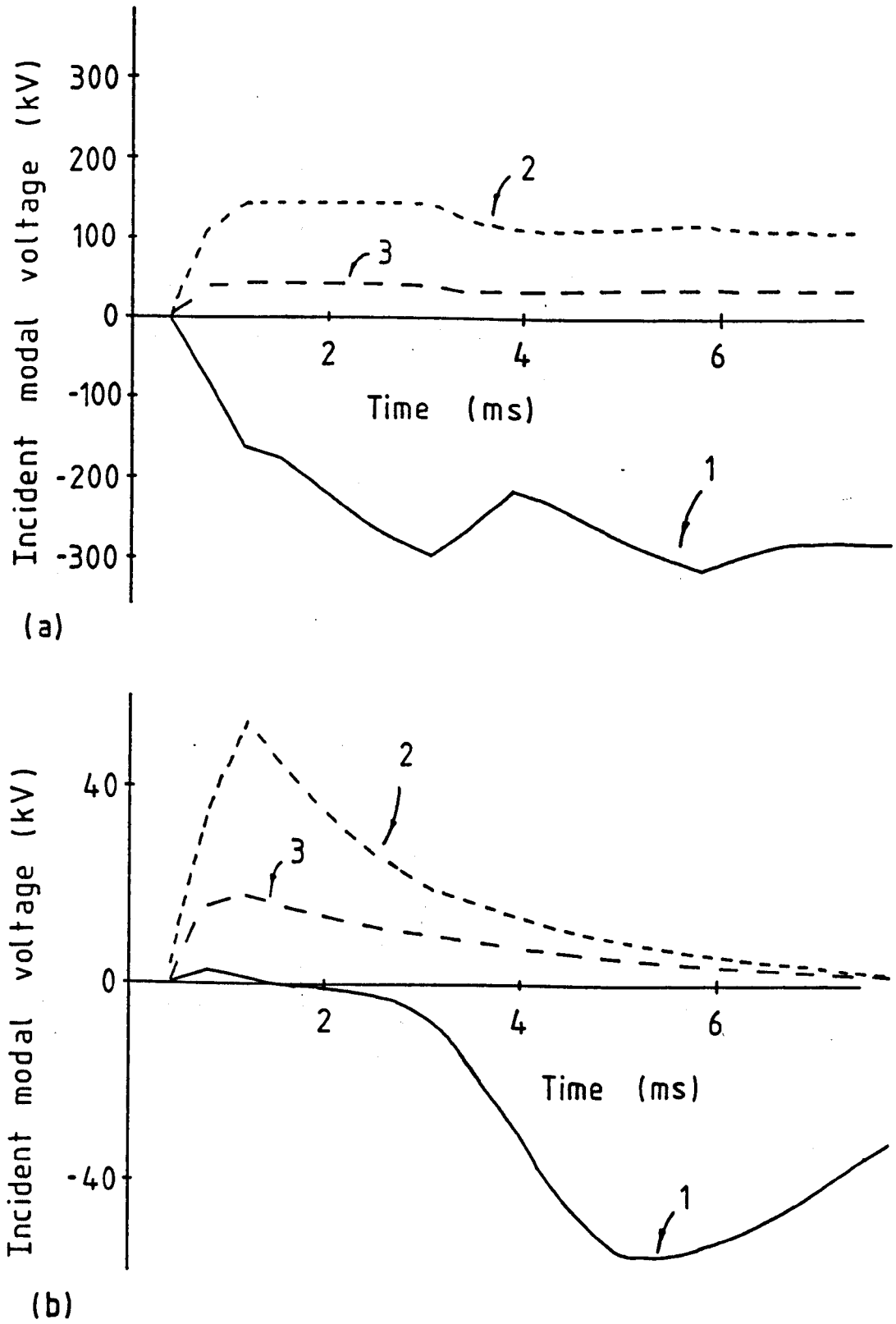

Figure 5.17 The incident modal transients, when only sampling one circuit, for a phase-a to ground fault on a double circuit line with each circuit connected in parallel.

(a) An internal fault located 160 km from the relaying point.

(b) An external fault located 360 km from the relaying point (160 km from the far busbar).

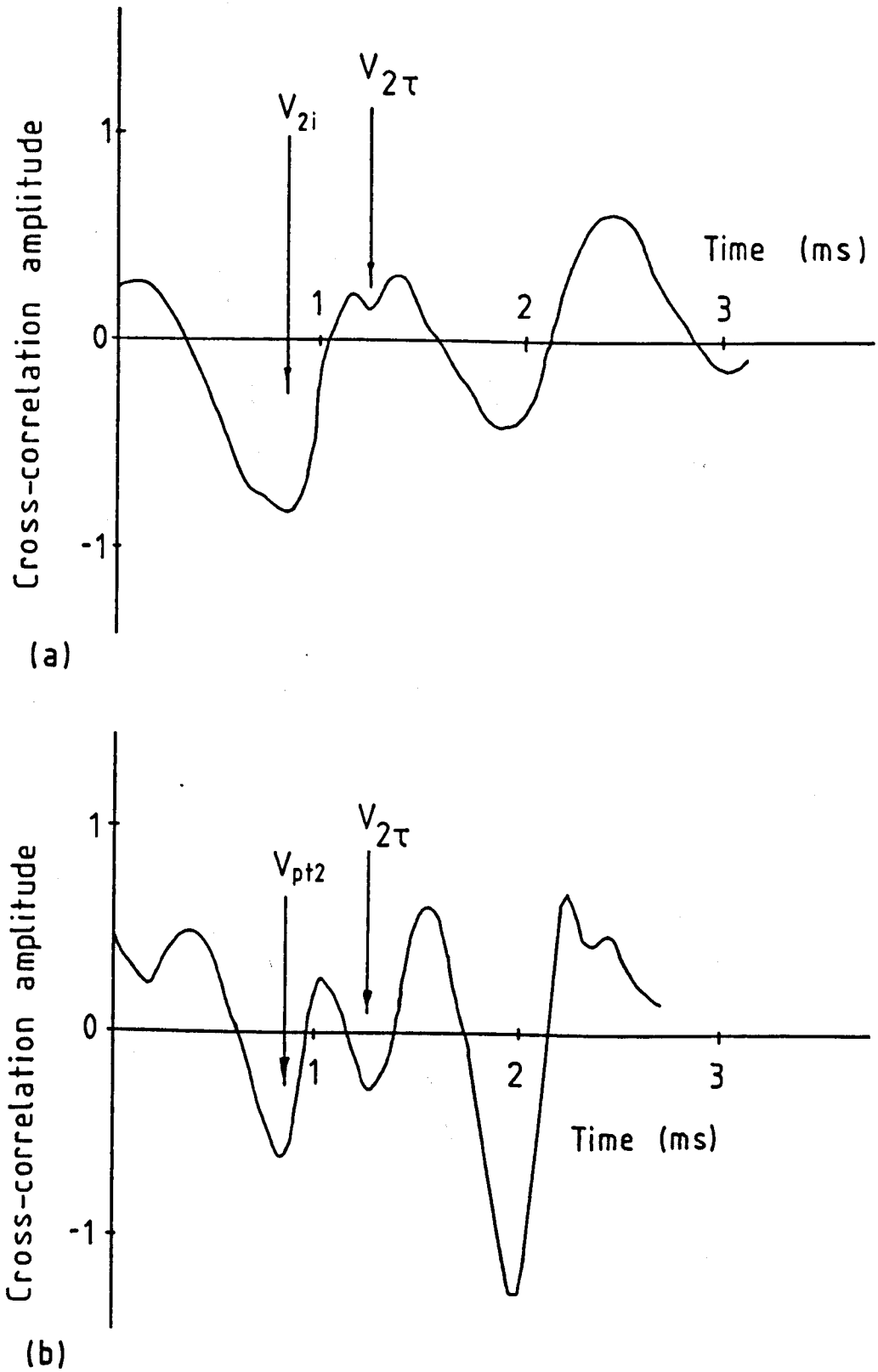

Figure 5.18 The cross-correlation functions using the long window (21 samples) for phase-a to phase-b faults on a double circuit line when sampling only one circuit. Both circuits are connected in parallel.

(a) An internal fault located 160 km from the relaying point of resistance 10 ohms.

(b) An external fault located 360 km from the relaying point (160 km from the far busbar) of resistance 10 ohms.

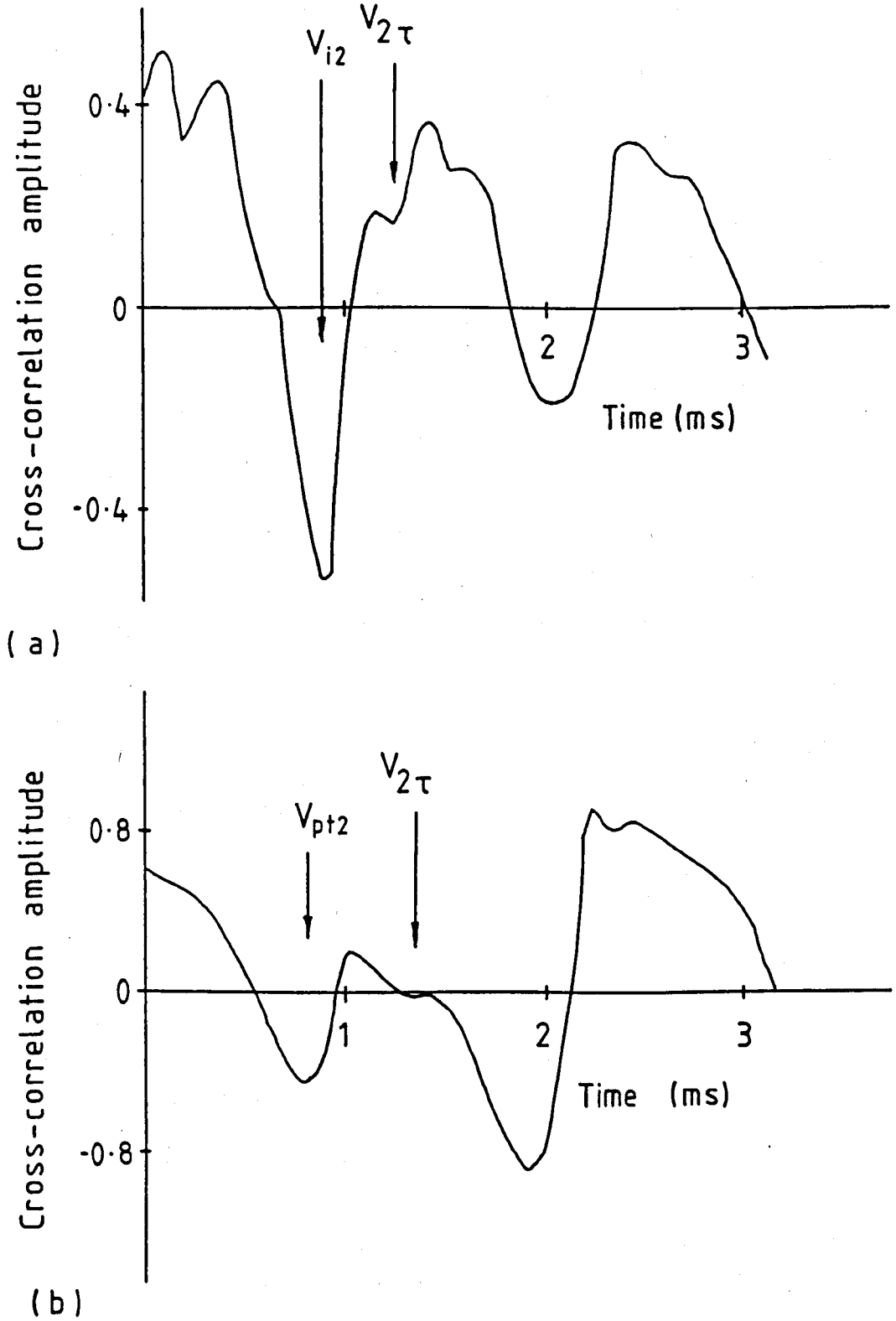

Figure 5.19 The cross-correlation functions using the long window (21 samples) for phase-a to phase-b faults on a double circuit line when sampling only one circuit. Both circuits are connected in parallel.

(a) An internal fault located 160 km from the relaying point of resistance 120 ohms and the far busbar short circuit capacity is 35 GVA.

(b) An external fault located 360 km from the relaying point (160 km from the far busbar) of resistance 10 ohms and the far busbar short circuit capacity is 10 GVA.

that the short circuit capacity connected to the far busbar is not less than 10 GVA, so that the minimum line round trip amplitude for an external fault gives a cross-correlation trough which is always greater than -0.3. Figure 5.19 shows a comparison of the cross-correlation functions between the two severest cases of an internal phase-a to phase-b fault of resistance 120 ohms with the far busbar short circuit capacity of 35 GVA and an external fault of resistance 10 ohms with the far busbar short circuit capacity of 10 GVA. From figure 5.19 it can be seen that even in the severest case the internal and external faults should be distinguishable.

In conclusion, good fault discrimination between internal and external phase to phase faults on a double circuit line should still be possible using the line round trip wave amplitude. In using the line round trip wave amplitude, however, the short circuit capacities of the line terminating busbars must be limited to not less than 10 GVA. It is expected that this limitation on the busbar short circuit capacities will not be too prohibitive as high speed relaying will only be required where high short circuit capacities are present (as these give large fault currents).

5.3.4 Simulation results

In this study the vertical CEGB double circuit type 02L, given in appendix c, will be used. This geometry will be a reasonably severe test as the mutual impedances are very asymmetrical. The fault transients studied were simulated on the line configuration given in figure 5.20. Sources connected to the protected lines terminating busbars were thought to give an adequately complicated system for the production of realistic transients. The double circuit lines are connected in parallel such that the corresponding phases (i.e. a-a',b-b' and c-c') were connected at the terminating busbars of the simulated lines. This would be typical of most systems where the reduced line impedance of the double circuit line is fully exploited [89].

The actual modal transform matrices and surge impedance matrices for the simulated line geometry (CEGB type 02L) are given in appendix c. It was found that the modal matrices and surge impedance matrix can be approximated by real constant values for the frequency range 50-5000 Hz. This is in agreement with the findings of Wasley and Slavavinayagamoorthy [34].

Using the scheme outlined in section 5.1.1, for fault conductance estimation when sampling only one circuit, specimen results for phase to ground faults and phase to phase faults were then obtained from simulations. Figure 5.21 shows the incremental voltage and current transients for a phase-a to ground fault 160 km from the relaying location occurring at phase-a voltage maximum. It appears in figure 5.21 that within a time of about 0.26 milliseconds, which roughly corresponds to $2\tau - 2t_1$ of figure 1.5, the incremental currents and voltages are of opposite sign for the faulted circuit and of the same sign for the healthy circuit. Directional information will then be sufficient to distinguish between the healthy and the faulted circuit, even when sampling just one circuit. It will not be possible to decide which is the faulted circuit for faults closer to the far busbar but such fault will be ignored as the relay will be limited to the protection of 80 % of the transmission line, in case series compensation is present (see section 5.1 on series compensation).

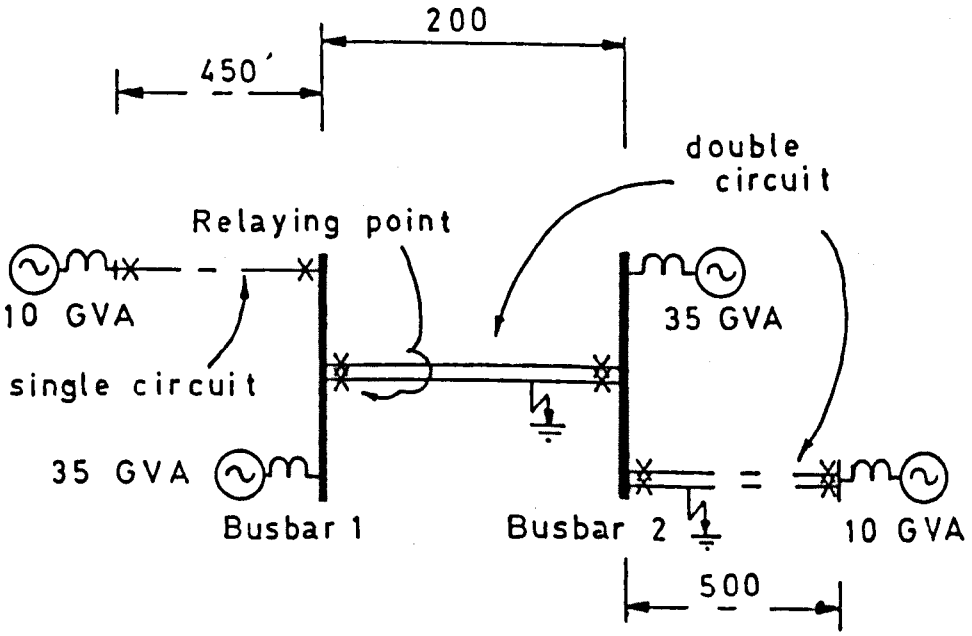

Line configuration of the double circuit geometery given below. All dimensions in km.

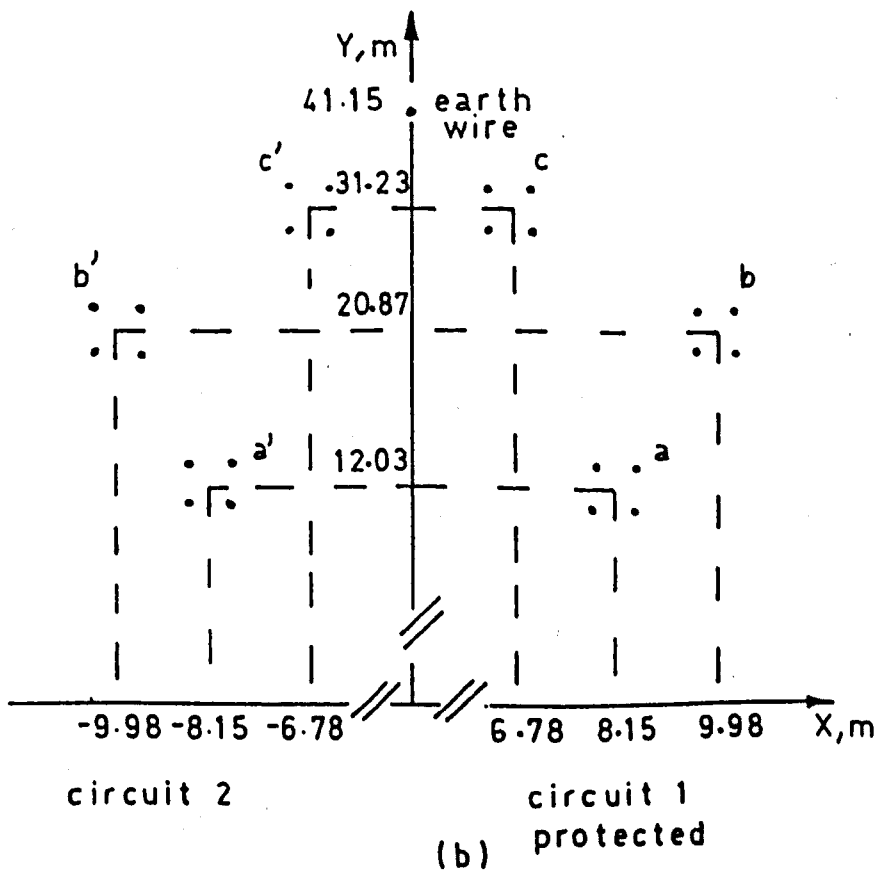

Figure 5.20 The simulated double circuit line configuration.

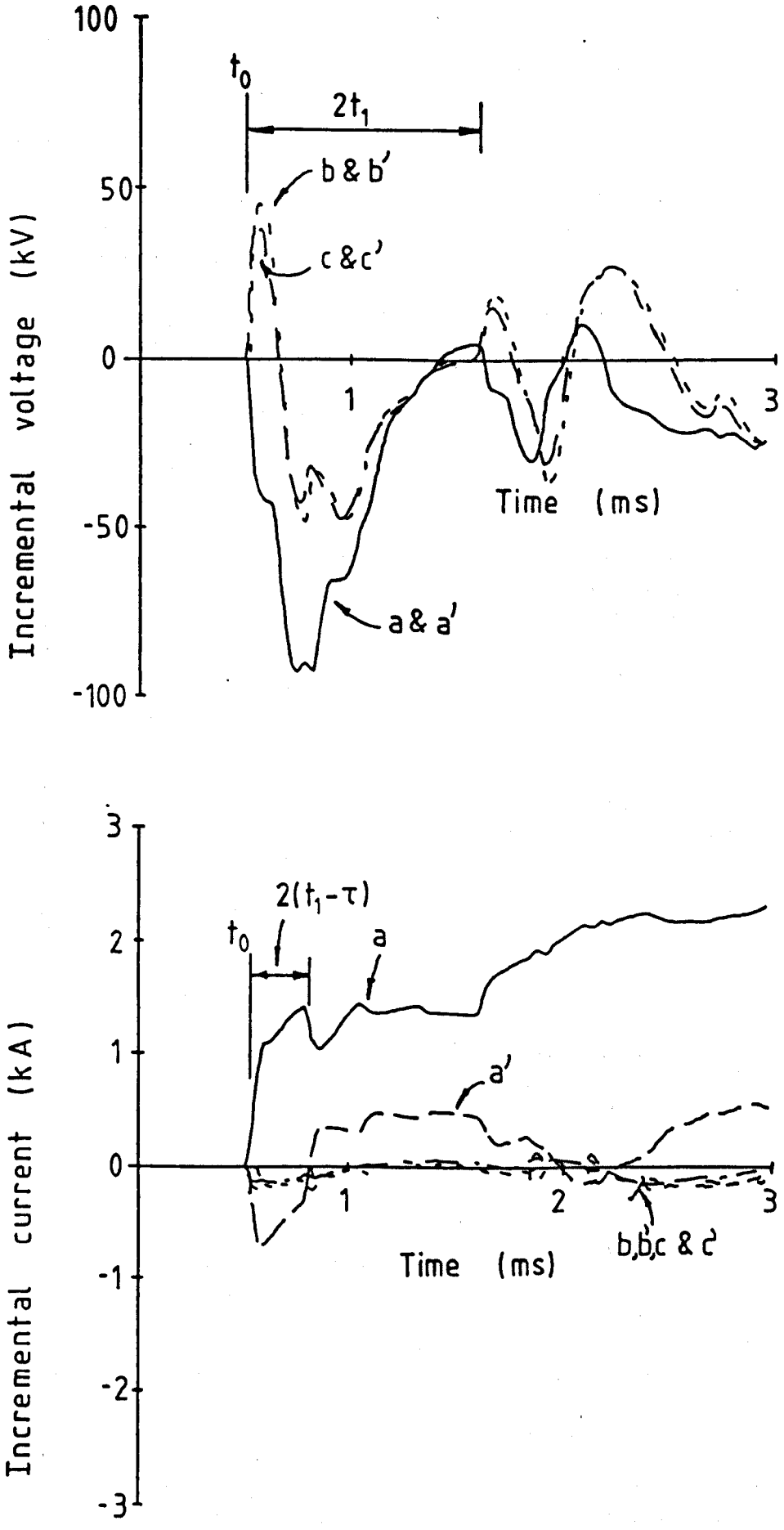

Figure 5.21 The incremental voltage and current transients for a phase-a to ground fault 160 km from the far busbar on the double cicruit line configuration given in figure 5.20. Directional information is correct on both circuits in the time range $t_0 < t < t_0 + 2\tau - 2t_1$

The fault resistance estimates for internal and external phase-a to ground faults against the initial fault voltage phase angle, are given in figure 5.22. The corresponding results for phase-a to phase-b faults are given in figure 5.23. From these results it appears that, for internal faults, good fault resistance estimation is possible to within $\pi/12$ radians of voltage zero. For external faults the fault resistances only agree at the special angles, but fault discrimination is ensured by the ground mode delay or the line round trip amplitudes as given in figures 5.17 and 5.18.

The fault resistance estimates against the actual fault resistance for internal phase-a to ground faults and internal phase-a to phase-b faults are given in figure 5.24. Figure 5.24 demonstrates that internal faults, up to about the line aerial-mode surge impedance ($Z_a \approx 260\Omega$), can be identified. In practice, however, the phase to phase faults can only be identified for fault resistances less than half the line surge impedance as larger resistances yield a large line round trip wave amplitude which is confused with that of external faults.

From these simulations it can be concluded that fault discrimination on double circuit lines should be possible. As with the single circuit case, however, internal faults can only be identified provided that significant voltage transients are present. Internal faults are then only identifiable when they do not occur within $\pi/12$ radians of voltage zero and have a fault resistance at least below the line surge impedance. On the other hand, all external faults are correctly identified and relay over reach should not occur.

5.3.5 Conclusions for the protection of double circuit lines

Travelling wave protection of double circuit transmission lines has been found to be possible. To achieve good fault discrimination, however, two limiting conditions are necessary which are

a The lines of the protected double circuit must be connected in parallel.

b The short circuit capacity of the protected lines terminating busbars must not be less than 10 GVA.

These conditions may not be significant, though, as double circuit lines are usually connected in parallel and high speed protection should only be required on lines connected to high short circuit capacity systems.

5.4 Relay noise tolerance and bandwidth requirements.

Up to this point the fault transients studied have been ideal broadband noiseless signals. On a real system it is expected that the fault transients will be band-limited by the transducers and that noise will also be present. In this section the noise tolerance and bandwidth requirements, of the proposed relay, will be quantified. It is then shown that the relay noise tolerance is adequate for EHV transmission lines but that the fidelity of the transducers in use at present is found to be insufficient, though suitable alternative transducers are available.

5.4.1 Fault transients with noise.

In the earlier chapters, care was taken to ensure that there will be a noise tolerance of up to 5% of the per unit levels. Information about the actual

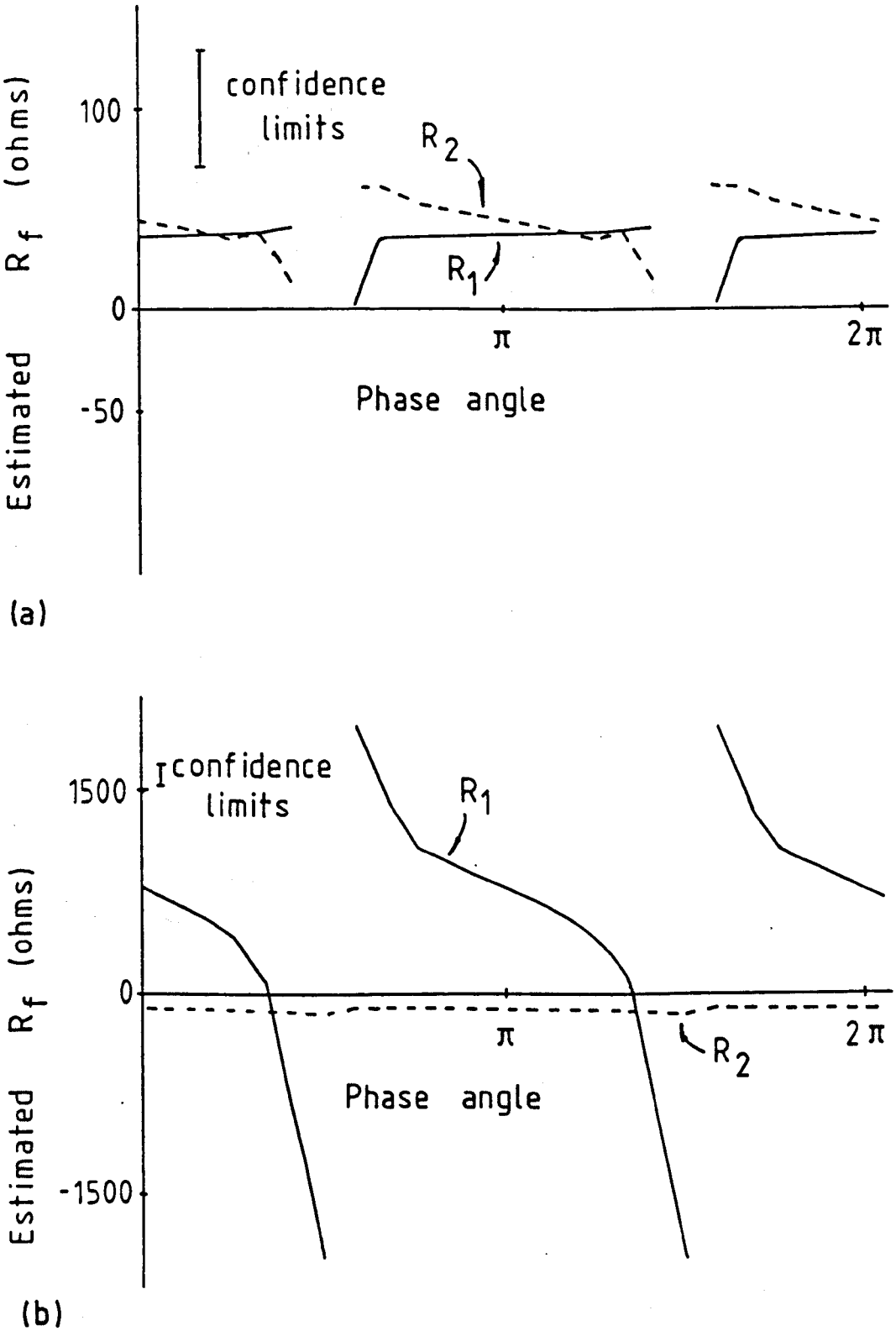

Figure 5.22 The fault resistance estimates for phase-a to ground faults against the initial phase-a voltage phase angle. The faults are located on the line configuration given in figure 5.20.

(a) An internal fault located 160 km from the relaying point of resistance 10 ohms.

(b) An external fault located 360 km from the relaying point (160 km from the far busbar) of resistance 10 ohms.

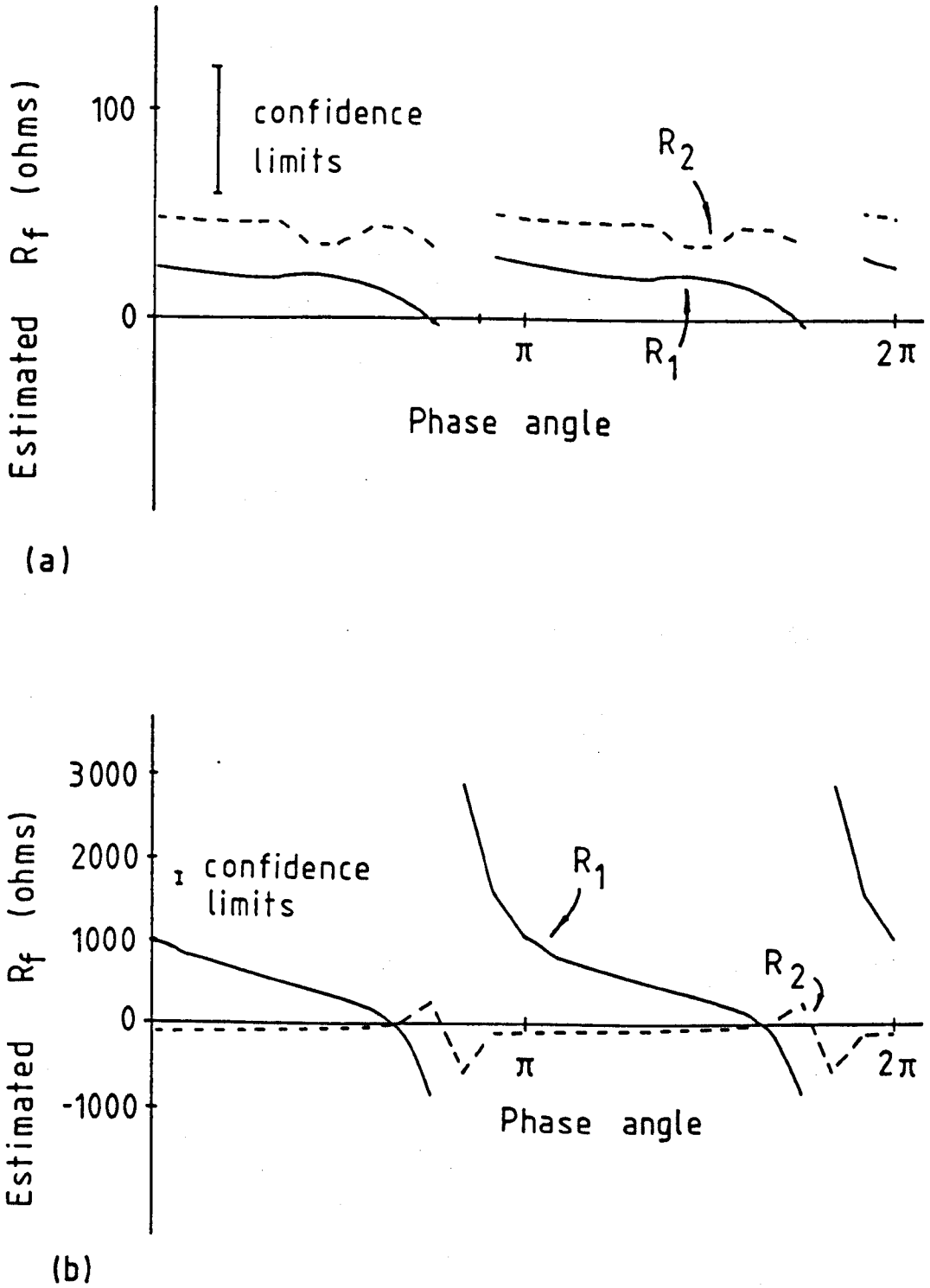

Figure 5.23 The fault resistance estimates for phase-a to phase-b faults against the initial phase-a voltage phase angle. The faults are located on the line configuration given in figure 5.20.

(a) An internal fault located 160 km from the relaying point of resistance 10 ohms.

(b) An external fault located 360 km from the relaying point (160 km from the far busbar) of resistance 10 ohms.

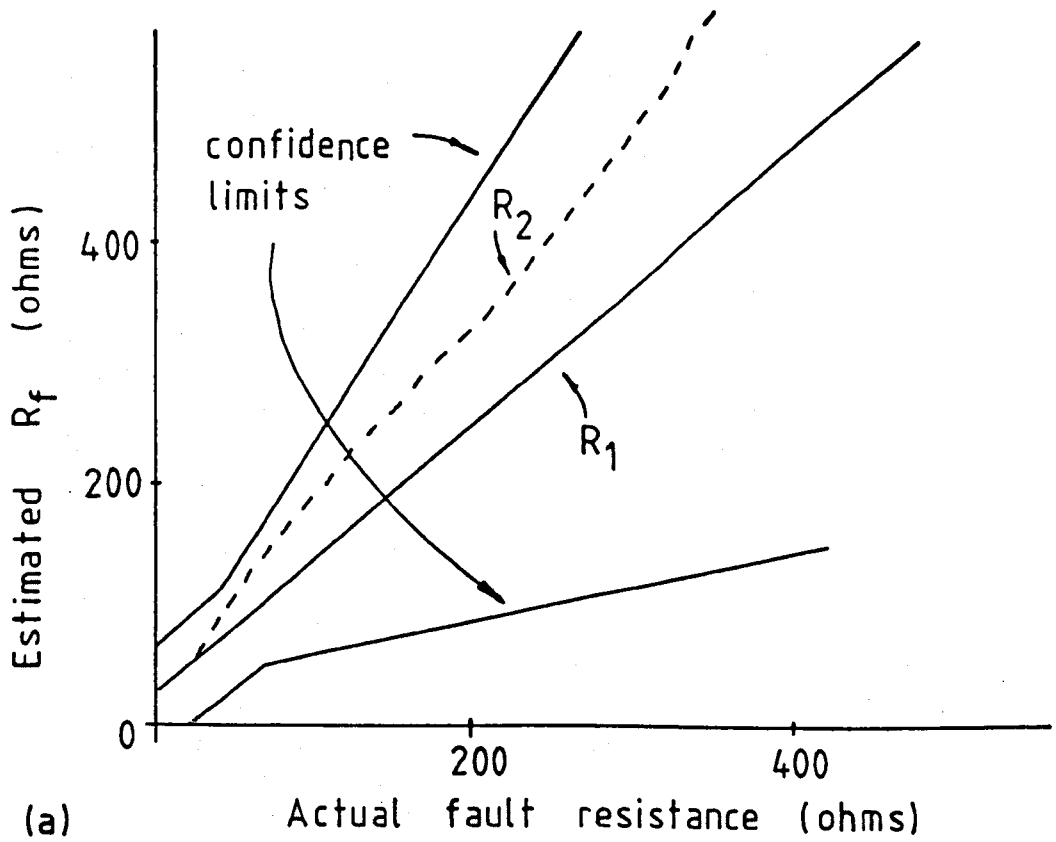

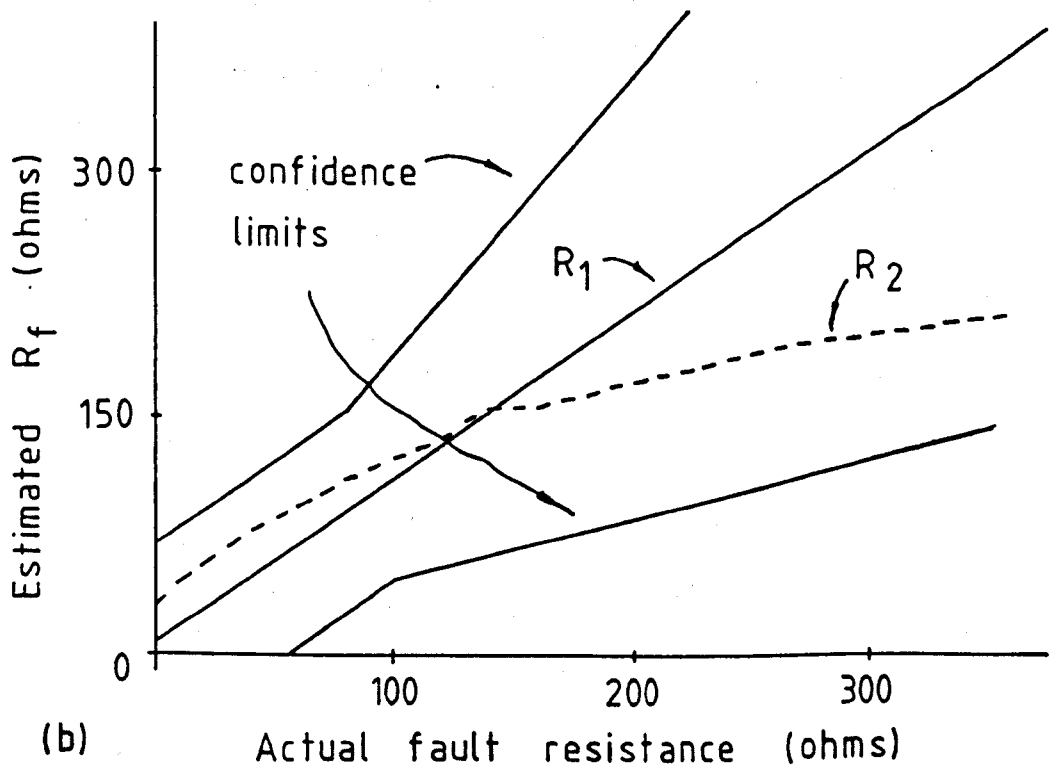

Figure 5.24 The fault resistance estimates against the actual fault resistance for internal faults on the double circuit line configuration given in figure 5.20.

(a) Phase-a to ground faults occurring at phase-a voltage maximum 160 km from the relaying point.

(b) Phase-a to phase-b faults occurring at phase-a voltage maximum 160 km from the relaying point.

noise levels on EHV transmission lines is difficult to find. What information there is [45] seems to suggest that between 1% and 2% per unit noise level (-34 db to -40 db) is typical. However, the exact nature of the system noise has not been studied. The system noise may be primarily harmonics or it could be purely random in content. The effects of system harmonics at the 5% per unit level and purely random noise has therefore been investigated.

In the initial study, purely random noise of Gaussian distribution was superimposed on the simulated fault transients. The noise was generated by a pseudo random noise algorithm on the university computer, which generates noise patterns of almost Gaussian distribution. Figure 5.25 shows a typical generated noise distribution compared with the ideal distribution. The standard deviation of the generated noise levels were adjusted through a range up to -22 decibels (8%) of the system per unit levels (400 kV and 1 kA). The single circuit line configuration of figure 4.3 was used in this study. Phase-a to ground fault transients were simulated for the full range of fault locations and the noise transients were then superimposed on these transients. The results were then interpreted in terms of the standard deviation of the fault resistance estimates for given noise levels. Results are given in figure 5.26 for phase-a to ground faults of fault resistance 10 ohms occurring at a phase-a voltage phase angle of 0 and $-5\pi/12$ radians.

Note that in this study on noise it was found that good fault selection, using the S parameters discussed in chapter 4, was only possible if the deduced S parameters were averaged over three samples. The incident aerial wave amplitude estimation $[V_1^a]$ was also better approximated by the average of three samples. In order that these three samples only include the initial incident transient $[V_1]$, the closest resolvable fault may have to be limited to within 50 km of the relaying point for a sampling rate of 25.6 kHz.

From the results given in figure 5.26, it can be seen that noise levels up to -26 decibels lead to errors in the fault resistance estimates of less than 30Ω. At present the noise threshold is limited to -32 decibels as the relay has to trip at this level to ensure that the ground mode delay is accurately determined at low initial fault voltages. Full implementation for noise levels up to -26 db may be possible, however, with a more sophisticated ground mode delay check. Low threshold levels in the presence of high noise levels will of course lead to the relay being constantly activated.

The fault location is also impaired by the presence of noise and can only be given to within 12 km for noise levels of -32 decibels.

System harmonics are tolerated up to 5% of the system per unit levels on EHV transmission lines [91]. Harmonic distortion on high voltage transmission lines (33-100 kV) has been found to be between 1% and 2% of the per unit levels [92], for up to the ninth harmonic, which suggests that about this level is expected on EHV transmission lines. Higher harmonics were found to be less significant (less than 1% p.u.).

The effects of system harmonics was investigated by superimposing various harmonics at the 5% per unit level on the phase-a to ground faults simulated on the line geometry given in figure 4.3. Two extreme cases were taken where the harmonic currents are exactly in phase with the harmonic voltages or were exactly out of phase with the harmonic voltages.

It is assumed that most system harmonics are created from non-linear loads. The harmonics on the system will then have the form [91]

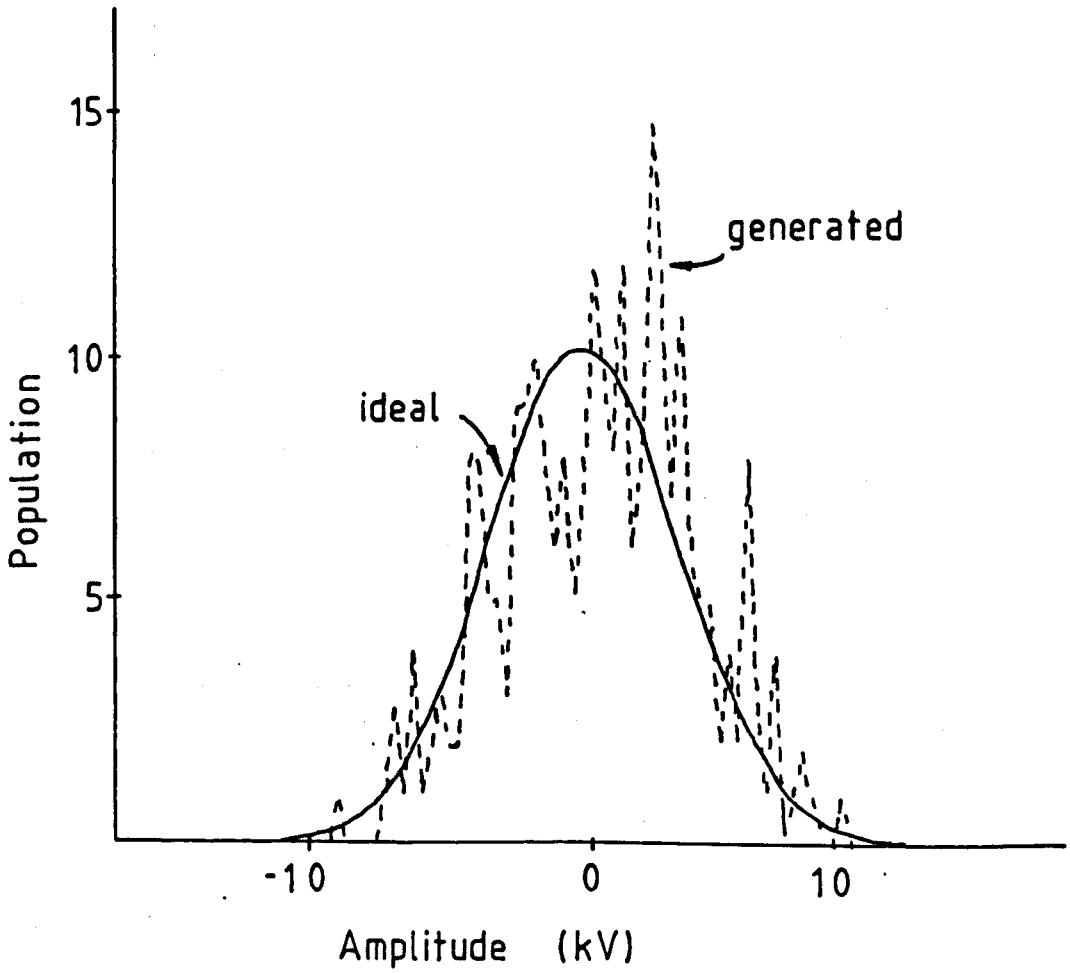

Figure 5.25 A typical amplitude distribution for the generated noise compared with the ideal normal distribution.

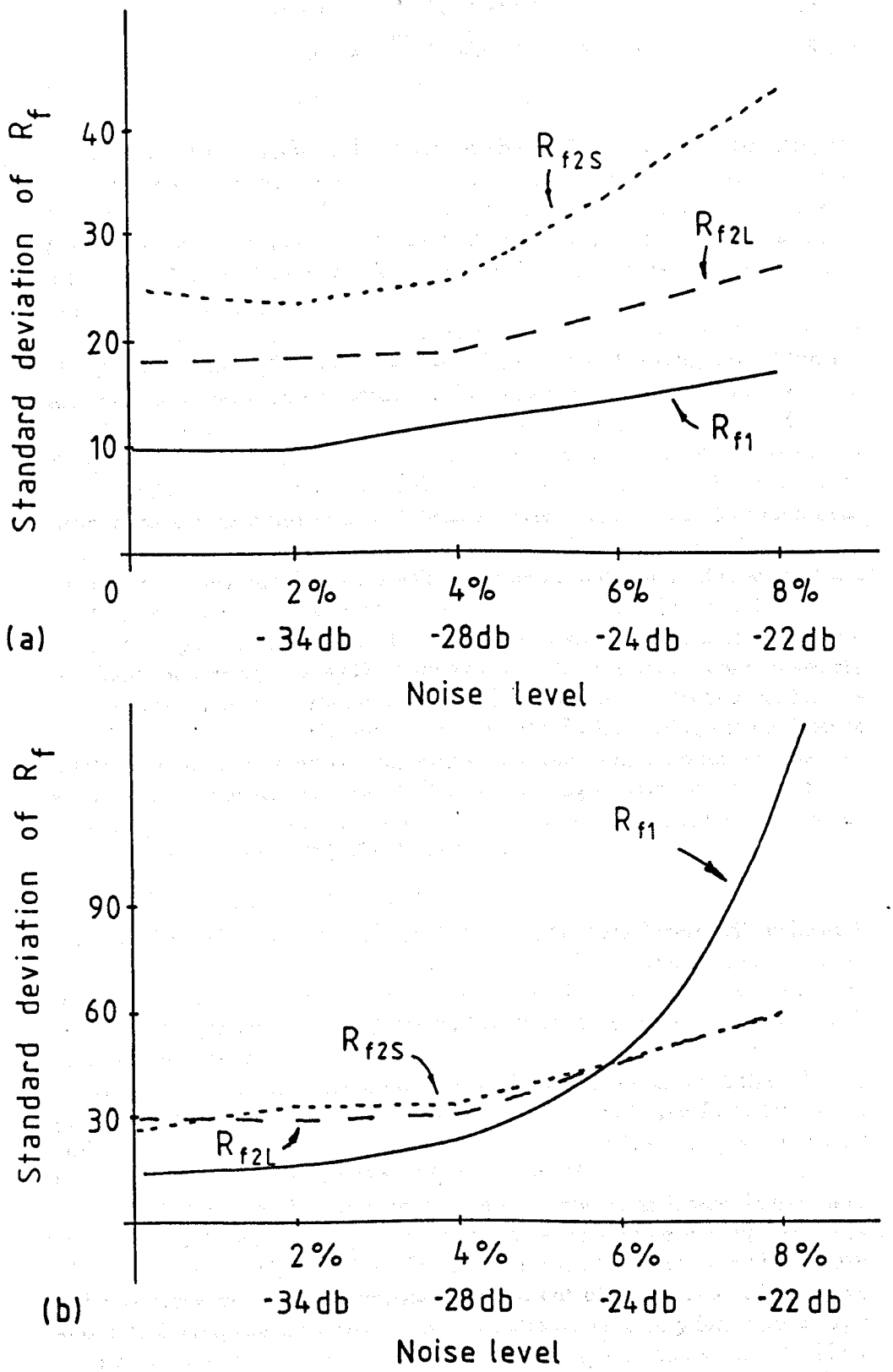

Figure 5.26 The standard deviation of the fault resistance estimates against the standard deviation of the noise superimposed on the fault transients. The faults were phase-a to ground faults on the line configuration given in figure 4.3. R_{f1} is the first resistance estimate. R_{f2S} is the second resistance estimate using the short cross-correlation window. R_{f2L} is the second resistance estimate using the long cross-correlation window.

(a) Faults occurring at phase-a voltage maximum.

(b) Faults occurring at phase-a voltage phase angle of $5\pi/12$.

$$\Delta v(a) = \sum V_n \sin(n\omega t) \quad (5.51)$$

$$\Delta v(b) = \sum V_n \sin(n(\omega t - 2\pi/3) \quad (5.52)$$

$$\Delta v(c) = \sum V_n \sin(n(\omega t + 2\pi/3) \quad (5.53)$$

The resulting standard deviation of the fault resistance estimates, for the two extreme conditions of the 5% harmonic levels, are given in figure 5.27, for up to the ninth harmonic. From figure 5.27 it can be seen that a 5% harmonic level should lead to a standard deviation in the fault resistance estimates of about 20 ohms. The phase angle of the current harmonics also appears to be unimportant.

It has been found, therefore, that random noise system harmonics of about -26 decibels (5% p.u.) can be tolerated by this relay algorithm for accurate fault resistance estimation. The tolerance will have to be lowered to -32 decibels (2.5 % p.u.) at present, to ensure that the ground mode delay can be accurately determined. Noise levels of about -26 decibels leads to a standard deviation in the fault resistance estimates of about 20 ohms near voltage maximum and a standard deviation of about 30 ohms near $\pi/12$ of voltage zero. The confidence limits for low impedance faults is set to 60 ohms which implies there will be a one in four hundred chance of the fault resistance estimates falling outside the confidence limits and the relay failing to trip on an internal fault for faults occurring near voltage maximum. For faults occurring near $\pi/12$ of voltage zero there is about a one in twenty chance of the fault resistance estimates falling outside the 60 ohms confidence limits. This can be greatly improved, however, by increasing the confidence limits to 80 ohms without risking relay over reach. There would then be over a one in ten thousand chance of the relay failing to trip on internal faults occurring near voltage maximum and about a one in a hundred chance for faults occurring near $\pi/12$ of voltage zero.

5.4.2 Filtering of the fault transients

As stated previously, real voltage and current transducers will exhibit a degree of low pass filtering of the fault transients. It would also be useful to filter out high frequency transients such as lightning spherics to ensure good noise rejection. It is important, therefore, to quantify the bandwidth required by this relay.

On a simple single phase transmission line, with a busbar at the relaying point, the dominant frequency component of the primary fault transients will have a period between two and four times the travelling wave transit time between the fault and the relaying point [5].

Figure 5.28 shows the fault resistance estimates of an internal phase-a to ground fault 40 km from the relaying point as the upper cut off frequency of the fault transients is varied. The fault transients were filtered by a sixth order Butterworth filter. It appears that, at cut off frequencies of less than about 3.75 kHz, the fault resistance estimates become very inaccurate. The time of separation of the first incident wave [V_1] and the second incident wave [V_{i2}] ($2t_1$ in figure 1.5) is about 0.26 milliseconds. Thus, the fault resistance estimates appear to become unreliable when the upper cut off frequency is less than about $1/2t_1$. This is a reasonable conclusion as not

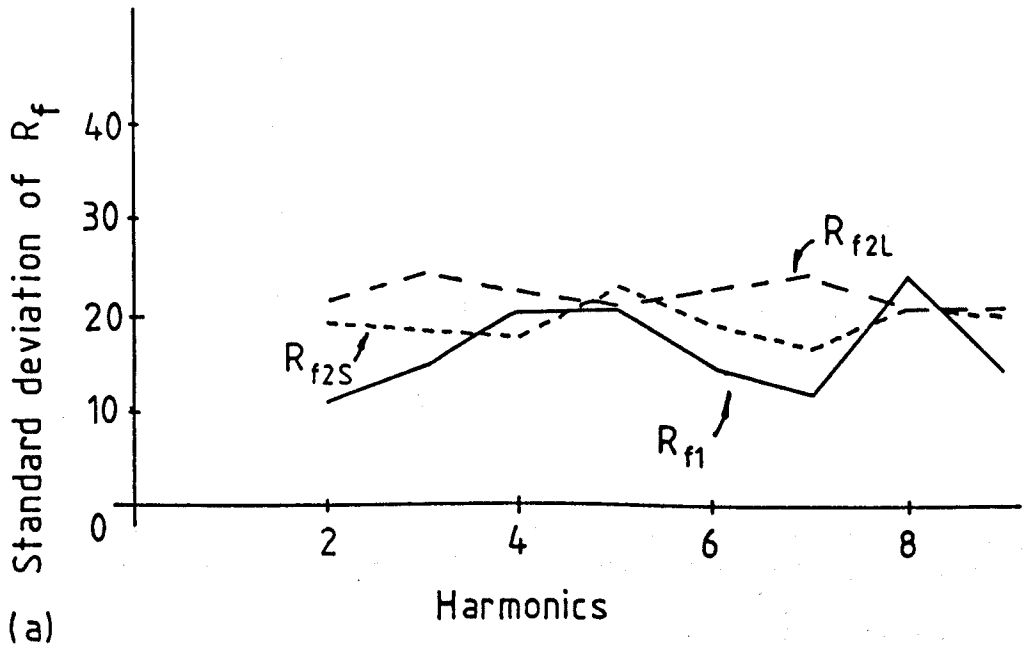

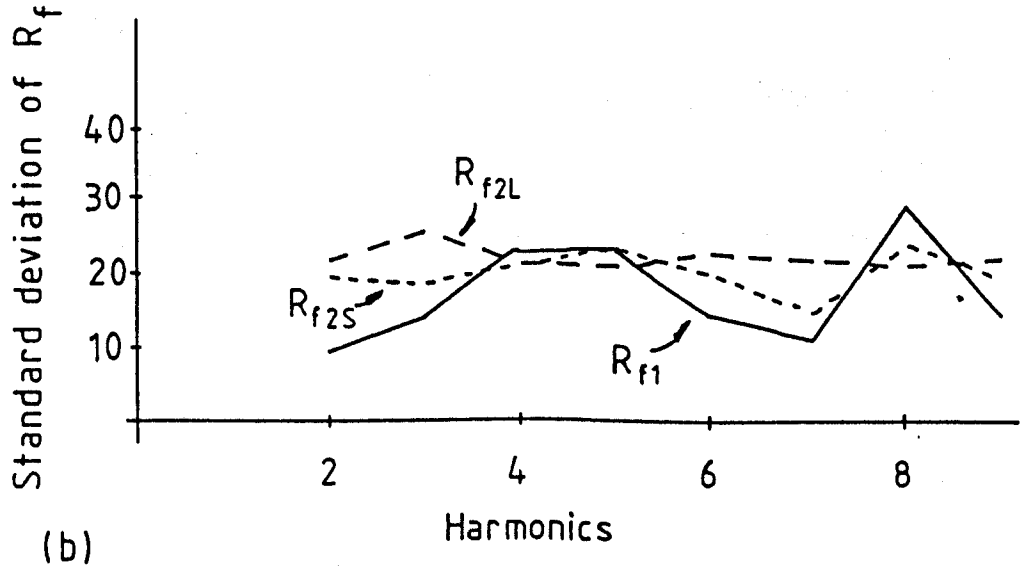

Figure 5.27 The standard deviation of the fault resistance estimates against the order of the harmonics superimposed on the fault transients. The amplitude of the harmonics was -26 db (5% p.u.). The faults were phase-a to ground faults located on the line configuration given in figure 4.3. R_{f1} is the first resistance estimate. R_{f2S} is the second resistance estimate using the short cross-correlation window. R_{f2L} is the second resistance estimate using the long cross-correlation window.

(a) The harmonic current in phase with the harmonic voltage.

(b) The harmonic current π out of phase with the harmonic voltage.

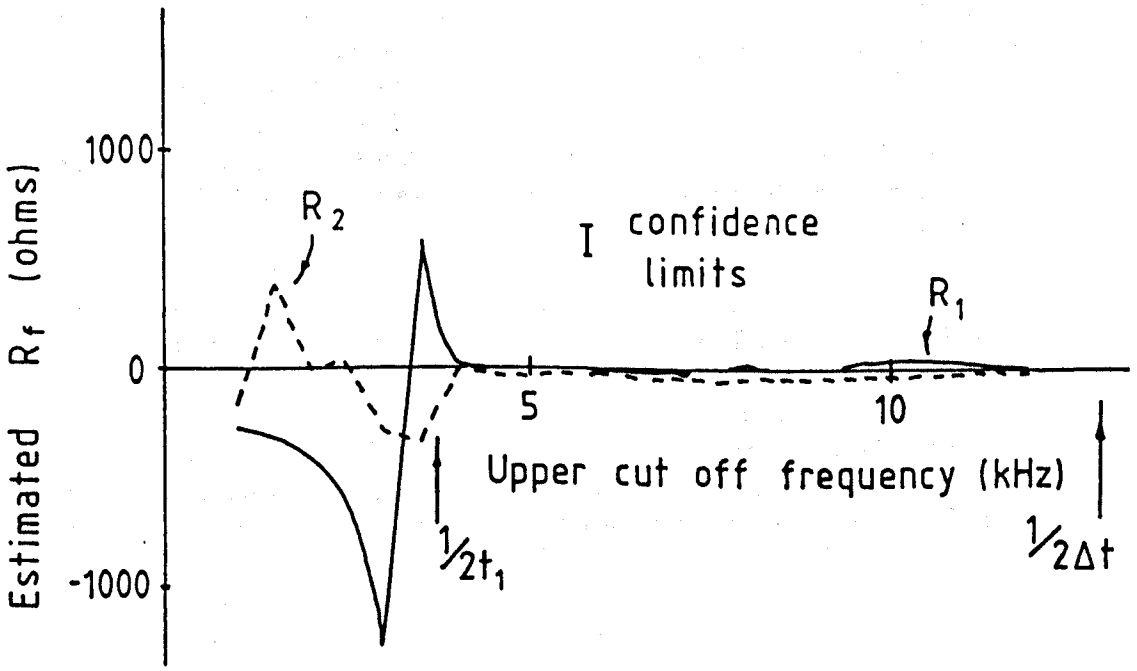

Figure 5.28 The fault resistance estimates against the fault transients upper cut off frequency. The fault was a phase-a to ground fault of resistance 10 ohms located 40 km from the relaying point on the configuration given in figure 4.3. The transients were filtered by a 6th order Butterworth low pass filter.

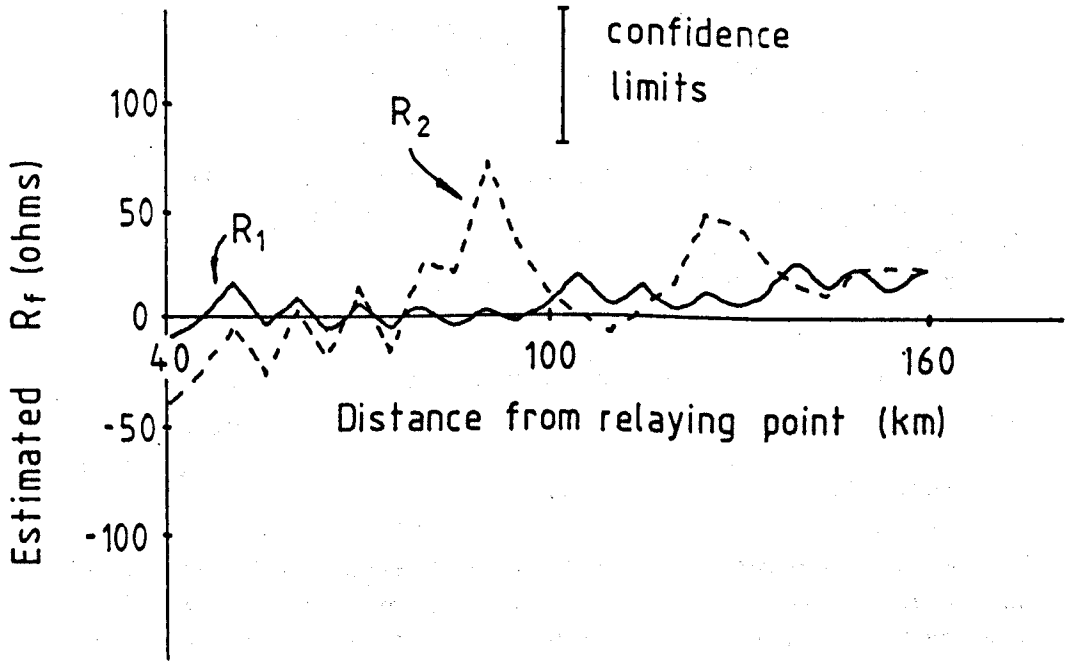

Figure 5.29 The fault resistance estimates against the fault location when the fault transients have been low pass filtered down to an upper cut off of 5 kHz. The faults were phase-a to ground faults occurring at phas-a voltage maximum on the line configuration given in figure 4.3.

only are the dominant transients at higher frequencies [5] but also resolving transients within the maximum frequency period must also be difficult.

This travelling wave relay is designed for the protection against faults at a distance greater than 40 km from the relaying point. It therefore seems reasonable to suggest that good fault discrimination can be achieved provided the transients are not low pass filtered below 3.75 kHz. Figure 5.29. shows the fault resistance estimates for fault locations along the whole protection zone of figure 4.3 when the transients are low pass filtered by a sixth order Butterworth filter of upper cut off frequency of 5 kHz. Good fault resistance agreement is achieved for all the fault locations.

In conclusion, the minimum frequency cut off of the transient signals, required for the resolution of faults within 40 km of the relaying point, is about 3.75 kHz. This is greater than the current bandwidth of the relaying transformers. In particular capacitive voltage transformers have bandwidths much less than 500 Hz [92, 93]. There are transducers available, such as capacitor-divider voltage sensors [93], which can achieve bandwidths of a few kHz. Therefore, though the required bandwidth is higher than the current relaying transducer fidelity, a bandwidth of 5 kHz is not an unreasonable requirement as transducers of the necessary bandwidth are available.

5.4.3 Conclusions for relaying noise tolerance and bandwidth.

From the preliminary investigations described, it appears that good fault resolution is possible for noise levels up to about -32 decibels of the system per unit levels and signal bandwidth of the order of 4 kHz. This should be adequate for application on EHV transmission lines which appear to have lower noise levels than this [45, 92].

The closest resolvable fault, however, may have to be limited to within 50 km of the relaying point so that the initial transient wave [V_1] can be averaged over three samples. This may not be too restrictive as traditional distance relaying schemes can adequately protect up to this distance

The relay algorithm requires transducers of a much larger bandwidth than those in current use. However, transducers of the appropriate bandwidth are available [93], therefore, this relay should still be a realistic proposition for the high speed protection of EHV transmission lines.

5.5 Measurement of the incident wave voltage gradient.

When a fault occurs at the line centre, the second incident wave at the relaying point arrives simultaneously with the first reflected wave from the far busbar (busbar 2). This is depicted in figure 5.30, which shows the Bewley lattice diagram of the fault transients for a fault occurring at the line centre. Though there are many other fault locations were the second incident wave arrives simultaneously with the other waves, faults at the line centre are a severe example as the waves from the far busbar are only attenuated by one reflection at a busbar and one transmission through the fault location. It is proposed, therefore, to protect against faults at the line centre by the use of the incident voltage gradient of the fault transients. It has then been found that this technique also differentiates between faults at the line centre and capacitor spark gap flashover at the line centre.

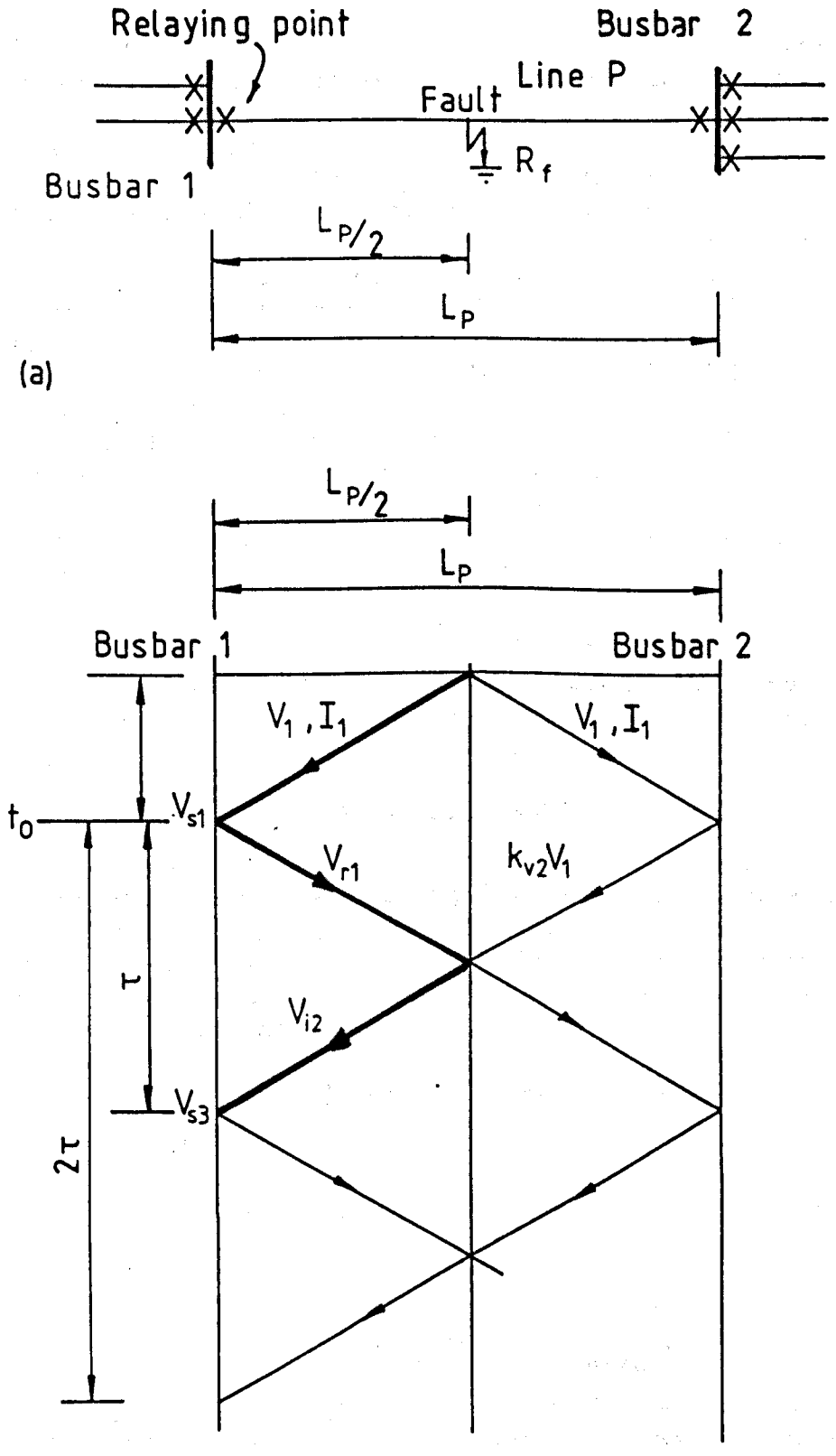

Figure 5.30 The line configuration (a) and Bewley lattice diagram (b) for a fault located at the protected line centre.

5.5.1 Estimation of the initial fault voltage phase angle.

In the vast majority of cases the long cross-correlation window is sufficient to resolve the second incident wave V_{i2} for faults at the centre of the protected line. However, with noise levels greater than -32 decibels it has been found that some single phase to ground faults may not be resolved. Fortunately, for faults at the line centre, there is plenty of time to confirm the fault location before another wave is incident at the relaying point.

From the Bewley lattice diagram given in figure 5.30 it can be seen that there is a period τ after the arrival of the first incident wave V_1 before another wave is incident at the protection point. It is therefore proposed to measure the gradient of the first incident wave V_1 in time τ to get a precise estimate of the initial fault voltage phase angle. If this measured fault voltage phase angle compares with the expected fault voltage phase angle for a fault at the line centre, then it will be assumed that there is a fault at the line centre and the relay will trip.

Given the voltage phase difference between the relaying point and the fault can be given as δ_1 as given in equation 2.24. The initial fault voltage v_f, at the steady state level, can be given as

$$v_f = |v_f| \cos(\omega_0 t + \theta_1 + \delta_1) \tag{5.54}$$

The first fault transient wave to propagate away from the fault will then have an amplitude which can be given by combining equations 5.54 and B.14 to give

$$V_1 = k_{vf} |v_f| \cos(\omega_0 t + \theta_1 + \delta_1) \tag{5.55}$$

From equation 4.4 and table 4.1 it was shown that the line impulse of the aerial transients has a very rapid rise time. Over the time period $t_0 + 0.08ms. < t < t_0 + \tau$, where t_0 is the arrival time of the first incident transient V_1 and $t_0 + \tau$ is the arrival time of the subsequent incident waves τ later, it is expected that the first incident aerial transients at the relaying point can be approximated by

$$V_{1a} = k^a_{vf} |v_f| \cos(\omega_0 (t - t_0) + \theta_1 + \delta_1) \tag{5.56}$$

The gradient of this wave form will then be

$$\frac{dV_{1a}}{dt} = -k^a_{vf} \omega_0 |v_f| \sin(\omega_0 (t - t_0) + \theta_1 + \delta_1) \tag{5.57}$$

thus

$$\omega_0 (t - t_0) + \theta_1 + \delta_1 = \tan^{-1} \left(-\frac{\frac{dV_{1a}}{dt}}{\omega_0 V_{1a}} \right) \tag{5.58}$$

Using equation 5.58, it should then be possible to estimate the initial fault voltage phase angle from the first incident aerial wave amplitude V_{1a} and its gradient.

The initial transient wave voltage gradient and amplitude can be found by using the traditional least squares technique [94]. This gives an accuracy in the measurement of the gradient σ_b of

$$\sigma_b = \sigma_v \sqrt{\frac{\sum_{n=1}^{N}(n\Delta t)}{N\sum_{n=1}^{N}(n\Delta t)^2 - (\sum_{n=1}^{N} n\Delta t)^2}} \tag{5.59}$$

where Δt is the sample period, σ_v is the standard deviation of the voltage transients and N is the total number of samples

The incident voltage amplitude is found from the average of the samples which will have an error of

$$\sigma_a = \frac{\sigma_v}{\sqrt{N}} \tag{5.60}$$

The precise fault locations which appear to give problems are just the relaying side of the line centre, where waves from the far busbar arrive between one and two samples before the second incident wave V_{i2}. For a 200 km line the problem locations lie between 90 to 100 km from the relaying point. The maximum number of samples N available for the fault phase angle estimates at a sampling rate of 25.6 kHz will then be thirteen. This can be greatly improved, however, by using the fact the all three phases of a single phase to ground fault's aerial transients are linearly dependent (as discussed in chapter 4). All three phases can then be averaged to increase the total number of samples to thirtynine.

Given a voltage noise level of -26 decibels (5% p.u.) the accuracy in estimating the initial fault voltage phase angle should then be about 0.01 radians. This is adequate to distinguish between internal and external faults provided the line is loaded to at least 40 megawatts. For lower line loadings there will not be enough phase difference between the line centre and the line ends to tell whether the fault is internal or at the far busbar.

This measured fault voltage phase angle is then compared with the estimated fault voltage phase angle assuming that the fault occurred between 90 to 100 km from the relaying point. The steady state fault voltage given by equation 2.20 can be rearranged to give

$$\delta_1 = \tan^{-1}\left(\frac{|i_0|Z_s\cos(\theta_1-\theta_2)\sin\beta x}{|v_0|\cos\beta x - |i_0|Z_s\sin(\theta_1-\theta_2)\sin\beta x}\right) \tag{5.61}$$

where x is set to 95 km from the relaying point.

Figure 5.31 shows the measured fault voltage phase angle from the gradient and amplitude of the incident voltage wave forms compared with the estimated fault voltage phase angle deduced using equation 5.61 for phase-a to ground faults occurring along the line given in figure 4.3 at a phase angle of $\pi/12$. The loading in this example was 500 megawatts. It can be seen that good fault resolution is possible for this loading.

It has therefore been found that faults near the line centre, occurring at small initial phase voltages, can be resolved using the initial transient voltage amplitude and gradient (Provided that the line loading is at least 40 megawatts).

If a cross-correlation trough is observed near the line travelling-wave travel time τ or no troughs are observed within the line round trip time 2τ, then it is proposed to implement this algorithm to ensure that there are no internal faults near the line centre.

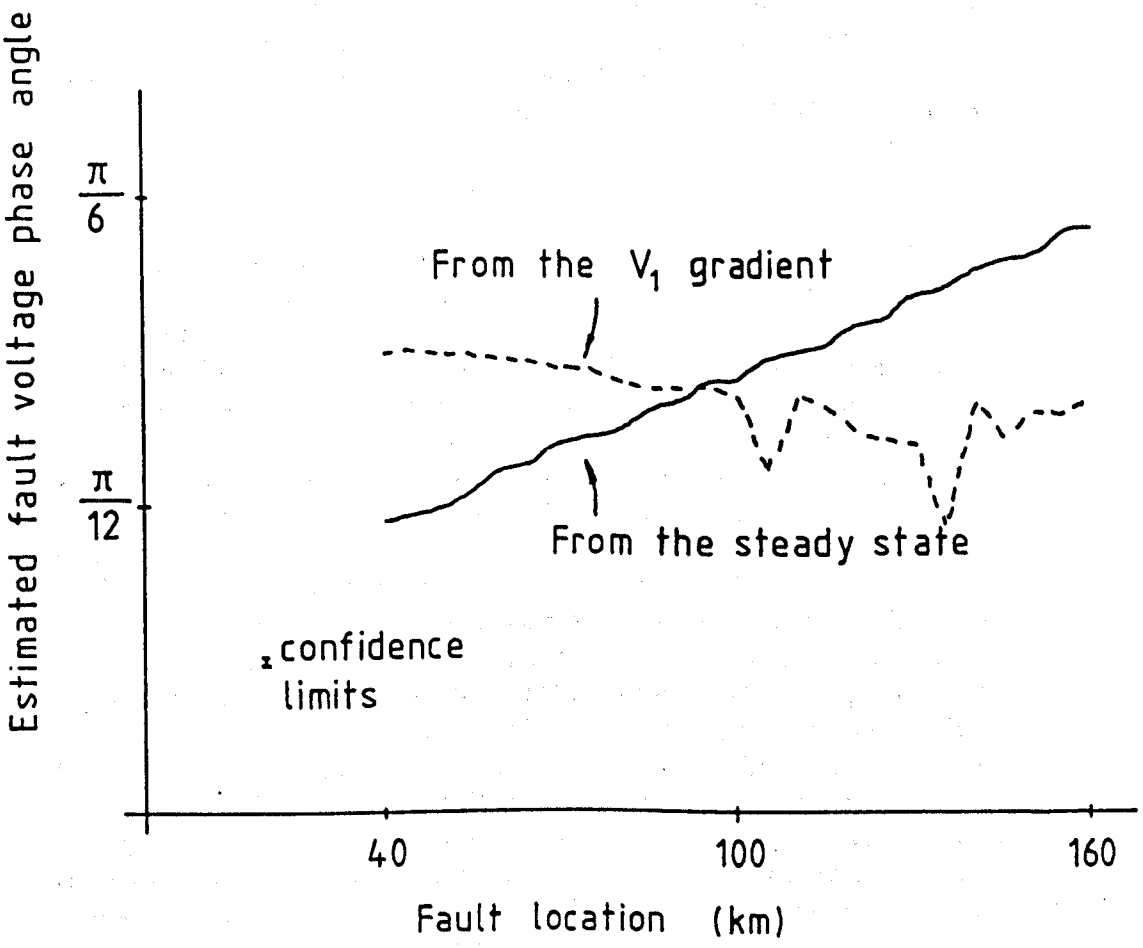

Figure 5.31 The estimated initial fault voltage phase angle for phase-a to ground faults occurring at phase-a voltage phase angle of $\pi/12$. Transient noise of -26 db (5% p.u.) was superimposed on the fault transients. The simulated line configuration is given in figure 4.3.

5.5.2 Sudden unexpected capacitor spark gap flashover

On EHV transmission lines it is not uncommon for series capacitor spark gaps to suddenly flash over for no apparent reason. The voltage across the series capacitors is only a few tens of kilovolts so that, in the vast majority of cases, the resulting transients will be below the relay threshold level. Unfortunately, the voltage across the series compensation is about $\pi/2$ radians out of phase with the line phase voltage. Maximum spark gap transients then coincide with the period when the relay is expecting small fault transient amplitudes from faults near phase voltage zero so the relay may trip on these transients.

For series compensation at the line ends, the cross-correlation functions will only display the line round trip wave $V_{2\tau}$ as shown in figure 5.32a. The relay will then ignore these transients.

When there is a capacitor spark gap flashover for compensation near the line centre, the resulting cross-correlation function will display a trough indicating a fault at the line centre as shown in figure 5.32b. Near line voltage zero these transients will also be of the correct amplitude to be confused with faults at the line centre. The relay may then trip on these transients.

For sudden capacitor spark gap flashover, the initial fault voltage profile of the incident wave V_1 will have the steady state variation of the voltage across the series compensation. The phase voltage phase angle across series capacitors varies by no more than $\pi/10$ radians. The voltage across the series compensation is $\pi/2$ out of phase with the phase current which in tern will only be a small angle out of phase with the phase voltage [89]. The measurement of the transient voltage phase angle from the initial transient voltage gradient and amplitude should then give a vastly different result to the estimated voltage phase angle from 5.61, for locations either side of the compensation. As an example the results for a typical sudden spark gap flashover on series compensation at the line centre are given below.

> Phase angle from the incident voltage wave $V_1^a = \pi/2$ radians.
>
> Phase angle estimate for the relay side of the compensation 3.2 radians.
>
> Phase angle estimate for the far side of the compensation 3.3 radians.

It can be seen that the phase angle estimate differences are very large, therefore, good precision in the measured transient phase angles is not necessary. It then follows that the, spark gap flashover transients should be distinguishable from fault transients even if the compensation is not located precisely at the line centre.

5.5.3 Conclusions for the measurement of voltage gradients.

In this section it has been proposed that, provided there is only one incident travelling wave transient from a fault or spark gap flashover, the voltage transient profile will be a good approximation of the steady state voltage variation across the fault or spark gap. Near phase voltage zero the phase angle of the steady state voltage at the fault or spark gap can then be estimated from the transient voltage gradient and its amplitude.

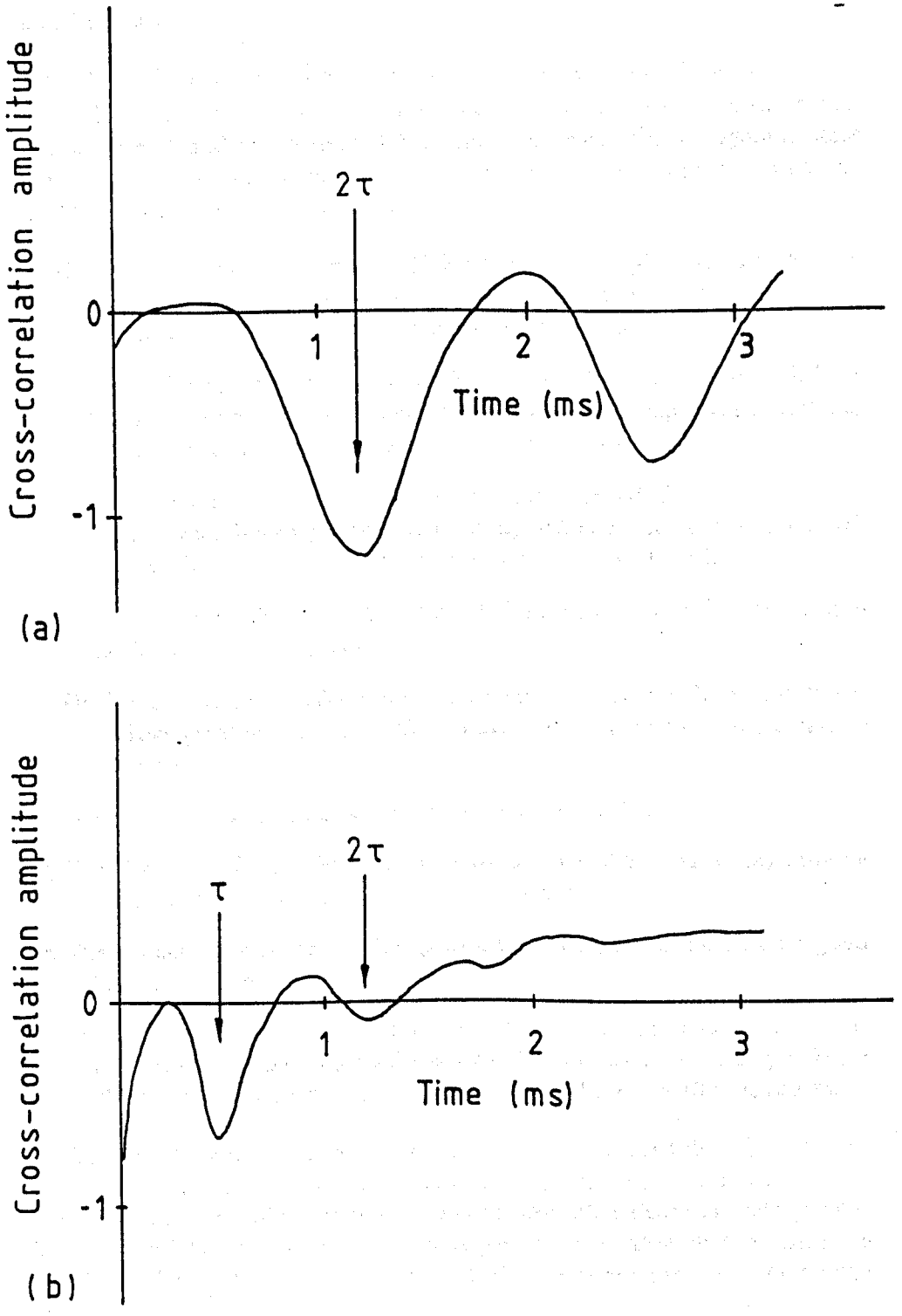

Figure 5.32 The cross-correlation functions for the long window (21 samples) when the series capacitor spark gaps suddenly flashover near capacitor voltage maximum. (a) Series compensation at the relaying point. (b) Series compensation at the line centre.

This technique will then enable the relay to resolve faults at the line centre and also to distinguish between faults and sudden capacitor spark gap flashover.

5.6 Conclusions for the protection of difficult conditions.

It has been shown that this travelling-wave relay should be able to protect double circuit and compensated transmission lines. Normal system noise can also be tolerated. There are limits to the line conditions which can be protected, however, and these are

a Only faults from a distance of 40 km from the relaying point to 80% of the line length can be protected. More distant faults are difficult to detect due to the capacitor spark gap transients.

b Lines no longer than 400 km can be protected. Longer lines will have travelling wave transit times comparable to the capacitor spark gap times so that all fault transients may not be identifiable.

c The transmission lines must not be excessively loaded. Excessively loaded transmission lines (greater than 2 p.u.) will cause the protective spark gaps to flashover before an internal fault can be identified.

d Double circuit lines must be connected in parallel so that the ground mode delay can be utilised.

e Double circuit line busbars must be connected to the short circuit capacities greater than 10 GVA so that the line round trip wave can be identified.

f The system noise must not exceed -26 decibels (5% p.u.)

g The closest resolvable fault for a sampling rate of 25.6 kHz may only be approximately 50 km from the relaying point.

h The transients must not be low pass filtered below about 4 kHz for good fault resolution.

i The transmission lines must not be lightly loaded so that faults at the line centre can be identified from the fault voltage phase angle. For a 200 km transmission line the minimum load limit is 40 megawatts.

Though there are quite a few restrictions it is expected that these conditions will not fall outside the usual range on EHV transmission lines and that normal distance relaying schemes can cover the other situations adequately. The required transducer bandwidth is greater than that of the currently installed relaying transducers, but, transducers of the required bandwidth are available.

Due to the nature of travelling-wave relays, where all information must be available in a short sample set (3 milliseconds), 100 % relay success can not be guaranteed. Travelling-wave relays must then be used as an extra facility in addition to the usual distance protection schemes. Travelling-wave routine will then offer a highly confident probability of rapid relay response

without the risk of relay over reach and the statistics for this response must be specified.

From the measured standard deviation of the fault resistance estimates it was found that, the present relaying setting ensures that only one in four hundred internal faults will be incorrectly identified as being external for faults occurring near voltage maximum. This may be greatly improved, without risking relay over reach, to over one in ten thousand. All external faults are correctly identified and relay over reach does not occur.

CHAPTER 6

Implementation of the relay algorithm in real time.

6.1 Introduction

In this chapter a real time implementation of the basic travelling-wave relay algorithm is described. This has been carried out to demonstrate that the complex signal processing requirements of the relay algorithm can be achieved in a reasonable time with reasonable accuracy for ultra high speed relay response.

The relay logic requires a large amount of signal processing. In particular the cross-correlation function with mean removal involves approximately a thousand multiplications and subtractions, which must be achieved within about a millisecond. It was decided, therefore, to use the Texas Instrument's TMS320C25 signal processor [95] which offers 100 nanosecond instruction cycle times with single cycle multiplications. This processor also has the advantage that it uses low power CMOS technology [96] which is ideal for substation equipment that has to have low maintenance and high reliability.

The important features of the TMS320C25 signal processor will be described and the implementation of the basic relay algorithm (without additional checks) will be outlined. The example data set shows that the implemented real time relay should have good precision and rapid response.

In this chapter the Texas Instrument's hexadecimal notation is used where `>1A` indicates the decimal value 26.

6.2 The TMS320C25 signal processor.

The TMS320C25 digital signal processor is a member of the Texas Instrument's TMS320 family of VLSI digital signal processors and peripherals. The TMS320 family processors have a 32-bit Harvard architecture, in which programme and data memory reside in separate address spaces, and a 16-bit external interface [95].

The TMS320C25 is a pin compatible CMOS version of the TMS32020 [97] with a faster instruction cycle and the inclusion of additional hardware and software features. The main enhancements include; a faster instruction cycle time (100 ns.), low power CMOS technology and eight auxiliary registers with a dedicated arithmetic unit.

Together the programme and data buses can carry data, from on-chip RAM and internal or external programme memory, to the 16-bit multiplier in a single cycle for multiply/accumulate operations. The central arithmetic logic unit (CALU) implements 32-bit two's compliment arithmetic and contains; a 16-bit scaling shifter, a 16x16-bit parallel multiplier, a 32-bit arithmetic logic unit (ALU), a 32-bit accumulator, and some additional 16-bit scaling shifters available at the outputs of both the accumulator and the

multiplier. The 32-bit arithmetic unit and accumulator can perform a wide range of arithmetic and logic instructions, the majority of which execute in a single cycle. The internal architecture of the TMS320C25 then offers a high degree of parallelism such that a powerful set of arithmetic, logic and bit manipulation operations may all be performed in a single cycle.

The TMS320C25 then appears to be ideal for the signal processing procedures envisaged in this travelling-wave relay algorithm and at present the TMS320C25 offers the most cost effective single processor solution.

It should be noted, however, that if data is being fetched from external memory locations then the processor instruction cycle will include an extra wait state increasing the access time to 200 nanoseconds. It is important, therefore, to make maximum use of the internal memory locations.

The TMS320C25 provides a total of 504 16-bit words of on-chip data RAM which is divided into three separate blocks (B0,B1 and B2). 256 words of the 544 words can be configured as either programme or data memory, this is block B0. The other 288 words (blocks B1 and B2) are always data memory. There are also 64 kwords of off chip programme memory locations and 64 kwords of off chip directly addressable data memory locations available. The programme and data memory maps for the TMS320C25 are given in figure 6.1. At present the TMS320C25 is run in microprocessor mode with the on chip ROM mapped out. In addition to the internal memory blocks B0, B1 and B2, the data memory map includes memory mapped registers and reserved locations. The registers have been mapped into data memory for easy modification, but, the reserved locations may not be used for storage and their contents are undefined when read.

The relay algorithm has been written in such a way as to make maximum use of the internal data memory addresses and the single cycle multiply and accumulate instructions. It will be demonstrated that this signal processor should be satisfactory for the signal processing requirements of the relay algorithm.

6.3 The relay algorithm for the TMS320C25

The Loughborough Sound Images TMS320C25 development system based on an IBM PC [98] was chosen as a suitable platform on which to develop the relay software. This development system essentially consists of a TMS320C25 processor board for an IBM PC compatible computer with support software. The boards main features are: a full speed TMS320C25 processor with no wait states, sockets to take full memory, an on board high precision A/D and D/A and timer, parallel and serial expansion connectors and complete support for assembler language programming. The board schematic is given in figure 6.2.

The basic relay algorithm can be summarised by the flow chart given in figure 2.5. In order to achieve as efficient an algorithm as possible, modern analysis methods of programme requirements were performed on the basic relay algorithm. This essentially involves the basic relay algorithm data processing requirements being represented by either the data flow diagram shown in figure 6.3 or the Warnier diagram shown below [99]

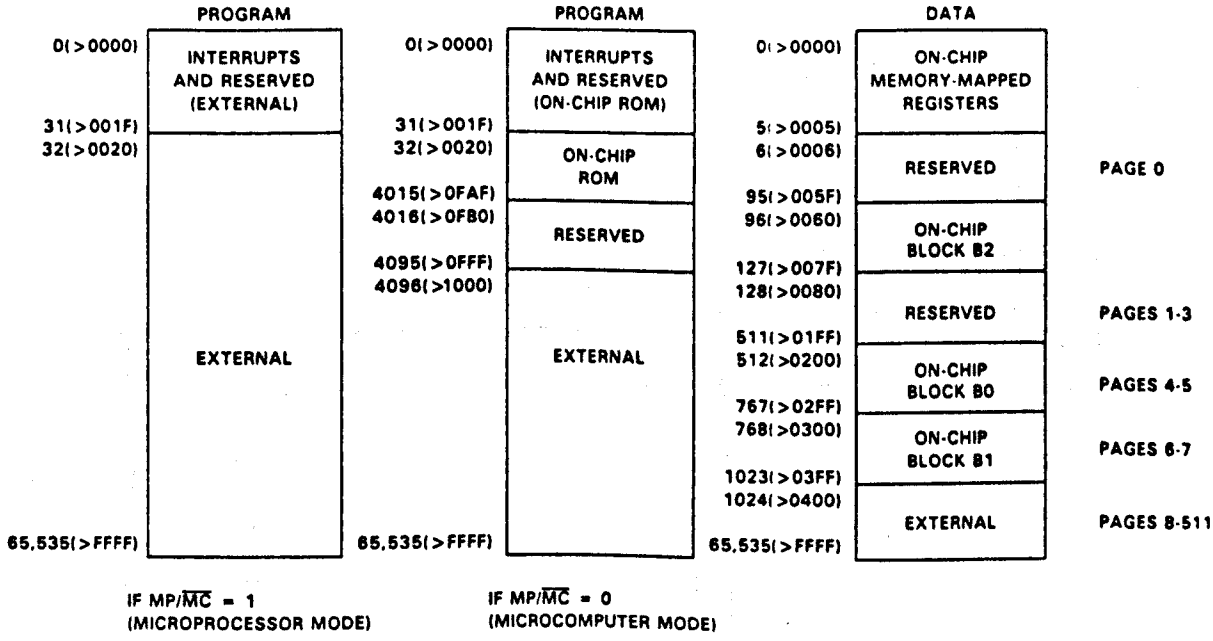

(a) MEMORY MAPS AFTER A CNFD INSTRUCTION

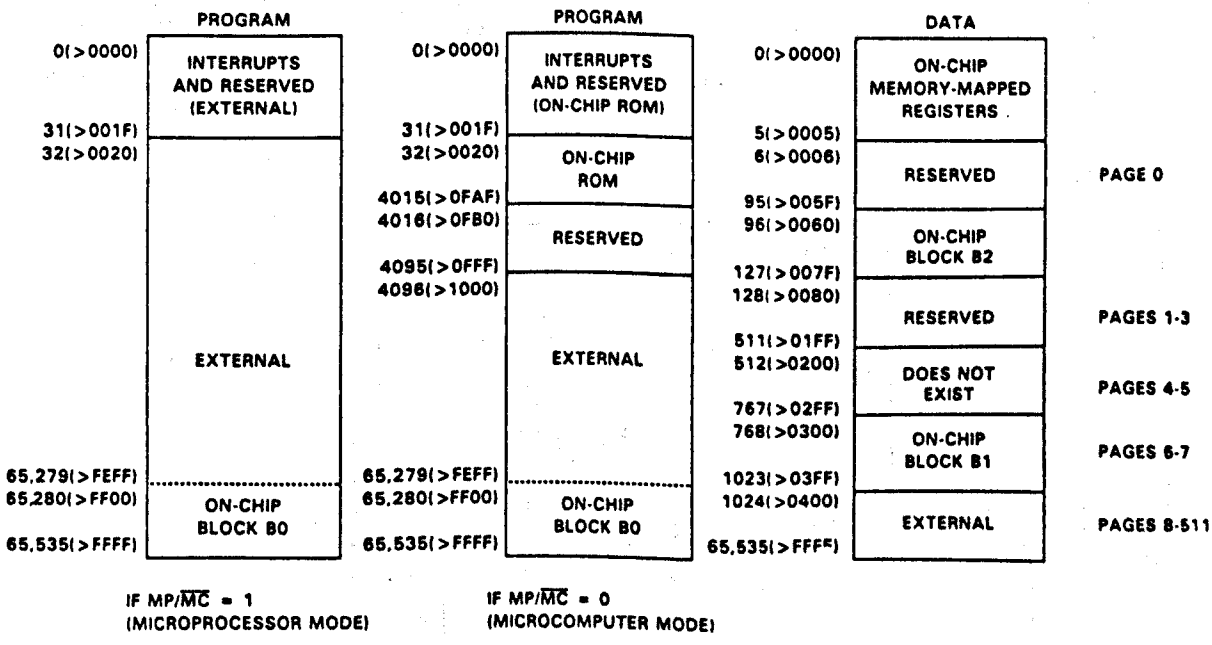

(b) MEMORY MAPS AFTER A CNFP INSTRUCTION

Figure 6.1 Memory maps for the TMS320C25. Microprocessor mode is with the on chip ROM mapped out. Microcomputer is with the on chip ROM mask-programmed at the factory and mapped into programme address space (After Texas Instruments [95]).

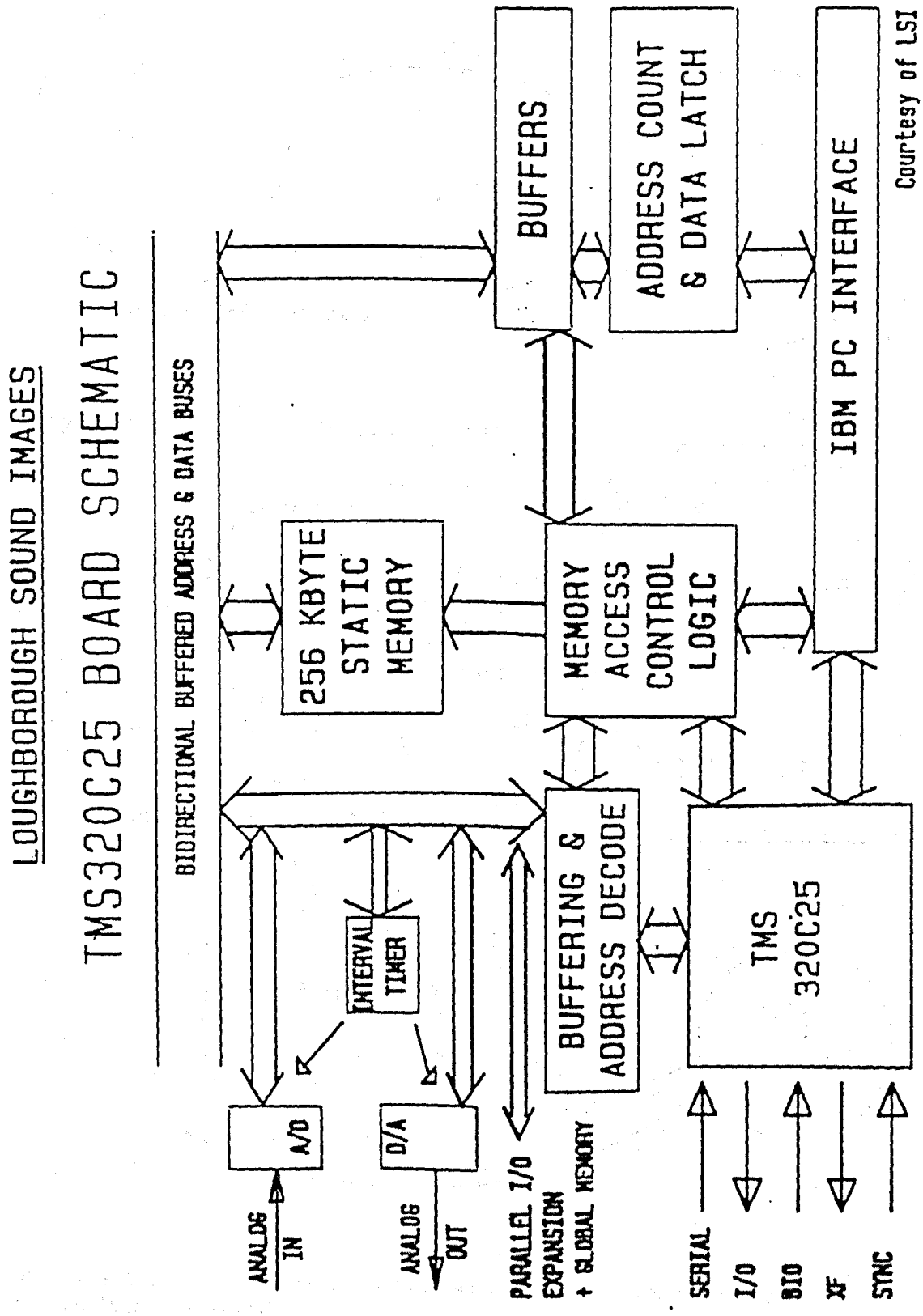

Figure 6.2 Loughborough Sound Images TMS320C25 development system (After Loughborough Sound Images [98]).

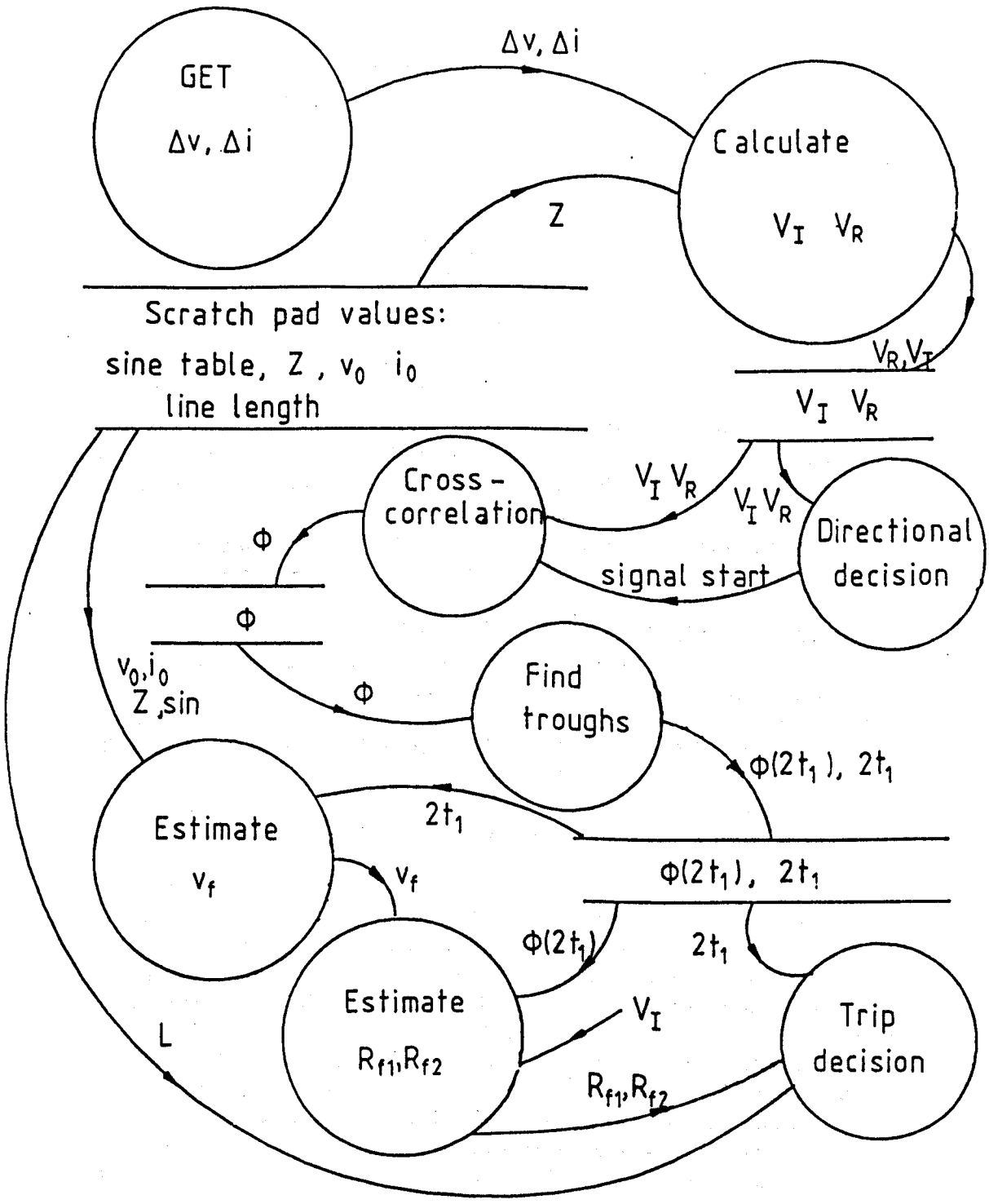

Figure 6.3 Data flow diagram for the basic relay algorithm without additional checks.

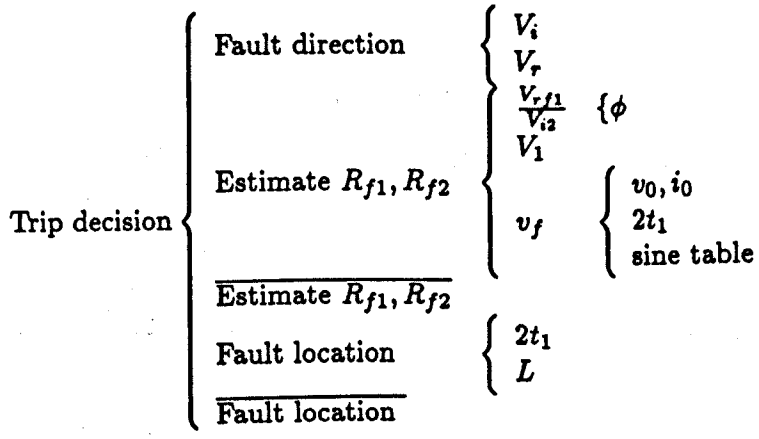

Warnier diagram of the basic relay algorithm.

The Warnier diagram considers information flow and functional hierarchy. In the Warnier diagram the bar over the process name indicates that it might not be implemented for some fault processing. The data flow diagram depicts information flow and the transforms that are applied as the data is moved from input to output. These two diagrams are valuable tools for producing an optimal relay algorithm.

The relay programme hierarchy is similar to the Warnier diagram shown above. Data memory allocation has been based on the data flow diagram shown in figure 6.3.

In order to demonstrate the action of the relay algorithm and its speed and accuracy, the results for an internal phase-a to ground fault are given. The example fault is the internal phase-a to ground fault, 140 km from the relaying point on the line configuration 4.3 at phase-a voltage maximum, discussed in section 4.4. The results deduced using the 16-bit integer arithmetic of the TMS320C25 compare favourably with that of the ideal study in section 4.4 which used 32-bit floating point arithmetic. The timing also shows that the basic routine can be implemented within 2.3 milliseconds.

6.3.1 Memory allocation

As stated earlier, single cycle operation of the TMS320C25 is not possible if both the programme and data reside in external address space. For this reason maximum use was made of the internal memory. The amount of internal memory available is limited however. From the data flow diagram in figure 6.3 and the Warnier diagram it has been found that, in general, only a few data values need be transferred between the algorithm routines so that external memory locations or just a few internal memory locations need be used. The cross-correlation function, on the other hand, requires a significant amount of processing with the transfer of a significant amount of data. The majority of the internal memory locations were then assigned for the cross-correlation function.

The data flow diagram for the cross-correlation function is shown in figure 6.4. The values stored in internal memory are; the reference waveform with mean removal T_R, the incident waveform section with mean removal T_I, the incident and reflected transients for the faulted phase (phase-a) V_{IA}

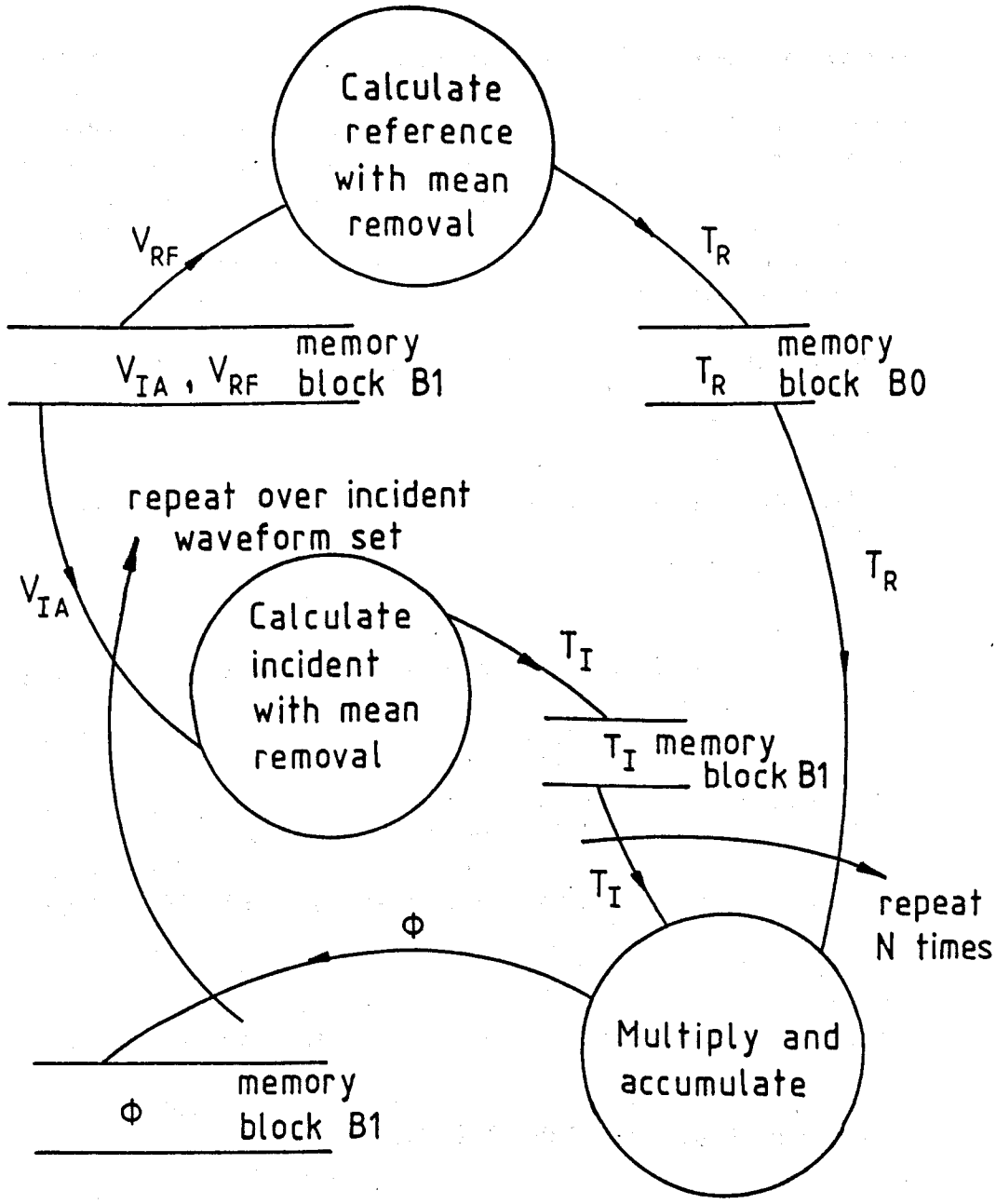

Figure 6.4 Data flow diagram for the cross-correlation function. V_{IA} and V_{RF} are given by equations 6.3 and 6.4. T_I and T_R are given by equations 6.12 and 6.13.

and V_{RF}, and the cross-correlation function ϕ. The reference values with mean removal T_R are stored in internal memory block B0 which can be reconfigured into programme address space. The values T_R and T_I can then be fetched simultaneously for the multiply and accumulate procedure. The cross-correlation function has then been implemented at maximum efficiency. Figures 6.5 and 6.6 show the internal memory allocation maps for the relay algorithm. Figure 6.7 shows the external data memory allocations.

For this initial study it is assumed that the incremental phase voltages and currents have already been captured and stored in external memory locations >0400 to >0567. The scaling of the incremental values is at present arbitrary and might need some modification in the future. At present they are stored assuming a transducer resolution of 12 bits. Each incremental voltage quantum represents 1 kV allowing a 10 per unit (1 p.u. = 400 kV) maximum incremental voltage level. Each current quantum represents 0.0039 kA allowing a 10 per unit (1 p.u. = 1 kA) maximum incremental current level. The sampled values are then stored as a 16-bit two's complement word at each address location in the format given in figure 6.8.

The sample period is 39 microseconds with a total of 60 samples per phase giving a period of 2.34 milliseconds. This is adequate for the protection of transmission lines up to 280 km. The deduced incident and reflected waveforms are also stored in external memory locations.

The deduced incident and reflected aerial transients for the faulted phase (in this case $V_i^a(a), V_r^a(a)$) are stored in internal memory locations >0300 to >0378, as they will constantly be required. They are stored in the internal memory locations at six times their true incident and reflected voltage amplitude. This format avoids any divisions which would take an excessive amount of processor time thus making the algorithm as efficient as possible.

In fact divisions are avoided throughout most of the algorithm. The data is simply scaled at suitable points in the routine to maintain a 16-bit resolution. The scaling is achieved by left or right shifting the data by the required number of bits (equivalent to multiplication by a power of 2). With the TMS320C25, this can be done in parallel with many of the instructions without incurring any delay. On the TMS320C25, 16-bit division is achieved by repeating a conditional subtract 16 times. Dividing 60 data values by a single number will take about 0.1 milliseconds which is a significant time compared the target overall operating time of 5 milliseconds. It is important, therefore, to avoid having to operate a division on significant parts of the data.

The reference waveform defined by equation 4.39 or 4.40 and the cross-correlation function are also stored in internal memory locations. The reference data is stored in internal memory block B0 which can be mapped into the top 256 programme memory locations by the CNFP instruction. The parallel Harvard architecture can then be used as a means of accessing two sets of data in one cycle. One data set residing in data address and the other in programme address space. This is a very powerful technique for processes like the cross-correlation function which require the access of two data sets.

The scratch pad values in block B2 consist mainly of data to be passed between the routines. These scratch pad values are normally accessed using direct mode addressing as they consist of individual data items.

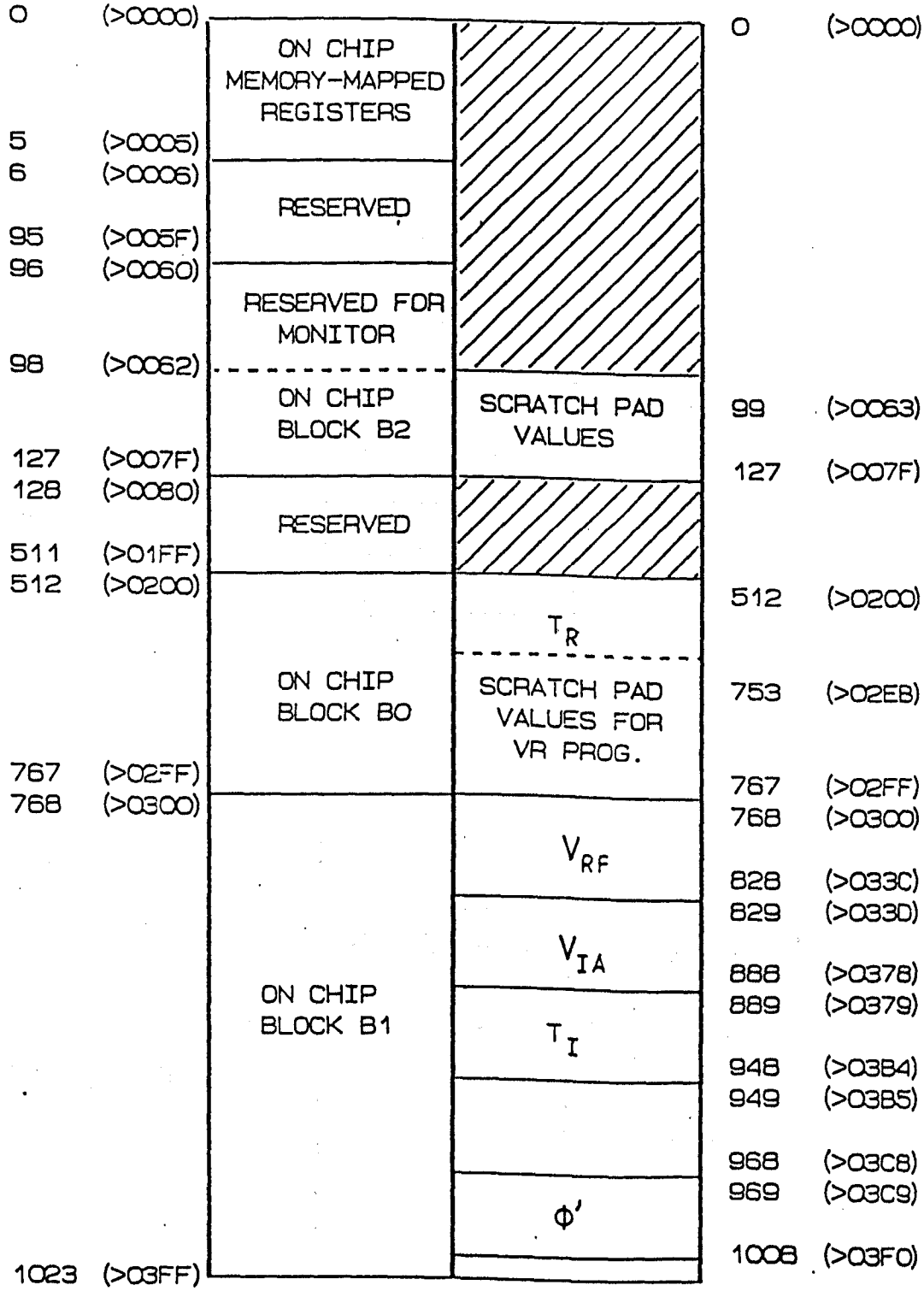

TMS320C25 INTERNAL MEMORY MAP FOR RELAY ALGORITHM

Figure 6.5 Internal data memory allocation for the basic relay algorithm.

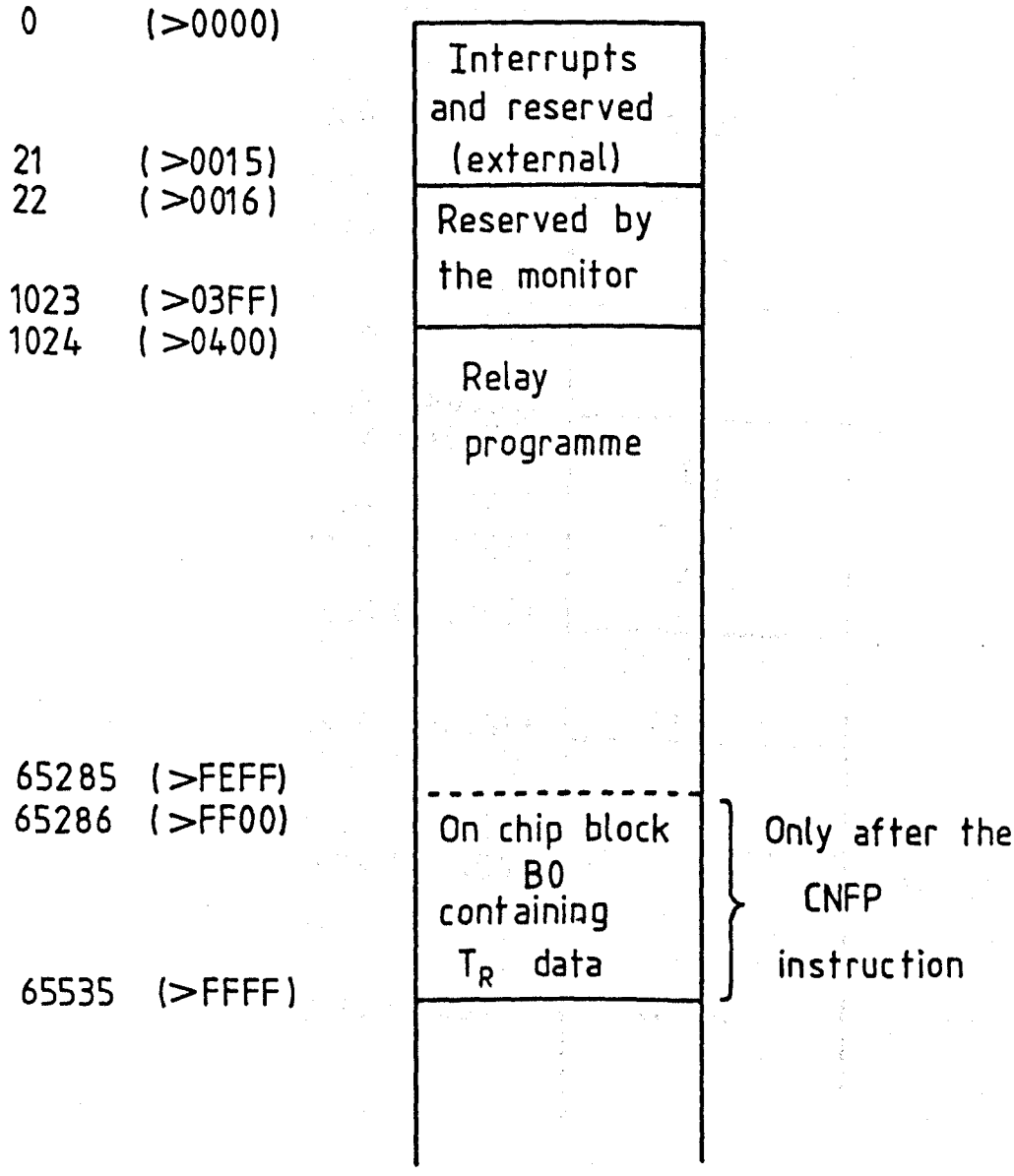

Figure 6.6 Programme memory allocation for the basic relay algorithm.

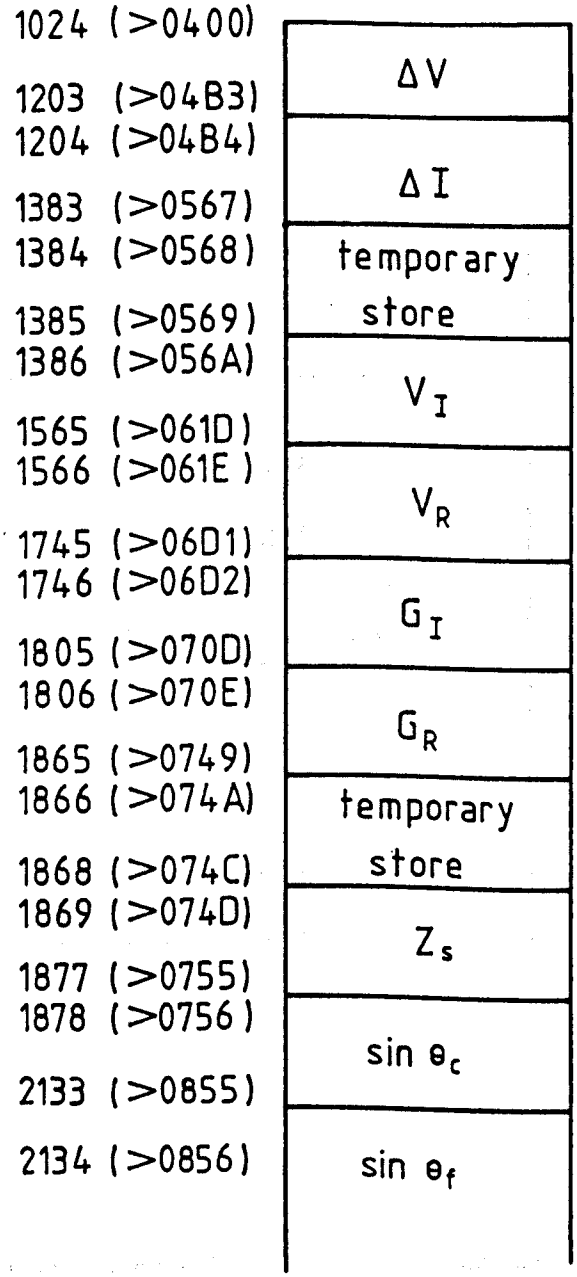

Figure 6.7 External data memory allocation for the basic relay algorithm.

DATA	ADDRESS
V(phase-a, t_{max})	> 0400
V(phase-b, t_{max})	> 0401
V(phase-c, t_{max})	> 0402
V(phase-a, $t_{max} - \Delta t$)	> 0403
etc....	
V(phase-c, t_{min})	> 04B3
I(phase-a, t_{max})	> 04B4
I(phase-b, t_{max})	> 04B5
etc....	

Figure 6.8 Format of the stored incremental values.

In conclusion, it has been found that there are enough internal memory locations for the protection of lines up to about 300 km in length. Longer transmission lines will require more internal memory address than is currently available. Lines longer than 300 km as data will have to have data either being constantly swapped in and out of internal memory locations or just residing in external data memory locations, causing the algorithm to be less efficient.

6.3.2 Calculation of the incident and reflected waveforms.

Once the incremental fault transients have been captured and stored in memory, the incident and reflected transients are calculated. These waveforms are found from the incremental voltages and currents using equations 2.40 and 2.41 where the divide by two is achieved by shifting the 16-bit numbers one bit to the right as they are stored in memory.

The incident and reflected ground mode are stored as three times their value to avoid a division by three. The stored values are given by

$$G_I = \sum_{n=a}^{c} V_i(n) = 3V_i^g \tag{6.1}$$

$$G_R = \sum_{n=a}^{c} V_r(n) = 3V_r^g \tag{6.2}$$

The incident and reflected aerial voltages are found using equation 4.10 at six times their actual amplitude in the form

$$[V_{IA}] = 6[V_i] - 2G_I = 6[V_i^a] \tag{6.3}$$

$$[V_{RF}] = 6[V_r] - 2G_R = 6[V_r^a] \tag{6.4}$$

From the deduced incident and reflected aerial voltages, directional discrimination can be performed. If the incident transients predominate then a forward fault will be assumed and the relay algorithm will continue. The directional discrimination can be carried out by comparing the incident and reflected aerial voltage amplitudes and averaging over three samples to avoid noise problems.

If there is a forward fault, pointers are set up to indicate the start and stop of the reference waveforms. The reference waveforms having been recalculated at six times the amplitude given by either equation 4.39 or 4.40. The incident and reference waveforms for the faulted phase are then stored in internal memory. In this example of a phase-a to ground fault, $V_{IA}(a)$ is given by the phase-a values of equation 6.3 and the phase-a reference waveform is stored as

$$V_{RF}(a) = 6V_{r1f}(a) \tag{6.5}$$

The resulting incident aerial voltage waveform on the faulted phase (phase-a), compared with the ideal results, is shown in figures 6.9b. Figures 6.9b. demonstrates that this 16-bit format with 12-bit transducer resolution gives perfectly adequate accuracy compared to the ideal case.

6.3.3 The cross-correlation routine

In order to find the second incident wave $[V_{i2}]$, the incident aerial voltage transients are cross-correlated with the reference waveforms. The cross-correlation routine involves over a thousand multiplications and subtractions and is therefore the most time consuming routine in the relay algorithm.

For a phase-a to ground fault, the cross-correlation function is given by equation 3.13 with the substitutions given in equations 4.25 and 4.26. In this implementation the cross-correlation function is not normalised but the normalising factor is calculated and stored in the scratch pad area. Other divisions are also avoided to make the cross-correlation routine as efficient as possible.

The cross-correlation function is then given by

$$\begin{aligned} \phi'(\nu) &= 2^{-22}\sum_{h=1}^{N}[NV_{IA}(h\Delta t+\nu)-N\bar{V}_{IA}(\nu)] \\ &\quad [NV_{RF}(h\Delta t)-N\bar{V}_{RF}] \qquad (6.6) \\ &= 2^{-22}36N^2\phi(\nu) \\ A' &= 2^{-22}\sum_{h=1}^{N}[NV_{RF}(h\Delta t)]-N\bar{V}_{RF}]^2 \qquad (6.7) \\ &= 2^{-22}36N^2A \end{aligned}$$

where

$$\begin{aligned} N\bar{V}_{IA}(\nu) &= \sum_{h=1}^{N}V_{IA}(h\Delta t+\nu) \qquad (6.8) \\ &= 6N\bar{V}_i^a \\ N\bar{V}_{RF} &= \sum_{h=1}^{N}V_{RF}(h\Delta t) \qquad (6.9) \\ &= 6N\bar{V}_{r1f} \\ N &= 21 \text{ or } 8 \qquad (6.10) \end{aligned}$$

The maximum cross-correlation amplitude will be approximately

$$\phi'_{max} = 2^{-22}36N^2\,V^2/4 \qquad (6.11)$$

If the transducer resolution is 12-bits then the maximum incremental voltages V will be 2^{12}. The scaling of 2^{-22} therefore ensures that the amplitude of the cross-correlation function does not exceed 2^{15} for the long window (21 samples). This scaling can be achieved by a combination of right shifting and only storing the high 16-bits of the the 32-bit accumulator. The scaling is therefore achieved without incurring any extra programming steps and is thus "transparent" to the algorithm.

The incident wave form with mean removal is stored as T_I in internal memory memory locations >03B4 downwards and the reflected waveform is stored as T_R in locations >0200 upwards. The form of the incident and reflected waves with mean removal is

$$T_I(h\Delta t) = NV_{IA}(h\Delta t + \nu) - N\bar{V}_{IA}(\nu) \quad (6.12)$$

$$T_R(h\Delta t) = NV_{RF}(h\Delta t) - N\bar{V}_{RF} \quad (6.13)$$

The cross-correlation function at delay time ν as given by equation 6.6 will then be

$$\phi'(\nu) = 2^{-22} \sum_{h=1}^{N} T_I(h\Delta t) T_R(h\Delta t) \quad (6.14)$$

The `CNFP` instruction is given to reconfigure the T_R data, in block B0, into internal programme memory so that the cross-correlation can be achieved by repeating a series of multiply and accumulate instructions `MAC` N times in the form

```
MAC  >FF00,*-
```  (6.15)

This multiplies two 16-bit values, one found at programme address `>FF00` (T_R) and the other in directly addressed by the current auxiliary register (T_I). Simultaneously with this multiplication; the direct address of the programme memory data location `>FF00` is incremented to `>FF01`, the auxiliary register pointer is decremented and the previous product is added to the accumulator. All this is achieved in one machine cycle (100 ns.) thus each sample of the cross-correlation function can be calculated within about N machine cycles. This is a good example of the processing power of dedicated signal processors.

For the next cross-correlation sample the normalised incident wave T_I is recalculated before the multiply and accumulate instruction is implemented a further N times.

The complete cross-correlation data flow diagram is shown in figure 6.4.

The cross-correlation function found using this algorithm is shown compared with the ideal results in figure 6.9c. From figure 6.9c it appears that the cross-correlation function deduced using this 16-bit integer arithmetic with 12-bit transducer resolution is virtually identical to that of the ideal case using 32-bit floating point arithmetic

6.3.4 Identification of the incident waves.

Once the cross-correlation function has been calculated, with either the short or long cross-correlation window, the troughs in the correlation function have to be identified. Each trough is identified in turn starting at time t_0 and working along to time $t_0 + 2\tau$. At time $t_0 + \tau$ the cross-correlation function is recalculated using the long window (21 samples).

For the cross-correlation trough with the long window (21 samples) indicated in figure 6.9c the following values are found

Delay time = 24 samples

Trough amplitude = -295

A' = 843

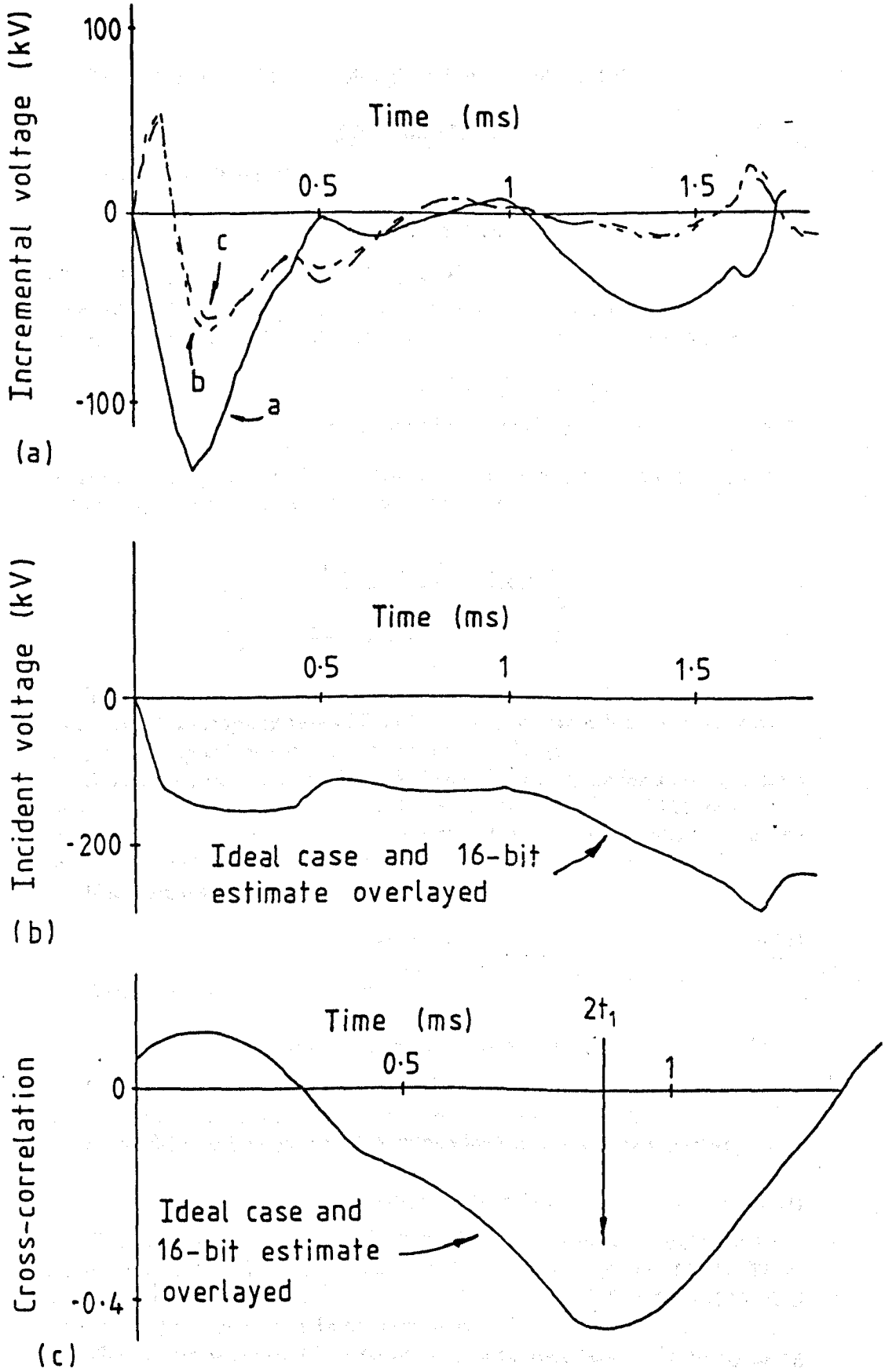

Figure 6.9 Relaying waveforms for the 12-bit resolution and 16-bit integer arithmetic of the TMS320C25 processor compared with the ideal results. (a) The incremental voltage transients. (b) The incident aerial voltage on phase-a. (c) The normalised cross-correlation function. The ideal results are indistinguishable from those using 12-bit transducer resolution and integer arithmetic.

The delay time of 24 samples gives from equation 2.19

$$\beta_0^p x = 0.1473\ rad. \tag{6.16}$$

Thus the fault location is

$$x_a = 141 \pm 6\ km \tag{6.17}$$

6.3.5 Estimation of the fault voltage level

The initial fault voltage amplitude on a three phase transmission line is given by equations 2.51,2.52 and 2.53 which can be combined to give

$$\begin{aligned} v_f(n) &= |\mathrm{v}_0^{\mathrm{p}}| \cos(\theta_1(n) - \beta_0^p x) \cos \beta_0^p x \\ &\quad - Z_s^p |\mathrm{i}_0^{\mathrm{p}}| \sin(\theta_2(n) - \beta_0^p x) \sin \beta_0^p x \end{aligned} \tag{6.18}$$

where n is the phases a, b, or c, the positive sequence line surge impedance Z_s^p and propagation constant β_0^p are given by

$$Z_s^p = \frac{z_{11}^s + z_{22}^s + z_{33}^s}{3} - \frac{z_{12}^s + z_{32}^s + z_{31}^s}{3} \tag{6.19}$$

$$\beta_0^p \approx \frac{\omega_0}{c} = 1.047 \times 10^{-3}\ rad./km \tag{6.20}$$

This calculation will require the estimate of sine and cos functions. Fortunately, at a sampling rate of 25.6 kHz, this can be achieved rapidly using simple look up tables that are not excessively large.

A sampling rate of 25.6 kHz is 512 samples per cycle for a 50 Hz system power frequency. This implies that a sine and cos table of 512 samples is required. This can be reduced, however, by using a combination of a fine and coarse look up table.

If an angle θ is given by $\theta = \theta_f + \theta_c$ such that

$$\cos \theta_f \approx 1 \tag{6.21}$$

then from basic trigonometry

$$\sin(\theta) = \sin(\theta_f) \cos(\theta_c) + \sin(\theta_c) \tag{6.22}$$

In this case this would only half the data set as condition 6.21 is only true, to within a 12-bit accuracy, for angles less than $\pi/128$.

It should also be noted that only one lookup table is required as

$$\cos \theta = \sin(\theta + \pi/2 \pm 2\pi) \tag{6.23}$$

Thus, at present, one coarse sin table is stored at external data locations >0756 to >0855 and one fine sine value is stored at address >0856. These values are stored as integer numbers in Q14 format [97] (i.e. 1= >4000 and -1= >C000) which gives a 14-bit accuracy.

The lookup table could be reduced by a further factor of four by using the fact that that these functions are cyclic so that only the first $\pi/2$ radians need be stored. The sine values for an angle θ are then given by

$$0 < \theta < \pi/2, \quad sin\theta = sin\theta \tag{6.24}$$
$$\pi/2 < \theta < \pi, \quad sin\theta = sin(\pi - \theta) \tag{6.25}$$
$$\pi < \theta < 3\pi/2, \quad sin\theta = sin(\theta - \pi) \tag{6.26}$$
$$3\pi/2 < \theta < 2\pi, \quad sin\theta = sin(2\pi - \theta) \tag{6.27}$$

The sine and cos functions would then require a single table of 65 samples. However, it was felt that the extra processing required would not merit the reduction in size of the already small data requirements.

The sine routine has been defined as a macro routine called SINANG. This is a set of source statements (machine instructions, macro statements and assembler directives), which represents a template for the generation of other statements within the source programme. When an assembler processes a macro call, it substitutes the predefined statements of the macro definition for the macro call statement in the source programme. It then assembles the substituted statements as if they had been included in the source programme. This greatly simplified the use of recurring routines such as the sine function.

The rest of the routine then simply evaluates the initial fault voltage from equation 6.18. The result is stored in the scratch pad area as an integer number which is twice the actual initial voltage level in kV. For the example data the initial fault voltage is estimated as

$$\begin{bmatrix} 351.5 \\ -181 \\ -171.5 \end{bmatrix} kV \tag{6.28}$$

6.3.6 The fault resistance estimates

In the basic relaying scheme, fault discrimination is achieved by the comparison of two fault resistance estimates. The first fault resistance estimate is given by the estimated initial fault voltage level v_f compared with the amplitude of the initial transients at the relaying point V_1. The second estimate of the fault resistance is given by the estimated initial incident transient at the fault V_{r1f} compared with the second incident transient at the relaying point V_{i2}.

For a phase-a to ground fault, these two fault resistance estimates are given by equations 4.27 and 4.28 and agreement is given by conditions 4.54 and 4.55. These conditions of agreement are based on the expected maximum error in the ratios $\frac{v_f(a)}{V_1^a(a)}$ and $\frac{v_{r1f}(a)}{V_{i2}^a(a)}$.

In the actual relay implementation the fault resistances do not have to be explicitly found but the conditions 4.54 and 4.55 have to be applied. Conditions 4.54 and 4.55 can then be reduced to the following ratio comparisons for the two defined zones.

In the first region $-1.7 \geq \frac{v_f(a)}{V_1^a(a)} \geq -3.2$, which corresponds to the first fault resistance estimate being in the region $-30\Omega \leq R_{f1} \leq 100\Omega$, fault resistance agreement is given by

$$\left|\left(\frac{v_f(a)}{V_1^a(a)} - \frac{V_{r1f}}{V_{i2}^a(a)}\right)\right| \leq 0.36 \left|\frac{V_{r1f}}{V_{i2}^a(a)}\right| \tag{6.29}$$

This corresponds to the condition given by 4.54.

In the second region $-3.2 > \frac{v_f(a)}{V_1^a(a)} \geq -4.8$, which corresponds to the first fault resistance estimate being in the region $100\Omega \leq R_{f1} \leq 240\Omega$, fault resistance agreement is given by

$$\left|\left(\frac{v_f(a)}{V_1^a(a)} - \frac{V_{r1f}}{V_{i2}^a(a)}\right)\right| \leq 0.5\left|\frac{V_{r1f}}{V_{i2}^a(a)}\right| \tag{6.30}$$

This corresponds to the condition given by 4.55.

Points outside these two regions are ignored as they correspond to a fault resistance estimate greater than the surge impedance of the line (approx 240 ohms) or estimates more negative than can be attributed to noise.

For the example data, the results were

$$\begin{aligned} v_f(a) &= 350.5\ kV \\ V_1^a(a) &= -146.3\ kV \\ \phi'(2t_1) &= -295 \\ A' &= 543 \end{aligned}$$

These results give

$$\frac{v_f(a)}{V_1^a(a)} = -2.4 \tag{6.31}$$

$$\frac{v_f(a)}{V_1^a(a)} = \frac{A'}{\phi'(2t_1)} = -1.8 \tag{6.32}$$

Thus the fault resistance estimates are in region one and condition 6.29 is met so the internal fault is correctly identified.

These results are equivalent to the fault resistance estimates of the ideal case given in chapter 4, which were

$$R_{f1} = 30\Omega \tag{6.33}$$

$$R_{f2} = -18\Omega \tag{6.34}$$

6.4 Timing

The relay routine has been shown to respond correctly to an internal fault 140 km from the protection point. The operation of this algorithm, from commencement of the processing of the stored incremental data to signalling that there is an internal fault, has been found to take about 2.3 milliseconds.

The initial filtering and sampling of the data should not cause a delay of more than about a millisecond as low pass filtering of only a few kHz is required. The inclusion of the other checks should also not delay the relay response more than a approximately 2 milliseconds as they involve the analysis of only a few data values.

The relay response time of the basic algorithm (without checks) therefore suggests that the travelling wave relay should respond within quarter of a power frequency cycle (5 ms. at 50 Hz).

6.5 Conclusion for the real time test

The basic relay algorithm without additional checks, for a phase-a to ground fault, has been successfully implemented on a TMS320C25 development system. The test fault demonstrated that good precision and rapid relay response can be achieved with the 12-bit resolution and 16-bit integer arithmetic of the TMS320C25 signal processor. The external memory demands of the algorithm are also not great as the basic routine requires about 1 kbytes of programme memory and about 1 kbytes of data memory. The relay response time of the basic routine indicates that the fully implemented routine should achieve a response time within about a quarter of a power system cycle (5 ms. at 50 Hz).

The whole relay algorithm might also be small enough to be incorporated into the on chip 4096 bytes of ROM which can be mask-programmed at the factory.

The precision assumed in the ideal tests in the earlier chapters should be achievable, therefore, the conclusions arrived at in the earlier chapters are realistic. The accuracy, timing and memory address space requirement of the proposed travelling-wave relay can also be met by currently available signal processors.

CHAPTER 7

Conclusions.

A travelling-wave relay has been developed which can be successfully applied to long EHV transmission lines.

The need for ultra high speed relays, which can respond within a quarter of a system power cycle (5 ms. at 50 Hz), has been identified as this gives a substantial improved stability and reduction in transmission costs. A review of the traditional relaying schemes showed that their optimum response times is only half a system cycle. It was then found that an ultra high speed relay has to operate from the information contained in just the fault transient travelling-waves received at the relaying point.

The basic theory for the operation of this travelling wave relay was first outlined for a single phase transmission line. The additional checks necessary to prevent relay over reach on multiphase transmission lines were then discussed. Throughout the work the emphasis has been on preventing relay over reach, as failure to do so would lead to unstable operation of the system network. In order to prevent relay over reach, however, limitations are imposed on the protectable system conditions and fault types. These conditions are not severe and in combination with conventional distance schemes an integrated scheme for complete protection can be devised. It is felt that this should be sufficient as this relay scheme is envisaged as an additional facility to the conventional schemes to offer a highly secure ultra high speed trip for internal faults without relay over reach. It is nevertheless important to specify the limitations and the probability of relay failure on internal faults. Relay over reach must definitely not occur.

This travelling-wave relay locates faults on the transmission lines by identifying incident travelling waves at the relaying point. After the arrival of the first incident travelling wave V_1 all subsequent travelling waves are identified by the cross-correlation with the first reflected wave V_{r1}. It has been found that good resolution of the second incident wave V_{2i} can be achieved, for fault locations along the whole line length, with the use of two cross-correlation windows at a sampling rate of 25.6 kHz. A short cross-correlation window (8 samples) is used to identify faults within half the line length of the relaying point. A long cross-correlation window (21 samples) is used to identify faults beyond half the line length from the relaying point.

In this study three common fault types were investigated and these were; symmetric three phase faults to ground, phase to ground faults and phase to phase faults. All symmetric internal faults can be identified up to about the line surge impedance (240 ohms). All external symmetric faults are correctly identified without the need for additional checks. Internal phase to ground faults, up to about the line surge impedance and occurring at initial voltage phase angles greater than $\pi/12$ from voltage zero, are correctly identified.

The ground mode or "mode 1" delay check ensures that all external phase to ground faults are correctly identified. All internal phase to phase faults, up to about half the line surge impedance and occurring at a phase angle greater than $\pi/12$ from the line voltage zero, are correctly identified. The amplitude of the line round trip wave $V_{2\tau}$ is used to ensure that all external phase to phase faults are correctly identified.

The protection of series compensated transmission lines and double circuit transmission line was also investigated and it was found that this travelling-wave relay should provide good protection for these configurations There are limitations which have to be imposed on these transmission lines, however, in order to ensure there is good fault discrimination between internal and external faults.

On series compensation care has to be taken to ensure that rapid protective spark gap flashover does not compromise the travelling wave protection. The transmission lines must not be excessively loaded, beyond twice their rated current level, so that the spark gap flashover does not occur before the time of arrival of the second incident wave V_{i2}. Compensated transmission lines can then be protected up to 80 % of there line length for lines of length 150 to 400 km. This is in stark contrast with conventional distance schemes which have severe problems in protecting compensated transmission lines. Faults can also be differentiated from sudden capacitor spark gap flashover by measuring the incident transient voltage gradient.

Double circuit lines can be protected when the two circuits are connected in parallel and the terminating busbar short circuit capacity is not less than 10 GVA. In the majority of cases the double circuit lines are connected in parallel to take full advantage of their reduced line impedance. It is also expected that this ultra high speed relay will only be required where there are strong sources and a risk of high fault current levels.

It should also be noted that, these restrictions on the double circuit lines are only to ensure that the extra checks for fault discrimination can be used. It may be possible to relax these line restrictions with the use of more sophisticated checks such as the measurement of the ground mode dispersion as well as its delay.

Noise susceptibility and transducer bandwidth were also investigated. The bandwidth requirement of the relay scheme depend solely on the closest fault to the relay which has to be resolved. For faults about 40 km from the relaying point a bandwidth of 4 kHz is required.

Care has been taken to ensure good noise tolerance up to about -26 decibels, however, at present the ground mode delay can only be accurately found if the noise level is less than -32 decibels. It should be possible to achieve a noise tolerance up to -26 decibels by using a more sophisticated ground mode delay check such as measuring the ground mode dispersion.

Given a noise level of -26 decibels it was found that the probability of failing to trip on an internal fault is 1/400 for faults occurring near voltage maximum and 1/20 for phase angles near voltage zero. It should be possible to greatly improve these statistics, as discussed in section 5.4, to better than 1/10000 for faults near voltage maximum and better than 1/100 for faults near voltage zero.

Real time implementation of the basic algorithm (without checks), using the TMS320C25 signal processor, showed that the currently available signal

processors can achieve the required speed and accuracy for ultra high speed relaying. Using 12-bit transducer resolution and 16-bit integer arithmetic the results were indistinguishable from the ideal results using 32-bit transducer resolution and floating point arithmetic. The algorithm response time to an internal fault 140 km from the relaying point, from initiating data analysis to signaling there is an internal fault, was about 2.3 milliseconds. This suggests that full implementation should achieve response times within 5 milliseconds.

In conclusion, a ultra high speed travelling-wave relay which should respond within 5 milliseconds, has been developed for the protection of of long EHV transmission lines. It has been shown that protection of a wide range of system conditions and fault types can be achieved. The relay has good system noise tolerance and the probability of failing to identify an internal fault is small. Relay over reach should not occur.

7.1 Further work.

To achieve full implementation of the relay on EHV transmission lines, there is still a large amount of work that needs to be done.

The relay algorithm needs to be fully implemented on a relay hardware to include all fault types and fault discriminating checks. The protection against phase to phase to ground faults also needs investigation. It should then be possible to tune the relay characteristics to the precise requirements of power system utilities.

Not only does the relay need further development but the electromagnetic interference in a substation during an EHV fault is at present only poorly understood. During EHV faults the large fault currents will give rise to large electromagnetic fields which could easily interfere with digital equipment. The security of digital relays can then only be fully guaranteed once substation electromagnetic interference has been fully investigated and controlled.

The monitoring of power system voltages and currents using wide-bandwidth recording equipment and transducers should then be undertaken to validate fully the results obtained using computer simulations.

References

[1] BERGLAND, R.O., MITTELSTADT, W.A, SHELTON, M.L., BARKEN, P., DEWEY, C.G., and SKREINER, K.M., "One cycle fault interruption at 500 kV. System benefits and breaker design." *IEEE trans. P.A.S., vol. PAS-93,* 1974, pp 1240-1251.

[2] KIMBARK, E.W., "Improvements of power system stability by changes in the network." *IEEE trans. P.A.S., vol. PAS-88(5),* 1969, pp 773-781.

[3] HICKS, K.L., and BUTT, W.H., "Feasibility and economics of Ultra-High-Speed fault clearing." *IEEE trans. P.A.S., vol. PAS-99(6),* 1980, pp 2138-2144.

[4] THORP, J.S., PHADKE, A.G., HOROWITZ, S.H., and BEEHLER, J.E., "Limits to impedance relaying." *IEEE trans. P.A.S., vol. PAS-98(1),* 1979, pp 246-256.

[5] SWIFT, G.W., "The spectra of fault induced transients." *IEEE trans. P.A.S., vol. PAS-98(3),* 1979, pp 940-947.

[6] MATHEWS, P., and NELLIST, B.D., "Transients in distance protection." *PROC. IEE pt. C, vol. 110(2),* 1963, pp 407-418.

[7] MANN, B.J., and MORRISON, I.F., "Digital calculation of impedance for transmission line protection." *IEEE trans. P.A.S., vol. PAS-90(1),* 1971, pp 270-279.

[8] WARRINGTON, A.R. van C., "Application of the ohm and mho principles to protective relays." *TRANS. AIEE, vol. 65,* 1946, pp 378-385.

[9] JACKSON, L., PATRICKSON, J.B., and WEDEPOHL, L.M., "Distance protection : optimum dynamic design of static relay comparators." *PROC. IEE pt. C, vol. 115(2),* 1968, pp 280-287.

[10] WRIGHT, A., "Limitations of distance-type protection equipment when applied to long Extremely-High Voltage power lines." *PROC. IEE pt C, vol. 108,* 1961, pp 271-280.

[11] DAVISON, E.B., and WRIGHT, A., "Some factors affecting the accuracy of distance-type protective equipment under earth-fault conditions." *PROC. IEE pt. C, vol. 110(9),* 1963, pp 1678-1688.

[12] WEDEPOHL, L.M., and MOHAMED, S.E.T., "Multiconductor transmission lines — Theory of natural modes and Fourier integral applied to transient analysis." *PROC. IEE pt. C, vol. 116(9),* 1969, pp 1553-1563.

[13] ROCKEFELLER, G.D., "Fault protection with a digital computer." *IEEE trans. P.A.S., vol. PAS-88(4),* 1969, pp 438-464.

[14] PHADKE, A.G., IBRAHIM, M., and HLIBKA, T., "Fundamental basis for distance relaying with symmetrical components." *IEEE trans. P.A.S., vol. PAS-96(2),* 1977, pp 635-645.

[15] GILBERT, J.G., and SHOVLIN, R.J., "High speed transmission line fault impedance calculation using a dedicated minicomputer." *IEEE trans. P.A.S., vol. PAS-94(3),* 1975, pp 872-883.

[16] KOTHARI, G.C., PARTHASARATHY, K., ASHOK KUMAR, B.S., and KHINCHA, H.P., "Computer-aided analysis of high-speed protective relays." *PROC. IEE pt. C, vol. 121(7),* 1974, pp 687-694.

[17] LAYCOCK, G.K., and MCLAREN, P.G., "Filtering applications in static distance relays." *PROC. IEE pt. C, vol. 119(3),* 1972, pp 313-317.

[18] JOHNS, A.T., and AGGARWAL, R.K., "Performance of high-speed distance relays with particular reference to travelling-wave effects." *PROC. IEE pt. C, vol. 124(7),* 1977, pp 639-646.

[19] HOPE, G.S., and UMAMAHESWAREN, V.S., "Sampling for computer protection of transmission lines." *IEEE trans. P.A.S., vol. PAS-93,* 1974, pp 1522-1534.

[20] HOPE, G.S., MALIK, D.P., and RASMY, M.E., "Digital transmission-line protection in real time." *PROC. IEE pt. C, vol. 123(12),* 1976, pp 1349-1354.

[21] WISZNIEWSKI, A., "How to reduce the errors of distance fault locating algorithms." *IEEE trans. P.A.S., vol. PAS-100(12),* 1981, pp 4815-4820.

[22] JOHNS, A.T., and MARTIN, M.A., "Fundamental digital approach to the distance protection of e.h.v. transmission lines." *PROC. IEE pt. C, vol. 125(5),* 1978, pp 377-384.

[23] SANDERSON, J.V.H., and WRIGHT, A., "Protective scheme for series compensated transmission lines." *PROC. IEE pt. C, vol. 121(11),* 1974, pp 1377-1384.

[24] RANJBAR, A.M., and CORY, B.J., "An improved method for the digital protection of high voltage transmission lines." *IEEE trans. P.A.S., vol. PAS-94(2),* 1975, pp 544-550.

[25] SMOLINSKI, W.J., "An algorithm for digital impedance calculation using a single Π section transmission line model." *IEEE trans. P.A.S., vol. PAS-98(5),* 1979, pp 1546-1551.

[26] JEYASURYA, B., and SMOLINSKI, W.J.,"Indentification of a best algorithm for digital distance protection of transmission lines." *IEEE trans. P.A.S., vol. PAS-102(10),* 1983, pp 3358-3369.

[27] KALMEN, R.E., "A new approach to linear filtering and prediction problems." *Journal of Basic Engineering*, vol. 82, 1960, pp 35-45.

[28] GIRGIS, A.A, and GROVER-BROWN, R., "Application of Kalman filtering in computer relaying." *IEEE trans. P.A.S., vol. PAS-100(7)*, 1981, pp 3387-3395.

[29] SACHDEV, M.S., WOOD, H.C., and JOHNSON, N.G., "Kalman filtering applied to power system measurements for relaying." *IEEE Power Engineering Review*, vol. 7(9), Sep. 1987, pp 21-27.

[30] SACHDEV, M.S., and BARIBEAU, M.A., "A new algorithm for digital impedance relays." *IEEE trans. P.A.S., vol. PAS-98(6)*, 1979, pp 2232-2240.

[31] DASH, P.K., and PANDA, D.K., "Digital impedance protection of power transmission lines using a spectral observer." *IEEE trans. Power Delivery, Vol. 3(1)*, 1988, pp 102-110.

[32] WEDEPOHL, L.M., "Application of matrix methods to the solution of travelling-wave phenomena in polyphase systems." *PROC. IEE pt. C, vol. 110(12)*, 1963, pp 2200-2212.

[33] MAGNUSSON, P.C., "Travelling waves on multi-conductor open-wire lines-A Numerical survey of the effects of frequency dependence of modal composition." *IEEE trans. P.A.S., vol. PAS-92*, 1973, pp 999-1008.

[34] WASLEY, R.G., and SELVAVINAYAGAMORTHY, S., "Approximate frequency-response values for transmission-line transient analysis." *PROC. IEE pt. C, vol. 121(4)*, 1974, pp 281-286.

[35] CABEZA-REZENDEZ L.Z., GREENWOOD, A.N., and LAUBER, T.S., "Evaluation of ultra-high speed relay algorithms." *EPRI Research project 1422-2 EL-3996*, Final report 1985.

[36] DOMMEL, H.W., and MICHELS, J.H, "High speed relaying using travelling-wave transient analysis." *IEEE Winter Power Meeting, New York*, Jan. 29 – Feb. 3, 1978, Paper No. A78 214-9

[37] CLARK, E., "Circuit analysis of A.C. power systems. vol. 1 Symmetrical and related components." Chapter X, pp 308-362, Pub. J. Wiley and Sons, 1965.

[38] MASOUR, M.M., and SWIFT, G.W., "Multi-Microprocessor based travelling-wave relay." *PROC. IEE Third International conference Developments in power system protection"* London, April 17-19, 1985.

[39] VITINS, M., "A fundamental concept for high speed relaying." *IEEE trans. P.A.S., vol. PAS-100(1)*, 1981, pp 163-168.

[40] CHAMIA, M., and LIBERMAN, S., "Ultra high speed relay for EHV/UHV transmission lines — Development, design and application." *IEEE trans. P.A.S., vol. PAS-97(6)*, 1978, pp 2104-2112.

[41] YEE, M.T., and ESZTERGALYOS, J., "Ultra high speed relay for EHV/UHV transmission lines — Installation-Staged fault tests and operational experience." *IEEE trans. P.A.S., vol. PAS-97(5),* 1978, pp 1814-1825.

[42] JOHNS, A.T., "New ultra-high speed directional comparison technique for the protection of EHV transmission lines." *PROC. IEE pt. C , Gen. Trans. and Distribution, vol. 127(4),* 1980, pp 228-239.

[43] JOHNS, A.T., MARTIN, M.A., BARKER, A., WALKER, E.P., and CROSSLEY, P.A., "A new approach to EHV directional comparison protection using digital signal processing techniques." *IEEE trans. power systems, vol. PWRD-1(2),* 1986 pp 24-34.

[44] AGGARWAL, R.K., JOHNS, A.T., and TRIPP, D.S., "The development and application of directional comparison protection for series compensated transmission systems." *IEEE trans. power systems, vol. PWRD-2,* 1987 pp 1037-1045.

[45] JOHNS, A.T., and WALKER, E.P., "Co-operative research into the engineering and design of a new digital directional comparison scheme." *PROC. IEE (C), vol. 135(4),* 1988, pp 334-368.

[46] BOLLEN, M.H.J., "Extensive testings for algorithms for travelling-wave-based protection." *PROC. IEE fourth international conference on developments in power system protection,* Edinburgh, April 1989, pp 135-139.

[47] TAGAKI, T., BABA, J., UEMURA, K., and SAKAGUCHI, T., "Fault protection based on travelling wave theory part-I Theory." *IEEE PES Summer Meeting,* July 1977, paper No. A77 750-3.

[48] TAGAKI, T., BABA, J., UEMURA, K., and SAKAGUCHI, T., "Fault protection based on travelling wave theory part-II Sensitivity analysis and laboratory test." *IEEE PES Winter Meeting,* 1978, paper No. A78 220-6.

[49] BEWLEY, L.V., "Travelling waves on transmission systems." 2nd Edition, Pub. Dover, NY. 1963, chapter 4, pp 90-106.

[50] STEVENS R.F., and STRINGFIELD, T.W., "A Transmission line fault locator using fault-generated surges." *AIEE trans. vol. 67,* 1948, pp 1168-1179.

[51] STRINGFIELD, T.W., MARIHART, D.J., STEVENS, R.F., "Fault location methods for overhead lines." *AIEE trans. vol. 76* , 1957, pp 518-530.

[52] VITINS, M., "A correlation method for transmission line protection ." *IEEE trans. P.A.S., vol. PAS-97(5),* 1978, pp 1607-1617.

[53] CROSSLEY, P.A., "Distance protection based on travelling waves." *Ph. D. Thesis,* University of Cambridge, Jan. 1983.

[54] CROSSLEY, P.A., and MCLAREN, P.G., "Distance protection based on travelling waves." *IEEE trans. P.A.S., vol. PAS-102(9),* 1983, pp 2971-2983.

[55] RAJENDRA, S., and MCLAREN, P.G., "Travelling-wave techniques applied to the protection of Teed circuits:- Principle of travelling-wave techniques." *IEEE trans. P.A.S., vol. PAS-104(12),* 1985, pp 3544-3550.

[56] RAJENDRA, S., and MCLAREN, P.G., "Travelling-wave techniques applied to the protection of Teed circuits:- Multi-phase/Multi-Circuit Systems." *IEEE trans. P.A.S., vol. PAS-104(12),* 1985, pp 3551-3557.

[57] SHEHAB-ELDIN, E.H., and MCLAREN, P.G., "Travelling-wave distance protection— problem areas and solutions." *IEEE trans. Power Delivery, Vol. 3(3),* 1988, pp

[58] KOGLIN, H., and ZHANG, B., "A new algorithm for digital distance protection based on travelling wave principle." *Power Systems computing and control 9th Conferance,* 1987 AUG/SEP, pp 746-750.

[59] NIMMERSJÖ, G., and SAHA, M.M., "A new approach to high speed relaying based on transient phenomena." *PROC. IEE fourth international conference on developments in power system protection,* Edinburgh, April 1989, pp 140-145.

[60] CHRISTOPOULOS, C., and WRIGHT, A., "The possibility of locating power system faults from the travelling-waves set up by them on transmission lines." *Seventeenth Universities Power Engineering Conference, UMIST.,* March 30—April 1, 1982.

[61] CHRISTOPOULOS, C., THOMAS, D.W.P., and WRIGHT, A., "Scheme, based on travelling-waves, for the protection of major transmission lines." *PROC. IEE pt. C, vol. 135(1),* 1988, pp 63-73.

[62] CHRISTOPOULOS, C., THOMAS, D.W.P., and WRIGHT, A., "Signal processing and discriminating techniques incorporated in the protective scheme based on travelling waves." *PROC. IEE pt. C, vol. 136(5),* 1989, pp 279-288.

[63] WEEDY B.M., "Electric Power Systems." Third edition, 1987, Chapter 3, pp 88-147, Pub. John-Wiley & Sons ltd.

[64] BICKFORD J.P., and ABDEL-RAHMAN, M.H., "Application of travelling-wave methods to the calculation of transient-fault currents and voltages in power-system networks." *PROC. IEE prt. C, vol. 127(3),* 1980, pp 153-168.

[65] GUILE, A.E., and PATERSON, W., "Electrical Power Systems." vol. 1, 2nd edition, 1977, Pub. Pergamon Press ltd., Chapter 8.3, pp 283-293.

[66] BEAUCHAMP K.G., "Signal processing using anolog and digital techniques." Pub. Allen and Unwin ltd., 1973, Chapter 9, pp 400-467.

[67] LEE, Y.W., CHEATHEM, T.P., and WIESNER, J.B., "Application of correlation analysis to the detection of periodic signals in noise." *PROC. IRE, vol. 38,* 1950, pp 1165-1170.

[68] ANDERS, G.J, DANDENO, P.L., and NEUDORF, E.E., "Computation of frequency of severe power system faults." *IEEE trans. P.A.S., vol. PAS-103(9),* 1984, pp 2369-2374.

[69] SCOTT-MAYER, W., " EMTP Rule book." Bonneville Power Administration, Portland, Oregan, USA, 1982.

[70] PEK, B., "Informal discussion and notes on GEC measurements power system simulation program." GEC measurements, Stafford, UK, 1980.

[71] DOMMEL, H.W., "Digital computer solutions of electromagnetic transients in single and multiphase networks." *IEEE trans. P.A.S., vol. PAS-88(4),* 1969, pp 388-399.

[72] DOMMEL, H.W., and SCOTT-MAYER, W., "Computation of electromagnetic transients." *PROC. IEEE, vol. 62(7),* 1974, pp 983-993.

[73] SEMLYEN, A., and DABULEANU, A., "Fast accurate switching transient calculations on transmission lines with ground return using recursive convolutions." *IEEE trans. P.A.S., vol. PAS-94(2),* 1975, pp 561-571.

[74] SEMLYEN, A., and DABULEANU, A., "A system approach to accurate switching transient calculations based on state variable component modelling." *IEEE trans. P.A.S., vol. PAS-94(2),* 1975, pp 572-578.

[75] HAUER J.F., "State-space modeling of transmission line dynamics via non-linear optimization." *IEEE trans. P.A.S., vol. PAS-100(12),* 1981, pp 4918-4924.

[76] HAUER, J.F., "Power system identification by fitting structured models to measured frequency response." *IEEE trans. P.A.S., vol. PAS-101(4),* 1982, pp 915-923.

[77] MARTI, J.R., "Accurate modelling of frequency-dependent transmission lines in electromagnetic transient simulations." *IEEE trans. P.A.S., vol. PAS-101(1),* 1982, pp 147-155.

[78] BATTISSON, M.J., DAY, S.J., MULLINEUX, N., PARTON, K.C., and REED, J.R., "Calculation of switching phenomina in power systems." *PROC. IEE, vol. 114(4),* 1967, pp 478-486.

[79] WEDEPOHL, L.M., and MOHAMED, S.E.T., "Multiconductor transmission lines. Theory of natural modes and Fourier integral applied to transient analysis." *PROC. IEE, vol. 116(9),* 1969, pp 1553-1563.

[80] MULLINEUX, N., REED, J.R., and SOPPITT, S.A., "Present mathematic syllabuses and analytical solution of field problems part-1." *International Journal of Electrical Engineering Education, vol. 8* 1970, pp 221-233.

[81] JOHNS, A.T., and EL-KATEB, M.M.T., "Developments in techniques for simulating faults on EHV transmission systems." *PROC IEE, vol. 125(3)* 1978, pp221-229

[82] LONG, R.W., and GELOPULOS, D., "Component transformations -Eigenvalue Analysis succinctly defines their relationship." *IEEE trans. P.A.S., vol. PAS-101(10),* 1982, pp 4055-4060.

[83] JOHNSON, A.A., BARKLE, J.E., and POVEJSIL, D.J., "Fundamental effects of series capacitors in high-voltage transmission lines." *AIEE trans., vol. 70,* 1951, pp 526-536.

[84] JANCKE, G., FAHLEN, N., and NERF, O., "Series capacitors in power systems." *IEEE trans. P.A.S., vol. PAS-94(3),* 1975, pp 915-925.

[85] MANEATIS, J.A., HUBACHER, E.J., RUTHENBUHLER, W.N., and SABETH. J., "500 kV series installations in California." *IEEE trans. P.A.S., vol. PAS-90,* 1971, pp 1138-1149.

[86] EL-KATEB, M.M., and CHEETHAM, W.J., "Problems in the protection of series compensated lines." *IEE Conference publication on power system protection No. 185,* 1980, pp215-220.

[87] TÜRELI, A., CARNEIRO, S., HAZAN, S.S., and SILVIA, A.M., "Comparison of protection schemes applied to series compensated long lines." *IEE Conference publication on power system protection No. 185,* 1980, pp221-225.

[88] MADZAREVIC, V., TSENG, F.K., WOO, D.H., NIEHBUHR, W.D., and ROCAMORA, R.G., "Overvoltages on EHV transmission lines due to faults and subsequent bypassing of series capacitors." *IEEE trans. P.A.S., vol. PAS-90,* 1971, pp 1874-1845.

[89] GUILE, A.E. and PATERSON, W., "Electrical power systems." *Second edition Pub. Pergamon press. vol. 1, chapter 1 and 2,* 1977, pp1-93.

[90] AGGORWAL, R.K., JOHNS, A.T., and KALEM, A., "Computer modelling of series-compensated EHV transmission lines." *PROC. IEE prt. C, vol. 131(5),* 1984, pp 188-196.

[91] WEEDY, B.M., "Electric power systems." *Third edition Pub. John Wiley and Sons, chapter 2* 1987, pp59-82.

[92] MEYNARD, P., BERGEAL, J., HEIKLILA, H., KENDALL, P., PILEGAARD, M., ROBERT, A., and WALDMANN, E., "Harmonics, characteristic parameters, methods of study, estimates of existing values in the network." *ELECTRA vol. 77,* 1981, pp 35-54.

[93] STALEWSKI, A., and WELLER, G.C., "Novel capacitor-divider voltage sensors for high-voltage transmission systems." *PROC. IEE, vol. 126(11),* 1979, pp 1186-1195.

[94] TOPPING. J., "Errors of observation and their treatment" 4th edition 1972, Pub. Chapman and Hill

[95] TEXAS INSTRUMENTS, "TMS320C25 User's guide (preliminary)" 1986, Pub. Texas Instruments Incorporated, USA.

[96] MILLMAN, J. " Microelectronics: digital and analog circuits and systems." 1979, chapter 8, pp 234-268.

[97] TEXAS INSTRUMENTS, "TMS32020 User's guide" 1986, Pub. Texas Instruments Incorporated, USA.

[98] LOUGHBOROUGH SOUND IMAGES LTD. "TMS320C25 PC board user manual issue 2." 1987, Loughborough Sound Images Ltd., Loughborough, U.K.

[99] PRESSMAN, R.S., "Software engineering a practitioner's approach." 1987, Pub. McGraw Hill.

[100] SANDER, K.F., and REED, G.A.L., "Transmission and propagation of electromagnetic waves." 2nd edition 1986, chapter 5, pp 153-205, Pub. Cambridge University Press.

APPENDIX A

Travelling waves on transmission lines.

The initial phase of any transmission line fault is dominated by travelling wave effects. On long EHV transmission lines, these effects can persist for a few milliseconds and can effect the performance of the traditional distance relays outlined in section 1.3. This appendix describes the form travelling waves take on transmission lines. A method of evaluating the transient behaviour of a multiphase transmission line using matrix algebra to deduce the independent modes of propagation will also be outlined.

The travelling waves, instigated by an internal fault on a long EHV transmission line, can be represented by the Bewley lattice diagram given in figure 1.5. These transients can be considered to be superimposed on the steady state voltages and currents. The travelling waves voltages and currents can then be found by subtracting the steady state values from the transducer outputs.

The relationship between the voltage and currents, for travelling waves on a transmission line, are given by the telegraphers equations [100]. For negligible losses these reduce to the well known wave equations

$$\frac{\partial^2 V}{\partial x^2} = LC\frac{\partial^2 V}{\partial t^2} \qquad \text{(A.1)}$$

$$\frac{\partial^2 I}{\partial x^2} = LC\frac{\partial^2 I}{\partial t^2} \qquad \text{(A.2)}$$

where L and C are the transmission line inductance and capacitance per unit length.

D'Alemberts solution for the wave equations, is expressed in terms of forward (F_1) and backward (F_2) waves

$$V(x,t) = \frac{1}{2}[F_1(ut-x) + F_2(ut+x)] \qquad \text{(A.3)}$$

$$I(x,t) = \frac{1}{2Z_s}[F_1(ut-x) - F_2(ut+x)] \qquad \text{(A.4)}$$

where;

$u = \frac{1}{\sqrt{LC}}$ = the surge velocity

$Z_s = \sqrt{\frac{L}{C}}$ = the line surge impedance

From the superposition theorem the incremental signals at the relaying point (Δv, Δi), found by removing the steady state signals, can be considered to be the travelling wave signals. We can then put

$$\Delta v = V(0,t) \qquad \text{(A.5)}$$

$$\Delta i = I(0,t) \qquad \text{(A.6)}$$

The forward and backward voltage amplitudes can then be found from the incremental voltages and currents using equations A.3 and A.4 to give

$$V_i = \frac{\Delta v - Z_s \Delta i}{2.0} \tag{A.7}$$

$$V_r = \frac{\Delta v + Z_s \Delta i}{2.0} \tag{A.8}$$

Note that equations A.7 and A.8 are independent of the source or load impedance at the protection point.

For multiphase conductors the mutual components of the phase surge impedance causes travelling waves to couple between all the phases. It is has been found, however, that for an "n" phase transmission line the travelling waves can be resolved into "n" independent modes of propagation [32].

The admittance and impedance matrices describing the multi-phase line are diagonalised by modal transformation matrices constructed from the Eigen vectors. Travelling waves on an n conductor and ground transmission line have n independent modes of propagation. The independent mode types, their attenuation and velocity of propagation are frequency dependent. This analysis was first proposed by Wedepohl [32].

In the frequency domain the partial differential equations, of the telegraphers equations describing the voltage and current transients [100], can be reduced to ordinary differential equations. The equations for an n phase line in the frequency domain become

$$\frac{d[V]}{dx} = -[Z_l][I] \tag{A.9}$$

$$\frac{d[I]}{dx} = -[Y_l][V] \tag{A.10}$$

where $[Z_l]$ and $[Y_l]$ are square matrices of order n which have elements given by

$Z_{rs} = j\omega M_{rs}(\omega) + R_r(\omega), \quad r \neq s$
$Z_{rs} = j\omega M_{rs}(\omega), \quad r = s$
$Y_{rs} = -j\omega C_{rs}(\omega), \quad r \neq s$
$Y_{rs} = \Sigma_{q=1}^{n} j\omega M_{rs}(\omega) + G_r(\omega), \quad r = s$

where $R_l(\omega), M_{ll}(\omega), C_{ll}(\omega), G_{ll}(\omega)$ are the resistance, inductance, capacitance and conductance per unit length of the lth wire. $M_{lk}(\omega), C_{lk}(\omega)$ are the mutual inductance and capacitance between the lth and kth wire per unit length.

As $[Z_l]$ and $[Y_l]$ are both symmetric matrices, the equations A.9 and A.10 can be combined to give

$$\frac{d^2[V]}{d^2x} = [P][I] \tag{A.11}$$

$$\frac{d^2[I]}{d^2x} = [P]^t[V] \tag{A.12}$$

where

$$[P] = [Z_l][Y_l] \tag{A.13}$$

$$[P]^t = [Y_l][Z_l] \tag{A.14}$$

$[\lambda]$ is a diagonal matrix where

$$[\lambda] = [S]^{-1}[P][S] \tag{A.15}$$

The matrix $[S]$ can then be formed by the eigen vectors of [P].

Using the transform of the phase voltages $[V] = [S][V_m]$, equation A.11 then becomes

$$\frac{d^2[V_m]}{dx^2} = [S]^{-1}[P][S][V_m] = [\lambda][V_m] \tag{A.16}$$

Similarly if $[\lambda] = [Q]^{-1}[P]^t[Q]$ and we use the transformation $[I] = [Q][I_m]$ then equation A.12 becomes

$$\frac{d^2[I_m]}{dx^2} = [Q]^{-1}[P]^t[Q][I_m] = [\lambda][I_m] \tag{A.17}$$

Equations A.16 and A.17 have the general solutions

$$[V_m] = [A][e^{-\gamma x}] + [B][e^{\gamma x}] \tag{A.18}$$
$$[I_m] = [C][e^{-\gamma x}] + [D][e^{\gamma x}] \tag{A.19}$$

where

$$\gamma_i^2 = \lambda_{ii} \tag{A.20}$$

The modes defined by the transformations given above, therefore, have a propagation coefficient γ_i given by equation A.20

The forward travelling modal wave is given by

$$[V_{mi}] = [A][e^{-\gamma x}] \tag{A.21}$$
$$[I_{mi}] = [C][e^{-\gamma x}] \tag{A.22}$$

The backward travelling modal wave is given by

$$[V_{mr}] = [B][e^{\gamma x}] \tag{A.23}$$
$$[I_{mr}] = [D][e^{\gamma x}] \tag{A.24}$$

These transient wave solutions can then be substituted into equations A.9 and A.10 to give

$$[V_{mi}] = [Z_m^0][I_{mi}] \tag{A.25}$$
$$[V_{mr}] = -[Z_m^0][I_{mr}] \tag{A.26}$$

where

$$[Z_m^0] = +[\gamma][S]^{-1}[Z_l][Q] \tag{A.27}$$

The modal impedance $[Z_m^0]$ is diagonal and the modal transients are independent. The first element in the modal voltage or current column matrix is termed mode 1 and the next is mode 2 etc. Mode 1 on fully transposed transmission line is known as the ground mode.

Equations A.25 and A.26 can also be written in the form

$$[V_i] = [Z_s][I_i] \tag{A.28}$$
$$[V_r] = -[Z_s][I_r] \tag{A.29}$$

where $[Z_s] = [S][Z_m^0][Q]^{-1}$ and is the phase surge impedance matrix.

Substitution of equations A.25 and A.26 into equations A.18 A.5, A.6 and A.19 gives at $x = 0$ (the relaying point)

$$[V_{mi}] = \frac{[S]^{-1}[\Delta v] - [Z_m^0][Q]^{-1}[\Delta i]}{2} \quad \text{(A.30)}$$

$$[V_{mr}] = \frac{[S]^{-1}[\Delta v] + [Z_m^0][Q]^{-1}[\Delta i]}{2} \quad \text{(A.31)}$$

or

$$[V_i] = \frac{[\Delta v] - [Z_s][\Delta i]}{2} \quad \text{(A.32)}$$

$$[V_r] = \frac{[\Delta v] + [Z_s][\Delta i]}{2} \quad \text{(A.33)}$$

These equations are then used to find the incident and reflected transient travelling waves at the relaying point.

The precise form of the modal transformation matrices depends on the conductor configuration and the conductivities of the conductors and the ground.

For a fully transposed three phase line there are two so called "aerial" modes which propagate at close to the speed of light and one so called "ground mode" or "common mode" which propagates at a much reduced velocity (typically 2/3 c).

For untransposed three phase lines there are two "aerial" modes which propagate at a velocity close to the speed of light and one termed mode 1 which propagates at a much reduced velocity. The modal transformation matrices and surge impedances are, however, frequency dependent and include complex terms. Studies have shown [34,35] that the frequency variation is negligible and the complex arguments are less than 5 %. Observations have then confirmed [36] that the model transient matrices on long EHV transmission lines can be represented, to a good approximation, by constant real quantities calculated in the frequency range 50-5000 Hz.

Travelling waves on multi phase transmission lines consist, therefore, of independent modes of propagation. The precise form of these modes depends on the line characteristics. These travelling waves can, however, be deduced from the transient incremental signals and form the basis of ultra high speed relaying on long EHV transmission lines.

APPENDIX B

The transient travelling-waves at the fault location.

This section quantifies the amplitudes of the transient travelling waves generated and reflected at the fault location. It is assumed that the fault is purely resistive.

A general fault on a multiphase line as depicted in figure 2.6 will have a conductance matrix $[Y_f]$ [64] which can be given as

$$[Y_f] = \begin{bmatrix} \frac{1}{R_{aa}} + \frac{1}{R_{ab}} + \frac{1}{R_{ac}} & -\frac{1}{R_{ab}} & -\frac{1}{R_{ac}} \\ -\frac{1}{R_{ab}} & \frac{1}{R_{bb}} + \frac{1}{R_{ab}} + \frac{1}{R_{bc}} & -\frac{1}{R_{cb}} \\ -\frac{1}{R_{ac}} & -\frac{1}{R_{cb}} & \frac{1}{R_{cc}} + \frac{1}{R_{ac}} + \frac{1}{R_{bc}} \end{bmatrix} \quad \text{(B.1)}$$

After a fault occurs on a healthy uniform multiphase transmission line of surge impedance $[Z_s]$, when the voltage level is $[v_f]$, then it will generate two transient travelling-waves which propagate away from the fault in each direction. From the line symmetry, the voltage and current amplitudes of the two waves will be identical $[V_1, I_1]$. Thévenins theorem states that the changes in the network currents and voltages caused by an added fault branch are equivalent to those caused by the addition of an emf, equal and opposite to the pre-fault steady state voltage at the fault point, in series with the fault impedance with all other active sources being zeroed. This is shown in figure B.1a. These changes are superimposed on the steady state values.

For continuity of the voltages the total voltage amplitude across the fault must be equal the the voltage amplitude of the generated propagating waves, therefore

$$[V_1] = -[v_f] + [Y_f]^{-1}[I_f] \quad \text{(B.2)}$$

where $[I_f]$ is the total current through the fault.

From the line symmetry the line currents along the two line sections must be identical so from Kirchhoff's second law

$$[I_f] = 2[I_1] \quad \text{(B.3)}$$

$$[I_f] = 2[Z_s]^{-1}[V_1] \quad \text{(B.4)}$$

This gives, from substitution into equation B.2.

$$[V_1] + 2[Y_f]^{-1}[Z_s]^{-1}[V_1] = -[v_f] \quad \text{(B.5)}$$

We can then put

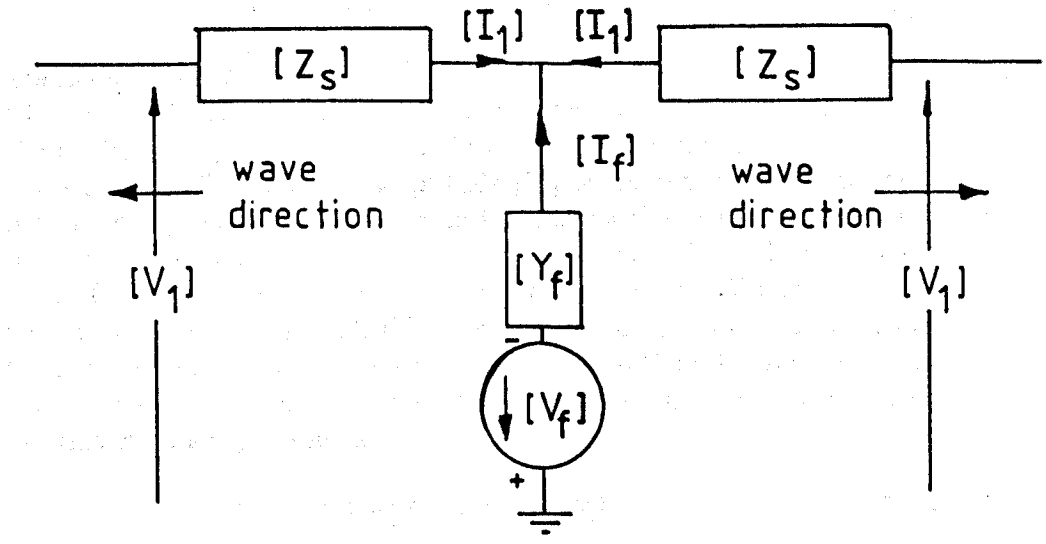

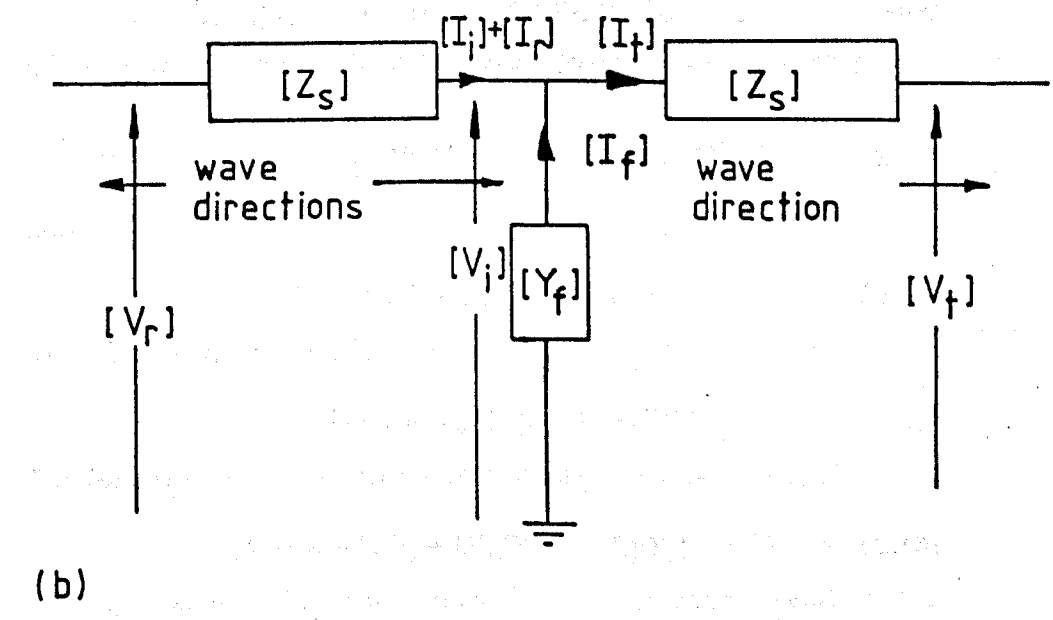

Figure B.1 The travelling-wave transients due to a fault on a multiphase transmission line. (a) The transients generated at fault inception. (b) The transients reflected and transmitted at the fault location due to an incident travelling-wave.

$$[V_1] = -[2[U] + [Z_s][Y_f]]^{-1}[Z_s][Y_f][v_f] \tag{B.6}$$

where $[U]$ is a unit matrix.

This is the form used in the relay algorithm to calculate the amplitude of the initial wave propagating away from the fault location.

When a travelling-wave of amplitude $[V_r]$ is incident at the fault location a travelling-wave will be reflected back along the line and a wave will be transmitted through the fault onto the other transmission line as shown in figure B.1b. Let the reflected wave have an amplitude $[V_i]$ and the transmitted wave have an amplitude $[V_t]$. For voltage continuity the total voltage of the incident and reflected wave must be equal to the total voltage across the fault and this in tern must be equal to the voltage of the transmitted wave. this can be expressed as

$$[V_i] + [V_r] = [V_f] = [V_t] \tag{B.7}$$

From Kirchhoff's second law

$$[I_i] + [I_r] = [I_f] + [I_t] \tag{B.8}$$

For positive current flow and wave propagation as shown in figure b.1b, the wave voltages given by equations A.25 and A.26 can be given by

$$[Z_s]^{-1}[V_r] - [Z_s]^{-1}[V_i] = [Y_f][V_f] + [Z_s]^{-1}[V_t] \tag{B.9}$$

Eliminating $[V_f]$ and $[V_t]$ by substituting equation B.7 will then give

$$[Z_s]^{-1}[V_r] - [Z_s]^{-1}[V_i] = [Y_f]([V_r] + [V_i]) + [Z_s]^{-1}([V_r] + [V_i]) \tag{B.10}$$

thus

$$-2[Z_s]^{-1}[V_i] - [Y_f][V_i] = [Y_f][V_r] \tag{B.11}$$

which can be rearranged to give

$$[V_i] = -[2[U] + [Z_s][Y_f]]^{-1}[Z][Y_f][V_r] \tag{B.12}$$

The fault travelling-wave reflection coefficient $[k_{vf}]$ is then

$$[k_{vf}] = -[2[U] + [Z_s][Y_f]]^{-1}[Z_s][Y_f] \tag{B.13}$$

This equation is in the form used by the relay algorithm to evaluate the fault impedance from the second incident wave amplitude at the protection point. Note that equation B.6 can also be written in the form

$$[V_1] = [k_{vf}][v_f] \tag{B.14}$$

APPENDIX C

Line configuration data

OVERHEAD LINE NUMBER 1

LINE IDENTIFICATION : TYPE 01L

LINE CONFIGURATION IN METERS

	PHASE-A	PHASE-B	PHASE-C	E.WIRE
X CO-ORD.	8.150	9.980	6.780	0.000
Y CO-ORD.	12.030	20.870	31.230	41.510

UNTRANSPOSED LINE

NUMBER OF EARTH WIRES	=	1	
NUMBER OF PHASE CONDUCTORS	=	3	
NUMBER OF CONDUCTORS IN THE BUNDLE	=	4	
EFFECTIVE DIAMETER OF PHASE BUNDLE	=	2.350E-01	M
DIAMETER OF THE EARTH WIRE	=	2.900E-02	M
EARTH RESISTIVITY	=	1.000E+02	Ω M
PHASE CONDUCTOR RESISTIVITY	=	3.147E-08	Ω M
EARTH WIRE RESISTIVITY	=	3.147E-08	Ω M
DIAMETER OF PHASE CONDUCTOR STRAND	=	3.180E-03	M
DIAMETER OF EARTH WIRE STRAND	=	3.180E-03	M
TOTAL STRANDS IN A PHASE CONDUCTOR	=	54	
TOTAL STRANDS IN AN EARTH WIRE	=	54	
STRANDS IN OUTER LAYER OF PH.COND.	=	24	
STRANDS IN OUTER LAYER OF E.WIRE	=	24	

Surge impedance $[Z_s]\Omega$			The modal transform matrices $[S]^{-1}$			$[Q]^{-1}$		
355	116	75	0.82	0.49	0.37	0.69	0.58	0.46
116	369	111	-0.71	0.32	0.66	-0.56	0.37	0.76
75	111	366	-0.27	0.78	-0.57	-0.19	0.79	-0.58

OVERHEAD LINE NUMBER 2
LINE IDENTIFICATION : TYPE 02L

LINE CONFIGURATION IN METERS

	CIRCUIT 2		
	PHASE A'	PHASE B'	PHASE C'
X CO-ORD.	-8.150	-9.980	-6.780
Y CO-ORD.	12.030	20.870	31.230

	CIRCUIT 1			
	PHASE A	PHASE B	PHASE C	E.WIRE
X CO-ORD.	8.150	9.980	6.780	0.000
Y CO-ORD.	12.030	20.870	31.230	41.510

UNTRANSPOSED LINE

NUMBER OF EARTH WIRES	=	1	
NUMBER OF PHASE CONDUCTORS	=	6	
NUMBER OF CONDUCTORS IN THE BUNDLE	=	4	
EFFECTIVE DIAMETER OF PHASE BUNDLE	=	2.350E-01	M
DIAMETER OF THE EARTH WIRE	=	2.900E-02	M
EARTH RESISTIVITY	=	1.000E+02	Ω M
PHASE CONDUCTOR RESISTIVITY	=	3.147E-08	Ω M
EARTH WIRE RESISTIVITY	=	3.147E-08	Ω M
DIAMETER OF PHASE CONDUCTOR STRAND	=	3.180E-03	M
DIAMETER OF EARTH WIRE STRAND	=	3.180E-03	M
TOTAL STRANDS IN A PHASE CONDUCTOR	=	54	
TOTAL STRANDS IN AN EARTH WIRE	=	54	
STRANDS IN OUTER LAYER OF PH.COND.	=	24	
STRANDS IN OUTER LAYER OF E.WIRE	=	24	

The surge impedance $\Omega[Z_s]$

369	116	75	78	72	63
116	383	111	72	77	77
75	111	381	63	77	95
78	72	63	369	116	75
72	77	77	116	383	111
63	77	95	75	111	381

The modal transform matrix $[S]^{-1}$

0.61	0.33	0.22	0.61	0.33	0.22
0.64	0.32	0.11	-0.64	-0.32	-0.11
-0.52	0.25	0.46	-0.52	0.25	0.46
0.42	-0.48	-0.28	-0.42	0.48	0.28
-0.04	0.33	-0.62	0.04	-0.33	0.62
-0.18	0.55	-0.41	-0.18	0.55	-0.41

The modal transform matrix $[Q]^{-1}$

0.48	0.40	0.33	0.48	0.40	0.33
0.56	0.39	0.17	-0.56	-0.39	-0.17
-0.35	0.28	0.54	-0.35	0.28	0.54
0.34	-0.56	-0.32	-0.34	0.56	0.32
-0.05	0.32	-0.63	0.05	-0.32	0.63
-0.13	0.53	-0.44	-0.13	0.53	-0.44

APPENDIX D

Publications

The work in this thesis has been presented in several publications which are as follows

1. CHRISTOPOULOS, C., THOMAS, D.W.P., WRIGHT, A., " Scheme, based on travelling-waves, for the protection of major transmission lines." *IEE Proceedings, Vol. 135 pt. c, No. 1,* January 1988, pp 63-73.

2. CHRISTOPOULOS, C., THOMAS, D.W.P., WRIGHT, A., " Developments in travelling-wave protection of long transmission lines", *23 rd. UPEC,* 20-22 September 1988, Trent Poly. Nottingham, c2 pp 1-4.

3. CHRISTOPOULOS, C., THOMAS, D.W.P., WRIGHT, A., " The performance of a protective scheme based on travelling waves ", *4 th Int. conference on Developments in power system protection, IEE conf.,* Publ. 302, 1989, pp 146-150.

4. CHRISTOPOULOS, C., THOMAS, D.W.P., WRIGHT, A., " The implementation of a fast protective algorithm using digital signal processors", *CIGRE symp. on digital technology in power systems,* Bournmouth 12-14 June 1989.

5. CHRISTOPOULOS, C., THOMAS, D.W.P., WRIGHT, A., " Signal processing and discrimination techniques incorporated in a protective scheme based on travelling-waves. " *IEE Proceedings, Vl. 136, pt. c, No. 5,* September 1989, pp 279-288.

6. CHRISTOPOULOS, C., THOMAS, D.W.P., WRIGHT, A., " Fast protection of long transmission lines ", *4th Int. Conf. Present day problems of power system automation and control, Gliwice, Poland,* 23-25 September 1989, 2.3.5 pp 203-208.

PAGES NOT SCANNED AT THE REQUEST OF THE UNIVERSITY

SEE ORIGINAL COPY OF THE THESIS FOR THIS MATERIAL